Theory on the local electromagnetic field in crystalline dielectrics

Dissertation

der Mathematisch - Naturwissenschaftlichen Fakultät
der Eberhard Karls Universität Tübingen
zur Erlangung des Grades eines
Doktors der Naturwissenschaften
(Dr. rer. nat.)

vorgelegt von
Marius Hermann Dommermuth
aus Limburg an der Lahn

Tübingen
2019

Gedruckt mit Genehmigung der Mathematisch - Naturwissenschaftlichen Fakultät der Eberhard Karls Universität Tübingen.

Tag der mündlichen Qualifikation:	31.05.2019
Dekan:	Prof. Dr. Wolfgang Rosenstiel
1. Berichterstatter:	Prof. Dr. Nils Schopohl
2. Berichterstatter:	Prof. Dr. Daniel Braun

Acknowledgements

With the completion of my PhD thesis, I would like to thank all the people who stood on my side and supported me during this time.

First of all, I would like to thank Prof. N. Schopohl for the opportunity to write my PhD thesis in his group and for proving, that there is still the chance to gain new knowledge in fields of research with long-lasting traditions, provided one is willing to put commonly accepted positions in question. In particular, I appreciate his active support as well as the exhaustive scientific discussions we had in this time, both substantially contributing to the successful outcome of this work.

In second place, I would like to thank Prof. D. Braun who took on the task of the second referee and thoroughly reviewed this work.

Further, I thank all my roommates and colleagues from the 8^{th} floor for the relaxed working atmosphere, cooperativeness as well as numerous scientific and non-scientific conversations we have had. In this context, special thanks is sent to Michael Benner and Anton Lebedev for various elucidations and support concerning mathematical and computer related problems, respectively.

I would particularly like to thank my parents Renate and Werner as well as my girlfriend Franziska, who always give me valuable advice and support in all situations and who never refrained from encouraging me in pursuing my objectives. Thank you!

Abstract

Starting from the microscopic Maxwell equations, a self-contained theory of the local electromagnetic field in crystalline dielectrics and its relation to macroscopic electrodynamics is established. Applying the Helmholtz decomposition theorem to the microscopic Maxwell equations, two independent sets of equations determining the solenoidal (transverse) and irrotational (longitudinal) contributions of the local electromagnetic field are initially identified. This enables to restate the microscopic Maxwell equations in terms of equivalent inhomogeneous integral equations, where the entire matter and its response to the local electromagnetic field is fully taken into account by the current density. Implementing a phenomenological material model into this current density, where the local electric field is assumed to polarize individual atoms/ions or subunits of the material in reaction to an externally applied electric field, the inhomogeneous integral equation determining the local electric field is specified first with respect to crystalline dielectrics, solely with the crystal structure and the individual polarizabilities as an input into the theory. Afterwards, it is solved exactly by making use of a newly discovered orthonormal and complete system of non-standard Bloch eigenfunctions of the crystalline translation operator. The propagable modes within the dielectric crystal as well as their dispersion relations $\omega_n(\mathbf{q})$, also called photonic band structure, are then obtained from the corresponding solvability condition of the associated homogeneous integral equation. Additionally, the impact of radiation damping and of a static external magnetic induction field on $\omega_n(\mathbf{q})$ is elucidated, followed by a discussion on the characteristics of the local electromagnetic field in crystalline dielectrics. Subsequently, the macroscopic electromagnetic field is consistently derived from the local electromagnetic field by applying a spatial low-pass filter to the latter one to eliminate all spatial variations that occur on length scales comparable to the lattice constant. The same filtering procedure is then deployed to the microscopic polarization, so that the dielectric tensor $\varepsilon_\Lambda(\mathbf{q},\omega)$ can be introduced in a tried and tested way as that quantity that relates the low-pass filtered microscopic polarization with the macroscopic electric field. Next, the differential equations satisfied by the longitudinal and transverse parts of the macroscopic electric field describing electric field screening or wave propagation are deduced in terms of the longitudinal and transverse dielectric tensor $\varepsilon^{(\mathrm{L})}(\mathbf{q},\omega)$ and $\varepsilon^{(\mathrm{T})}(\mathbf{q},\omega)$ respectively, followed by a comparison of the local and macroscopic radiation field in dielectric crystals. Finally, the dielectric tensor and its transverse counterpart are discussed. It is shown, that the derived expression for the dielectric tensor $\varepsilon_\Lambda(\mathbf{q},\omega)$ conforms in the static limit with general principles such as causality and thermodynamic stability and eventually reduces to the well-known Clausius-Mossotti equation when monatomic simple cubic crys-

tals are considered. Furthermore, its frequency dependence is proven to comply well with the Lyddane-Sachs-Teller relation. In the end, the Taylor expansion of the transverse dielectric tensor $\boldsymbol{\varepsilon}^{(\mathrm{T})}(\mathbf{q},\omega)$ up to second order around $\mathbf{q}=\mathbf{0}$ gives insight into various optical effects or quantities, that are related to non-locality (spatial dispersion) and retardation (chromatic dispersion), in full agreement with the phenomenological theory of Agranovich and Ginzburg [1]. This includes the index of refraction, natural optical activity and spatial dispersion induced birefringence as well as their respective frequency dependencies. The utility of the presented theory is then proven by demonstrating, that the calculations regarding the previously mentioned optical effects or quantities coincide well with experimental data for a variety of highly diverse and complex crystal structures. In particular, the disruptive influence of spatial dispersion induced birefringence in cubic crystals is highlighted in view of the design of optical imaging systems for lithographic applications in the deep ultraviolet spectral region.

Contents

Chapter 1

Introduction

On a microscopic level any material consists of charged particles, namely electrons and their associated nuclei. Therefore, the classical fundamental theoretical framework of electrodynamics in matter is based on *microscopic* Maxwell equations, complemented by a model of the material under consideration, that has to be incorporated into the total charge and current densities $\bar{\rho}(\mathbf{r},t)$ and $\bar{\mathbf{j}}(\mathbf{r},t)$. In this context, $\bar{\rho}(\mathbf{r},t)$ and $\bar{\mathbf{j}}(\mathbf{r},t)$ reflect the spatial structure of the medium on a microscopic level and the motion of the particles in it, including their electromagnetic response [2]. The solution of the *microscopic* Maxwell equations when taking into account the respective material model then provides the true spatial and temporal electromagnetic field distribution interacting with the individual charges within the medium, which is in this work called the *local* electromagnetic field[1]. Consequently, the calculation of the local field constitutes the basis for studying electrodynamics in different sorts of materials like e.g. dielectrics, conductors or superconductors on a microscopic level, irrespective of whether these are in a gaseous, liquid or solid state. In particular, this includes the propagation of light in as well as the optical properties of crystalline dielectrics, which is in the focus of this work.

Although the *macroscopic* Maxwell equations are commonly deployed for the theoretical description of electrodynamics in matter, including light propagation therein, it should be emphasized that this macroscopic approach is purely phenomenological, in contrast to that of the *local* field described above. For

[1] Originally, the term "local field" goes back to Lorentz. However, his approach for calculating the local electric field polarizing an individual atom within a medium is purely phenomenological and substantially differs from that presented in this work. In Lorentz's theory, the aim is to determine the local electric field $\mathbf{E}_{\text{local}}$ acting on a particular atom at position $\mathbf{r}_{\text{atom}}$ inside a polarizable dielectric medium coming from the *macroscopic* Maxwell equations. To do so, the respective atom located at $\mathbf{r}_{\text{atom}}$ is imagined to be surrounded by a sphere whose radius is large compared to the interatomic distance within the medium but small compared to the length scale on which the *macroscopic* electric field $\mathscr{E}$ varies. Outside the sphere the medium is treated as a continuum where $\mathscr{E}$ gives rise to a *macroscopic* polarization $\mathscr{P}$, while the electric field contribution to the local field from inside the sphere $\mathbf{E}_{\text{near}}$, that induces a polarization $\mathbf{P}_{\text{near}}$, is obtained by considering the medium's specific microstructure. To be precise, $\mathbf{E}_{\text{near}}$ results by summing up the dipole fields of the individual atoms arranged around the atom at $\mathbf{r}_{\text{atom}}$. Due to the boundary condition for the normal component of the *macroscopic* dielectric displacement $\mathscr{D}$ at the sphere's surface, a surface charge density is induced on the sphere, giving rise to an electric field $\mathbf{E}_{\text{sphere}}$. Then, the local field is given as the superposition $\mathbf{E}_{\text{local}} = \mathscr{E} + \mathbf{E}_{\text{near}} + \mathbf{E}_{\text{sphere}}$ and has to be understood as a, for the medium's microscopic structure, corrected macroscopic electric field. For details see e.g. [3, 4].

instance, the origin of natural optical activity occurring in various crystals is inherently included in the *local* field formalism because the precise arrangement of atoms/ions in a crystal lattice is fully taken into account. Additionally, quantum mechanical considerations on the interaction among individual atoms and the local electric field in presence of an externally controlled static magnetic induction field naturally give rise to the Faraday effect. In contrast, both optical effects just mentioned have to be incorporated by hand into the *macroscopic* description by means of one polar and one axial 3^{rd} rank material tensor, where both tensors have to reflect the point group symmetry of the respective crystal, a requirement set by Neumanns principle [1, 5]. For this reason, the fundamental physical mechanisms causing various effects like e.g. the Faraday effect remain hidden in the framework of macroscopic electrodynamics. In particular, drawing conclusions from a phenomenological/macroscopic theory to microscopic mechanisms is a delicate affair, as diverse microscopic theories may possess the same asymptotic/macroscopic limit. In contrast, the phenomenological electrodynamic theory based on macroscopic Maxwell equations is totally included in the local field formalism and can be deduced from this by a simple filtering process, as is shown in this work. As a consequence, the local field formalism provides access to macroscopic material parameters like e.g. the dielectric tensor or the 3^{rd} rank material tensors describing natural optical activity and the Faraday effect. Furthermore, it allows to relate them to microscopic quantities like e.g. the polarizabilities of the individual atoms/ions that build up the material under investigation.

Paying special attention to electromagnetic wave or light propagation, the theory on the local electromagnetic field including its relation to the macroscopic field description is elaborated by using the example of crystalline dielectrics. On the one hand this kind of material possesses a variety of optical effects that are related to its material structure as well as to the electromagnetic response of its individual constituents. On the other hand dielectric crystals are multilaterally applicable in all fields of optical sciences as they allow a tailored manipulation of technically relevant properties of light like its polarization, phase and intensity. For instance, dielectric crystals are utilized as polarizers and analyzers in ellipsometry, a widely used technique in material sciences for measuring the complex dielectric function of a material or also for determining the thickness of a thin film with a precision on the nanometer scale [6, 7]. In addition, their usage in form of e.g. $\frac{\lambda}{4}-$waveplates allows the conversion of linear polarized laser light to circular polarized light, which is essential for trapping atoms in magneto-optical traps [8]. Also, optical imaging systems for lithographic applications operating in the deep ultraviolet spectral regime are fabricated from crystals like BaF_2 and CaF_2, as they are less absorptive than glasses in this spectral range [9]. Furthermore, the range of application of crystalline dielectrics can be enlarged significantly by manipulating their optical properties with the aid of externally controlled electromagnetic fields. In particular, deploying a static magnetic induction field to a dielectric crystal like terbium-gallium-garnet allows its usage as a Faraday rotator, a magneto-optical device that rotates linear polarized light in a non-reciprocal way and therefore facilitates the realization of optical isolators, which are widely employed in interferometers to suppress perturbing back reflections. In addition, when an electric field is applied to a crystalline dielectric that does not possess a center of inversion like

e.g. KDP or $LiNbO_3$, the crystal acts as a Pockels cell, an electro-optic modulator that allows e.g. the realization of Q-switched lasers [10], these having a versatile scope in clinical applications like laser tattoo removal or pigmented and vascular lesion removal [11–13].

Due to the multitude of qualitatively distinct optical effects exhibited by crystalline dielectrics as well as their numerous fields of applications in the optical sciences it is worthwhile to develop a profound knowledge on the electrodynamics of these materials from a *microscopic* point of view. This is the objective of this thesis, that is organized as follows:

In chapter 2, the microscopic Maxwell (differential) equations determining the local electromagnetic field exactly in arbitrary materials are restated in terms of equivalent inhomogeneous integral equations by making use of the Helmholtz decomposition theorem. In chapter 3, the material model represented by $\bar{\rho}(\mathbf{r},t)$ and $\bar{\mathbf{j}}(\mathbf{r},t)$ is initially specified to crystalline dielectrics. Afterwards, the inhomogeneous integral equations are solved exactly by expanding the local electromagnetic field with respect to a complete and orthonormal set of non-standard Bloch functions. The propagable modes of the radiation field are then identified from the solvability condition of the associated homogeneous integral equations, which reflects the photonic band structure. Finally, the characteristics of the local electromagnetic field in dielectric crystals are discussed. In chapter 4, the macroscopic electromagnetic field is deduced from the local one by means of a low-pass filtering process. In this context the dielectric tensor is identified and the differential equations of macroscopic electrodynamics are derived. Subsequently, the local and the macroscopic radiation field are contrasted and their commonalities as well as their varieties are highlighted. In what follows, the dielectric tensor is thoroughly discussed. This includes besides certain limiting cases also the calculation of optical quantities like the index of refraction, rotatory power or spatial dispersion induced birefringence for a variety of crystalline dielectrics and their comparison with experimental data. The main text ends with a summary and an outlook on potential extensions of the presented theory in chapters 5 and 6, respectively. Appendices A - H provide several derivations as well as auxiliary calculations that would have disturbed the line of thought within the main text. Appendix I gives a brief introduction in the local field description of magnetizable crystals.

Chapter 2

The integral equations of the local electromagnetic field

On a fundamental level any material consists of charged particles carrying some spin, namely electrons and their allocated nuclei, which may interact with electromagnetic fields. As emphasized by Keldysh [2], each particle responds to the fields of all other constituent particles of the material in exactly the same way as to the fields generated by external charge and current densities. As a consequence, when an external field is applied to a material, the actual field, i.e. the *local* field interacting with a particular particle, will be a superposition of the externally applied field and the fields generated by all the other constituent particles of the medium. Thus, the material's microstructure is inherently encoded in the local field. Since all the fields are treated classically in this work, the *microscopic* Maxwell equations serve as the elemental starting point for the calculation of the local field, as they govern the laws of classical electrodynamics exactly. The specific material model is then fully taken into account by the *total* charge or current density, where the response of the individual charged particles to the local electromagnetic field is driven by the Lorentz force.

This section is organized as follows. Once the microscopic Maxwell equations have been introduced in space-time domain, they will be Fourier transformed to space-frequency domain, before the current density as well as the local electromagnetic field are decomposed into their irrotational (longitudinal) and solenoidal (transverse) contributions with the aid of Helmholtz's theorem. The resulting (differential) equations determine unambiguously the longitudinal and transverse components of the local electromagnetic field. Assuming that the current density does not vanish in two spatially disjoint domains of three dimensional space, where one domain constitutes the source of an externally applied electromagnetic field and where the other one represents the probe volume of the material under investigation, these (differential) equations can be reformulated in terms of integral equations, that form the basis for the investigation of the local electromagnetic field in arbitrary materials.

2.1 Helmholtz decomposition of Maxwell's equations

The microscopic Maxwell equations in space-time domain read in SI units

$$\nabla_{\mathbf{r}} \cdot \bar{\mathbf{E}}(\mathbf{r},t) = \frac{1}{\varepsilon_0}\bar{\rho}(\mathbf{r},t) \tag{2.1.1}$$

$$\nabla_{\mathbf{r}} \cdot \bar{\mathbf{B}}(\mathbf{r},t) = 0 \tag{2.1.2}$$

$$\nabla_{\mathbf{r}} \times \bar{\mathbf{E}}(\mathbf{r},t) = -\frac{\partial \bar{\mathbf{B}}(\mathbf{r},t)}{\partial t} \tag{2.1.3}$$

$$\nabla_{\mathbf{r}} \times \bar{\mathbf{B}}(\mathbf{r},t) = \mu_0\varepsilon_0\frac{\partial \bar{\mathbf{E}}(\mathbf{r},t)}{\partial t} + \mu_0\bar{\mathbf{j}}(\mathbf{r},t), \tag{2.1.4}$$

where $\bar{\rho}(\mathbf{r},t)$ and $\bar{\mathbf{j}}(\mathbf{r},t)$ denote the *total* charge or current density and thus represent on a fundamental level the material distribution in space. The response of the individual charges of magnitude $Z|e|$ to the local electromagnetic field, where $Z \in \mathbb{Z}$ and $|e|$ denotes the elementary charge, is governed by the Lorentz force according to

$$\bar{\mathbf{F}}(\mathbf{r},t) = Z|e|\left(\bar{\mathbf{E}}(\mathbf{r},t) + \frac{d\mathbf{r}}{dt} \times \bar{\mathbf{B}}(\mathbf{r},t)\right). \tag{2.1.5}$$

Due to the linearity of Maxwell's equations (2.1.1)-(2.1.4), any wanted time dependence of the quantities $\bar{\mathbf{E}}(\mathbf{r},t)$, $\bar{\mathbf{B}}(\mathbf{r},t)$, $\bar{\rho}(\mathbf{r},t)$ and $\bar{\mathbf{j}}(\mathbf{r},t)$ can be constructed by a superposition of monochromatic signals out of the set $\left\{e^{-i\omega t}\right\}_{\omega\in\mathbb{R}}$. Therefore, it is easy and convenient to get rid of the time derivatives in Maxwell's equations by Fourier transforming them from time to frequency domain. By convention, the Fourier transform of a function from time to frequency domain or vice versa, where the mutually Fourier transformed functions are denoted by $\bar{f}(\mathbf{r},t)$ and $f(\mathbf{r},\omega)$, is defined by

$$\bar{f}(\mathbf{r},t) = \frac{1}{2\pi}\int_{-\infty}^{\infty} d\omega\, e^{-i\omega t} f(\mathbf{r},\omega) \tag{2.1.6}$$

$$f(\mathbf{r},\omega) = \int_{-\infty}^{\infty} dt\, e^{i\omega t}\bar{f}(\mathbf{r},t). \tag{2.1.7}$$

Similarly, a function $f(\mathbf{r},\omega)$ living in real space is related to its Fourier transform $\tilde{f}(\mathbf{k},\omega)$ that lives in reciprocal space via

$$f(\mathbf{r},\omega) = \frac{1}{(2\pi)^3}\int_{\mathbb{R}^3} d^3k\, e^{i\mathbf{k}\cdot\mathbf{r}}\tilde{f}(\mathbf{k},\omega) \tag{2.1.8}$$

$$\tilde{f}(\mathbf{k},\omega) = \int_{\mathbb{R}^3} d^3r\, e^{-i\mathbf{k}\cdot\mathbf{r}} f(\mathbf{r},\omega). \tag{2.1.9}$$

Consequently, from (2.1.1)-(2.1.4) one readily obtains the corresponding Maxwell equations in space-frequency domain according to

$$\nabla_{\mathbf{r}} \cdot \mathbf{E}(\mathbf{r},\omega) = \frac{1}{\varepsilon_0}\rho(\mathbf{r},\omega) \tag{2.1.10}$$

$$\nabla_{\mathbf{r}} \cdot \mathbf{B}(\mathbf{r},\omega) = 0 \tag{2.1.11}$$

$$\nabla_{\mathbf{r}} \times \mathbf{E}(\mathbf{r},\omega) = i\omega\mathbf{B}(\mathbf{r},\omega) \tag{2.1.12}$$

$$\nabla_{\mathbf{r}} \times \mathbf{B}(\mathbf{r},\omega) = -i\omega\mu_0\varepsilon_0\mathbf{E}(\mathbf{r},\omega) + \mu_0\mathbf{j}(\mathbf{r},\omega), \tag{2.1.13}$$

which constitute the basis for further purposes. In accordance with Helmholtz's theorem [14–17], a smooth vector field $\mathbf{V}(\mathbf{r},\omega)$ that decays fast enough when $|\mathbf{r}| \to \infty$, can be decomposed uniquely into a sum of its irrotational (longitudinal) and solenoidal (transverse) components $\mathbf{V}^{(\mathrm{L})}(\mathbf{r},\omega)$ and $\mathbf{V}^{(\mathrm{T})}(\mathbf{r},\omega)$ according to[1]

$$\mathbf{V}(\mathbf{r},\omega) = \mathbf{V}^{(\mathrm{L})}(\mathbf{r},\omega) + \mathbf{V}^{(\mathrm{T})}(\mathbf{r},\omega) \tag{2.1.14}$$

$$\nabla_{\mathbf{r}} \times \mathbf{V}^{(\mathrm{L})}(\mathbf{r},\omega) = \mathbf{0} \tag{2.1.15}$$

$$\nabla_{\mathbf{r}} \cdot \mathbf{V}^{(\mathrm{T})}(\mathbf{r},\omega) = 0. \tag{2.1.16}$$

The explicit construction of $\mathbf{V}^{(\mathrm{L})}(\mathbf{r},\omega)$ and $\mathbf{V}^{(\mathrm{T})}(\mathbf{r},\omega)$ out of $\mathbf{V}(\mathbf{r},\omega)$ can be realized with the help of the so-called longitudinal and transverse projection operators[2], whose matrix elements in real space are given in cartesian coordinates by

$$a,b \in \{1,2,3\}$$

$$\Pi^{(\mathrm{L})}_{ab}(\mathbf{r}-\mathbf{r}') = \frac{1}{3}\delta_{ab}\delta(\mathbf{r}-\mathbf{r}') + \Theta_{\mathrm{H}}(|\mathbf{r}-\mathbf{r}'|-0^+)\,\frac{\delta_{ab}|\mathbf{r}-\mathbf{r}'|^2 - 3(r_a-r'_a)(r_b-r'_b)}{4\pi|\mathbf{r}-\mathbf{r}'|^5} \tag{2.1.17}$$

$$\Pi^{(\mathrm{T})}_{ab}(\mathbf{r}-\mathbf{r}') = \frac{2}{3}\delta_{ab}\delta(\mathbf{r}-\mathbf{r}') - \Theta_{\mathrm{H}}(|\mathbf{r}-\mathbf{r}'|-0^+)\,\frac{\delta_{ab}|\mathbf{r}-\mathbf{r}'|^2 - 3(r_a-r'_a)(r_b-r'_b)}{4\pi|\mathbf{r}-\mathbf{r}'|^5}, \tag{2.1.18}$$

[1] For a detailed derivation of (2.1.14), see appendix A.1. Also note, that the terms irrotational and longitudinal as well as solenoidal and transverse will be used synonymously in this work, although there is a subtle difference. The terms longitudinal and transverse usually refer to reciprocal space, where a field orientated parallel to the "wave vector" is called longitudinal while a field that is perpendicular to the "wave vector" is said to be transverse. In real space instead, there is no such geometrical picture due to the *non-local* relationship between a vector field and its irrotational and solenoidal components (see (2.1.19)).

[2] The projection operators given by (2.1.17) and (2.1.18) are also known as longitudinal and transverse delta function. For their derivation as well as that of the projection procedure (2.1.19), see appendix A.2 or alternatively [18].

where $\Theta_{\mathrm{H}}(x)$ denotes the Heaviside step function. The components of $\mathbf{V}^{(\mathrm{L})}(\mathbf{r},\omega)$ or $\mathbf{V}^{(\mathrm{T})}(\mathbf{r},\omega)$ in cartesian coordinates are then related to those of $\mathbf{V}(\mathbf{r},\omega)$ via the convolution integral

$$a \in \{1,2,3\}$$
$$V_a^{(A)}(\mathbf{r},\omega) = \sum_{b=1}^{3} \int_{\mathbb{R}^3} d^3r' \, \Pi_{ab}^{(A)}(\mathbf{r}-\mathbf{r}') \, V_b(\mathbf{r}',\omega) \quad ; \quad A \in \{\mathrm{L},\mathrm{T}\}, \tag{2.1.19}$$

which corresponds in reciprocal space to the *local* relationship

$$\tilde{V}_a^{(A)}(\mathbf{k},\omega) = \sum_{b=1}^{3} \tilde{\Pi}_{ab}^{(A)}(\mathbf{k}) \, \tilde{V}_b(\mathbf{k},\omega) \quad ; \quad A \in \{\mathrm{L},\mathrm{T}\}, \tag{2.1.20}$$

with the associated projection operators given by

$$\tilde{\Pi}_{ab}^{(\mathrm{L})}(\mathbf{k}) = \frac{k_a k_b}{|\mathbf{k}|^2} \tag{2.1.21}$$
$$\tilde{\Pi}_{ab}^{(\mathrm{T})}(\mathbf{k}) = \delta_{ab} - \frac{k_a k_b}{|\mathbf{k}|^2}. \tag{2.1.22}$$

Due to the extensive use of the projection operators in this work, their characteristic properties are briefly summarized in abstract operator notation according to

$$\Pi^{(\mathrm{L})} + \Pi^{(\mathrm{T})} = \mathbb{I} \tag{2.1.23}$$
$$\Pi^{(\mathrm{L})} \circ \Pi^{(\mathrm{L})} = \Pi^{(\mathrm{L})} \tag{2.1.24}$$
$$\Pi^{(\mathrm{T})} \circ \Pi^{(\mathrm{T})} = \Pi^{(\mathrm{T})} \tag{2.1.25}$$
$$\Pi^{(\mathrm{L})} \circ \Pi^{(\mathrm{T})} = \Pi^{(\mathrm{T})} \circ \Pi^{(\mathrm{L})} = \mathbb{O}, \tag{2.1.26}$$

where "$\circ$" denotes the common matrix product in reciprocal space or a convolution in real space, while $\mathbb{I}$ and $\mathbb{O}$ represent the corresponding unity and zero operator, respectively.

It should be stressed again, that the projection process (2.1.19) in real space is *non-local*, i.e. even if $\mathbf{V}(\mathbf{r},\omega)$ vanishes in any region of three-dimensional space, it does not have to hold true for the projected fields $\mathbf{V}^{(\mathrm{L})}(\mathbf{r},\omega)$ and $\mathbf{V}^{(\mathrm{T})}(\mathbf{r},\omega)$. As will be seen in the course of this work, the Helmholtz decomposition of Maxwell's equations will allow an unambiguous identification of the radiative and non-radiative contributions of the electromagnetic field including their associated sources[3].

According to equation (2.1.11) the magnetic induction field has vanishing divergence and is thus always transverse, so that in the remainder of this work the notation

$$\mathbf{B}(\mathbf{r},\omega) \equiv \mathbf{B}^{(\mathrm{T})}(\mathbf{r},\omega) \tag{2.1.27}$$

[3] In other words, the Helmholtz decomposition permits the identification of the independent degrees of freedom of the electromagnetic theory, which is important in the context of quantizing the electromagnetic radiation field. See e.g. [18].

is introduced. Now, applying the Helmholtz decomposition (2.1.14) to Maxwell's equations (2.1.10)-(2.1.13) with regard to the current density $\mathbf{j}(\mathbf{r},\omega)$ as well as to the fields $\mathbf{E}(\mathbf{r},\omega)$ and $\mathbf{B}(\mathbf{r},\omega)$, one readily obtains

$$\nabla_{\mathbf{r}} \cdot \mathbf{E}^{(\mathrm{L})}(\mathbf{r},\omega) = \frac{1}{\varepsilon_0}\rho(\mathbf{r},\omega) \tag{2.1.28}$$

$$\nabla_{\mathbf{r}} \cdot \mathbf{B}(\mathbf{r},\omega) = 0 \tag{2.1.29}$$

$$\nabla_{\mathbf{r}} \times \mathbf{E}^{(\mathrm{T})}(\mathbf{r},\omega) = i\omega\mathbf{B}(\mathbf{r},\omega) \tag{2.1.30}$$

$$\begin{aligned}\nabla_{\mathbf{r}} \times \mathbf{B}(\mathbf{r},\omega) &= -i\omega\mu_0\varepsilon_0\left(\mathbf{E}^{(\mathrm{L})}(\mathbf{r},\omega)+\mathbf{E}^{(\mathrm{T})}(\mathbf{r},\omega)\right)+\mu_0\left(\mathbf{j}^{(\mathrm{L})}(\mathbf{r},\omega)+\mathbf{j}^{(\mathrm{T})}(\mathbf{r},\omega)\right)\\ &= -i\omega\mu_0\varepsilon_0\mathbf{E}^{(\mathrm{T})}(\mathbf{r},\omega)+\mu_0\mathbf{j}^{(\mathrm{T})}(\mathbf{r},\omega),\end{aligned} \tag{2.1.31}$$

where in the second line of the last equation the orthogonality of longitudinal and transverse vector fields was exploited, leading to the important identity

$$-i\omega\varepsilon_0\mathbf{E}^{(\mathrm{L})}(\mathbf{r},\omega)+\mathbf{j}^{(\mathrm{L})}(\mathbf{r},\omega) = \mathbf{0}. \tag{2.1.32}$$

Obviously, (2.1.32) reflects the continuity equation in space-frequency domain, as taking the divergence and employing (2.1.28) directly gives[4]

$$-i\omega\rho(\mathbf{r},\omega)+\nabla_{\mathbf{r}} \cdot \mathbf{j}^{(\mathrm{L})}(\mathbf{r},\omega) = 0. \tag{2.1.33}$$

It should be pointed out that the longitudinal electric field $\mathbf{E}^{(\mathrm{L})}(\mathbf{r},\omega)$ can be determined from a scalar potential $\phi(\mathbf{r},\omega)$ due to its vanishing curl, i.e. it can be written as

$$\mathbf{E}^{(\mathrm{L})}(\mathbf{r},\omega) = -\nabla_{\mathbf{r}}\phi(\mathbf{r},\omega). \tag{2.1.34}$$

When taking the divergence of (2.1.32), subsequent application of the continuity equation (2.1.33) together with (2.1.34) yields the Poisson equation

$$-\nabla_{\mathbf{r}}^2\phi(\mathbf{r},\omega) = \frac{1}{\varepsilon_0}\rho(\mathbf{r},\omega) \tag{2.1.35}$$

for the scalar potential $\phi(\mathbf{r},\omega)$, that possesses the particular solution

$$\phi(\mathbf{r},\omega) = \frac{1}{4\pi\varepsilon_0}\int_{\mathbb{R}^3} d^3r' \,\frac{\rho(\mathbf{r}',\omega)}{|\mathbf{r}-\mathbf{r}'|}, \tag{2.1.36}$$

which is well known from electrostatics. Consequently, the longitudinal electric field $\mathbf{E}^{(\mathrm{L})}(\mathbf{r},\omega)$ constitutes a *non-radiative* field. To obtain an equation for the transverse electric field alone, the respective Maxwell equations determining $\mathbf{E}^{(\mathrm{T})}(\mathbf{r},\omega)$ and $\mathbf{B}(\mathbf{r},\omega)$ have to be decoupled. This can be achieved by

[4] Recall, that because of (2.1.6) the equivalence $\frac{\partial}{\partial t} \leftrightarrow -i\omega$ is established. Similarly, there holds $\nabla_{\mathbf{r}} \leftrightarrow i\mathbf{k}$ due to (2.1.8).

taking the curl of (2.1.30) and subsequent employment of the identity

$$\nabla_{\mathbf{r}} \times \nabla_{\mathbf{r}} \times \mathbf{V}(\mathbf{r},\omega) = \nabla_{\mathbf{r}} \nabla_{\mathbf{r}} \cdot \mathbf{V}(\mathbf{r},\omega) - \nabla_{\mathbf{r}}^2 \mathbf{V}(\mathbf{r},\omega) \tag{2.1.37}$$

together with (2.1.31). As a result[5], the transverse electric field $\mathbf{E}^{(\mathrm{T})}(\mathbf{r},\omega)$ is described by the Helmholtz equation

$$-\nabla_{\mathbf{r}}^2 \mathbf{E}^{(\mathrm{T})}(\mathbf{r},\omega) - \frac{\omega^2}{c^2}\mathbf{E}^{(\mathrm{T})}(\mathbf{r},\omega) = i\omega\mu_0 \mathbf{j}^{(\mathrm{T})}(\mathbf{r},\omega), \tag{2.1.38}$$

indicating unambiguously that $\mathbf{E}^{(\mathrm{T})}(\mathbf{r},\omega)$ is a *radiative* field[6]. Of course, there holds a similar Helmholtz equation for the magnetic induction field, which can be obtained by taking the curl of (2.1.31) with ensuing application of (2.1.30) and (2.1.37). It reads

$$-\nabla_{\mathbf{r}}^2 \mathbf{B}(\mathbf{r},\omega) - \frac{\omega^2}{c^2}\mathbf{B}(\mathbf{r},\omega) = \mu_0 \nabla_{\mathbf{r}} \times \mathbf{j}^{(\mathrm{T})}(\mathbf{r},\omega) \tag{2.1.39}$$

and thus indicates the radiative character of $\mathbf{B}(\mathbf{r},\omega)$. Finally, another advantage of the Helmholtz decomposition becomes obvious at this point, as each cartesian component of the fields $\mathbf{E}^{(\mathrm{T})}(\mathbf{r},\omega)$ and $\mathbf{B}(\mathbf{r},\omega)$ satisfies the Helmholtz equation separately, so that a solution based on a scalar instead of a dyadic Green function is possible.

In this section, the fundamental (differential) equations determining the longitudinal and transverse components of the local electric field as well as that of the purely transverse local magnetic induction field have been identified by applying Helmholtz's decomposition to the microscopic Maxwell equations. In the next section, these equations will be transformed to integral equations that form an effective basis for the investigation of the local electromagnetic field in arbitrary materials. In particular it is shown in the course of this work, that these integral equations can be solved exactly when polarizable or magnetizable crystalline materials are considered.

2.2 Integral representation of the local electromagnetic field

The transformation of a differential equation to an integral equation has a long tradition in physics[7], because the treatment of physical problems by means of integral equations instead of differential equations provides several advantages. To obtain a unique solution of a differential equation, it has to be supplemented by particular boundary conditions, that have to be imposed at the final stage of the calculation. In contrast, when an integral equation is constructed, which is equivalent to a particular differential equation including the imposed boundary conditions, the definite form of the integral equation depends on the boundary conditions and therefore these are inherently built into the integral equation. Further,

[5] Recall the identity $c = \frac{1}{\sqrt{\varepsilon_0\mu_0}}$.

[6] As photons describe quantized radiation, they are exclusively the quanta of the transverse electric field $\mathbf{E}^{(\mathrm{T})}(\mathbf{r},\omega)$.

[7] An outstanding example can be found in quantum mechanical scattering theory, where the Schrödinger equation is transformed to an integral equation. See e.g. [19].

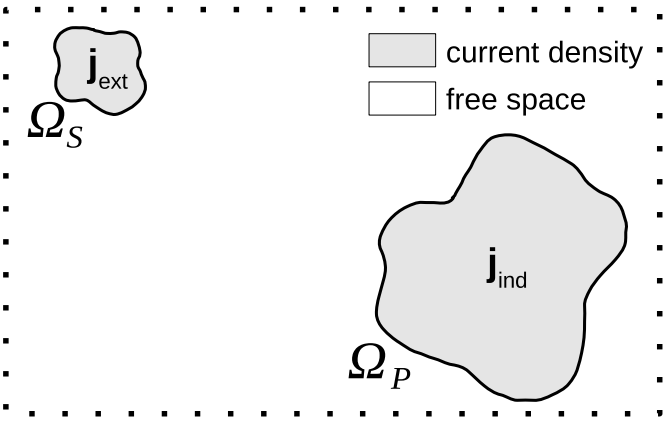

Figure 2.2.1: Schematic illustration of the externally controlled source volume Ω_S and the probe volume to be investigated Ω_P embedded in free space. Both disjoint domains exhibit non vanishing current densities $\mathbf{j}_{ext}(\mathbf{r},\omega)$ and $\mathbf{j}_{ind}(\mathbf{r},\omega)$, respectively. The figure is taken from [23].

an integral equation is non-local, i.e. it relates the unknown function to its values throughout a specific region including the boundary [20]. Hence, imposing conditions for the normal and tangential components of a vector field at an interface, as is usually done in the differential equation formulation of electrodynamics, is redundant in the integral equation approach. Finally it should be mentioned, that physical problems exist which can not be represented by differential equations but by integral equations, granting the integral equations a wider generality [21, 22].

In the following, the equations (2.1.32), (2.1.38) and (2.1.39) determining the local electromagnetic field are supposed to be solved for the geometry shown in figure 2.2.1. The setup consists of two disjoint domains Ω_S and Ω_P which are referred to as the source and the probe volume, respectively. They are embedded in free three-dimensional space and filled with material at rest. Obviously, there holds by construction $\Omega_S \cap \Omega_P = \emptyset$ where $\Omega = \Omega_S \cup \Omega_P$ denotes the total domain of non-vanishing current densities. Accordingly, the current density is split into

$$\mathbf{j}(\mathbf{r},\omega) = \begin{cases} \mathbf{j}_{ext}(\mathbf{r},\omega) & \mathbf{r} \in \Omega_S \\ \mathbf{j}_{ind}(\mathbf{r},\omega) & \mathbf{r} \in \Omega_P \\ \mathbf{0} & \mathbf{r} \notin \Omega \end{cases}, \tag{2.2.1}$$

where $\mathbf{j}_{ext}(\mathbf{r},\omega)$ is an externally controlled and a priori known current density, whereas $\mathbf{j}_{ind}(\mathbf{r},\omega)$ represents the induced current density in the material to be investigated[8]. What type of material is dealt with, depends on the specific model of the material which has to be incorporated into $\mathbf{j}_{ind}(\mathbf{r},\omega)$. Furthermore, it is assumed that charge transfer between Ω_S and Ω_P is prohibited, having the consequence that the

[8] As was shown in the previous section, the sources of the local electromagnetic field are the longitudinal and transverse components of the current density, see (2.1.32) and (2.1.38) for the electric field as well as (2.1.39) for the magnetic induction field. Hence, there is no necessity to incorporate the material model into the charge density separately. If desired, the charge density can always be deduced from the continuity equation (2.1.33) by calculating the divergence of the (longitudinal) current density.

continuity equation (2.1.33) holds separately in the domains concerned, i.e.

$$-i\omega\rho_{\text{ext}}(\mathbf{r},\omega)+\nabla_{\mathbf{r}}\cdot\mathbf{j}_{\text{ext}}^{(\text{L})}(\mathbf{r},\omega)=0 \quad \text{for } \mathbf{r}\in\Omega_{\text{S}} \tag{2.2.2}$$

$$-i\omega\rho_{\text{ind}}(\mathbf{r},\omega)+\nabla_{\mathbf{r}}\cdot\mathbf{j}_{\text{ind}}^{(\text{L})}(\mathbf{r},\omega)=0 \quad \text{for } \mathbf{r}\in\Omega_{\text{P}}. \tag{2.2.3}$$

Additionally, the source is allowed to affect the probe, while it is required that the reverse does not hold true[9]. As a reminder, the projection process (2.1.19) relates $\mathbf{j}^{(\text{L})}(\mathbf{r},\omega)$ or $\mathbf{j}^{(\text{T})}(\mathbf{r},\omega)$ to $\mathbf{j}(\mathbf{r},\omega)$ in a *non-local* way, i.e. though $\mathbf{j}(\mathbf{r},\omega)\neq\mathbf{0}$ only holds for $\mathbf{r}\in\Omega$, there is *no* such restriction for $\mathbf{j}^{(\text{L})}(\mathbf{r},\omega)$ and $\mathbf{j}^{(\text{T})}(\mathbf{r},\omega)$, respectively. Hence, for the geometry under consideration, the longitudinal electric field is readily determined from equation (2.1.32) according to

$$\begin{aligned}E_a^{(\text{L})}(\mathbf{r},\omega)&=\frac{1}{\varepsilon_0}\frac{1}{i\omega}j_a^{(\text{L})}(\mathbf{r},\omega)\\&=E_{\text{ext},a}^{(\text{L})}(\mathbf{r},\omega)+\frac{1}{\varepsilon_0}\frac{1}{i\omega}j_{\text{ind},a}^{(\text{L})}(\mathbf{r},\omega),\end{aligned} \tag{2.2.4}$$

where the externally controlled longitudinal electric field is defined by

$$E_{\text{ext},a}^{(\text{L})}(\mathbf{r},\omega)=\frac{1}{\varepsilon_0}\frac{1}{i\omega}j_{\text{ext},a}^{(\text{L})}(\mathbf{r},\omega). \tag{2.2.5}$$

It turns out that for the exact analytical calculation of the transverse electric field, a transformation of Helmholtz's equation (2.1.38) into an integral equation is appropriate. The latter reads[10]

$$E_a^{(\text{T})}(\mathbf{r},\omega)=E_{\text{ext},a}^{(\text{T})}(\mathbf{r},\omega)+i\omega\mu_0\int_{\mathbb{R}^3}d^3r'\,g(\mathbf{r}-\mathbf{r}',\omega)\,j_{\text{ind},a}^{(\text{T})}(\mathbf{r}',\omega), \tag{2.2.6}$$

where the externally controlled transverse electric field is defined by

$$E_{\text{ext},a}^{(\text{T})}(\mathbf{r},\omega)=i\omega\mu_0\int_{\mathbb{R}^3}d^3r'\,g(\mathbf{r}-\mathbf{r}',\omega)\,j_{\text{ext},a}^{(\text{T})}(\mathbf{r}',\omega). \tag{2.2.7}$$

Here,

$$g(\mathbf{r}-\mathbf{r}',\omega)=\frac{1}{4\pi}\frac{e^{i\frac{\omega}{c}|\mathbf{r}-\mathbf{r}'|}}{|\mathbf{r}-\mathbf{r}'|} \tag{2.2.8}$$

denotes the retarded Green function of Helmholtz's equation, behaving like an outgoing spherical wave and being determined by

$$\left(-\nabla_{\mathbf{r}}^2-\frac{\omega^2}{c^2}\right)g(\mathbf{r}-\mathbf{r}',\omega)=\delta(\mathbf{r}-\mathbf{r}'). \tag{2.2.9}$$

[9] For instance, imagine a setup where a laser (the source) irradiates a crystal (the probe). At the crystal's surface an amount of the emitted laser light will be reflected and possibly a small fraction of it may enter the laser cavity, thus inducing a current density inside the source and consequently modulating the laser emission. This effect, where the crystal affects the laser as a consequence of being irradiated, is a kind of backlash and will be neglected in the remainder of this work. It should be emphasized that the suppression of such retroactive effects can be realized in experiments with the help of optical insulators.

[10] For a detailed derivation of the integral equation (2.2.6) determining $E_a^{(\text{T})}(\mathbf{r},\omega)$, see appendix B.

It should be emphasized, that the external transverse electric field given by (2.2.7) represents a particular solution of an *inhomogeneous* Helmholtz equation. Hence, there is *no* need to satisfy the dispersion relation $|\mathbf{k}| = \frac{\omega}{c}$ of free space, that represents the solvability condition of the associated *homogeneous* Helmholtz equation, where $\mathbf{k}$ denotes the so-called wave vector which is usually associated with a plane wave proportional to $e^{i\mathbf{k}\cdot\mathbf{r}}$. As the Helmholtz equation (2.1.39) establishing the magnetic induction field can be received from that of the transverse electric field (2.1.38) just by replacing $\mathbf{E}^{(\mathrm{T})}(\mathbf{r},\omega) \to \mathbf{B}(\mathbf{r},\omega)$ and $i\omega\mathbf{j}^{(\mathrm{T})}(\mathbf{r},\omega) \to \nabla_{\mathbf{r}} \times \mathbf{j}^{(\mathrm{T})}(\mathbf{r},\omega)$, its integral representation can be readily deduced from (2.2.6), yielding

$$B_a(\mathbf{r},\omega) = B_{\mathrm{ext},a}(\mathbf{r},\omega) + \mu_0 \int_{\mathbb{R}^3} d^3r'\, g(\mathbf{r}-\mathbf{r}',\omega) \left[\nabla_{\mathbf{r}'} \times \mathbf{j}^{(\mathrm{T})}_{\mathrm{ind}}(\mathbf{r}',\omega)\right]_a, \tag{2.2.10}$$

where the externally controlled magnetic induction field is defined by

$$B_{\mathrm{ext},a}(\mathbf{r},\omega) = \mu_0 \int_{\mathbb{R}^3} d^3r'\, g(\mathbf{r}-\mathbf{r}',\omega) \left[\nabla_{\mathbf{r}'} \times \mathbf{j}^{(\mathrm{T})}_{\mathrm{ext}}(\mathbf{r}',\omega)\right]_a. \tag{2.2.11}$$

The local electric field $E_a(\mathbf{r},\omega)$ is then obtained by superimposing its longitudinal and transverse components according to Helmholtz's theorem, reading

$$\begin{aligned} E_a(\mathbf{r},\omega) &= E^{(\mathrm{L})}_a(\mathbf{r},\omega) + E^{(\mathrm{T})}_a(\mathbf{r},\omega) \\ &= E^{(\mathrm{L})}_{\mathrm{ext},a}(\mathbf{r},\omega) + E^{(\mathrm{T})}_{\mathrm{ext},a}(\mathbf{r},\omega) + \frac{1}{\varepsilon_0}\frac{1}{i\omega} j^{(\mathrm{L})}_{\mathrm{ind},a}(\mathbf{r},\omega) + i\omega\mu_0 \int_{\mathbb{R}^3} d^3r'\, g(\mathbf{r}-\mathbf{r}',\omega)\, j^{(\mathrm{T})}_{\mathrm{ind},a}(\mathbf{r}',\omega). \end{aligned} \tag{2.2.12}$$

Identifying the externally controlled electric field as

$$E_{\mathrm{ext},a}(\mathbf{r},\omega) = E^{(\mathrm{L})}_{\mathrm{ext},a}(\mathbf{r},\omega) + E^{(\mathrm{T})}_{\mathrm{ext},a}(\mathbf{r},\omega) \tag{2.2.13}$$

and expressing the induced longitudinal and transverse current densities $j^{(\mathrm{L})}_{\mathrm{ind},a}(\mathbf{r},\omega)$ and $j^{(\mathrm{T})}_{\mathrm{ind},a}(\mathbf{r},\omega)$, respectively, in terms of $j_{\mathrm{ind},a}(\mathbf{r},\omega)$ by means of (2.1.19), the local electric field finally assumes the guise (with $c = \frac{1}{\sqrt{\varepsilon_0\mu_0}}$)

$$\begin{aligned} &E_a(\mathbf{r},\omega) \\ =&E_{\mathrm{ext},a}(\mathbf{r},\omega) + \frac{i}{\omega}\frac{1}{\varepsilon_0}\sum_{b=1}^{3}\int_{\mathbb{R}^3} d^3r' \left[\frac{\omega^2}{c^2}\int_{\mathbb{R}^3} d^3x\, g(\mathbf{r}-\mathbf{x},\omega)\,\Pi^{(\mathrm{T})}_{ab}(\mathbf{x}-\mathbf{r}') - \Pi^{(\mathrm{L})}_{ab}(\mathbf{r}-\mathbf{r}')\right] j_{\mathrm{ind},b}(\mathbf{r}',\omega) \\ =&E_{\mathrm{ext},a}(\mathbf{r},\omega) + \frac{i}{\omega}\frac{1}{\varepsilon_0}\sum_{b=1}^{3}\int_{\mathbb{R}^3} d^3r'\, \mathscr{G}_{ab}(\mathbf{r},\mathbf{r}',\omega)\, j_{\mathrm{ind},b}(\mathbf{r}',\omega), \end{aligned} \tag{2.2.14}$$

which has already been obtained following the outlined procedure by [24]. In the last line of (2.2.14)

the cartesian components of the electromagnetic kernel have been defined as[11]

$$\mathscr{G}_{ab}\left(\mathbf{r},\mathbf{r}',\omega\right)=\frac{\omega^2}{c^2}\int_{\mathbb{R}^3}d^3x\,g\left(\mathbf{r}-\mathbf{x},\omega\right)\Pi_{ab}^{(\mathrm{T})}\left(\mathbf{x}-\mathbf{r}'\right)-\Pi_{ab}^{(\mathrm{L})}\left(\mathbf{r}-\mathbf{r}'\right). \tag{2.2.15}$$

As is shown in appendix C, there holds for the electromagnetic kernel

$$\mathscr{G}_{ab}\left(\mathbf{r},\mathbf{r}',\omega\right)=\mathscr{G}_{ab}\left(\mathbf{r}-\mathbf{r}',\omega\right), \tag{2.2.16}$$

expressing its translation invariance with respect to a simultaneous shift of its spatial arguments by a constant vector. Furthermore, its Fourier transform $\tilde{\mathscr{G}}_{ab}\left(\mathbf{k},\omega\right)$ which will be used extensively for the representation and evaluation of lattice sums in the course of this work, is given by

$$\tilde{\mathscr{G}}_{ab}\left(\mathbf{k},\omega\right)=\frac{\omega^2}{c^2}\frac{1}{|\mathbf{k}|^2-\frac{\omega^2}{c^2}}\tilde{\Pi}_{ab}^{(\mathrm{T})}\left(\mathbf{k}\right)-\tilde{\Pi}_{ab}^{(\mathrm{L})}\left(\mathbf{k}\right) \tag{2.2.17}$$

$$=\frac{\frac{\omega^2}{c^2}\delta_{ab}-k_ak_b}{|\mathbf{k}|^2-\frac{\omega^2}{c^2}}. \tag{2.2.18}$$

Equation (2.2.14) determines the total local electric field exactly and constitutes the starting point for the investigation of electromagnetic wave propagation in as well as the optical properties of arbitrary media. What kind of material is dealt with, say insulators, semiconductors, conductors or even superconductors, irrespective of their state of aggregation, solely depends on the model of the material that is incorporated into the induced current density $\mathbf{j}_{\mathrm{ind}}\left(\mathbf{r},\omega\right)$.

In the next chapter, a material model for crystalline dielectrics is proposed, that allows to solve (2.2.14) analytically for $E_a\left(\mathbf{r},\omega\right)$ by means of a special orthonormal and complete system of Bloch functions[12]. Once the propagable modes of the local field have been identified with the eigenmodes of the crystalline dielectric, $E_a\left(\mathbf{r},\omega\right)$ will be discussed extensively, where special attention is paid with respect to its longitudinal (non-radiative) and transverse (radiative) components.

[11] The formal structure of the local electric field's integral representation (2.2.14) may remind on the solution of the vector wave equation for the electric field by means of a dyadic Green function. Indeed, there is a close relationship between that dyadic Green function and the electromagnetic kernel given by (2.2.15), as is shown in appendix C.3.

[12] Both, the material model as well as the function system have been established by Prof. N. Schopohl [23, 24].

Chapter 3

The local electromagnetic field in crystalline dielectrics

To investigate the local electromagnetic field in as well as the optical properties of crystalline dielectrics, an appropriate material model is initially established concerning the induced current density. Starting from a phenomenological model of polarizable atoms or ions arranged in a three-dimensional (crystal) lattice, the integral equation (2.2.14) determining the local electric field is specified first. Then, by expanding the local electric field with respect to a newly discovered complete and orthonormal system of non-standard Bloch functions, this integral equation is solved analytically. Driven by the question, which modes of the local electromagnetic radiation field are capable to propagate within dielectric crystals, the concept of the photonic band structure is elaborated in detail. In particular this includes the impact of radiation damping as well as that of an additionally applied static magnetic induction field on the photonic bands. Based on these findings, the local electric field in crystalline dielectrics is discussed, where special attention is paid to its radiative (transverse) and non-radiative (longitudinal) contributions.

3.1 Model of light-matter interaction

Initially, consider again the geometry shown in figure 2.2.1, where within a fixed inertial frame an externally controlled and a priori known current source as well as the probe under investigation, both at rest in that frame, occupy volumes Ω_S and Ω_P, respectively. The probe is assumed to be a charge-neutral, non-polar dielectric material with crystalline order, so that in equilibrium each individual constituent (e.g. an atom or ion) comprised by the crystal is located at a site $\mathbf{R}^{(j)} = \mathbf{R} + \eta^{(j)}$, where $\mathbf{R} \in \Lambda$ denotes a lattice vector (in real space) of a Bravais lattice Λ and $\eta^{(j)} \in C_\Lambda$, with $j \in \{1,2,\ldots,M\}$, indicates the position of the j^{th}-constituent inside the Wigner-Seitz cell C_Λ. Actually, the probe volume Ω_P will be of finite size, so that it can be thought of to be filled by translating a finite number N_P of Wigner-Seitz

cells C_Λ with volume $|C_\Lambda|$ by lattice vectors $\mathbf{R} \in \Lambda_\mathrm{P}$, where $\Lambda_\mathrm{P} \subseteq \Lambda$ denotes the finite, with the material probe filled subset of the infinitely extended Bravais lattice Λ.

A full microscopic theory of the interaction of such a crystalline dielectric with an electromagnetic radiation field would require the consideration of a Hamiltonian that includes the coupling of all charged particles, i.e. the (atomic or ionic) nuclei as well as the electrons, to the electromagnetic potentials by taking into account the laws of quantum statistical physics and (low energy) quantum electrodynamics [2]. Because this is a formidable task, in the remainder of this work a phenomenological model of light-matter interaction is adopted, relying on the empirical knowledge, that matter is stable, i.e. in absence of any external fields, the dielectric crystal remains in its most favorable energetic state. But, when an externally applied (not too strong) electromagnetic field $\bar{\mathbf{E}}_\mathrm{ext}(\mathbf{r},t)$ irradiates the crystal, its prior most favorable energetic state is disturbed due to the change of the local electric field $\bar{\mathbf{E}}(\mathbf{r},t)$, and a small additional force is exerted onto each charge carrier within the crystal.

Regarding each constituent (i.e. atom or ion) of the crystal individually, the positively charged nucleus and its associated bound electrons are pulled apart in opposite directions by that additional force, resulting in a small displacement of the barycenters of the positive and negative charge distributions within the constituent, while the position of the constituent's center of mass remains unchanged. As the positively charged nucleus is much heavier than the multitude of its associated bound electrons, the resulting shift of its barycenter is tiny compared to the shift experienced by the barycenter of the bound electrons. Consequently, each individual constituent acquires an *induced* electric dipole moment[1] proportional to the *local* electric field $\bar{\mathbf{E}}(\mathbf{r},t)$ as retarded response to the externally applied field $\bar{\mathbf{E}}_\mathrm{ext}(\mathbf{r},t)$. This is Lorentz's basic idea of the effect of *induced electronic polarization*, who described the induced electric dipole moment of electrons that are bound to a heavy immobile nucleus on the basis of a classical harmonic oscillator model with the local electric field $\bar{\mathbf{E}}(\mathbf{r},t)$ as a drive (see e.g. [3]). As a result, the proportionality factor between the induced electric dipole moment and the local electric field for the j^th-constituent inside the Wigner-Seitz cell C_Λ is described by the cartesian components of the 3×3 *electronic* polarizability tensor $\alpha_{ab}^{(\mathrm{el})}\left(\eta^{(j)},\omega\right)$, where $a,b \in \{1,2,3\}$. Provided the electronic polarizability is isotropic, $\alpha_{ab}^{(\mathrm{el})}\left(\eta^{(j)},\omega\right)$ possesses the well-known functional frequency dependence [2]

$$\alpha_{ab}^{(\mathrm{el})}\left(\eta^{(j)},\omega\right) = \frac{\alpha_0^{(j)}}{1-\left(\frac{\omega+\frac{i}{2}\gamma^{(j)}}{\omega_0^{(j)}}\right)^2}\delta_{ab} \ \text{(isotropic)}. \tag{3.1.1}$$

Here $\alpha_0^{(j)}$ and $\omega_0^{(j)}$ represent the static electronic polarizability or the resonance frequency of an elec-

[1] Notice that once the frequency of the externally applied (disturbing) field becomes high enough so that field strength can no longer be taken as constant on the atomic length scale, the rather simple dipole interaction model described in this section has to be supplemented by electric quadrupole as well as magnetic dipole interactions, where the last two are of comparable strength and therefore have to be treated on equal footing [25].

[2] A quantum mechanical justification of this successful but rather simple model proposed by Lorentz in terms of first-order time-dependent perturbation theory as well as its discussion is given by Prof. N. Schopohl in [24] as well as in the supplementary material to [23].

tronic transition within the j^{th}-constituent, each treated as a fitting parameter. Furthermore, $\gamma^{(j)}$ denotes a small damping parameter originating from spontaneous emission, where it is assumed that $\gamma^{(j)} \to 0^+$, unless ω approaches the transition frequency $\omega_0^{(j)}$. Notice that when the crystal is additionally exposed to rather strong (quasi-) static electric or magnetic induction fields $\mathbf{E}^{(0)}$ or $\mathbf{B}^{(0)}$, this will directly affect the electronic polarizability tensor. In the latter case, the off-diagonal elements of $\alpha_{ab}^{(\text{el})}\left(\eta^{(j)},\omega;\mathbf{B}^{(0)}\right)$ give rise in first order in $\mathbf{B}^{(0)}$ to the well-known Faraday effect [26].

In real crystalline materials, the Wigner-Seitz cell C_Λ usually contains more than a single atom or ion, so that $M \geq 2$. In the case of ionic crystals like e.g. RbCl, SiO_2 or $CaCO_3$, the charge neutral Wigner-Seitz cell C_Λ comprises various positively and negatively charged ions located at positions $\eta^{(j)}$ with $j \in \{1,2,\ldots,M\}$. Of course, under the influence of an externally applied electromagnetic field $\bar{\mathbf{E}}_{\text{ext}}(\mathbf{r},t)$, the local field within the crystal changes and an additional force is exerted onto each ion inside the crystal. This results in a displacement of all ions from the equilibrium positions they hold in the absence of $\bar{\mathbf{E}}_{\text{ext}}(\mathbf{r},t)$, so that their rearrangement inside C_Λ is initiated. Consequently, oppositely charged ions located at different sites $\eta^{(j)}$ and $\eta^{(j')}$ with $j,j' \in \{1,2,\ldots,M\}$ and $j \neq j'$ may contribute to the total polarization of the crystal due to their relative displacement, which is induced by the change of the local electric field $\bar{\mathbf{E}}(\mathbf{r},t)$ due to $\bar{\mathbf{E}}_{\text{ext}}(\mathbf{r},t)$, an effect known as *ionic displacement* polarizability. Obviously, this effect is related to lattice vibrations whose frequencies ω_{ph} are typically of the order $10^{12}-10^{13}s^{-1}$ [3], so that it will only be noticed for electromagnetic radiation of frequencies ω that correspond to the infrared spectral region and below, because the "heavy" ions are not able to respond to radiation with frequencies $\omega \gg \omega_{\text{ph}}$ due to their relatively large moment of inertia. Thus, when ω corresponds to the visible regime (i.e. $\omega \sim 10^{15}s^{-1}$) and above, ionic displacement polarizability can be neglected confidently. Though not derived from a microscopic theory, the Lorentz oscillator also proves useful for modeling the cartesian components of the 3×3 *ionic displacement* polarizability tensor $\alpha_{ab}^{(\text{ion})}\left(\eta^{(j)},\eta^{(j')},\omega\right)$ with $a,b \in \{1,2,3\}$, when two oppositely charged ions located at $\eta^{(j)}$ and $\eta^{(j')}$ inside the Wigner-Seitz cell are considered[3]. In case the ionic displacement polarizability is isotropic, $\alpha_{ab}^{(\text{ion})}\left(\eta^{(j)},\eta^{(j')},\omega\right)$ then assumes the guise

$$\alpha_{ab}^{(\text{ion})}\left(\eta^{(j)},\eta^{(j')},\omega\right) = \frac{\alpha_0^{(j,j')}}{1-\left(\frac{\omega+\frac{i}{2}\gamma^{(j,j')}}{\omega_0^{(j,j')}}\right)^2}\delta_{ab} \text{ (isotropic)}, \tag{3.1.2}$$

where $\alpha_0^{(j,j')}$ as well as $\omega_0^{(j,j')}$ constitute fitting parameters that represent the static ionic displacement polarizability of the ion pair j and j' as well as the resonance frequency of their associated vibration. $\gamma^{(j,j')}$ indicates a small damping term[4], that only becomes relevant when ω approaches $\omega_0^{(j,j')}$. It should be emphasized, that the distinction between electronic and ionic displacement polarizability as outlined

[3]For instance, see the calculated chromatic dispersion of the index of refraction $n(\omega)$ for CsI and RbCl in figure 4.4.3 (a) and (b) with the parameters taken from table 4.4.2.

[4]It should be pointed out, that the damping term $\gamma^{(j,j')}$ is *not* related to spontaneous emission, contrary to $\gamma^{(j)}$. Instead, it subsumes all relevant physical processes in crystalline dielectrics that cause a damping of lattice vibrations such as electromagnetic interactions, scattering processes et cetera.

above is only reasonable, if the time scales associated with both effects are well separable, i.e. if $\max_{j\neq j'}\left(\omega_0^{(j,j')}\right) \ll \min_j\left(\omega_0^{(j)}\right)$ holds for $j,j' \in \{1,2,\ldots,M\}$.

As indicated in section 2.2, the local electric field within arbitrary materials can be calculated on the basis of equation (2.2.14), provided an appropriate model for the material under investigation can be incorporated into the induced current density. Following the outline given by Keldysh [2], there is *no* physical justification for the decomposition of the induced current density $\bar{\mathbf{j}}_{\text{ind}}(\mathbf{r},t)$ into polarization or magnetization currents as response to high frequency electromagnetic fields. In particular, in the optical regime and beyond, there is *no* qualitative criterion for such a distinction. Therefore, $\bar{\mathbf{j}}_{\text{ind}}(\mathbf{r},t)$ is assumed to consist of polarization currents alone[5], so that it is determined by the time derivative of the microscopic polarization $\bar{\mathbf{P}}(\mathbf{r},t)$. For time harmonic signals there directly follows

$$\mathbf{j}_{\text{ind}}(\mathbf{r},\omega) = -i\omega\mathbf{P}(\mathbf{r},\omega). \tag{3.1.3}$$

The integral equation (2.2.14) determining the cartesian components of the local electric field therefore becomes

$$E_a(\mathbf{r},\omega) = E_{\text{ext},a}(\mathbf{r},\omega) + \frac{1}{\varepsilon_0}\sum_{b=1}^{3}\int_{\mathbb{R}^3} d^3r'\,\mathscr{G}_{ab}\left(\mathbf{r}-\mathbf{r}',\omega\right)P_b\left(\mathbf{r}',\omega\right), \tag{3.1.4}$$

where all the information about the material is contained in $\mathbf{P}(\mathbf{r},\omega)$. As elucidated previously, the (microscopic) polarization experienced by a charge-neutral, non-polar dielectric crystal is related to the local electric field as well as to the individual electronic and ionic displacement polarizabilities of each of the material's constituents. Thus, $\mathbf{P}(\mathbf{r},\omega)$ and $\mathbf{E}(\mathbf{r},\omega)$ are related by a dielectric susceptibility kernel $\chi_{ab}(\mathbf{r},\mathbf{r}',\omega)$ according to[6]

$$P_a(\mathbf{r},\omega) = \varepsilon_0\sum_{b=1}^{3}\int_{\mathbb{R}^3} d^3r'\,\chi_{ab}\left(\mathbf{r},\mathbf{r}',\omega\right)E_b\left(\mathbf{r}',\omega\right), \tag{3.1.5}$$

where the integration may be carried out about $\mathbb{R}^3$ instead of the probe volume Ω_{P}, because $\chi_{ab}(\mathbf{r},\mathbf{r}',\omega)$ is a material quantity and can only contribute to the polarization when $\mathbf{r},\mathbf{r}' \in \Omega_{\text{P}}$. A simple *phenomeno-*

[5] For a discussion of the special case of a purely magnetizable crystalline material, where $\bar{\mathbf{j}}_{\text{ind}}(\mathbf{r},t)$ originates from magnetization currents formed by induced infinitesimal current loops, where the latter are equivalent to point-like magnetic dipoles, see appendix I.

[6] Note, that (3.1.5) must *not* be understood as a linear response theory in the sense of Kubo (for this, see e.g. [27]), which would require to calculate the microscopic polarization $P_a(\mathbf{r},\omega)$ for $\mathbf{r}\in\Omega_{\text{P}}$ in response to the (perturbing) external electric field $E_{\text{ext},b}(\mathbf{r}',\omega)$, where their connection would be established by the response kernel $\chi_{ab}^{(\text{ext})}(\mathbf{r},\mathbf{r}',\omega)$ via

$$P_a(\mathbf{r},\omega) = \varepsilon_0\sum_{b=1}^{3}\int_{\Omega_{\text{P}}} d^3r'\,\chi_{ab}^{(\text{ext})}\left(\mathbf{r},\mathbf{r}',\omega\right)E_{\text{ext},b}\left(\mathbf{r}',\omega\right).$$

Even if the knowledge of $\chi_{ab}^{(\text{ext})}(\mathbf{r},\mathbf{r}',\omega)$ from a full microscopic theory with Kubo's formula is desirable, its calculation for real materials constitutes a formidable task. Hence, this problem is circumvented in this work by invoking equation (3.1.5), where a phenomenological model for the dielectric susceptibility kernel $\chi_{ab}(\mathbf{r},\mathbf{r}',\omega)$ is applied (see (3.1.6)), that turns out to be suitable to describe the propagation of light in as well as the optical properties of dielectric crystals in sufficient detail. Nevertheless, there is a close connection between $\chi_{ab}^{(\text{ext})}(\mathbf{r},\mathbf{r}',\omega)$ and $\chi_{ab}(\mathbf{r},\mathbf{r}',\omega)$, as is shown by Prof. N. Schopohl in the supplementary material of [23].

logical model for the dielectric susceptibility kernel, taking into account the afore depicted polarization processes hold by dielectric crystals, proves to be [23, 24]

$$\chi_{ab}\left(\mathbf{r},\mathbf{r}',\omega\right)=\frac{1}{\varepsilon_0}\sum_{\mathbf{R}\in\Lambda_{\mathrm{P}}}\sum_{j,j'=1}^{M}\alpha_{ab}\left(\eta^{(j)},\eta^{(j')},\omega\right)\delta\left(\mathbf{r}-\mathbf{R}-\eta^{(j)}\right)\delta\left(\mathbf{r}'-\mathbf{R}-\eta^{(j')}\right) \tag{3.1.6}$$

together with

$$\alpha_{ab}\left(\eta^{(j)},\eta^{(j')},\omega\right)=\delta_{jj'}\alpha_{ab}^{(\mathrm{el})}\left(\eta^{(j)},\omega\right)+\left(1-\delta_{jj'}\right)\alpha_{ab}^{(\mathrm{ion})}\left(\eta^{(j)},\eta^{(j')},\omega\right), \tag{3.1.7}$$

where in (3.1.6) first the contributions from the atoms located at positions $\eta^{(j)}$ and $\eta^{(j')}$ within the Wigner-Seitz cell C_Λ arranged around the lattice site $\mathbf{R}=\mathbf{0}$ are gathered, followed by a summation over all cells filling the probe volume Ω_{P}. Obviously, the diagonal terms $j=j'$ in (3.1.7) correspond to the effect of induced electronic polarization, that affects single atoms or ions positioned at $\eta^{(j)}$, while the off-diagonal terms $j\neq j'$ may be attributed to the ionic displacement polarizability, which concerns oppositely charged ions located at $\eta^{(j)}$ and $\eta^{(j')}$ within C_Λ. Because of its block-matrix structure that enters forthcoming calculations, the proposed model for $\alpha_{ab}\left(\eta^{(j)},\eta^{(j')},\omega\right)$ should not to be confused with just adding up electronic and ionic displacement polarizabilities, especially as there is no justification for such an oversimplification [3]. Additionally, it should be emphasized that in the limit of an infinitely extended crystal, i.e. if $\Lambda_{\mathrm{P}}=\Lambda$, the dielectric susceptibility kernel (3.1.6) is invariant under a translation by an arbitrary lattice vector $\mathbf{R}'\in\Lambda$ (compare with von Laue [28])

$$\chi_{ab}\left(\mathbf{r}+\mathbf{R}',\mathbf{r}'+\mathbf{R}',\omega\right)=\chi_{ab}\left(\mathbf{r},\mathbf{r}',\omega\right). \tag{3.1.8}$$

Finally, the integral equation determining the local electric field inside crystalline dielectrics emerges by utilizing (3.1.4) in conjunction with the polarization model (3.1.5) according to

$$\begin{aligned}E_a\left(\mathbf{r},\omega\right)&=E_{\mathrm{ext},a}\left(\mathbf{r},\omega\right)+\sum_{b=1}^{3}\int_{\mathbb{R}^3}d^3r'\left[\sum_{c=1}^{3}\int_{\mathbb{R}^3}d^3r''\,\mathscr{G}_{ac}\left(\mathbf{r}-\mathbf{r}'',\omega\right)\chi_{cb}\left(\mathbf{r}'',\mathbf{r}',\omega\right)\right]E_b\left(\mathbf{r}',\omega\right)\\&\equiv E_{\mathrm{ext},a}\left(\mathbf{r},\omega\right)+\sum_{b=1}^{3}\int_{\mathbb{R}^3}d^3r'\,\left[\mathscr{G}\circ\chi\right]_{ab}\left(\mathbf{r},\mathbf{r}',\omega\right)E_b\left(\mathbf{r}',\omega\right),\end{aligned} \tag{3.1.9}$$

where in the second line the abbreviation

$$\left[\mathscr{G}\circ\chi\right]_{ab}\left(\mathbf{r},\mathbf{r}',\omega\right)=\sum_{c=1}^{3}\int_{\mathbb{R}^3}d^3r''\,\mathscr{G}_{ac}\left(\mathbf{r}-\mathbf{r}'',\omega\right)\chi_{cb}\left(\mathbf{r}'',\mathbf{r}',\omega\right) \tag{3.1.10}$$

has been introduced.

In this section, the integral equation (3.1.9) determining the local electric field in crystalline dielectrics has been deduced by invoking the phenomenological model (3.1.6) for the dielectric susceptibility kernel $\chi_{ab}\left(\mathbf{r},\mathbf{r}',\omega\right)$, where the latter includes the effects of electronic and ionic displacement polarization

as well. Consequently, the next section is about solving this integral equation. As will be shown, (3.1.9) can be solved exactly, when the local electric field is expanded in terms of a non-standard system of Bloch functions, that has been discovered by Prof. N. Schopohl [24].

3.2 Solution of the local electric field integral equation

Because of the lattice periodicity of the dielectric susceptibility tensor $\chi_{ab}(\mathbf{r},\mathbf{r}',\omega)$, as indicated by (3.1.8), it seems natural to approach the integral equation (3.1.9) by means of Bloch's theorem[7], i.e. to expand the local electric field in terms of a complete (and orthonormal) set of eigenfunctions of the translation operator $\hat{T}_{\mathbf{R}}$, that shifts the argument of an arbitrary function $f(\mathbf{r})$ by a lattice vector $\mathbf{R}\in\Lambda$ according to

$$\hat{T}_{\mathbf{R}} f(\mathbf{r}) = f(\mathbf{r}+\mathbf{R}). \tag{3.2.1}$$

Obviously, an eigenfunction $\psi_{\mathbf{k}}(\mathbf{r})$ of $\hat{T}_{\mathbf{R}}$ can always be written as

$$\psi_{\mathbf{k}}(\mathbf{r}) = e^{i\mathbf{k}\cdot\mathbf{r}} u(\mathbf{r}), \tag{3.2.2}$$

provided that

$$u(\mathbf{r}+\mathbf{R}) = u(\mathbf{r}). \tag{3.2.3}$$

The associated eigenvalue is then given by $e^{i\mathbf{k}\cdot\mathbf{R}}$. Here $\mathbf{k}\in C_{\Lambda^{-1}}$ is located inside the first Brillouin zone $C_{\Lambda^{-1}}$, which represents the analogue to the Wigner-Seitz cell C_{Λ} in the reciprocal lattice Λ^{-1}, the latter being generated by all reciprocal lattice vectors $\mathbf{G}\in\Lambda^{-1}$ that obey to the condition $e^{i\mathbf{G}\cdot\mathbf{R}}=1$ for all $\mathbf{R}\in\Lambda$.

Due to the required lattice periodicity (3.2.3), the function $u(\mathbf{r})$ to be determined is routinely expanded in terms of a complete and orthonormal set of plane waves via

$$u(\mathbf{r}) = \sum_{\mathbf{G}\in\Lambda^{-1}} u_{\mathbf{G}} e^{i\mathbf{G}\cdot\mathbf{r}}, \tag{3.2.4}$$

where the $u_{\mathbf{G}}$ denote the Fourier coefficients to be identified. The drawback of this expansion, when deployed to the local electric field determined by the integral equation (3.1.9), manifests itself in the fact, that the kernel $[\mathscr{G}\circ\chi]_{ab}(\mathbf{r},\mathbf{r}',\omega)$ basically turns out to be a huge completely filled matrix, whose components are labeled by $\mathbf{k},\mathbf{k}'\in C_{\Lambda^{-1}}$ and an infinite set of reciprocal lattice vectors $\mathbf{G},\mathbf{G}'\in\Lambda^{-1}$. Hence, this ansatz would necessitate a big effort of numerical calculations[8].

[7] Let $\hat{H}$ denote the Hamiltonian for a single particle moving in a lattice periodic potential $V(\mathbf{r}+\mathbf{R})=V(\mathbf{r})$ for $\mathbf{R}\in\Lambda$. Then $\left[\hat{H},\hat{T}_{\mathbf{R}}\right]=\hat{0}$, so that a set of functions $\{\psi_{\mathbf{k}}(\mathbf{r})\}_{\mathbf{k}\in C_{\Lambda^{-1}}}$ can be found, which constitute simultaneously eigenfunctions of $\hat{H}$ and the shift operator $\hat{T}_{\mathbf{R}}$ defined by equation (3.2.1). Here $C_{\Lambda^{-1}}$ denotes the first Brillouin zone. Accordingly, such an eigenfunction can always be written as $\psi_{\mathbf{k}}(\mathbf{r})=e^{i\mathbf{k}\cdot\mathbf{r}}u(\mathbf{r})$, provided that $u(\mathbf{r}+\mathbf{R})=u(\mathbf{r})$. For details regarding Bloch's theorem and its proove, see e.g. [3].

[8] For a rigorous theory of the microscopic electrodynamic response kernel of crystalline systems that rests on its matrix

For this reason, an alternative to the plane wave expansion (3.2.4) is desirable, that allows to represent the kernel $[\mathscr{G} \circ \chi]_{ab}(\mathbf{r}, \mathbf{r}', \omega)$ in terms of a small sparse matrix. Noticing that any lattice periodic function $u(\mathbf{r})$ may be generated from a function $u^{(0)}(\mathbf{r})$, that coincides with $u(\mathbf{r})$ inside the Wigner-Seitz cell C_Λ and identically vanishes outside, $u(\mathbf{r})$ can be represented by

$$u(\mathbf{r}) = \sum_{\mathbf{R}' \in \Lambda} u^{(0)}(\mathbf{r} + \mathbf{R}'), \tag{3.2.5}$$

where

$$u^{(0)}(\mathbf{r}) = \begin{cases} u(\mathbf{r}) & \mathbf{r} \in C_\Lambda \\ 0 & \mathbf{r} \notin C_\Lambda \end{cases}. \tag{3.2.6}$$

The ensuing identification of $u^{(0)}(\mathbf{r})$ as the position space representation of a state $|\, u^{(0)}\rangle$, i.e. $u^{(0)}(\mathbf{r}) = \langle \mathbf{r} |\, u^{(0)}\rangle$, suggests the representation of the state $|\, u^{(0)}\rangle$ inside the Wigner-Seitz cell C_Λ in terms of the complete and orthonormal set of continuous position eigenstates $\{|\, \mathbf{s}\rangle\}_{\mathbf{s} \in C_\Lambda}$ of the position operator $\hat{\mathbf{x}}$, that obeys to the well-known relations

$$\begin{aligned} \hat{\mathbf{x}} |\, \mathbf{s}\rangle &= \mathbf{s} |\, \mathbf{s}\rangle \\ \int_{C_\Lambda} d^3 s \, |\, \mathbf{s}\rangle\langle \mathbf{s} \,| &= \hat{1} \\ \langle \mathbf{s}' |\, \mathbf{s}\rangle &= \delta(\mathbf{s} - \mathbf{s}'). \end{aligned} \tag{3.2.7}$$

Consequently, for $\mathbf{s} \in C_\Lambda$ the state $|\, u^{(0)}\rangle$ can be represented by

$$|\, u^{(0)}\rangle = \int_{C_\Lambda} d^3 s \, u^{(0)}(\mathbf{s}) \,|\, \mathbf{s}\rangle. \tag{3.2.8}$$

Motivated by what has been said, there emerges a complete and orthonormal set $\{w(\mathbf{r}; \mathbf{s}, \mathbf{k})\}_{\mathbf{s} \in C_\Lambda, \mathbf{k} \in C_{\Lambda^{-1}}}$ of non-standard Bloch-eigenfunctions[9] of the translation operator $\hat{T}_\mathbf{R}$ according to

$$\begin{aligned} w(\mathbf{r}; \mathbf{s}, \mathbf{k}) &= \frac{e^{i\mathbf{k}\cdot\mathbf{r}}}{\sqrt{N_\mathrm{P}}} \sum_{\mathbf{R}' \in \Lambda} \langle \mathbf{s} + \mathbf{R}' |\, \mathbf{r}\rangle \\ &= \frac{e^{i\mathbf{k}\cdot\mathbf{r}}}{\sqrt{N_\mathrm{P}}} \sum_{\mathbf{R}' \in \Lambda} \delta(\mathbf{r} - \mathbf{s} - \mathbf{R}'), \end{aligned} \tag{3.2.9}$$

which are labeled by a continuous position vector $\mathbf{s} \in C_\Lambda$ and a discrete wave vector $\mathbf{k} \in C_{\Lambda^{-1}}$, where the latter ranges in accordance with a Born-von Karman boundary condition (for details see [3]) through a number of N_P values inside the first Brillouin zone[10]. In contrast to the unbounded label $\mathbf{G} \in \Lambda^{-1}$

representation with respect to a basis of plane waves, inclusive of a profound analysis of the associated dielectric function, see Dolgov and Maksimov [29].

[9] The system of functions $\{w(\mathbf{r}; \mathbf{s}, \mathbf{k})\}_{\mathbf{s} \in C_\Lambda, \mathbf{k} \in C_{\Lambda^{-1}}}$ was established by Prof. N. Schopohl in [23, 24].

[10] For a proof regarding the completeness and orthonormality of the set of eigenfunctions $\{w(\mathbf{r}; \mathbf{s}, \mathbf{k})\}_{\mathbf{s} \in C_\Lambda, \mathbf{k} \in C_{\Lambda^{-1}}}$ of the translation operator $\hat{T}_\mathbf{R}$, see appendix D.

appearing in the plane wave expansion (3.2.4), the labels $\mathbf{s} \in C_\Lambda$ and $\mathbf{k} \in C_{\Lambda^{-1}}$ of the non-standard Bloch functions (3.2.9) are restricted to compact domains. As a consequence, the kernel $[\mathscr{G} \circ \chi]_{ab}(\mathbf{r}, \mathbf{r}', \omega)$ can be represented in terms of a small sparse matrix instead of a huge completely filled matrix, when it is expanded with respect to $\{w(\mathbf{r};\mathbf{s},\mathbf{k})\}_{\mathbf{s}\in C_\Lambda, \mathbf{k}\in C_{\Lambda^{-1}}}$ instead of $\left\{e^{i\mathbf{G}\cdot\mathbf{r}}\right\}_{\mathbf{G}\in\Lambda^{-1}}$.

In what follows (compare with [23]), the integral equation (3.1.9) determining the local electric field in crystalline dielectrics will be solved exactly, by expanding the local field with respect to the non-standard Bloch-eigenfunctions (3.2.9) of the translation operator $\hat{T}_{\mathbf{R}}$. For this purpose, the a$^{\text{th}}$ cartesian component with $a \in \{1,2,3\}$ of the local electric field $E_a(\mathbf{r}, \omega)$ for $\mathbf{r} \in \Omega_{\text{P}}$ is written as

$$E_a(\mathbf{r}, \omega) = \sum_{\mathbf{k}\in C_{\Lambda^{-1}}} \int_{C_\Lambda} d^3s\, w(\mathbf{r};\mathbf{s},\mathbf{k})\, \mathfrak{e}_a(\mathbf{s},\mathbf{k},\omega), \tag{3.2.10}$$

where the expansion coefficients to be determined $\mathfrak{e}_a(\mathbf{s},\mathbf{k},\omega)$ are defined by

$$\mathfrak{e}_a(\mathbf{s},\mathbf{k},\omega) = \int_{\Omega_{\text{P}}} d^3r\, w^\dagger(\mathbf{r};\mathbf{s},\mathbf{k})\, E_a(\mathbf{r},\omega). \tag{3.2.11}$$

Analogously, the expansion coefficients $\mathfrak{e}_{\text{ext},a}(\mathbf{s},\mathbf{k},\omega)$ of the externally applied electric field $E_{\text{ext},a}(\mathbf{r},\omega)$ are given by

$$\mathfrak{e}_{\text{ext},a}(\mathbf{s},\mathbf{k},\omega) = \int_{\Omega_{\text{P}}} d^3r\, w^\dagger(\mathbf{r};\mathbf{s},\mathbf{k})\, E_{\text{ext},a}(\mathbf{r},\omega), \tag{3.2.12}$$

so that insertion of (3.1.9) into (3.2.11) directly yields

$$\mathfrak{e}_a(\mathbf{s},\mathbf{k},\omega) = \mathfrak{e}_{\text{ext},a}(\mathbf{s},\mathbf{k},\omega) + \sum_{b=1}^{3} \int_{\Omega_{\text{P}}} d^3r \int_{\mathbb{R}^3} d^3r'\, w^\dagger(\mathbf{r};\mathbf{s},\mathbf{k})\, [\mathscr{G}\circ\chi]_{ab}(\mathbf{r},\mathbf{r}',\omega)\, E_b(\mathbf{r}',\omega). \tag{3.2.13}$$

By subsequent elimination of $E_b(\mathbf{r}', \omega)$ in terms of (3.2.10),

$$\begin{aligned}\mathfrak{e}_a(\mathbf{s},\mathbf{k},\omega) =& \mathfrak{e}_{\text{ext},a}(\mathbf{s},\mathbf{k},\omega) + \sum_{b=1}^{3} \sum_{\mathbf{k}'\in C_{\Lambda^{-1}}} \\ &\cdot \int_{C_\Lambda} d^3s' \int_{\Omega_{\text{P}}} d^3r \int_{\mathbb{R}^3} d^3r'\, w^\dagger(\mathbf{r};\mathbf{s},\mathbf{k})\, [\mathscr{G}\circ\chi]_{ab}(\mathbf{r},\mathbf{r}',\omega)\, w(\mathbf{r}';\mathbf{s}',\mathbf{k}')\, \mathfrak{e}_b(\mathbf{s}',\mathbf{k}',\omega)\end{aligned} \tag{3.2.14}$$

is readily obtained, which constitutes a system of equations that determines the expansion coefficients $\mathfrak{e}_a(\mathbf{s},\mathbf{k},\omega)$. Obviously,

$$\langle \mathbf{s},\mathbf{k}\,|\,[\mathscr{G}\circ\chi]_{ab}\,|\,\mathbf{s}',\mathbf{k}'\rangle \equiv \int_{\Omega_{\text{P}}} d^3r \int_{\mathbb{R}^3} d^3r'\, w^\dagger(\mathbf{r};\mathbf{s},\mathbf{k})\, [\mathscr{G}\circ\chi]_{ab}(\mathbf{r},\mathbf{r}',\omega)\, w(\mathbf{r}';\mathbf{s}',\mathbf{k}') \tag{3.2.15}$$

defines the matrix elements of the kernel $[\mathscr{G}\circ\chi]_{ab}$ with respect to the basis $\{w(\mathbf{r};\mathbf{s},\mathbf{k})\}_{\mathbf{s}\in C_\Lambda, \mathbf{k}\in C_{\Lambda^{-1}}}$, so

that (3.2.14) can be abbreviated by

$$\mathfrak{e}_a(\mathbf{s},\mathbf{k},\omega) = \mathfrak{e}_{\mathrm{ext},a}(\mathbf{s},\mathbf{k},\omega) + \sum_{b=1}^{3}\sum_{\mathbf{k}'\in C_{\Lambda^{-1}}}\int_{C_\Lambda} d^3s'\,\langle \mathbf{s},\mathbf{k}|[\mathscr{G}\circ\chi]_{ab}|\mathbf{s}',\mathbf{k}'\rangle \mathfrak{e}_b\left(\mathbf{s}',\mathbf{k}',\omega\right). \tag{3.2.16}$$

Assuming from now on the crystal to be infinitely extended[11], i.e. $N_\mathrm{P}\to\infty$ and $\Lambda_\mathrm{P}=\Lambda$, the sum over wave vectors $\mathbf{k}'\in C_{\Lambda^{-1}}$ in (3.2.16) can be replaced by an integral according to

$$\sum_{\mathbf{k}'\in C_{\Lambda^{-1}}} \longrightarrow \frac{|\Omega_\mathrm{P}|}{(2\pi)^3}\int_{C_{\Lambda^{-1}}} d^3k', \tag{3.2.17}$$

so that $\langle \mathbf{s},\mathbf{k}|[\mathscr{G}\circ\chi]_{ab}|\mathbf{s}',\mathbf{k}'\rangle$ assumes the guise[12]

$$\begin{aligned}\langle \mathbf{s},\mathbf{k}|[\mathscr{G}\circ\chi]_{ab}|\mathbf{s}',\mathbf{k}'\rangle =& \frac{e^{-i\mathbf{k}\cdot\mathbf{s}}}{\varepsilon_0}\frac{(2\pi)^3}{|C_\Lambda|}\frac{1}{N_\mathrm{P}}\sum_{c=1}^{3}\sum_{j,j'=1}^{M}\sum_{\mathbf{R}'\in\Lambda}\\ &\cdot\mathscr{G}_{ac}\left(\mathbf{s}-\mathbf{R}'-\eta^{(j)},\omega\right)\alpha_{cb}\left(\eta^{(j)},\eta^{(j')},\omega\right)e^{i\mathbf{k}'\cdot(\mathbf{s}'+\mathbf{R}')}\delta\left(\mathbf{s}'-\eta^{(j')}\right)\delta\left(\mathbf{k}-\mathbf{k}'\right).\end{aligned} \tag{3.2.18}$$

The equation determining the expansion coefficients $\mathfrak{e}_a(\mathbf{s},\mathbf{k},\omega)$ now turns out to be algebraic and reads

$$\begin{aligned}\mathfrak{e}_a(\mathbf{s},\mathbf{k},\omega) =& \mathfrak{e}_{\mathrm{ext},a}(\mathbf{s},\mathbf{k},\omega) + \frac{e^{-i\mathbf{k}\cdot\mathbf{s}}}{\varepsilon_0}\sum_{b,c=1}^{3}\sum_{j,j'=1}^{M}\sum_{\mathbf{R}\in\Lambda}\\ &\cdot\mathscr{G}_{ab}\left(\mathbf{s}-\mathbf{R}-\eta^{(j)},\omega\right)\alpha_{bc}\left(\eta^{(j)},\eta^{(j')},\omega\right)e^{i\mathbf{k}\cdot\left(\eta^{(j')}+\mathbf{R}\right)}\mathfrak{e}_c\left(\eta^{(j')},\mathbf{k},\omega\right)\\ =& \mathfrak{e}_{\mathrm{ext},a}(\mathbf{s},\mathbf{k},\omega) + \frac{1}{\varepsilon_0}\sum_{b,c=1}^{3}\sum_{j,j'=1}^{M}\left[\zeta_\Lambda\left(\mathbf{s}-\eta^{(j)},\mathbf{k},\omega\right)\right]_{ab}\alpha_{bc}^{(j,j')}(\mathbf{k},\omega)\,\mathfrak{e}_c^{(j')}(\mathbf{k},\omega),\end{aligned} \tag{3.2.19}$$

where in the last line the abbreviation $\mathfrak{e}_c^{(j')}(\mathbf{k},\omega)\equiv\mathfrak{e}_c\left(\eta^{(j')},\mathbf{k},\omega\right)$ and the notations

$$\alpha_{bc}^{(j,j')}(\mathbf{k},\omega)\equiv e^{-i\mathbf{k}\cdot\eta^{(j)}}\alpha_{bc}\left(\eta^{(j)},\eta^{(j')},\omega\right)e^{i\mathbf{k}\cdot\eta^{(j')}} \tag{3.2.20}$$

as well as

$$[\zeta_\Lambda(\mathbf{s},\mathbf{k},\omega)]_{ab} = \begin{cases}\sum_{\mathbf{R}\in\Lambda}e^{-i\mathbf{k}\cdot(\mathbf{s}+\mathbf{R})}\mathscr{G}_{ab}(\mathbf{s}+\mathbf{R},\omega) & \text{if } \mathbf{s}\neq\mathbf{0}\\ \sum_{\mathbf{R}\in\Lambda\setminus\{\mathbf{0}\}}e^{-i\mathbf{k}\cdot\mathbf{R}}\mathscr{G}_{ab}(\mathbf{R},\omega) & \text{if } \mathbf{s}=\mathbf{0}\end{cases} \tag{3.2.21}$$

have been introduced[13]. Here, $[\zeta_\Lambda(\mathbf{s},\mathbf{k},\omega)]_{ab}$ with $a,b\in\{1,2,3\}$ denotes the cartesian components

[11] It should be emphasized, that any crystalline material of finite extent can always be described by means of an infinitely extended lattice Λ, provided a lattice site dependent, say electronic polarizability $\alpha_{ab}^{(\mathrm{el})}\left(\mathbf{R}+\eta^{(j)},\omega\right)$ is introduced, which vanishes if $\mathbf{R}\notin\Lambda_\mathrm{P}$.

[12] For a derivation of (3.2.18), see appendix E.1.

[13] The definition by cases of the lattice sum $[\zeta_\Lambda(\mathbf{s},\mathbf{k},\omega)]_{ab}$ in (3.2.21) avoids, that an atom gets polarized by its self-generated electromagnetic field in the case if $\mathbf{s}=\mathbf{0}$. This distinction between $\mathbf{s}\neq\mathbf{0}$ and $\mathbf{s}=\mathbf{0}$ will become relevant, when the

of a 3×3 matrix of *lattice sums*, whose evaluation[14] plays a central role in the calculation of the local electromagnetic field as well as that of the dielectric function, as will be seen later. Obviously, $\zeta_\Lambda(\mathbf{s},\mathbf{k},\omega)$ is invariant with respect to a translation by any lattice vector $\mathbf{R}' \in \Lambda$ if $\mathbf{s} \neq \mathbf{0}$, i.e.

$$\zeta_\Lambda\left(\mathbf{s}+\mathbf{R}',\mathbf{k},\omega\right) = \zeta_\Lambda(\mathbf{s},\mathbf{k},\omega)\,. \tag{3.2.22}$$

For this reason, $[\zeta_\Lambda(\mathbf{s},\mathbf{k},\omega)]_{ab}$ exhibits an alternative representation according to [15]

$$[\zeta_\Lambda(\mathbf{s},\mathbf{k},\omega)]_{ab} = \frac{1}{|C_\Lambda|}\sum_{\mathbf{G}\in\Lambda^{-1}} e^{i\mathbf{G}\cdot\mathbf{s}}\left(\frac{\omega^2}{c^2}\frac{1}{|\mathbf{k}+\mathbf{G}|^2-\frac{\omega^2}{c^2}}\tilde{\Pi}^{(\mathrm{T})}_{ab}(\mathbf{k}+\mathbf{G}) - \tilde{\Pi}^{(\mathrm{L})}_{ab}(\mathbf{k}+\mathbf{G})\right) \tag{3.2.23}$$

$$= \frac{1}{|C_\Lambda|}\sum_{\mathbf{G}\in\Lambda^{-1}} \tilde{\mathscr{G}}_{ab}(\mathbf{k}+\mathbf{G},\omega)\,e^{i\mathbf{G}\cdot\mathbf{s}}, \tag{3.2.24}$$

that will turn out to be valuable when identifying the longitudinal and transverse components of the local electric field. Particular attention should be paid to the definition by cases (3.2.21) of the lattice sum, as

$$\zeta^{(0)}_\Lambda(\mathbf{k},\omega) \equiv \zeta_\Lambda(\mathbf{0},\mathbf{k},\omega) \neq \lim_{|\mathbf{s}|\to 0}\zeta_\Lambda(\mathbf{s},\mathbf{k},\omega)\,. \tag{3.2.25}$$

Instead there holds

$$\left[\zeta^{(0)}_\Lambda(\mathbf{k},\omega)\right]_{ab} = \lim_{|\mathbf{s}|\to 0}\left([\zeta_\Lambda(\mathbf{s},\mathbf{k},\omega)]_{ab} - \mathscr{G}_{ab}(\mathbf{s},\omega)\right). \tag{3.2.26}$$

In the end, the expansion coefficients $\mathfrak{e}_a(\mathbf{s},\mathbf{k},\omega)$ at any point $\mathbf{s} \in C_\Lambda$ inside the Wigner-Seitz cell can be obtained from equation (3.2.19), provided that the expansion coefficients $\mathfrak{e}^{(j')}_c(\mathbf{k},\omega)$ are known at each atomic position $\eta^{(j')} \in C_\Lambda$ with $j' \in \{1,2,\ldots,M\}$. By successively taking the limit $\mathbf{s} \to \eta^{(j'')}$ for any $j'' \in \{1,2,\ldots,M\}$ in (3.2.19) and abbreviating $\mathfrak{e}^{(j'')}_{\mathrm{ext},a}(\mathbf{k},\omega) \equiv \mathfrak{e}_{\mathrm{ext},a}\left(\eta^{(j'')},\mathbf{k},\omega\right)$, a closed $3M \times 3M$ system of linear equations determining $\mathfrak{e}^{(j'')}_a(\mathbf{k},\omega)$ emerges according to

$$\mathfrak{e}^{(j'')}_a(\mathbf{k},\omega) = \mathfrak{e}^{(j'')}_{\mathrm{ext},a}(\mathbf{k},\omega) + \frac{1}{\varepsilon_0}\sum_{b,c=1}^{3}\sum_{j,j'=1}^{M}\left[\zeta_\Lambda\left(\eta^{(j'')}-\eta^{(j)},\mathbf{k},\omega\right)\right]_{ab}\alpha^{(j,j')}_{bc}(\mathbf{k},\omega)\,\mathfrak{e}^{(j')}_c(\mathbf{k},\omega)\,. \tag{3.2.27}$$

Here, the definition by cases of the lattice sum $\zeta_\Lambda(\mathbf{s},\mathbf{k},\omega)$ applies in (3.2.27), thus avoiding for $j'' = j$ the polarization of the respective atom by its self-generated electromagnetic field[16]. Introducing $\Gamma^{(j'',j')}_{ac}(\mathbf{k},\omega)$ and $\delta^{(j'',j')}_{ac}$ with $a,c \in \{1,2,3\}$ and $j',j'' \in \{1,2,\ldots,M\}$ via

$$\Gamma^{(j'',j')}_{ac}(\mathbf{k},\omega) = \frac{1}{\varepsilon_0}\sum_{b=1}^{3}\sum_{j=1}^{M}\left[\zeta_\Lambda\left(\eta^{(j'')}-\eta^{(j)},\mathbf{k},\omega\right)\right]_{ab}\alpha^{(j,j')}_{bc}(\mathbf{k},\omega) \tag{3.2.28}$$

---

expansion coefficients $\mathfrak{e}^{(j)}_a(\mathbf{k},\omega)$ are explicitly determined (see (3.2.27) and in particular appendix E.2).

[14] A fast and precise numerical method for the calculation of $\zeta_\Lambda(\mathbf{s},\mathbf{k},\omega)$ given by (3.2.21) in the sense of Ewald's summation technique [30–33] is presented in appendix F.2.

[15] For a derivation of (3.2.23) or (3.2.24) that requires $\mathbf{s} \neq \mathbf{0}$, see appendix F.1.

[16] A detailed derivation of (3.2.27), which highlights the significance of the definition by cases of the lattice sum $\zeta_\Lambda(\mathbf{s},\mathbf{k},\omega)$, is given in appendix E.2.

and

$$\delta_{ac}^{(j'',j')} = \delta_{j''j'}\delta_{ac}, \tag{3.2.29}$$

where both represent the components of their corresponding $3M \times 3M$ matrices, (3.2.27) can be easily cast into

$$\sum_{c=1}^{3}\sum_{j'=1}^{M}\left(\delta_{ac}^{(j'',j')} - \Gamma_{ac}^{(j'',j')}(\mathbf{k},\omega)\right)\mathfrak{e}_{c}^{(j')}(\mathbf{k},\omega) = \mathfrak{e}_{\mathrm{ext},a}^{(j'')}(\mathbf{k},\omega), \tag{3.2.30}$$

so that the explicit solution for the expansion coefficients $\mathfrak{e}_{c}^{(j')}(\mathbf{k},\omega)$ at the atomic positions reads

$$\mathfrak{e}_{c}^{(j')}(\mathbf{k},\omega) = \sum_{d=1}^{3}\sum_{j''=1}^{M}\left[(\delta - \Gamma(\mathbf{k},\omega))^{-1}\right]_{cd}^{(j'j'')}\mathfrak{e}_{\mathrm{ext},d}^{(j'')}(\mathbf{k},\omega). \tag{3.2.31}$$

Inserting (3.2.31) in (3.2.19) finally determines the expansion coefficients $\mathfrak{e}_a(\mathbf{s},\mathbf{k},\omega)$ for any $\mathbf{s} \in C_\Lambda$. Consequently, under the previously made assumption of an infinitely extended crystal, the expansion of the local electric field $E_a(\mathbf{r},\omega)$ in terms of the system of functions $\{w(\mathbf{r};\mathbf{s},\mathbf{k})\}_{\mathbf{s}\in C_\Lambda,\mathbf{k}\in C_{\Lambda^{-1}}}$ is given by[17]

$$\begin{aligned}E_a(\mathbf{r},\omega) =& E_{\mathrm{ext},a}(\mathbf{r},\omega) + \frac{1}{\varepsilon_0}\frac{1}{(2\pi)^3}\frac{|\Omega_\mathrm{P}|}{\sqrt{N_\mathrm{P}}}\sum_{b,c,d=1}^{3}\sum_{j,j',j''=1}^{M}\\ &\cdot\int_{C_{\Lambda^{-1}}} d^3k\, e^{i\mathbf{k}\cdot\mathbf{r}}\left[\zeta_\Lambda\left(\mathbf{r}-\eta^{(j)},\mathbf{k},\omega\right)\right]_{ab}\alpha_{bc}^{(j,j')}(\mathbf{k},\omega)\left[(\delta-\Gamma(\mathbf{k},\omega))^{-1}\right]_{cd}^{(j'j'')}\mathfrak{e}_{\mathrm{ext},d}^{(j'')}(\mathbf{k},\omega).\end{aligned} \tag{3.2.32}$$

It is important to realize, that the externally applied electric field $E_{\mathrm{ext},a}(\mathbf{r},\omega)$ is generated by an externally controlled current density $j_{\mathrm{ext},a}(\mathbf{r},\omega)$ that flows inside a source volume Ω_S, which is positioned at a finite distance from the probe volume Ω_P. Thus, $E_{\mathrm{ext},a}(\mathbf{r},\omega)$ represents a solution of the *inhomogeneous* Maxwell equations (see (2.2.5) and (2.2.7)), so that when it is expanded with respect to the basis system of plane waves according to

$$E_{\mathrm{ext},a}(\mathbf{r},\omega) = \sum_{\mathbf{q}}\tilde{E}_{\mathbf{q}\omega,a}^{(\mathrm{ext})}e^{i\mathbf{q}\cdot\mathbf{r}}, \tag{3.2.33}$$

any real external signal $E_{\mathrm{ext},a}(\mathbf{r},\omega)$ of fixed frequency ω is composed of a bunch of wave vectors $\mathbf{q}$. This feature enables to treat ω and $\mathbf{q}$ from now on as *independent* variables[18] [2]. Nonetheless, only specific relations of ω and $\mathbf{q}$ that comply with the photonic band structure $\omega_n(\mathbf{q})$ of the crystal will facilitate the propagation of the local electric field within the crystal, as is shown in sections 3.3 and 3.4. Assuming $\mathbf{q} \in C_{\Lambda^{-1}}$ in the remainder of this work, a simple relation between the distinct expansion coefficients

[17] For a detailed derivation of (3.2.32), see appendix E.3.

[18] It should be stressed, that the well-known dispersion relation $|\mathbf{q}| = \frac{\omega}{c}$ of light in vacuum constitutes the solvability condition required by the *homogeneous* Maxwell equations in free space for time harmonic signals $E_a(\mathbf{r},\omega) \sim e^{i\mathbf{q}\cdot\mathbf{r}}$. Similarly, assuming $E_{\mathrm{ext},a}(\mathbf{r},\omega) = 0$ in (3.1.9), a *homogeneous* integral equation determining $E_a(\mathbf{r},\omega)$ emerges, whose solvability condition is reflected by the photonic band structure $\omega_n(\mathbf{q})$ (for details, see section 3.3).

$\mathfrak{e}_{\mathrm{ext},a}(\mathbf{s},\mathbf{k},\omega)$ and $\tilde{E}^{(\mathrm{ext})}_{\mathbf{q}\omega,a}$ of the external electric field $E_{\mathrm{ext},a}(\mathbf{r},\omega)$ can be established according to[19]

$$\mathfrak{e}_{\mathrm{ext},a}(\mathbf{s},\mathbf{k},\omega) = \frac{e^{-i\mathbf{k}\cdot\mathbf{s}}}{\sqrt{N_{\mathrm{P}}}}\frac{(2\pi)^3}{|C_\Lambda|}\sum_{\mathbf{q}\in C_{\Lambda^{-1}}}\tilde{E}^{(\mathrm{ext})}_{\mathbf{q}\omega,a}e^{i\mathbf{q}\cdot\mathbf{s}}\delta(\mathbf{k}-\mathbf{q}), \tag{3.2.34}$$

that allows to rewrite (3.2.32) in the guise

$$\begin{aligned}E_a(\mathbf{r},\omega) = &\sum_{\mathbf{q}\in C_{\Lambda^{-1}}}\tilde{E}^{(\mathrm{ext})}_{\mathbf{q}\omega,a}e^{i\mathbf{q}\cdot\mathbf{r}} + \frac{1}{\varepsilon_0}\sum_{b,c,d=1}^{3}\sum_{j,j',j''=1}^{M}\sum_{\mathbf{q}\in C_{\Lambda^{-1}}}\\ &\cdot\left[\zeta_\Lambda\left(\mathbf{r}-\eta^{(j)},\mathbf{q},\omega\right)\right]_{ab}\alpha^{(j,j')}_{bc}(\mathbf{q},\omega)\left[(\delta-\Gamma(\mathbf{q},\omega))^{-1}\right]^{(j'j'')}_{cd}\tilde{E}^{(\mathrm{ext})}_{\mathbf{q}\omega,d}e^{i\mathbf{q}\cdot\mathbf{r}}.\end{aligned} \tag{3.2.35}$$

In the representation (3.2.35), the composition of the local electric field by multiple beams with same frequency ω but with different wave vectors $\mathbf{q}\in C_{\Lambda^{-1}}$ is manifest for real external signals[20] like (3.2.33). In what follows, the external electric field is assumed to be a *single beam* in the guise of a plane wave with wave vector $\mathbf{q}\in C_{\Lambda^{-1}}$. Thus, (3.2.33) reduces to

$$E_{\mathrm{ext},a}(\mathbf{r},\omega) = \tilde{E}^{(\mathrm{ext})}_{\mathbf{q}\omega,a}e^{i\mathbf{q}\cdot\mathbf{r}}, \tag{3.2.36}$$

where the corresponding Fourier transform in reciprocal space is given by

$$\tilde{E}_{\mathrm{ext},a}(\mathbf{k},\omega) = \int_{\mathbb{R}^3} d^3r\, e^{-i\mathbf{k}\cdot\mathbf{r}}E_{\mathrm{ext},a}(\mathbf{r},\omega) = (2\pi)^3\delta(\mathbf{k}-\mathbf{q})\tilde{E}^{(\mathrm{ext})}_{\mathbf{q}\omega,a}. \tag{3.2.37}$$

Now, representing the lattice sum $\zeta_\Lambda\left(\mathbf{r}-\eta^{(j)},\mathbf{q},\omega\right)$ for $\mathbf{r}-\eta^{(j)}\neq\mathbf{0}$ in terms of its Fourier series (3.2.24) and subsequently introducing the kernel

$$\tilde{K}_{bd}(\mathbf{G},\mathbf{q},\omega) = \frac{1}{\varepsilon_0}\sum_{c=1}^{3}\sum_{j,j',j''=1}^{M}e^{-i\mathbf{G}\cdot\eta^{(j)}}\alpha^{(j,j')}_{bc}(\mathbf{q},\omega)\left[(\delta-\Gamma(\mathbf{q},\omega))^{-1}\right]^{(j'j'')}_{cd}, \tag{3.2.38}$$

the local electric field, originally given by (3.2.35) for multiple beams, finally reduces in the case of a *single beam* to

$$E_a(\mathbf{r},\omega) = \tilde{E}^{(\mathrm{ext})}_{\mathbf{q}\omega,a}e^{i\mathbf{q}\cdot\mathbf{r}} + \frac{1}{|C_\Lambda|}\sum_{b,d=1}^{3}\sum_{\mathbf{G}\in\Lambda^{-1}}e^{i(\mathbf{q}+\mathbf{G})\cdot\mathbf{r}}\mathscr{G}_{ab}(\mathbf{q}+\mathbf{G},\omega)\tilde{K}_{bd}(\mathbf{G},\mathbf{q},\omega)\tilde{E}^{(\mathrm{ext})}_{\mathbf{q}\omega,d}. \tag{3.2.39}$$

The representation (3.2.39) of $E_a(\mathbf{r},\omega)$ requires that $\mathbf{r}$ does *not* coincide with an atomic position, a fact owed to the Fourier series expansion of the lattice sum $\zeta_\Lambda\left(\mathbf{r}-\eta^{(j)},\mathbf{q},\omega\right)$, that only exists for

[19] The insistence that $\mathbf{q}\in C_{\Lambda^{-1}}$ does not pose strong limitations on the applicability of the theory, because wave vectors $\mathbf{q}$ which are associated with typical external signals $E_{\mathrm{ext},a}(\mathbf{r},\omega)$ for frequencies ω well below the x-ray regime (e.g. within the optical regime) are completely contained within the first Brillouin zone. However, for external signals of particularly high frequency where $\mathbf{q}$ reaches out of $C_{\Lambda^{-1}}$, i.e. in and beyond the x-ray regime, the electric point dipole ansatz (3.1.6) for the dielectric susceptibility kernel $\chi_{ab}(\mathbf{r},\mathbf{r}',\omega)$ has to be extended to include also electric quadrupoles and magnetic dipoles, both to be treated on an equal footing [25]. For a derivation of the relation (3.2.34), see appendix E.4.

[20] For a discussion of multiple beam effects, see for example [28].

$\mathbf{r}-\eta^{(j)}\neq\mathbf{0}$ (see appendix F.1). If one is interested in the electric field strength at an atomic position $\eta^{(j)}$, the representation (3.2.21) of the lattice sum is valuable, because it exists even if $\mathbf{r}=\eta^{(j)}$ due to its definition by cases.

It is instructive to decompose the local electric field $E_a(\mathbf{r},\omega)$ given by (3.2.39) into its transverse and longitudinal components $E_a^{(\mathrm{T})}(\mathbf{r},\omega)$ and $E_a^{(\mathrm{L})}(\mathbf{r},\omega)$ respectively, because it allows to identify the radiative and non-radiative parts of the local electric field inside crystalline dielectrics. This decomposition also turns out to be inevitable when discussing the optical properties of crystals like e.g the index of refraction or natural optical activity, as these effects are assigned to the macroscopic radiation field $\mathscr{E}_a^{(\mathrm{T})}(\mathbf{r},\omega)$, which can be deduced from $E_a^{(\mathrm{T})}(\mathbf{r},\omega)$ by a low-pass filtering process, as is shown in section 4.1. But also in the polariton model, where phonons are coupled to electromagnetic radiation [34], it is $E_a^{(\mathrm{T})}(\mathbf{r},\omega)$ that enters the model instead of $E_a(\mathbf{r},\omega)$. The longitudinal and transverse components of the local electric field are obtained by applying the projection procedure (2.1.19) to (3.2.39) and subsequent identification of the Fourier transforms of the projection operators, so that at first glance

$$\begin{aligned}E_a^{(\mathrm{L,T})}(\mathbf{r},\omega)=&\sum_{b=1}^{3}\tilde{\Pi}_{ab}^{(\mathrm{L,T})}(\mathbf{q})\tilde{E}_{\mathbf{q}\omega,b}^{(\mathrm{ext})}e^{i\mathbf{q}\cdot\mathbf{r}}\\&+\frac{1}{|C_\Lambda|}\sum_{b,c,d=1}^{3}\sum_{\mathbf{G}\in\Lambda^{-1}}e^{i(\mathbf{q}+\mathbf{G})\cdot\mathbf{r}}\tilde{\Pi}_{ab}^{(\mathrm{L,T})}(\mathbf{q}+\mathbf{G})\tilde{\mathscr{G}}_{bc}(\mathbf{q}+\mathbf{G},\omega)\tilde{K}_{cd}(\mathbf{G},\mathbf{q},\omega)\tilde{E}_{\mathbf{q}\omega,d}^{(\mathrm{ext})}\end{aligned}\tag{3.2.40}$$

follows. Representing now the electromagnetic kernel in terms of the projection operators according to (2.2.17) and subsequently utilizes the projection operator identities (2.1.24)-(2.1.26), the longitudinal and transverse components of $E_a(\mathbf{r},\omega)$ finally assume the guise

$$E_a^{(\mathrm{L})}(\mathbf{r},\omega)=\tilde{E}_{\mathbf{q}\omega,a}^{(\mathrm{ext})(\mathrm{L})}e^{i\mathbf{q}\cdot\mathbf{r}}-\frac{1}{|C_\Lambda|}\sum_{c,d=1}^{3}\sum_{\mathbf{G}\in\Lambda^{-1}}e^{i(\mathbf{q}+\mathbf{G})\cdot\mathbf{r}}\tilde{\Pi}_{ac}^{(\mathrm{L})}(\mathbf{q}+\mathbf{G})\tilde{K}_{cd}(\mathbf{G},\mathbf{q},\omega)\tilde{E}_{\mathbf{q}\omega,d}^{(\mathrm{ext})}\tag{3.2.41}$$

$$\begin{aligned}E_a^{(\mathrm{T})}(\mathbf{r},\omega)=&\tilde{E}_{\mathbf{q}\omega,a}^{(\mathrm{ext})(\mathrm{T})}e^{i\mathbf{q}\cdot\mathbf{r}}\\&+\frac{1}{|C_\Lambda|}\sum_{c,d=1}^{3}\sum_{\mathbf{G}\in\Lambda^{-1}}e^{i(\mathbf{q}+\mathbf{G})\cdot\mathbf{r}}\frac{\frac{\omega^2}{c^2}}{|\mathbf{q}+\mathbf{G}|^2-\frac{\omega^2}{c^2}}\tilde{\Pi}_{ac}^{(\mathrm{T})}(\mathbf{q}+\mathbf{G})\tilde{K}_{cd}(\mathbf{G},\mathbf{q},\omega)\tilde{E}_{\mathbf{q}\omega,d}^{(\mathrm{ext})}.\end{aligned}\tag{3.2.42}$$

Recall, that the projection operators in reciprocal space are given by

$$\tilde{\Pi}_{ab}^{(\mathrm{L})}(\mathbf{k})=\frac{k_ak_b}{|\mathbf{k}|^2}\tag{3.2.43}$$

$$\tilde{\Pi}_{ab}^{(\mathrm{T})}(\mathbf{k})=\delta_{ab}-\frac{k_ak_b}{|\mathbf{k}|^2}.\tag{3.2.44}$$

A detailed discussion of the local electric field as well as of its longitudinal and transverse components in dielectric crystals is given in section 3.4. However, previously it has to be worked out, which relation has to be satisfied by the independent variables $\mathbf{q}$ and ω, so that an external signal $E_{\mathrm{ext},a}(\mathbf{r},\omega)=\tilde{E}_{\mathbf{q}\omega,a}^{(\mathrm{ext})}e^{i\mathbf{q}\cdot\mathbf{r}}$ incident on a crystal is also capable to induce a propagable field within that crystal. This

issue leads to the concept of photonic band structures, that will be dealt with in the next section.

Addendum: Local magnetic induction field Due to Faraday's law (2.1.12), the local electric field $E_a(\mathbf{r},\omega)$ induces a local magnetic induction field $B_a(\mathbf{r},\omega)$ according to

$$B_a(\mathbf{r},\omega) = \frac{1}{i\omega}\left[\nabla_{\mathbf{r}} \times \mathbf{E}(\mathbf{r},\omega)\right]_a. \tag{3.2.45}$$

Deploying (3.2.39), one readily obtains

$$\begin{aligned} B_a(\mathbf{r},\omega) =& \frac{1}{\omega}\left[\mathbf{q}\times\tilde{\mathbf{E}}^{(\mathrm{ext})}_{\mathbf{q}\omega}\right]_a e^{i\mathbf{q}\cdot\mathbf{r}} \\ &+ \frac{1}{\omega}\frac{1}{|C_\Lambda|}\sum_{b,c,d,e=1}^{3}\sum_{\mathbf{G}\in\Lambda^{-1}} e^{i(\mathbf{q}+\mathbf{G})\cdot\mathbf{r}}\varepsilon_{abc}(q_b+G_b)\tilde{\mathscr{G}}_{ce}(\mathbf{q}+\mathbf{G},\omega)\tilde{K}_{ed}(\mathbf{G},\mathbf{q},\omega)\tilde{E}^{(\mathrm{ext})}_{\mathbf{q}\omega,d}. \end{aligned} \tag{3.2.46}$$

For a discussion of the induced magnetic induction field, the reader is referred to section 4.3, where the local field $B_a(\mathbf{r},\omega)$ is compared with its macroscopic counterpart $\mathscr{B}_a(\mathbf{r},\omega)$.

For a brief discussion of the magnetic induction field in as well as the magnetic permeability tensor of crystalline materials that are only magnetizable rather than polarizable, the reader is referred to appendix I.

3.3 Photonic band structure

As has been reasoned in the previous section, the two variables ω and $\mathbf{q}\in C_{\Lambda^{-1}}$, representing the frequency and the wave vector respectively, have to be regarded as independent in equation (3.2.39) that determines the local electric field $E_a(\mathbf{r},\omega)$, because the latter represents a solution of the *inhomogenous* Maxwell equations including a source term $j_{\mathrm{ext},a}(\mathbf{r},\omega)\in\Omega_{\mathrm{S}}$, which is located at a finite distance to the probe volume Ω_{P} under investigation. With regard to (3.2.39), naturally the question arises whether any external signal $E_{\mathrm{ext},a}(\mathbf{r},\omega)=\tilde{E}^{(\mathrm{ext})}_{\mathbf{q}\omega,a}e^{i\mathbf{q}\cdot\mathbf{r}}$ of arbitrary ω and $\mathbf{q}$ is capable to induce a propagable local electric field $E_a(\mathbf{r},\omega)$ within a dielectric crystal polarizing its individual constituents, or if a specific constraint imposed on ω and $\mathbf{q}$ is required to allow for wave propagation inside crystalline dielectrics. Indeed, experience shows that a crystal especially prefers propagating waves, that correspond to the crystal's (photonic) eigenmodes, which in turn obey to the dispersion relation $\omega_n(\mathbf{q})$, also called photonic band structure[21]. To obtain these eigenmodes and their associated photonic band structure $\omega_n(\mathbf{q})$, the external source term is eliminated [24], i.e. $j_{\mathrm{ext},a}(\mathbf{r},\omega)=0$ or $E_{\mathrm{ext},a}(\mathbf{r},\omega)=0$. Then, the *inhomogeneous* integral equation (3.1.9) determining $E_a(\mathbf{r},\omega)$ as response to $E_{\mathrm{ext},a}(\mathbf{r},\omega)$, reduces to the

[21] The term band structure is usually employed in solid state physics to describe the energies $\varepsilon_n(\mathbf{k})$ of electrons moving in a periodic potential. Albeit, it should be emphasized, that the manifestation of a band structure is *not* a quantum mechanical effect. Instead, it is the result of solving a homogeneous partial differential equation with a *periodic* "potential" such as e.g. the Schrödinger eigenvalue problem for an electron moving within a crystal potential. Concerning the emergence of the band structure concept in electromagnetic theory, the reader is referred to [35–37].

homogeneous integral equation

$$E_a(\mathbf{r},\omega) = \sum_{b=1}^{3} \int_{\mathbb{R}^3} d^3r' \, [\mathscr{G} \circ \chi]_{ab}(\mathbf{r},\mathbf{r}',\omega) \, E_b(\mathbf{r}',\omega), \tag{3.3.1}$$

which solely contains the material dielectric susceptibility kernel $\chi(\mathbf{r},\mathbf{r}',\omega)$ as an input. When expanding the local electric field with respect to $\{w(\mathbf{r};\mathbf{s},\mathbf{q})\}_{\mathbf{s}\in C_\Lambda, \mathbf{q}\in C_{\Lambda^{-1}}}$, the *homogeneous* equation

$$\sum_{c=1}^{3} \sum_{j'=1}^{M} \left(\delta_{ac}^{(j'',j')} - \Gamma_{ac}^{(j'',j')}(\mathbf{q},\omega) \right) \mathfrak{e}_c^{(j')}(\mathbf{q},\omega) = 0 \tag{3.3.2}$$

can readily be inferred from (3.2.30), as $\mathfrak{e}_{\mathrm{ext},a}^{(j'')}(\mathbf{q},\omega) = 0$ for all $j'' \in \{1,2,\ldots,M\}$. (3.3.2) constitutes a homogeneous, linear system of $3M$ equations, thus possessing non-trivial solutions with regard to the expansion coefficients $\mathfrak{e}_c^{(j')}(\mathbf{q},\omega)$, provided that

$$\det[\delta - \Gamma(\mathbf{q},\omega)] = 0. \tag{3.3.3}$$

It should be stressed, that the $3M \times 3M$ matrix $\Gamma(\mathbf{q},\omega)$ comprises the lattice sum $\zeta_\Lambda^{(0)}(\mathbf{q},\omega)$, which exhibits an imaginary part for $\omega > 0$ representing radiation damping. It reads[22]

$$\Im\left\{ \left[\zeta_\Lambda^{(0)}(\mathbf{q},\omega) \right]_{ab} \right\} = -\frac{1}{6\pi} \left(\frac{\omega}{c} \right)^3 \delta_{ab} \tag{3.3.4}$$

and can be attributed to dissipative phenomena associated with the radiative energy loss [18] and may therefore *not* be confused with the damping term $\gamma^{(j)}$, that describes spontaneous emission in a quantum mechanical model of the electronic polarizability[23] $\alpha_{ab}^{(\mathrm{el})}(\eta^{(j)},\omega)$. Due to (3.3.4), the strict requirement (3.3.3), which implicitly contains the photonic band structure $\omega_n(\mathbf{q})$ as its solvability condition, will *never* be satisfied for frequencies $\omega > 0$ and real wave vectors $\mathbf{q} \in C_{\Lambda^{-1}}$, as the roots of the determinant's real and imaginary part emerge for given $\mathbf{q}$ at different frequencies. This has important consequences regarding the uniqueness of the solution of the *inhomogeneous* integral equation (3.1.9) determining the local electric field $E_a(\mathbf{r},\omega)$. As the *homogeneous* equation (3.3.1) only possesses the trivial solution for $\omega > 0$ and real $\mathbf{q} \in C_{\Lambda^{-1}}$ because of the non-vanishing radiation damping (3.3.4), the solution of the *inhomogeneous* equation is unique in the sense of Fredholm's alternative [40]. In presence of radiation damping, $\omega_n(\mathbf{q})$ is determined for given $\mathbf{q} \in C_{\Lambda^{-1}}$ by searching that frequency $\omega > 0$, that minimizes

[22] For a derivation of (3.3.4), see appendix F.2.2. For a discussion in the literature, see for example [18, 31, 38, 39].
[23] See (3.1.1) and especially the supplemental material to [23].

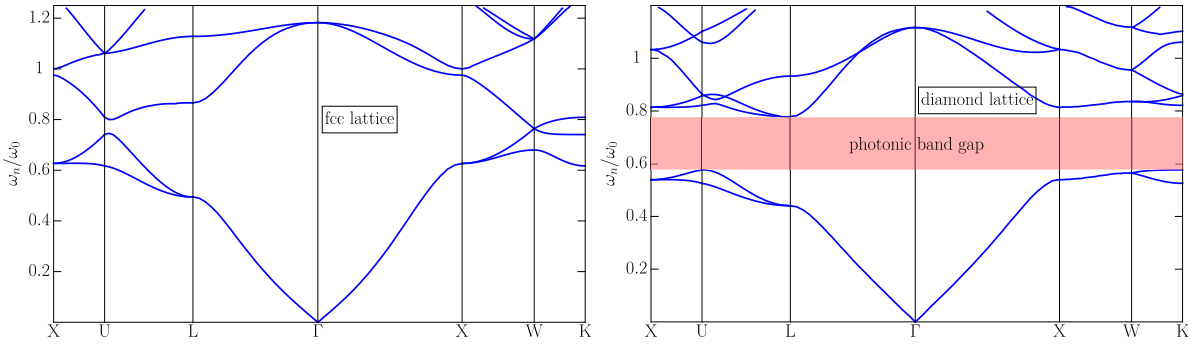

(a) (b)

Figure 3.3.1: Photonic band structure $\omega_n(\mathbf{q})$ in units of $\omega_0 = \frac{2\pi c}{a_\Lambda}$ as calculated from (3.3.3) by neglecting radiation damping, where the wave vector $\mathbf{q}$ is orientated along various symmetry lines of the first Brillouin zone $C_{\Lambda^{-1}}$ for (a) a face-centered cubic (fcc) lattice with lattice constant $a_\Lambda = 4\text{Å}$ and a constant scalar electronic polarizability of $\frac{\alpha^{(\mathrm{el})}}{4\pi\varepsilon_0} = 2\text{Å}^3$ and (b) for a diamond lattice with lattice constant $a_\Lambda = 6\text{Å}$ and a constant scalar electronic polarizability of $\frac{\alpha^{(\mathrm{el})}}{4\pi\varepsilon_0} = 3\text{Å}^3$.

the function[24]

$$f(\Omega) = |\det[\delta - \Gamma(\mathbf{q},\Omega)]|, \tag{3.3.5}$$

in other words, there holds

$$\lim_{\Omega\to\omega} \frac{\partial}{\partial\Omega} f(\Omega) = 0 \tag{3.3.6}$$

$$\lim_{\Omega\to\omega} \frac{\partial^2}{\partial\Omega^2} f(\Omega) > 0. \tag{3.3.7}$$

However, assume for the moment that radiation damping can be ignored. Then, the dispersion relation $\omega_n(\mathbf{q})$ can be readily determined for given $\mathbf{q} \in C_{\Lambda^{-1}}$ by calculating $\det[\delta - \Gamma(\mathbf{q},\omega)]$ in dependence of ω and then solving the implicit equation (3.3.3) with respect to the unknown ω's. After that, varying $\mathbf{q}$ along different symmetry lines inside the first Brillouin zone $C_{\Lambda^{-1}}$ and repeating the previously outlined procedure for every $\mathbf{q}$, the photonic band structure $\omega_n(\mathbf{q})$ emerges, as is exemplarily shown in figure 3.3.1 for the monatomic face-centered-cubic (fcc) lattice as well as the diatomic diamond lattice[25]. Both crystal structures display multiple bands along different symmetry lines of the first Brillouin zone, some

[24] The determination of $\omega_n(\mathbf{q})$ with or without radiation damping includes the evaluation of determinants. Therefore, this procedure is due to its computational cost only valuable for rather small matrices $\Gamma(\mathbf{q},\omega)$, i.e. if only few atoms are comprised by C_Λ. For many atoms contained within C_Λ, it turns out to be useful to grasp (3.3.2) as the $3M \times 3M$ eigenvalue problem

$$\sum_{c=1}^{3}\sum_{j'=1}^{M} \Gamma_{ac}^{(j'',j')}(\mathbf{q},\omega)\,\mathfrak{e}_c^{(j')}(\mathbf{q},\omega) = \mathfrak{e}_a^{(j'')}(\mathbf{q},\omega),$$

that can numerically be solved effectively even for large matrices $\Gamma(\mathbf{q},\omega)$.

[25] While the monatomic fcc-lattice is a Bravais lattice, the diatomic diamond lattice is not, though it is fcc as well.

of them being degenerate[26] such as the lowest bands of the fcc-lattice along the paths $\overline{L\Gamma}$ and $\overline{\Gamma X}$. In contrast to the fcc-lattice, the diamond lattice exhibits a complete photonic band gap, i.e. there exists a frequency interval, where electromagnetic wave propagation is prohibited irrespective of propagation direction and polarization. This feature constitutes a qualitatively new effect, that gives rise to a variety of applications concerning the guidance of light in the context of integrated optical circuits [42–44] and fibre-optic communications [45, 46], but it can also allow the realization of highly efficient optical reflectors or optical resonant microcavities [47].

All photonic band structures calculated within the framework of the presented theory comply well with calculations carried out for atomic dipole lattices in the spirit of the Fano-Hopfield model [41, 48] in the case of weakly coupled oscillators. But in comparison to earlier calculations carried out for dielectric superlattices on the basis of the macroscopic Maxwell equations [49–51], the current results of this work only agree with these for low frequencies ω, where the associated (free-space) wavelength $\lambda = \frac{2\pi c}{\omega}$ is large compared to the lattice constant and to the extension of the scatterers. However, at high frequencies ω, the electromagnetic wave is able to resolve the crystalline structure in detail, so that the extension of the scatterers, which is incorporated into the macroscopic Maxwell equations by a lattice periodic dielectric function $\varepsilon(\mathbf{r}) = \varepsilon(\mathbf{r}+\mathbf{R})$ with $\mathbf{R} \in \Lambda$, matters. This naturally leads to a discrepancy of the theory based on macroscopic Maxwell equations and the present one that assumes a point dipole model. Furthermore, the former ansatz employs the expansion with respect to plane waves $\left\{e^{i\mathbf{G}\cdot\mathbf{r}}\right\}_{\mathbf{G}\in\Lambda^{-1}}$, which requires the solution of a $3N \times 3N$ matrix equation, provided N reciprocal lattice vectors are retained. Unfortunately, these calculations show a number N of zero eigenvalues, which are attributed to longitudinal modes, that have to be eliminated afterwards by invoking the transversality of electromagnetic waves. In contrast, (3.3.2) involves only the solution of a $3M \times 3M$ matrix equation, with M denoting the number of atoms comprised by the Wigner-Seitz cell C_Λ.

Taking account of radiation damping, the concept of a photonic band structure $\omega_n(\mathbf{q})$ including many band branches looses its meaning for real crystalline materials of microscopic lattice constants a_Λ if ω exceeds a critical frequency ω_c. This is because for frequencies $\omega > \omega_c$ far and beyond the ultraviolet, radiation damping given by (3.3.4) becomes dominant, so that no frequency Ω can be found that minimizes the function $f(\Omega)$ given by (3.3.5) anymore. Figure 3.3.2 exemplifies what has been said by comparing the lowest bands, once calculated with and once without radiation damping taken into account, of the monatomic fcc and the diatomic diamond lattice along the symmetry lines $\overline{L\Gamma}$ and $\overline{\Gamma X}$. Obviously, the appearance of higher bands is suppressed for both crystal structures as a consequence of radiation damping, so that the formation of a photonic band gap, as has been observed for the diamond lattice in absence of radiation damping (see figure 3.3.1), is not possible. Additionally, the radiationally damped bands are shifted with respect to the undamped bands to lower frequencies, which is in accordance with the resonance behaviour of a periodically driven, damped harmonic oscillator. In contrast to real naturally occuring crystalline materials like NaCl or CsCl, the concept of a photonic band structure

[26] The degeneracy of the bands can be lifted, for example, by applying an additional static electric [41] or magnetic induction field, where the latter is demonstrated in figure 3.3.5.

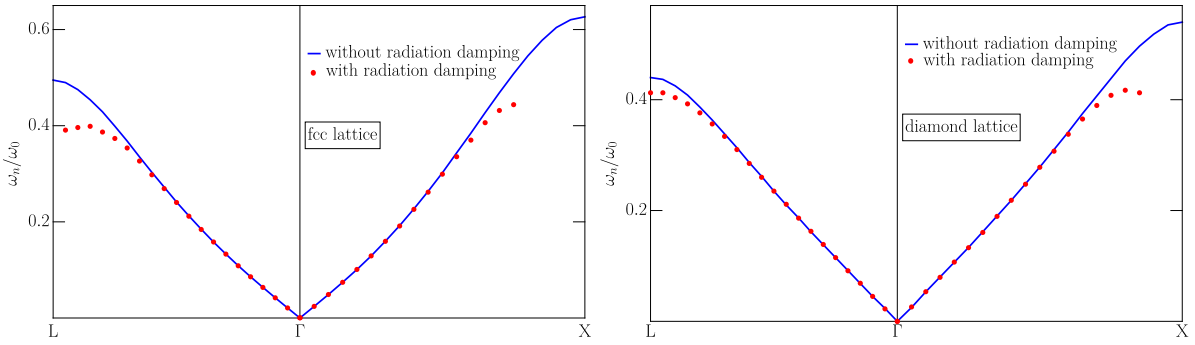

Figure 3.3.2: Comparison of photonic band structures $\omega_n(\mathbf{q})$ in units of $\omega_0 = \frac{2\pi c}{a_\Lambda}$ in the vicinity of the Γ point, once calculated with (red dots) and once without (blue line) radiation damping taken into account for (a) a fcc - lattice and (b) a diamond lattice. The deployed parameters are the same as in figure 3.3.1. With radiation damping taken into account, $\omega_n(\mathbf{q})$ has been determined by minimizing $f(\Omega)$ given by (3.3.5) with respect to $\Omega > 0$.

$\omega_n(\mathbf{q})$ with many band branches applies well for (artificial) dielectric superlattices with a mesoscopic lattice constant a_Λ. In this case, the photonic band structure including many band branches already evolves in the low frequency regime, where radiation damping is immaterial. For this reason, dielectric superlattices are promising materials for technical applications, as they allow the realization of a complete photonic band gap in the visible and near-infrared spectral regime [52, 53].

Addendum: Photonic band structures for the monatomic simple cubic (sc) and body-centred-cubic (bcc) lattices For the sake of completeness, figures 3.3.3 and 3.3.4 show the photonic band structure $\omega_n(\mathbf{q})$ for the monatomic sc- and bcc-lattices respectively, as well as the influence of radiation damping on their lowest bands around the Γ-point. Similar to the previously discussed fcc - and diamond lattices, the meaning of a photonic band structure ceases to make sense also for sc - or bcc - lattices with microscopic lattice constants, once the boundary of the first Brillouin zone is approached and $\omega_n(\mathbf{q})$ enters the x - ray regime, as radiation damping suppresses the existence of any photonic bands.

Addendum: Impact of an external static magnetic induction field on the photonic band structure Suppose that the dielectric (non-magnetic) crystal under consideration is put into an externally controlled *static* magnetic induction field $\mathbf{B}^{(0)}$. Then, the former state of equilibrium of the crystal's constituents, which is represented by their individual electronic polarizabilities $\alpha_{ab}^{(\mathrm{el})}\left(\eta^{(j)},\omega\right)$ with $j \in \{1,2,\ldots,M\}$, is changed due to the interaction of $\mathbf{B}^{(0)}$ with the charge carriers comprised by each constituent. Consequently, in every constituent a new atomic/ionic state of equilibrium is established, which now depends on $\mathbf{B}^{(0)}$ and is thus described by a polarizability $\alpha_{ab}^{(\mathrm{el})}\left(\eta^{(j)},\omega;\mathbf{B}^{(0)}\right)$.

Restricting the discussion from now on to crystals with only one atom per unit cell (i.e. $M = 1$),

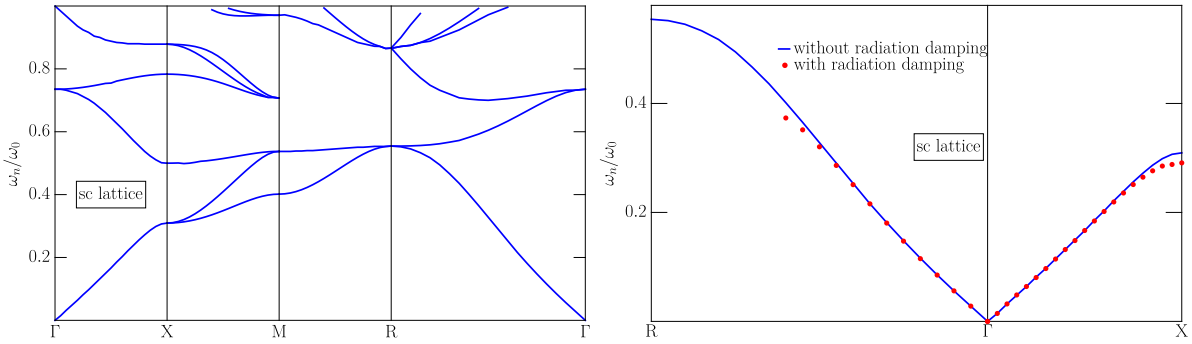

(a) (b)

Figure 3.3.3: (a) Photonic band structure $\omega_n(\mathbf{q})$ in units of $\omega_0 = \frac{2\pi c}{a_\Lambda}$ as calculated from (3.3.3) by neglecting radiation damping, where the wave vector $\mathbf{q}$ is orientated along various symmetry lines of the first Brillouin zone $C_{\Lambda^{-1}}$ for a simple cubic (sc) lattice with lattice constant $a_\Lambda = 4\text{Å}$ and a constant scalar electronic polarizability of $\frac{\alpha^{(\mathrm{el})}}{4\pi\varepsilon_0} = 5\text{Å}^3$. (b) Comparison of photonic band structures $\omega_n(\mathbf{q})$ of a sc - lattice in the vicinity of the Γ point, once calculated with (red dots) and once without (blue line) radiation damping taken into account.

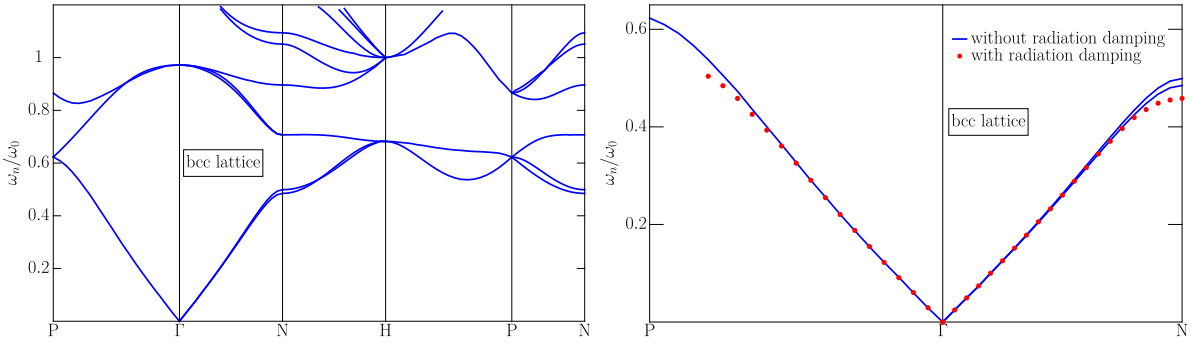

(a) (b)

Figure 3.3.4: (a) Photonic band structure $\omega_n(\mathbf{q})$ in units of $\omega_0 = \frac{2\pi c}{a_\Lambda}$ as calculated from (3.3.3) by neglecting radiation damping, where the wave vector $\mathbf{q}$ is orientated along various symmetry lines of the first Brillouin zone $C_{\Lambda^{-1}}$ for a body - centered cubic (bcc) lattice with lattice constant $a_\Lambda = 4\text{Å}$ and a constant scalar electronic polarizability of $\frac{\alpha^{(\mathrm{el})}}{4\pi\varepsilon_0} = 2\text{Å}^3$. (b) Comparison of photonic band structures $\omega_n(\mathbf{q})$ of a bcc - lattice in the vicinity of the Γ point, once calculated with (red dots) and once without (blue line) radiation damping taken into account.

the abbreviation $\alpha_{ab}^{(\mathrm{el})}\left(\eta^{(j)},\omega;\mathbf{B}^{(0)}\right)\equiv\alpha_{ab}^{(\mathrm{el})}\left(\omega;\mathbf{B}^{(0)}\right)$ is introduced. Assuming $\alpha_{ab}^{(\mathrm{el})}\left(\omega;\mathbf{B}^{(0)}\right)$ to be an analytic function, it can formally be expanded into a Taylor series with respect to $\mathbf{B}^{(0)}$ around $\mathbf{B}^{(0)}=\mathbf{0}$. Requiring that the static magnetic induction field is not too strong, $\alpha_{ab}^{(\mathrm{el})}\left(\omega;\mathbf{B}^{(0)}\right)$ will vary linearly with $\mathbf{B}^{(0)}$, so that one obtains

$$\alpha_{ab}^{(\mathrm{el})}\left(\omega;\mathbf{B}^{(0)}\right)=\alpha_{ab}\left(\omega\right)+i\sum_{c=1}^{3}\beta_{abc}\left(\omega\right)B_{c}^{(0)} \tag{3.3.8}$$

in accordance with quantum mechanical considerations, where $\beta_{abc}\left(\omega\right)\in\mathbb{R}$. Obviously, $\alpha_{ab}\left(\omega\right)$ denotes the electronic polarizability in the absence of $\mathbf{B}^{(0)}$, so that its frequency dependence is determined by the Lorentz oscillator model (3.1.1). The quantum mechanical derivation of (3.3.8) including the formal frequency dependence of $\beta_{abc}\left(\omega\right)$ follows the lines indicated in the supplemental material to [23] regarding the calculation of the atomic polarizability by means of first order time dependent perturbation theory and was explicitly elaborated by Prof. N. Schopohl in [24]. However, in presence of the *static* magnetic induction field $\mathbf{B}^{(0)}$, the multi-electron atom Hamiltonian has to be complemented by the additional term $\frac{|e|}{2m}\left(\mathbf{L}+2\mathbf{S}\right)\cdot\mathbf{B}^{(0)}$, that might give rise to a field dependent shift of the atom's spectral lines or even to Zeeman splitting. Additionally, $\mathbf{B}^{(0)}$ breaks the time reversal symmetry, so that the eigenstates of the multi-electron atom Hamiltonian can *not* all be chosen real anymore, thus the dipole matrix elements are becoming complex and magnetic field dependent. Accordingly, the atomic polarizability tensor decomposes into symmetric and antisymmetric parts, where the latter vanishes if $\mathbf{B}^{(0)}=\mathbf{0}$. Then, expanding that polarizability tensor with respect to $\mathbf{B}^{(0)}$ to linear order and just keeping terms that describe qualitatively new effects, i.e. omitting all terms that simply give rise to a small quantitative correction to the atomic polarizability in absence of the static magnetic induction field, the functional form (3.3.8) of the polarizability tensor emerges. In particular there holds $\beta_{abc}\left(0\right)=0$.

The objective is now to study the impact of $\mathbf{B}^{(0)}$, mediated by $\beta_{abc}\left(\omega\right)$, on the photonic band structure of a dielectric crystal. In order to do that, consider exemplarily a simple cubic crystal and neglect for the sake of simplicity the frequency dependence of $\alpha_{ab}^{(\mathrm{el})}\left(\omega;\mathbf{B}^{(0)}\right)$, i.e. it is required that $\alpha_{ab}^{(\mathrm{el})}\left(\omega;\mathbf{B}^{(0)}\right)=\alpha_{ab}^{(\mathrm{el})}\left(\mathbf{B}^{(0)}\right)$ with $\alpha_{ab}\left(\omega\right)=\alpha_{ab}$ and $\beta_{abc}\left(\omega\right)=\beta_{abc}$. If now the $m\bar{3}m$ (or O_h) point group symmetry of the simple cubic crystal is assigned to the tensors α_{ab} and β_{abc}, these assume the guise $\alpha_{ab}=\alpha\delta_{ab}$ and $\beta_{abc}=\beta\varepsilon_{abc}$ [5], so that finally

$$\alpha^{(\mathrm{el})}\left(\mathbf{B}^{(0)}\right)=\begin{pmatrix}\alpha & i\beta B_3^{(0)} & -i\beta B_2^{(0)}\\ -i\beta B_3^{(0)} & \alpha & i\beta B_1^{(0)}\\ i\beta B_2^{(0)} & -i\beta B_1^{(0)} & \alpha\end{pmatrix} \tag{3.3.9}$$

emerges. To illustrate the effect of the purely imaginary off-diagonal components of the polarizability tensor (3.3.9) on the photonic band structure of a monatomic simple cubic crystal, its lowest bands are calculated by means of (3.3.3) around the Γ-point for a static magnetic induction field $\mathbf{B}^{(0)}=B_2^{(0)}\mathbf{e}_2$ pointing in y-direction, once for $B_2^{(0)}=0$ and once for $B_2^{(0)}\neq 0$. The result is shown in figure 3.3.5. In the absence of $\mathbf{B}^{(0)}$ (blue line), the variation of the wave vector $\mathbf{q}$ along the symmetry lines $\overline{\Gamma X}$ and $\overline{R\Gamma}$

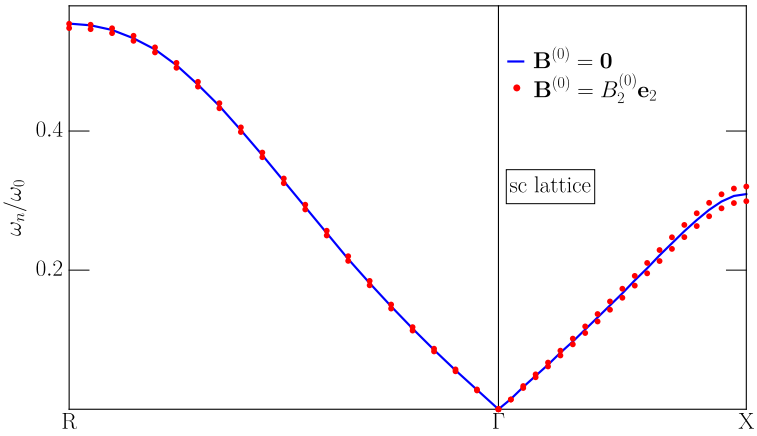

Figure 3.3.5: Comparison of photonic band structures $\omega_n(\mathbf{q})$ in units of $\omega_0 = \frac{2\pi c}{a_\Lambda}$ for a sc - lattice with lattice constant $a_\Lambda = 4\text{Å}$ in the vicinity of the Γ point, once calculated with non-vanishing (red dots) and once with vanishing (blue line) static magnetic induction field $\mathbf{B}^{(0)} = B_2^{(0)}\mathbf{e}_2$. The deployed parameters entering the polarizability model (3.3.9) are $\frac{\alpha}{4\pi\varepsilon_0} = 5\text{Å}^3$ and $\frac{\beta B_2^{(0)}}{4\pi\varepsilon_0} = 0.5\text{Å}^3$.

is associated with wave propagation along highly symmetric directions within the crystal, accompanied by time-reversal symmetry. Therefore, both propagable modes of the transverse electric field obey to the same dispersion relation, resulting in twofold degenerated photonic bands. In presence of a non-vanishing magnetic induction field $\mathbf{B}^{(0)}$ (red dots), time-reversal symmetry is locally broken[27] [54, 55], so that the degeneracy of the photonic bands is removed. Noticing that the orientation of $\mathbf{B}^{(0)}$ is parallel to the wave vectors $\mathbf{q}$ lying on the symmetry line $\overline{\Gamma X}$, the two bands reflect in the optical regime the well-known, non-reciprocal Faraday effect [26, 54, 56, 57].

Similar to an external static magnetic induction field, an external static electric field can also remove the degeneracy of the photonic bands. For a discussion see [41].

3.4 Discussion of the local electric field

As has been elucidated in section 3.2, frequency ω and wave vector $\mathbf{q} \in C_{\Lambda^{-1}}$ are independent variables in the present theory of the local electric field $E_a(\mathbf{r},\omega)$, which is determined by (3.2.39). Anyway, only external signals $E_{\text{ext},a}(\mathbf{r},\omega) = \tilde{E}^{(\text{ext})}_{\mathbf{q}\omega,a} e^{i\mathbf{q}\cdot\mathbf{r}}$ of particular polarization as well as of specific frequency ω and wave vector $\mathbf{q}$ that obey to the crystal's photonic band structure $\omega_n(\mathbf{q})$ correspond to the photonic eigenmodes of the crystal and are thus favoured to induce the (propagable) local electric field $E_a(\mathbf{r},\omega)$,

[27] Because $\mathbf{B}^{(0)}$ is regarded as an external field generated by an external current density $\mathbf{j}^{(0)}$ that does *not* belong the (crystalline) system under consideration, the source of $\mathbf{B}^{(0)}$ is supposed to be unaffected by a time-reversal operation that is applied to the (crystalline) system. Therefore $\mathbf{B}^{(0)}$ remains unchanged and the time-reversal symmetry is locally broken within the (crystalline) system. Of course, if the source $\mathbf{j}^{(0)}$ of the magnetic induction field $\mathbf{B}^{(0)}$ would be a part of the (crystalline) system, then the (crystalline) system would be invariant under a time-reversal operation, because $\mathbf{B}^{(0)}$ is reversed, too.

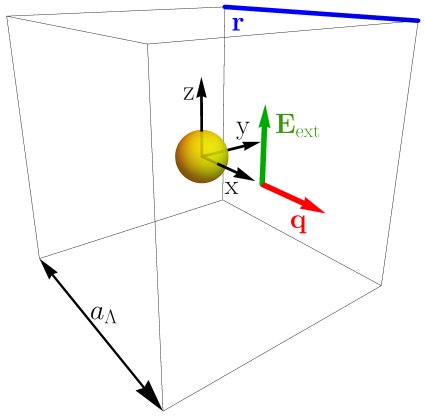

Figure 3.4.1: Schematic illustration of the crystal structure and the externally applied signal $\mathbf{E}_{\text{ext}}(\mathbf{r},\omega_{\text{ext}})$, for which the local electric field $\mathbf{E}(\mathbf{r},\omega)$ is calculated along the path $\mathbf{r}(x)$. For details, see text.

which polarizes the individual atoms and ions within the crystal[28].

In this context, the local electric field $E_a(\mathbf{r},\omega)$ in dielectric crystals is discussed in the remainder of this section for the setup illustrated in figure 3.4.1. Here, the crystal is assumed to be a monatomic simple cubic structure with lattice constant a_Λ and constant isotropic electronic polarizability $\alpha_{ab}^{(\text{el})}\left(\eta^{(1)},\omega\right) = \alpha^{(\text{el})}\delta_{ab}$, where the externally applied (time harmonic) plane wave signal $\mathbf{E}_{\text{ext}}(\mathbf{r},\omega_{\text{ext}}) = \mathbf{e}_3 e^{i\mathbf{q}\cdot\mathbf{r}}\left[\frac{V}{m}\right]$ of frequency ω_{ext} and wave vector $\mathbf{q} = |\mathbf{q}|\,\mathbf{e}_1$ propagates along the x-direction while it is linearly polarized in z-direction. The local electric field $\mathbf{E}(\mathbf{r},\omega)$ is then calculated along the path $\mathbf{r}(x) = x\mathbf{e}_1 + \frac{a_\Lambda}{2}(\mathbf{e}_2+\mathbf{e}_3)$ with $x\in\mathbb{R}$, so that the respective path never encounters an atom or ion positioned within the crystal.

While the externally applied field $\mathbf{E}_{\text{ext}}(\mathbf{r},\omega_{\text{ext}})$ displays spatial variations on a length scale comparable to its free space wavelength $\lambda_{\text{ext}} = \frac{2\pi c}{\omega_{\text{ext}}}$ because of $\mathbf{q}\in C_{\Lambda^{-1}}$, the local electric field $\mathbf{E}(\mathbf{r},\omega)$ given by (3.2.39) comprises rapid spatial variations according to $e^{i\mathbf{G}\cdot\mathbf{r}}$ for $\mathbf{G}\in\Lambda^{-1}\setminus\{\mathbf{0}\}$ on the back of the slowly varying envelope $e^{i\mathbf{q}\cdot\mathbf{r}}$, as is shown in figure[29] 3.4.2. Obviously, the distance between two adjacent peaks equals exactly the lattice constant a_Λ, this being a consequence of the lattice periodicity of the lattice sum $\zeta_\Lambda(\mathbf{s},\mathbf{k},\omega)$ if $\mathbf{s}\neq\mathbf{0}$. It is also noticeable, that in compliance with the external signal, only the local electric field's z-component is non-vanishing. This should not be taken for granted, because the external signal in guise of a plane wave is purely transverse, while the local field is comprised by longitudinal and transverse contributions (see (3.2.41) as well as (3.2.42) and in particular figure 3.4.4). One should not be confused by the fact, that the amplitude of the local field inside the crystal by far exceeds that of

[28] Of course, the requirement that ω and $\mathbf{q}\in C_{\Lambda^{-1}}\subset\mathbb{R}^3$ are in entire accordance with the photonic band structure $\omega_n(\mathbf{q})$ to allow wave propagation within a crystal is not absolutely strict, because due to radiation damping the rigorous solvability condition (3.3.3) is never satisfied as long as $\omega>0$. Instead, $\omega_n(\mathbf{q})$ is determined by minimizing $f(\Omega)$ given by (3.3.5) with respect to Ω for given $\mathbf{q}$, implicitly implying that it is sufficient, when ω and $\mathbf{q}$ are situated in close proximity of $\omega_n(\mathbf{q})$. This approach is legit, provided that radiation damping is a weak effect (see section 3.3 and also figure 3.4.3).

[29] Notice the quantity n appearing in the caption of figure 3.4.2 (not to be confused with the band index of $\omega_n(\mathbf{q})$), which measures the modulus of the wave vector $|\mathbf{q}|$ with respect to $\frac{\omega_{\text{ext}}}{c}$. In chapter 4, n turns out as the index of refraction, that constitutes the major contribution to the dielectric tensor $\varepsilon(\mathbf{q},\omega)$ and additionally provides an appropriate parametrization of the photonic band structure in the low-frequency regime, when $\mathbf{q}$ is restricted to the proximity of the Γ-point within $C_{\Lambda^{-1}}$.

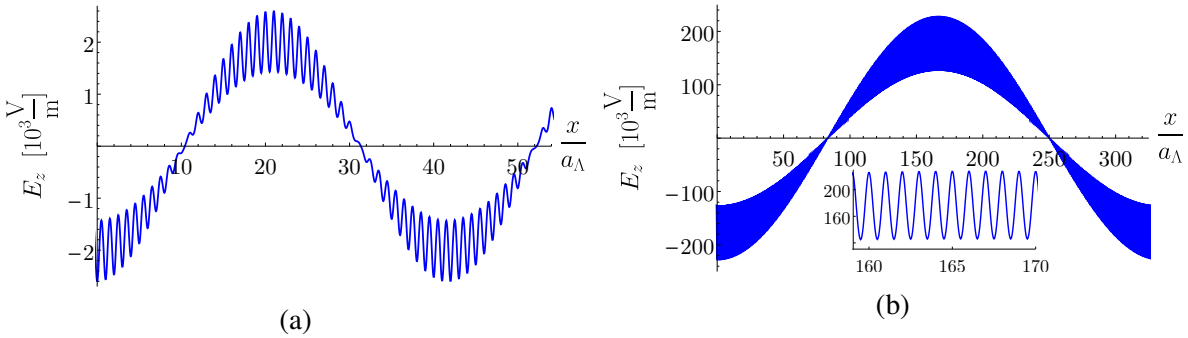

Figure 3.4.2: Spatial variation of the local electric field's z-component $E_z(\mathbf{r},\omega)$ given by (3.2.39) for the setup shown in figure 3.4.1. While the crystal's lattice constant as well as the electronic polarizability are the same in both plots, namely $a_\Lambda = 3.5\text{Å}$ and $\frac{\alpha^{(\mathrm{el})}}{4\pi\varepsilon_0} = 8\text{Å}^3$ respectively, the externally applied electric field possesses in (a) a rather short ultraviolet wavelength $\lambda_{\mathrm{ext}} = \frac{2\pi c}{\omega_{\mathrm{ext}}} = 50nm$ with $|\mathbf{q}| = \frac{2\pi}{\lambda_{\mathrm{ext}}} n$ and $n = 3.42077$ and in (b) a visible violet wavelength $\lambda_{\mathrm{ext}} = \frac{2\pi c}{\omega_{\mathrm{ext}}} = 400nm$ with $|\mathbf{q}| = \frac{2\pi}{\lambda_{\mathrm{ext}}} n$ and $n = 3.4256$. The inset zooms to a smaller scale to reveal the rapid spatial variations of the local electric field in the visible regime.

the external field. Because in the present case ω_{ext} and $\mathbf{q}$ agree well with the photonic band structure $\omega_n(\mathbf{q})$, $\tilde{K}(\mathbf{G},\mathbf{q},\omega)$ given by (3.2.38) becomes large because of the term $(\delta - \Gamma(\mathbf{q},\omega))^{-1}$ that reflects the solvability condition (3.3.3) (or rather (3.3.6)) of the *homogeneous* integral equation (3.3.1), but at last remains *finite* due to radiation damping. Therefore, the amplitude of the local electric field given by (3.2.39) is large compared to that of the external field but always finite, too.

To investigate the dependence of the local electric field's amplitude with respect to the choice of ω_{ext} and $\mathbf{q}$, consider again the setup shown in figure 3.4.1 and calculate the maximal field strength $\max_x E_z(\mathbf{r}(x),\omega_{\mathrm{ext}})$ along the path $\mathbf{r}(x)$ for a fixed frequency ω_{ext} in dependence of $|\mathbf{Q}|$, which denotes the modulus of the wave vector $\mathbf{Q} = |\mathbf{Q}|\,\mathbf{e}_1$ of the external signal $\mathbf{E}_{\mathrm{ext}}(\mathbf{r},\omega_{\mathrm{ext}}) = \mathbf{e}_3 e^{i\mathbf{Q}\cdot\mathbf{r}}\ \left[\frac{V}{m}\right]$. The result is shown in figure 3.4.3. Obviously, the amplitude of the local electric field in crystalline dielectrics is very sensitive with respect to the choice of ω_{ext} and $\mathbf{q}$. In particular, if frequency ω_{ext} and wave vector $\mathbf{q}$ of the external signal coincide with the photonic band structure, i.e. if $\omega_{\mathrm{ext}} = \omega_n(\mathbf{q})$, the local electric field turns out to be maximal. But if ω_{ext} and $\mathbf{q}$ do not meet the requirements set by $\omega_n(\mathbf{q})$, the electric field strength rapidly decreases, even if ω_{ext} and $\mathbf{q}$ are located in the vicinity of $\omega_n(\mathbf{q})$. As a result, the amplitude of the local electric field is a sharply peaked function of ω_{ext} and $\mathbf{q}$ around $\omega_n(\mathbf{q})$ so that solely optical modes associated with the immediate proximity of $\omega_n(\mathbf{q})$ are capable to propagate with sufficient intensity within the crystal. It should be noticed, that the position as well as the width of this peak depends on the density of polarizable atoms ν_{P}. With increasing lattice constant a_Λ (see figure 3.4.3 (b)), its position is shifted to lower values of $|\mathbf{Q}|$ and its width decreases. In the limit $a_\Lambda \to \infty$ the peak is positioned at $|\mathbf{q}| = \frac{\omega_{\mathrm{ext}}}{c}$ and of infinitesimal width, thus reflecting the propagation of plane waves in free space.

Finally, it is instructive to identify the non-radiative and radiative contributions $E_a^{(\mathrm{L})}(\mathbf{r},\omega)$ and $E_a^{(\mathrm{T})}(\mathbf{r},\omega)$

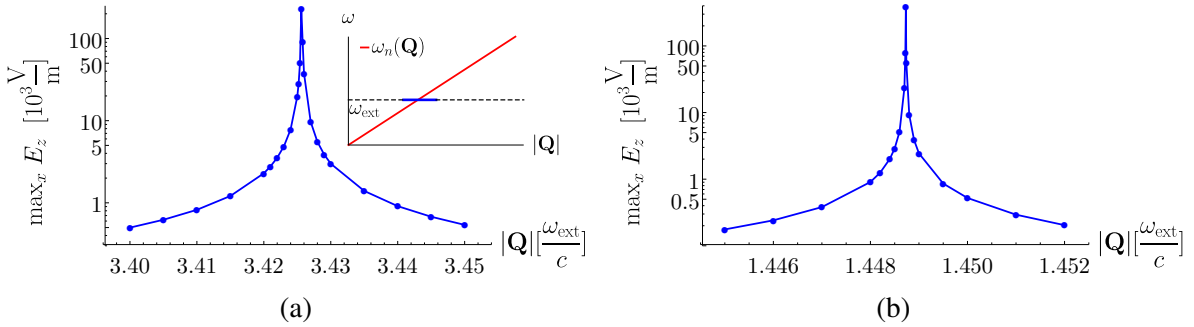

(a) (b)

Figure 3.4.3: Maximal electric field strength $\max_x E_z(\mathbf{r}(x), \omega_{\mathrm{ext}})$ for a fixed frequency ω_{ext} in dependence of the modulus $|\mathbf{Q}|$ of the external signal's wave vector $\mathbf{Q}$ along the path $\mathbf{r}(x)$ shown in figure 3.4.1. The applied parameters regarding frequency and electronic polarizability are the same in both plots and read $\lambda_{\mathrm{ext}} = \frac{2\pi c}{\omega_{\mathrm{ext}}} = 400nm$ and $\frac{\alpha^{(\mathrm{el})}}{4\pi\varepsilon_0} = 8\text{Å}^3$ respectively. While in (a) the lattice constant $a_\Lambda = 3.5\text{Å}$ is rather small, in (b) it has been increased to $a_\Lambda = 5\text{Å}$. The inset in (a) shows the variation of $|\mathbf{Q}|$ within the $\omega - |\mathbf{Q}|$ plane as well as the photonic band structure $\omega_n(\mathbf{Q})$. For $\omega_{\mathrm{ext}} = \omega_n(\mathbf{Q})$, the electric field strength is always maximal.

of the local electric field in dielectric crystals, which can be calculated according to (3.2.41) and (3.2.42) respectively. Therefore consider the local electric field $E_z(\mathbf{r}, \omega)$ shown in figure 3.4.2 (b) and decompose it according to $E_z(\mathbf{r}, \omega) = E_z^{(\mathrm{L})}(\mathbf{r}, \omega) + E_z^{(\mathrm{T})}(\mathbf{r}, \omega)$ into its longitudinal and transverse contributions. The result is shown in figure 3.4.4. Obviously, in the present case the non-radiative part of the local electric field $E_z(\mathbf{r}, \omega)$ is predominant, as the amplitude of $E_z^{(\mathrm{L})}(\mathbf{r}, \omega)$ is distinctly larger than the amplitude of $E_z^{(\mathrm{T})}(\mathbf{r}, \omega)$. This is intuitively accessible, because in materials with a high density ν_{P} of polarizable atoms, i.e. in materials of high refractive index, every point $\mathbf{r} \in \Omega_{\mathrm{P}}$ is surrounded by nearby positioned induced atomic dipoles, whose emitted fields are dominated by their static longitudinal parts on such microscopic length scales. Additionally, in contrast to $E_z(\mathbf{r}, \omega)$ and $E_z^{(\mathrm{L})}(\mathbf{r}, \omega)$, the pure radiative part $E_z^{(\mathrm{T})}(\mathbf{r}, \omega)$ seems at first glance to be free of rapid spatial variations on the length scale of the lattice constant a_Λ. That this is *not* true is shown in section 4.3 and especially in figure 4.3.1, when it is compared to the *macroscopic* electric field.

It is important to realize, that the contribution $\rho^{(\mathrm{L})}$ of the non-radiative part $E_z^{(\mathrm{L})}(\mathbf{r}, \omega)$ to the total field $E_z(\mathbf{r}, \omega)$ increases rapidly when the density ν_{P} of polarizable atoms/ions within the crystal is increased, while the contribution $\rho^{(\mathrm{T})}$ of the radiative part $E_z^{(\mathrm{T})}(\mathbf{r}, \omega)$ decreases rapidly, and vice versa. See therefor figure 3.4.5 (a). In the low density limit $\nu_{\mathrm{P}} \to 0$, the non-radiative field $E_z^{(\mathrm{L})}(\mathbf{r}, \omega)$ does not contribute to $E_z(\mathbf{r}, \omega)$, so that the radiative field $E_z^{(\mathrm{T})}(\mathbf{r}, \omega)$ coincides with the total local electric field. Conversely, in the limit $\nu_{\mathrm{P}} \to \nu_{\mathrm{P}}^{(c)}$ where matter becomes unstable in absence of a counteracting damping term, the transverse field $E_z^{(\mathrm{T})}(\mathbf{r}, \omega)$ is strongly suppressed while the longitudinal field $E_z^{(\mathrm{L})}(\mathbf{r}, \omega)$ essentially coincides with $E_z(\mathbf{r}, \omega)$. Whether the local electric field is of radiative or non-radiative nature or even a mixture of both thus strongly depends on the density of polarizable atoms ν_{P} within the crystal, which is a measure for the optical density of a material. An alternative measure of optical density in the sense of macroscopic electrodynamics is the index of refraction n, that can be

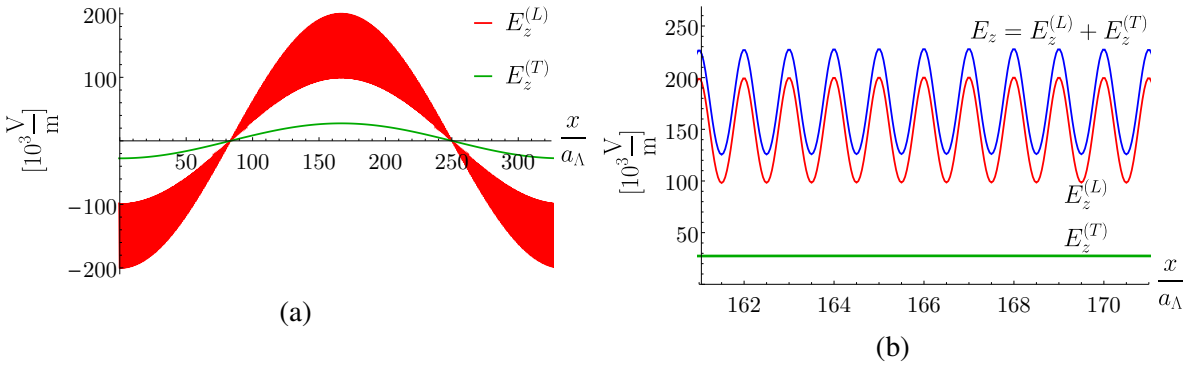

Figure 3.4.4: (a) Spatial variation of the z-components of the longitudinal (red) and transverse (green) local electric fields $E_z^{(\mathrm{L})}(\mathbf{r},\omega)$ and $E_z^{(\mathrm{T})}(\mathbf{r},\omega)$ given by (3.2.41) and (3.2.42), constituting the non-radiative and radiative contributions of the local electric field $E_z(\mathbf{r},\omega)$, where the latter is shown in figure 3.4.2 (b). (b) Zoom to a smaller scale to reveal the local field's rapid spatial oscillations. For the sake of completeness, $E_z(\mathbf{r},\omega) = E_z^{(\mathrm{L})}(\mathbf{r},\omega) + E_z^{(\mathrm{T})}(\mathbf{r},\omega)$ (blue) taken from figure 3.4.2 (b) is also shown.

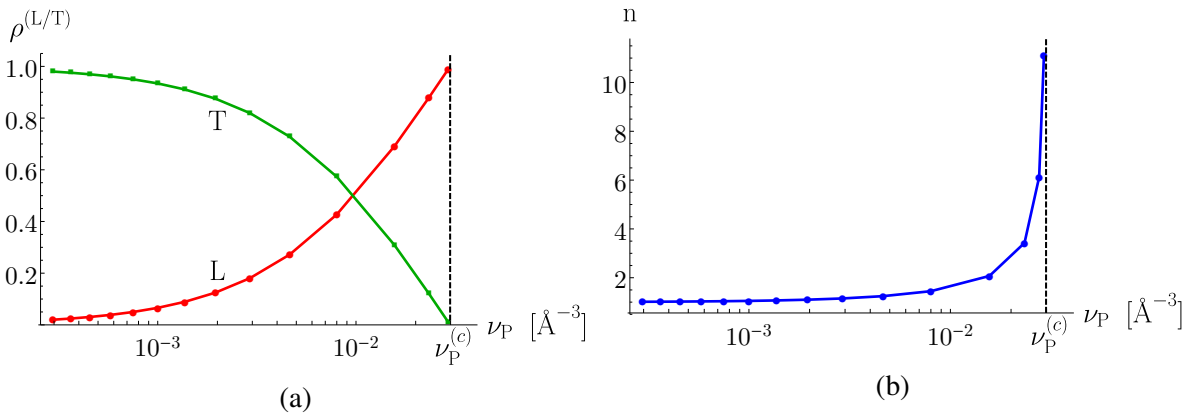

Figure 3.4.5: (a) Contributions $\rho^{(\mathrm{L,T})} = \frac{\max_x \left| E_z^{(\mathrm{L,T})}(\mathbf{r}(x),\omega_\mathrm{ext}) \right|}{\max_x |E_z(\mathbf{r}(x),\omega_\mathrm{ext})|}$ of the longitudinal and transverse parts $E_z^{(\mathrm{L})}(\mathbf{r},\omega)$ and $E_z^{(\mathrm{T})}(\mathbf{r},\omega)$ to the total local electric field $E_z(\mathbf{r},\omega)$ in dependence of the density ν_P of polarizable atoms (basically with parameters as in figure 3.4.4). (b) Variation of the index of refraction $n(\omega_\mathrm{ext})$ of the crystal, which can be taken as an alternative measure for its optical density. It can be calculated from the transverse dielectric tensor given in (4.2.20) in dependence of ν_P. Here, $\nu_\mathrm{P}^{(c)}$ denotes the border to instability, where the transverse dielectric tensor exhibits a pole, provided the damping term $\gamma^{(1)} > 0$ associated with the electronic polarizability $\alpha_{ab}^{(\mathrm{el})}\left(\eta^{(1)},\omega_\mathrm{ext}\right)$ is neglected.

calculated from the transverse dielectric tensor given by (4.2.20) in the limit $\mathbf{q} = \mathbf{0}$. That there is a close correlation between ν_{P} and n is exemplified in figure 3.4.5 (b). While a high density always implicates a large index of refraction, a low density brings along a refractive index which is only slightly larger than that of free space.

It should be emphasized again, that up to this point the presented theory of the *local* electromagnetic field solely relies on the *microscopic* Maxwell equations. Thus, there has been no need to introduce macroscopic quantities like a dielectric tensor or an index of refraction to describe the electrodynamics of dielectric crystals. However, when one is interested in the electrodynamics on a macroscopic length scale, as is the case in a variety of engineering applications, it is reasonable to discard information that is contained in the local electromagnetic field about the material's precise microstructure. Instead of the local electromagnetic field, one considers its spatially slowly varying envelope, representing the macroscopic electromagnetic field[30]. In view of applications in the optical sciences, the equations determining the macroscopic electromagnetic field are deduced in the next chapter. These then allow the identification of the (transverse) dielectric tensor in a tried and tested way, so that a multitude of optical properties owned by crystalline dielectrics can be investigated on its basis.

[30]For an illustration of what has been said, consider e.g. figure 3.4.2

Chapter 4

Macroscopic electromagnetic field in crystalline dielectrics and the dielectric tensor

When investigating electrostatic or electrodynamic phenomena in matter, one is usually not interested in the spatially rapidly varying *local* electromagnetic field, that is determined by the *microscopic* Maxwell equations. Instead, one considers the *macroscopic* electromagnetic field as well as *macroscopic* material parameters like e.g. the dielectric tensor, that only show a significant spatial variation on length scales that are large when compared to the (inter-) atomic length scale. This widely accepted perspective applies well when investigating optical phenomena in the visible spectral regime, but massively fails when studying x-ray related effects, of course [3]. The macroscopic electromagnetic field is obtained by solving the macroscopic Maxwell equations, the latter being commonly deduced from the microscopic ones by averaging the therein included quantities over a macroscopic but "physically infinitesimal" volume comprising many particles. However, this averaging procedure exhibits some shortcomings. On the one hand, it is purely phenomenological as the exclusion of the structure of the local electromagnetic field on the atomic length scale from the very outset does not allow to relate the dielectric tensor to the microscopic structure of the medium under consideration. On the other hand, this averaging procedure presupposes the neglect of non-local response effects when applied consistently, because averaging itself is non-local [2].

The procedure presented in this chapter for deriving the macroscopic electromagnetic field in crystalline dielectrics follows [23, 24] and avoids the subtle difficulties mentioned before. As the local electromagnetic field is known exactly (see (3.2.39) and (3.2.46)), the macroscopic field is readily deduced from this by means of a low-pass filtering procedure that solely retains the spatially slowly varying contribution of the local field. In this way, the dielectric tensor introduced in this chapter includes the microscopic material structure, so that the investigation of different non-local optical effects like natu-

ral optical activity or spatial dispersion induced birefringence is possible. Additionally it is shown, that the such derived macroscopic electromagnetic field obeys to the differential equations of macroscopic electrodynamics.

Finally it should be stressed, that the exposition of the macroscopic electromagnetic theory presented in this chapter solely makes use of the macroscopic electric and magnetic induction field $\mathscr{E}(\mathbf{r},\omega)$ or $\mathscr{B}(\mathbf{r},\omega)$ instead of displacement and magnetic field $\mathscr{D}(\mathbf{r},\omega)$ and $\mathscr{H}(\mathbf{r},\omega)$, respectively. This approach is highly favorable, as the last two fields are *not* uniquely determined, so that they can *not* be taken as genuine physical fields (see [25, 29]).

4.1 Derivation of the macroscopic electromagnetic field equations and the dielectric tensor

As has been shown in section 3.4 and in particular in figure 3.4.2, the *local* electric field component $E_a(\mathbf{r},\omega)$ given by (3.2.39) comprises rapid spatial variations due to $e^{i\mathbf{G}\cdot\mathbf{r}}$ for $\mathbf{G}\in\Lambda^{-1}\setminus\{\mathbf{0}\}$ on the back of the slowly varying envelope $e^{i\mathbf{q}\cdot\mathbf{r}}$ with $\mathbf{q}\in C_{\Lambda^{-1}}$. It is exactly this slowly varying envelope, which represents the *macroscopic* electric field component $\mathscr{E}_a(\mathbf{r},\omega)$, that obeys to the *macroscopic* Maxwell equations, as is shown in section 4.2. But first, $\mathscr{E}_a(\mathbf{r},\omega)$ has to be derived from the exact local electric field $E_a(\mathbf{r},\omega)$. Therefore, the macroscopic field is conceived as the low-pass filtered local field [24], where the filtering process can be easily realized by means of Fourier transform methods. While

$$\tilde{E}_a(\mathbf{k},\omega)=\int_{\mathbb{R}^3} d^3r\, e^{-i\mathbf{k}\cdot\mathbf{r}}E_a(\mathbf{r},\omega) \tag{4.1.1}$$

with $\mathbf{k}\in\mathbb{R}^3$ denotes the Fourier amplitude of the local electric field, its low-pass filtered Fourier amplitude which likewise constitutes the Fourier amplitude of the macroscopic electric field, is defined by

$$\tilde{\mathscr{E}}_a(\mathbf{q},\omega)=\int_{\mathbb{R}^3} d^3r\, e^{-i\mathbf{q}\cdot\mathbf{r}}E_a(\mathbf{r},\omega)\quad\text{with}\quad\mathbf{q}\in C_{\Lambda^{-1}}, \tag{4.1.2}$$

so that

$$\mathscr{E}_a(\mathbf{r},\omega)=\frac{1}{(2\pi)^3}\int_{C_{\Lambda^{-1}}} d^3q\, e^{i\mathbf{q}\cdot\mathbf{r}}\tilde{\mathscr{E}}_a(\mathbf{q},\omega). \tag{4.1.3}$$

The requirement $\mathbf{q}\in C_{\Lambda^{-1}}$ in (4.1.2) or (4.1.3) ensures, that one gets rid of the rapid spatial variations of $E_a(\mathbf{r},\omega)$ caused by reciprocal lattice vectors $\mathbf{G}\in\Lambda^{-1}\setminus\{\mathbf{0}\}$, while its slowly varying envelope is

preserved. Combining (3.2.39) and (4.1.2) yields

$$\begin{aligned}
&\tilde{\mathscr{E}}_a(\mathbf{q},\omega)\\
&=\int_{\mathbb{R}^3} d^3r\, e^{-i\mathbf{q}\cdot\mathbf{r}}\left[\tilde{E}^{(\mathrm{ext})}_{\mathbf{q}'\omega,a}e^{i\mathbf{q}'\cdot\mathbf{r}}+\frac{1}{|C_\Lambda|}\sum_{b,d=1}^{3}\sum_{\mathbf{G}\in\Lambda^{-1}} e^{i(\mathbf{q}'+\mathbf{G})\cdot\mathbf{r}}\tilde{\mathscr{G}}_{ab}\left(\mathbf{q}'+\mathbf{G},\omega\right)\tilde{K}_{bd}\left(\mathbf{G},\mathbf{q}',\omega\right)\tilde{E}^{(\mathrm{ext})}_{\mathbf{q}'\omega,d}\right]\\
&=(2\pi)^3\,\delta\left(\mathbf{q}-\mathbf{q}'\right)\left[\tilde{E}^{(\mathrm{ext})}_{\mathbf{q}'\omega,a}+\frac{1}{|C_\Lambda|}\sum_{b,d=1}^{3}\tilde{\mathscr{G}}_{ab}\left(\mathbf{q}',\omega\right)\tilde{K}_{bd}\left(\mathbf{0},\mathbf{q}',\omega\right)\tilde{E}^{(\mathrm{ext})}_{\mathbf{q}'\omega,d}\right],
\end{aligned}\tag{4.1.4}$$

where in the last line use has been made of $\mathbf{q},\mathbf{q}'\in C_{\Lambda^{-1}}$. Introducing the abbreviation

$$\tilde{K}_{bd}\left(\mathbf{q}',\omega\right)\equiv\tilde{K}_{bd}\left(\mathbf{0},\mathbf{q}',\omega\right)\overset{(3.2.38)}{=}\frac{1}{\varepsilon_0}\sum_{c=1}^{3}\sum_{j,j',j''=1}^{M}\alpha^{(j,j')}_{bc}\left(\mathbf{q}',\omega\right)\left[\left(\delta-\Gamma\left(\mathbf{q}',\omega\right)\right)^{-1}\right]^{(j'j'')}_{cd},\tag{4.1.5}$$

the Fourier amplitude of the macroscopic electric field finally reads

$$\tilde{\mathscr{E}}_a(\mathbf{q},\omega)=(2\pi)^3\,\delta\left(\mathbf{q}-\mathbf{q}'\right)\sum_{d=1}^{3}\left[\delta_{ad}+\frac{1}{|C_\Lambda|}\sum_{b=1}^{3}\tilde{\mathscr{G}}_{ab}(\mathbf{q},\omega)\,\tilde{K}_{bd}(\mathbf{q},\omega)\right]\tilde{E}^{(\mathrm{ext})}_{\mathbf{q}\omega,d}.\tag{4.1.6}$$

Consequently, the macroscopic electric field $\mathscr{E}_a(\mathbf{r},\omega)$ in real space is readily obtained from (4.1.3) according to

$$\mathscr{E}_a(\mathbf{r},\omega)=\sum_{d=1}^{3}\left[\delta_{ad}+\frac{1}{|C_\Lambda|}\sum_{b=1}^{3}\tilde{\mathscr{G}}_{ab}(\mathbf{q},\omega)\,\tilde{K}_{bd}(\mathbf{q},\omega)\right]\tilde{E}^{(\mathrm{ext})}_{\mathbf{q}\omega,d}e^{i\mathbf{q}\cdot\mathbf{r}}.\tag{4.1.7}$$

With regard to the discussion of electromagnetic wave propagation, it is useful to decompose $\mathscr{E}_a(\mathbf{r},\omega)$ into its longitudinal and transverse contributions to identify the non-radiative and radiative parts of the macroscopic electric field, yielding

$$\mathscr{E}^{(\mathrm{L})}_a(\mathbf{r},\omega)=\sum_{d=1}^{3}\left[\tilde{\Pi}^{(\mathrm{L})}_{ad}(\mathbf{q})-\frac{1}{|C_\Lambda|}\sum_{c=1}^{3}\tilde{\Pi}^{(\mathrm{L})}_{ac}(\mathbf{q})\,\tilde{K}_{cd}(\mathbf{q},\omega)\right]\tilde{E}^{(\mathrm{ext})}_{\mathbf{q}\omega,d}e^{i\mathbf{q}\cdot\mathbf{r}}\tag{4.1.8}$$

$$\mathscr{E}^{(\mathrm{T})}_a(\mathbf{r},\omega)=\sum_{d=1}^{3}\left[\tilde{\Pi}^{(\mathrm{T})}_{ad}(\mathbf{q})+\frac{1}{|C_\Lambda|}\frac{\omega^2}{c^2}\frac{1}{|\mathbf{q}|^2-\frac{\omega^2}{c^2}}\sum_{c=1}^{3}\tilde{\Pi}^{(\mathrm{T})}_{ac}(\mathbf{q})\,\tilde{K}_{cd}(\mathbf{q},\omega)\right]\tilde{E}^{(\mathrm{ext})}_{\mathbf{q}\omega,d}e^{i\mathbf{q}\cdot\mathbf{r}}.\tag{4.1.9}$$

Applying the afore introduced low-pass filtering process to the *microscopic* polarization component $P_a(\mathbf{r},\omega)$ given by (3.1.5), one obtains the *macroscopic* polarization component $\mathscr{P}_a(\mathbf{r},\omega)$ that enters the *macroscopic* Maxwell equations. It is derived in analogy to the macroscopic electric field by first calculating the low-pass filtered Fourier amplitude

$$\tilde{\mathscr{P}}_a(\mathbf{q},\omega)=\int_{\mathbb{R}^3}d^3r\,e^{-i\mathbf{q}\cdot\mathbf{r}}P_a(\mathbf{r},\omega)\quad\text{with}\quad\mathbf{q}\in C_{\Lambda^{-1}}\tag{4.1.10}$$

and subsequent evaluation of

$$\mathscr{P}_a(\mathbf{r},\omega) = \frac{1}{(2\pi)^3}\int_{C_{\Lambda^{-1}}} d^3q\, e^{i\mathbf{q}\cdot\mathbf{r}}\,\tilde{\mathscr{P}}_a(\mathbf{q},\omega)\,. \tag{4.1.11}$$

The result of this procedure is given by

$$\tilde{\mathscr{P}}_a(\mathbf{q},\omega) = \varepsilon_0\frac{(2\pi)^3}{|C_\Lambda|}\delta\left(\mathbf{q}-\mathbf{q}'\right)\sum_{d=1}^{3}\tilde{K}_{ad}(\mathbf{q},\omega)\,\tilde{E}^{(\mathrm{ext})}_{\mathbf{q}\omega,d} \tag{4.1.12}$$

and

$$\mathscr{P}_a(\mathbf{r},\omega) = \frac{\varepsilon_0}{|C_\Lambda|}\sum_{d=1}^{3}\tilde{K}_{ad}(\mathbf{q},\omega)\,\tilde{E}^{(\mathrm{ext})}_{\mathbf{q}\omega,d}e^{i\mathbf{q}\cdot\mathbf{r}} \tag{4.1.13}$$

respectively[1]. With the help of (4.1.13), the macroscopic electric field (4.1.7) can be cast into

$$\mathscr{E}_a(\mathbf{r},\omega) = \underbrace{\tilde{E}^{(\mathrm{ext})}_{\mathbf{q}\omega,a}e^{i\mathbf{q}\cdot\mathbf{r}}}_{\equiv E_{\mathrm{ext},a}(\mathbf{r},\omega)} + \frac{1}{\varepsilon_0}\sum_{b=1}^{3}\tilde{\mathscr{G}}_{ab}(\mathbf{q},\omega)\,\mathscr{P}_b(\mathbf{r},\omega)\,, \tag{4.1.14}$$

which reflects Lorentz's well-known local field correction[2]. Introducing the dielectric 3×3 tensor $\varepsilon_\Lambda(\mathbf{q},\omega)$, a relation between the Fourier amplitudes of the macroscopic electric field $\tilde{\mathscr{E}}_a(\mathbf{q},\omega)$ and the macroscopic polarization $\tilde{\mathscr{P}}_a(\mathbf{q},\omega)$ can be established in the common way owed to macroscopic electrodynamics

$$\tilde{\mathscr{P}}_a(\mathbf{q},\omega) = \varepsilon_0\sum_{b=1}^{3}\left(\varepsilon_\Lambda(\mathbf{q},\omega)-\delta\right)_{ab}\tilde{\mathscr{E}}_b(\mathbf{q},\omega)\,. \tag{4.1.15}$$

Notice, while (4.1.15) is local in reciprocal space, it is non-local in real space. Thus, the dielectric tensor in real space does not solely depend on a single reference point $\mathbf{r}$, but also on its environment. Inserting (4.1.6) and (4.1.12) into (4.1.15) readily yields (in matrix notation)

$$\frac{1}{|C_\Lambda|}\tilde{K}(\mathbf{q},\omega)\cdot\tilde{\mathbf{E}}^{(\mathrm{ext})}_{\mathbf{q}\omega} = \left(\varepsilon_\Lambda(\mathbf{q},\omega)-\delta\right)\cdot\left[\delta+\frac{1}{|C_\Lambda|}\tilde{\mathscr{G}}(\mathbf{q},\omega)\cdot\tilde{K}(\mathbf{q},\omega)\right]\cdot\tilde{\mathbf{E}}^{(\mathrm{ext})}_{\mathbf{q}\omega}, \tag{4.1.16}$$

[1] For calculational details, see appendix E.5.

[2] In appendix G.2 it is shown, that for a simple cubic lattice $\tilde{\mathscr{G}}_{ab}(\mathbf{q},\omega)$ reduces in the static limit (i.e. when $\omega\to 0$ and $|\mathbf{q}|\to 0$) to the famous prefactor $-\frac{1}{3}\delta_{ab}$. In this case, (4.1.14) becomes

$$\mathscr{E}(\mathbf{r}) = \tilde{\mathbf{E}}_{\mathrm{ext}} - \frac{1}{3}\frac{1}{\varepsilon_0}\mathscr{P}(\mathbf{r})$$

and is thus in total agreement with [58]. Additionally it should be emphasized, that in the present theory there was no need to construct a Lorentz sphere or any other equivalent volume (see e.g. [3, 58]) to obtain this well-known result.

so that the dielectric tensor is identified as (see also [23])

$$\begin{aligned}\varepsilon_\Lambda(\mathbf{q},\omega) &= \delta + \frac{1}{|C_\Lambda|}\tilde{K}(\mathbf{q},\omega)\cdot\left[\delta + \frac{1}{|C_\Lambda|}\tilde{\mathscr{G}}(\mathbf{q},\omega)\cdot\tilde{K}(\mathbf{q},\omega)\right]^{-1} \\ &= \delta + \frac{1}{|C_\Lambda|}\left[\tilde{K}^{-1}(\mathbf{q},\omega) + \frac{1}{|C_\Lambda|}\tilde{\mathscr{G}}(\mathbf{q},\omega)\right]^{-1}. \end{aligned} \tag{4.1.17}$$

It should be emphasized, that $\varepsilon_\Lambda(\mathbf{q},\omega)$ solely depends on the crystal structure via the lattice sums and on the individual electronic and ionic displacement polarizabilities. For a thorough discussion of the dielectric tensor including chromatic and spatial dispersion effects represented by its arguments ω and $\mathbf{q}$, see section 4.4.

Last but not least, the induced macroscopic magnetic induction field $\mathscr{B}_a(\mathbf{r},\omega)$ emerges by low-pass filtering the induced local magnetic induction field $B_a(\mathbf{r},\omega)$ given by (3.2.46) according to

$$\begin{aligned}\tilde{\mathscr{B}}_a(\mathbf{q},\omega) &= \int_{\mathbb{R}^3} d^3r\, e^{-i\mathbf{q}\cdot\mathbf{r}} B_a(\mathbf{r},\omega) \quad \text{with} \quad \mathbf{q}\in C_{\Lambda^{-1}} \\ &= \frac{(2\pi)^3}{\omega}\delta(\mathbf{q}-\mathbf{q}')\sum_{b,c,d=1}^{3}\varepsilon_{abc}q_b\left[\delta_{cd} + \frac{1}{|C_\Lambda|}\sum_{e=1}^{3}\tilde{\mathscr{G}}_{ce}(\mathbf{q},\omega)\tilde{K}_{ed}(\mathbf{q},\omega)\right]\tilde{E}^{(\mathrm{ext})}_{\mathbf{q}\omega,d}, \end{aligned} \tag{4.1.18}$$

so that finally in real space

$$\begin{aligned}\mathscr{B}_a(\mathbf{r},\omega) &= \frac{1}{(2\pi)^3}\int_{C_{\Lambda^{-1}}} d^3q\, e^{i\mathbf{q}\cdot\mathbf{r}}\tilde{\mathscr{B}}_a(\mathbf{q},\omega) \\ &= \frac{1}{\omega}\sum_{b,c,d=1}^{3}\varepsilon_{abc}q_b\left[\delta_{cd} + \frac{1}{|C_\Lambda|}\sum_{e=1}^{3}\tilde{\mathscr{G}}_{ce}(\mathbf{q},\omega)\tilde{K}_{ed}(\mathbf{q},\omega)\right]\tilde{E}^{(\mathrm{ext})}_{\mathbf{q}\omega,d}e^{i\mathbf{q}\cdot\mathbf{r}} \\ &= \frac{1}{i\omega}\sum_{b,c=1}^{3}\varepsilon_{abc}\frac{\partial}{\partial r_b}\mathscr{E}_c(\mathbf{r},\omega) \end{aligned} \tag{4.1.19}$$

results.

In the presented theory, the macroscopic electromagnetic field naturally emerges by filtering out the rapid spatial variations of the local electromagnetic field appearing on a microscopic length scale set by the lattice constant a_Λ, while the local field's slowly varying envelope, whose length scale is set by the wavelength of the externally applied electric field, is maintained. As the local fields $E_a(\mathbf{r},\omega)$ and $B_a(\mathbf{r},\omega)$ constitute solutions of the microscopic Maxwell equations, the in this manner identified macroscopic fields $\mathscr{E}_a(\mathbf{r},\omega)$ and $\mathscr{B}_a(\mathbf{r},\omega)$ should obey to the common differential equations deduced from macroscopic Maxwell equations for reasons of consistency. This issue will be addressed in the next section.

4.2 Deducing the differential equations of macroscopic electrodynamics

When one is dealing with materials corresponding to (non-magnetic) crystalline dielectrics, the local electromagnetic field represented by $E_a(\mathbf{r},\omega)$ and $B_a(\mathbf{r},\omega)$ (see (3.2.39) and (3.2.46)) respectively, constitutes the solution of the microscopic Maxwell equations (2.1.10)-(2.1.13). If the presented theory is taken seriously, then the macroscopic electromagnetic field represented by $\mathscr{E}_a(\mathbf{r},\omega)$ and $\mathscr{B}_a(\mathbf{r},\omega)$, which are given by (4.1.7) or (4.1.19), should correspond to the macroscopic Maxwell fields (see [24]). To check this consistency requirement, start with the Fourier transform of (4.1.14) from real to reciprocal space and subsequently deploy (4.1.15), yielding[3]

$$\tilde{\mathscr{E}}_a(\mathbf{q},\omega) = \tilde{E}_{\mathrm{ext},a}(\mathbf{q},\omega) + \sum_{b,c=1}^{3} \tilde{\mathscr{G}}_{ab}(\mathbf{q},\omega)\left(\varepsilon_\Lambda(\mathbf{q},\omega)-\delta\right)_{bc}\tilde{\mathscr{E}}_c(\mathbf{q},\omega). \tag{4.2.1}$$

In general, according to (2.2.5), (2.2.7) and (2.2.13), the externally applied electric field in real space reads

$$E_{\mathrm{ext},a}(\mathbf{r},\omega) = \frac{1}{\varepsilon_0}\frac{1}{i\omega} j^{(\mathrm{L})}_{\mathrm{ext},a}(\mathbf{r},\omega) + i\omega\mu_0 \int_{\mathbb{R}^3} d^3r'\, g\left(\mathbf{r}-\mathbf{r}',\omega\right) j^{(\mathrm{T})}_{\mathrm{ext},a}\left(\mathbf{r}',\omega\right) \tag{4.2.2}$$

and is thus given in reciprocal space by

$$\begin{aligned}\tilde{E}_{\mathrm{ext},a}(\mathbf{q},\omega) &= \frac{1}{\varepsilon_0}\frac{1}{i\omega}\tilde{j}^{(\mathrm{L})}_{\mathrm{ext},a}(\mathbf{q},\omega) + i\omega\mu_0\tilde{g}(\mathbf{q},\omega)\,\tilde{j}^{(\mathrm{T})}_{\mathrm{ext},a}(\mathbf{q},\omega)\\ &= -\frac{1}{\varepsilon_0}\frac{1}{i\omega}\sum_{b=1}^{3}\tilde{\mathscr{G}}_{ab}(\mathbf{q},\omega)\,\tilde{j}_{\mathrm{ext},b}(\mathbf{q},\omega),\end{aligned} \tag{4.2.3}$$

where $\tilde{g}(\mathbf{q},\omega) = \frac{1}{|\mathbf{q}|^2-\frac{\omega^2}{c^2}}$ denotes the Fourier transform of the Helmholtz propagator $g(\mathbf{r}-\mathbf{r}',\omega)$. Additionally, in the second line use has been made of (2.2.17). Insertion of (4.2.3) into (4.2.1) and subsequent multiplication from the left hand side by

$$\left[\tilde{\mathscr{G}}^{-1}(\mathbf{q},\omega)\right]_{ab} = \frac{c^2}{\omega^2}|\mathbf{q}|^2\tilde{\Pi}^{(\mathrm{T})}_{ab}(\mathbf{q}) - \delta_{ab} \tag{4.2.4}$$

readily results in

$$\sum_{b=1}^{3}\left[\tilde{\mathscr{G}}^{-1}(\mathbf{q},\omega)\right]_{ab}\tilde{\mathscr{E}}_b(\mathbf{q},\omega) = -\frac{1}{\varepsilon_0}\frac{1}{i\omega}\tilde{j}_{\mathrm{ext},a}(\mathbf{q},\omega) + \sum_{b=1}^{3}\left(\varepsilon_\Lambda(\mathbf{q},\omega)-\delta\right)_{ab}\tilde{\mathscr{E}}_b(\mathbf{q},\omega), \tag{4.2.5}$$

which is equivalent to

$$\sum_{b=1}^{3}\left[|\mathbf{q}|^2\tilde{\Pi}^{(\mathrm{T})}(\mathbf{q}) - \frac{\omega^2}{c^2}\varepsilon_\Lambda(\mathbf{q},\omega)\right]_{ab}\tilde{\mathscr{E}}_b(\mathbf{q},\omega) = i\omega\mu_0\tilde{j}_{\mathrm{ext},a}(\mathbf{q},\omega). \tag{4.2.6}$$

[3] Recall, that $\tilde{E}_{\mathrm{ext},a}(\mathbf{q},\omega)$ denotes the Fourier transform of $E_{\mathrm{ext},a}(\mathbf{r},\omega)$.

It should be noticed that (4.2.6) represents the so-called vector wave equation for the macroscopic electric field in reciprocal space, provided that spatial dispersion can be ignored, i.e. if $\varepsilon_\Lambda(\mathbf{q},\omega) \to \varepsilon_\Lambda(\omega)$. As $|\mathbf{q}|^2 \leftrightarrow -\nabla_\mathbf{r}^2$ and $-\nabla_\mathbf{r}^2 \mathscr{E}^{(\mathrm{T})}(\mathbf{r},\omega) = \nabla_\mathbf{r} \times \nabla_\mathbf{r} \times \mathscr{E}(\mathbf{r},\omega)$, in this special case (4.2.6) can directly be rewritten in real space according to

$$\nabla_\mathbf{r} \times \nabla_\mathbf{r} \times \mathscr{E}(\mathbf{r},\omega) - \frac{\omega^2}{c^2}\varepsilon_\Lambda(\omega) \cdot \mathscr{E}(\mathbf{r},\omega) = i\omega\mu_0 \mathbf{j}_\mathrm{ext}(\mathbf{r},\omega). \tag{4.2.7}$$

It should be stressed, that the interpretation of (4.2.7) as a wave equation describing the propagation of photons is misleading, because of $\mathscr{E}(\mathbf{r},\omega) = \mathscr{E}^{(\mathrm{L})}(\mathbf{r},\omega) + \mathscr{E}^{(\mathrm{T})}(\mathbf{r},\omega)$ the macroscopic electric field $\mathscr{E}(\mathbf{r},\omega)$ may still exhibit non-radiative contributions determined by its curl-free part $\mathscr{E}^{(\mathrm{L})}(\mathbf{r},\omega)$. To find the respective differential equations determining the longitudinal or transverse macroscopic electric field alone, the *general* equation (4.2.6) has to be decomposed into its longitudinal and transverse parts first. By means of the Helmholtz decomposition of vector fields as well as the following block matrix notation for the longitudinal and transverse projections of the dielectric tensor

$$\varepsilon_{ab}^{(A,B)}(\mathbf{q},\omega) = \sum_{c,d=1}^{3} \tilde{\Pi}_{ac}^{(A)}(\mathbf{q}) \left[\varepsilon_\Lambda(\mathbf{q},\omega)\right]_{cd} \tilde{\Pi}_{db}^{(B)}(\mathbf{q}) \quad \text{with} \quad A,B \in \{\mathrm{L},\mathrm{T}\}, \tag{4.2.8}$$

(4.2.6) can be cast into

$$\begin{aligned} &|\mathbf{q}|^2 \tilde{\mathscr{E}}_a^{(\mathrm{T})}(\mathbf{q},\omega) - \frac{\omega^2}{c^2}\sum_{b=1}^{3}\left[\varepsilon^{(\mathrm{L,L})} + \varepsilon^{(\mathrm{L,T})} + \varepsilon^{(\mathrm{T,L})} + \varepsilon^{(\mathrm{T,T})}\right]_{ab}(\mathbf{q},\omega)\left(\tilde{\mathscr{E}}_b^{(\mathrm{L})}(\mathbf{q},\omega) + \tilde{\mathscr{E}}_b^{(\mathrm{T})}(\mathbf{q},\omega)\right) \\ =&i\omega\mu_0\left(\tilde{j}_{\mathrm{ext},a}^{(\mathrm{L})}(\mathbf{q},\omega) + \tilde{j}_{\mathrm{ext},a}^{(\mathrm{T})}(\mathbf{q},\omega)\right), \end{aligned} \tag{4.2.9}$$

where $\tilde{\Pi}_{ab}^{(\mathrm{L})}(\mathbf{q}) + \tilde{\Pi}_{ab}^{(\mathrm{T})}(\mathbf{q}) = \delta_{ab}$ has been utilized. As longitudinal and transverse fields are orthogonal, (4.2.9) can now easily be separated into one longitudinal and one transverse equation according to

$$-\frac{\omega^2}{c^2}\sum_{b=1}^{3}\left[\varepsilon_{ab}^{(\mathrm{L,L})}(\mathbf{q},\omega)\,\tilde{\mathscr{E}}_b^{(\mathrm{L})}(\mathbf{q},\omega) + \varepsilon_{ab}^{(\mathrm{L,T})}(\mathbf{q},\omega)\,\tilde{\mathscr{E}}_b^{(\mathrm{T})}(\mathbf{q},\omega)\right] = i\omega\mu_0 \tilde{j}_{\mathrm{ext},a}^{(\mathrm{L})}(\mathbf{q},\omega) \tag{4.2.10}$$

$$\sum_{b=1}^{3}\left[|\mathbf{q}|^2\delta_{ab} - \frac{\omega^2}{c^2}\varepsilon_{ab}^{(\mathrm{T,T})}(\mathbf{q},\omega)\right]\tilde{\mathscr{E}}_b^{(\mathrm{T})}(\mathbf{q},\omega) - \frac{\omega^2}{c^2}\sum_{b=1}^{3}\varepsilon_{ab}^{(\mathrm{T,L})}(\mathbf{q},\omega)\,\tilde{\mathscr{E}}_b^{(\mathrm{L})}(\mathbf{q},\omega) = i\omega\mu_0 \tilde{j}_{\mathrm{ext},a}^{(\mathrm{T})}(\mathbf{q},\omega). \tag{4.2.11}$$

Under which requirements the equations (4.2.10) and (4.2.11) correspond to differential equations that can be deduced from macroscopic Maxwell equations for the longitudinal and transverse electric field, will be elaborated in the next two subsections.

Finally regarding the macroscopic magnetic induction field $\mathscr{B}(\mathbf{r},\omega)$, the situation turns out to be simpler than in the case of the electric field, because of (4.1.19) it can be easily calculated from the macro-

scopic electric field by the induction law

$$i\omega\mathscr{B}(\mathbf{r},\omega)=\nabla_{\mathbf{r}}\times\mathscr{E}(\mathbf{r},\omega) \tag{4.2.12}$$

and thus inherently satisfies $\nabla_{\mathbf{r}}\cdot\mathscr{B}(\mathbf{r},\omega)=0$.

4.2.1 Electric field screening

Assuming a purely longitudinal external current density, i.e. $\tilde{j}^{(\mathrm{T})}_{\mathrm{ext},a}(\mathbf{q},\omega)=0$, (4.2.11) allows to solve for the transverse macroscopic electric field according to

$$\tilde{\mathscr{E}}^{(\mathrm{T})}_a(\mathbf{q},\omega)=\sum_{b,c=1}^{3}\left[\frac{\frac{\omega^2}{c^2}}{|\mathbf{q}|^2\,\delta-\frac{\omega^2}{c^2}\varepsilon^{(\mathrm{T,T})}(\mathbf{q},\omega)}\right]_{ab}\varepsilon^{(\mathrm{T,L})}_{bc}(\mathbf{q},\omega)\,\tilde{\mathscr{E}}^{(\mathrm{L})}_c(\mathbf{q},\omega), \tag{4.2.13}$$

provided that $\det\left(|\mathbf{q}|^2\,\delta-\frac{\omega^2}{c^2}\varepsilon^{(\mathrm{T,T})}(\mathbf{q},\omega)\right)\neq 0$. Defining the longitudinal dielectric tensor by

$$\varepsilon^{(\mathrm{L})}(\mathbf{q},\omega)=\varepsilon^{(\mathrm{L,L})}(\mathbf{q},\omega)+\varepsilon^{(\mathrm{L,T})}(\mathbf{q},\omega)\circ\frac{\frac{\omega^2}{c^2}}{|\mathbf{q}|^2\,\delta-\frac{\omega^2}{c^2}\varepsilon^{(\mathrm{T,T})}(\mathbf{q},\omega)}\circ\varepsilon^{(\mathrm{T,L})}(\mathbf{q},\omega), \tag{4.2.14}$$

there follows from (4.2.10) by eliminating $\tilde{\mathscr{E}}^{(\mathrm{T})}_a(\mathbf{q},\omega)$ by means of (4.2.13)

$$\sum_{b=1}^{3}\varepsilon^{(\mathrm{L})}_{ab}(\mathbf{q},\omega)\,\tilde{\mathscr{E}}^{(\mathrm{L})}_b(\mathbf{q},\omega)=-\frac{c^2}{\omega}i\mu_0\tilde{j}^{(\mathrm{L})}_{\mathrm{ext},a}(\mathbf{q},\omega), \tag{4.2.15}$$

so that subsequent multiplication with iq_a and summation over $a\in\{1,2,3\}$ reveals

$$\sum_{a,b=1}^{3}iq_a\varepsilon^{(\mathrm{L})}_{ab}(\mathbf{q},\omega)\,\tilde{\mathscr{E}}^{(\mathrm{L})}_b(\mathbf{q},\omega)=\frac{1}{\varepsilon_0}\tilde{\rho}_{\mathrm{ext}}(\mathbf{q},\omega), \tag{4.2.16}$$

where $c^2=\frac{1}{\varepsilon_0\mu_0}$ as well as the continuity equation $\mathbf{q}\cdot\tilde{\mathbf{j}}^{(\mathrm{L})}_{\mathrm{ext}}(\mathbf{q},\omega)=\omega\tilde{\rho}_{\mathrm{ext}}(\mathbf{q},\omega)$ (see (2.2.2)) have been deployed. Equation (4.2.16) determines in a very general manner the longitudinal macroscopic electric field $\tilde{\mathscr{E}}^{(\mathrm{L})}(\mathbf{q},\omega)$ in reciprocal space in terms of the external charge density $\tilde{\rho}_{\mathrm{ext}}(\mathbf{q},\omega)$ and the longitudinal dielectric tensor $\varepsilon^{(\mathrm{L})}(\mathbf{q},\omega)$, the latter describing electric field screening for all frequencies.

At rather low frequencies there holds the approximation $\varepsilon^{(\mathrm{L})}(\mathbf{q},\omega)\approx\varepsilon^{(\mathrm{L,L})}(\mathbf{q},\omega)$, so that from (4.2.16)

$$\sum_{a,b=1}^{3}iq_a\left[\varepsilon_\Lambda(\mathbf{q},\omega)\right]_{ab}\tilde{\mathscr{E}}^{(\mathrm{L})}_b(\mathbf{q},\omega)=\frac{1}{\varepsilon_0}\tilde{\rho}_{\mathrm{ext}}(\mathbf{q},\omega) \tag{4.2.17}$$

is obtained by invoking (4.2.8). Thus, in the low frequency limit, electric field screening is exactly described by the dielectric tensor $\varepsilon_\Lambda(\mathbf{q},\omega)$. Additionally, if spatial dispersion can be neglected, i.e. if

$\varepsilon_\Lambda(\mathbf{q},\omega) \to \varepsilon_\Lambda(\omega)$, (4.2.17) conforms in real space to the well-known equation

$$\nabla_{\mathbf{r}} \cdot \left(\varepsilon_\Lambda(\omega) \cdot \mathscr{E}^{(\mathrm{L})}(\mathbf{r},\omega) \right) = \frac{1}{\varepsilon_0} \rho_{\mathrm{ext}}(\mathbf{r},\omega). \tag{4.2.18}$$

With $\mathscr{E}^{(\mathrm{L})}(\mathbf{r},\omega) = -\nabla_{\mathbf{r}}\phi(\mathbf{r},\omega)$, (4.2.18) then assumes the guise of a Poisson type equation and it becomes manifest, that $\varepsilon_\Lambda(\omega)$ describes electric field screening similar to electrostatics.

4.2.2 Wave equation and the renormalized speed of light

If the external current density is purely transverse, i.e. $\tilde{j}^{(\mathrm{L})}_{\mathrm{ext},a}(\mathbf{q},\omega) = 0$, (4.2.10) allows to solve for the longitudinal macroscopic electric field according to

$$\tilde{\mathscr{E}}^{(\mathrm{L})}_a(\mathbf{q},\omega) = -\sum_{b,c=1}^{3} \left[\frac{1}{\varepsilon^{(\mathrm{L,L})}(\mathbf{q},\omega)} \right]_{ab} \varepsilon^{(\mathrm{L,T})}_{bc}(\mathbf{q},\omega)\, \tilde{\mathscr{E}}^{(\mathrm{T})}_c(\mathbf{q},\omega), \tag{4.2.19}$$

provided that $\det\left(\varepsilon^{(\mathrm{L,L})}(\mathbf{q},\omega)\right) \neq 0$. Introducing the transverse dielectric tensor by

$$\varepsilon^{(\mathrm{T})}(\mathbf{q},\omega) = \varepsilon^{(\mathrm{T,T})}(\mathbf{q},\omega) - \varepsilon^{(\mathrm{T,L})}(\mathbf{q},\omega) \circ \left[\frac{1}{\varepsilon^{(\mathrm{L,L})}(\mathbf{q},\omega)} \right] \circ \varepsilon^{(\mathrm{L,T})}(\mathbf{q},\omega), \tag{4.2.20}$$

there follows from (4.2.11) by eliminating $\tilde{\mathscr{E}}^{(\mathrm{L})}_a(\mathbf{q},\omega)$ by means of (4.2.19)

$$\sum_{b=1}^{3} \left(|\mathbf{q}|^2 \delta_{ab} - \frac{\omega^2}{c^2} \varepsilon^{(\mathrm{T})}_{ab}(\mathbf{q},\omega) \right) \tilde{\mathscr{E}}^{(\mathrm{T})}_b(\mathbf{q},\omega) = i\omega\mu_0 \tilde{j}^{(\mathrm{T})}_{\mathrm{ext},a}(\mathbf{q},\omega). \tag{4.2.21}$$

Equation (4.2.21) determines in a quite general way the transverse macroscopic electric field $\tilde{\mathscr{E}}^{(\mathrm{T})}(\mathbf{q},\omega)$ in reciprocal space in terms of the transverse external current density $\tilde{\mathbf{j}}^{(\mathrm{T})}_{\mathrm{ext}}(\mathbf{q},\omega)$ and the transverse dielectric tensor $\varepsilon^{(\mathrm{T})}(\mathbf{q},\omega)$, which renormalizes the propagation speed of an electromagnetic wave traversing a crystalline dielectric and that also includes a variety of optical effects[4]. The rather complicated structure of $\varepsilon^{(\mathrm{T})}(\mathbf{q},\omega)$ given by (4.2.20) is owed to the fact, that in general within a solid, a purely longitudinal electric field can induce a transverse current density and consequently a transverse electric field. Of course, the converse is also possible [59]. If for any reason this induction is *not* possible, then $\sum_{b=1}^{3} \varepsilon^{(\mathrm{T,L})}_{ab}(\mathbf{q},\omega)\, \tilde{\mathscr{E}}^{(\mathrm{L})}_b(\mathbf{q},\omega) = 0$ in (4.2.11), so that the transverse dielectric tensor assumes the simple guise $\varepsilon^{(\mathrm{T})}(\mathbf{q},\omega) = \varepsilon^{(\mathrm{T,T})}(\mathbf{q},\omega)$. Similarly, if $\sum_{b=1}^{3} \varepsilon^{(\mathrm{L,T})}_{ab}(\mathbf{q},\omega)\, \tilde{\mathscr{E}}^{(\mathrm{T})}_b(\mathbf{q},\omega) = 0$ in (4.2.10), the longitudinal dielectric tensor (4.2.14) reduces to $\varepsilon^{(\mathrm{L})}(\mathbf{q},\omega) = \varepsilon^{(\mathrm{L,L})}(\mathbf{q},\omega)$.

If spatial dispersion can be ignored, i.e. if $\varepsilon^{(\mathrm{T})}(\mathbf{q},\omega) \to \varepsilon^{(\mathrm{T})}(\omega)$, (4.2.21) conforms in real space to the

[4] For a thorough discussion of $\varepsilon^{(\mathrm{T})}(\mathbf{q},\omega)$, see section 4.4.3.

well-known wave equation

$$\sum_{b=1}^{3}\left(-\nabla_{\mathbf{r}}^{2}\delta_{ab}-\frac{\omega^{2}}{c^{2}}\varepsilon_{ab}^{(\mathrm{T})}(\omega)\right)\mathscr{E}_{b}^{(\mathrm{T})}(\mathbf{r},\omega)=i\omega\mu_{0}j_{\mathrm{ext},a}^{(\mathrm{T})}(\mathbf{r},\omega), \tag{4.2.22}$$

that determines the cartesian components of the transverse macroscopic electric field and is thus in full agreement with the standard theory of electromagnetic wave propagation in dielectric crystals. Finally, in view of the familiar and popularly accepted wave equation (4.2.22) it should be pointed out again, that it is the transverse dielectric tensor $\varepsilon^{(\mathrm{T})}(\mathbf{q},\omega)$ which governs wave propagation in crystalline dielectrics within the framework of macroscopic electrodynamics instead of $\varepsilon_{\Lambda}(\mathbf{q},\omega)$ and thus $\varepsilon^{(\mathrm{T})}(\mathbf{q},\omega)$ includes all optical effects originating from chromatic and spatial dispersion.

In this section it has been shown, that the macroscopic electromagnetic field which has been identified as the spatially low-pass filtered local electromagnetic field, obeys to differential equations that are commonly associated with those of macroscopic electrodynamics, whereas the presented approach provides a deeper insight into the radiative and non-radiative nature of the electromagnetic field in dielectric crystals as well as the correct macroscopic description of those materials by means of the longitudinal and transverse dielectric tensor. In the next section, the local field will be opposed to its associated macroscopic field in view of a possible starting point for a transport theory of radiation inside arbitrary (possibly disordered) materials.

4.3 Comparison of the local and macroscopic electromagnetic field

In this section, the macroscopic electric and magnetic induction fields $\mathscr{E}_{a}(\mathbf{r},\omega)$ and $\mathscr{B}_{a}(\mathbf{r},\omega)$ are calculated with the same parameters as the local electric and magnetic induction fields $E_{a}(\mathbf{r},\omega)$ and $B_{a}(\mathbf{r},\omega)$ for the setup shown in figure 3.4.1. This allows a direct comparison of the local and macroscopic fields and in consequence to highlight certain aspects, in which both descriptions are more or less equivalent and in which they may lead to quite different results.

Comparing the components of the local electric field $E_{a}(\mathbf{r},\omega)$ given by (3.2.39) with those of the macroscopic electric field $\mathscr{E}_{a}(\mathbf{r},\omega)$ determined by (4.1.7), enables to express $E_{a}(\mathbf{r},\omega)$ in terms of $\mathscr{E}_{a}(\mathbf{r},\omega)$ according to

$$E_{a}(\mathbf{r},\omega)=\mathscr{E}_{a}(\mathbf{r},\omega)+\delta E_{a}(\mathbf{r},\omega) \tag{4.3.1}$$

with

$$\delta E_{a}(\mathbf{r},\omega)=\frac{1}{|C_{\Lambda}|}\sum_{b,d=1}^{3}\sum_{\mathbf{G}\in\Lambda^{-1}\setminus\{\mathbf{0}\}}e^{i(\mathbf{q}+\mathbf{G})\cdot\mathbf{r}}\tilde{\mathscr{G}}_{ab}(\mathbf{q}+\mathbf{G},\omega)\,\tilde{K}_{bd}(\mathbf{G},\mathbf{q},\omega)\,\tilde{E}_{\mathbf{q}\omega,d}^{(\mathrm{ext})}. \tag{4.3.2}$$

Obviously, the local and macroscopic electric field differ by $\delta E_{a}(\mathbf{r},\omega)$, which represents the contribution of the sum over reciprocal lattice vectors $\mathbf{G}\in\Lambda^{-1}\setminus\{\mathbf{0}\}$. In figure 4.3.1 the spatial variation of the transverse local electric field $E_{z}^{(\mathrm{T})}(\mathbf{r},\omega)$ (as already displayed in figure 3.4.4) is compared to the spatial variation of its associated transverse macroscopic electric field $\mathscr{E}_{z}^{(\mathrm{T})}(\mathbf{r},\omega)$, revealing that

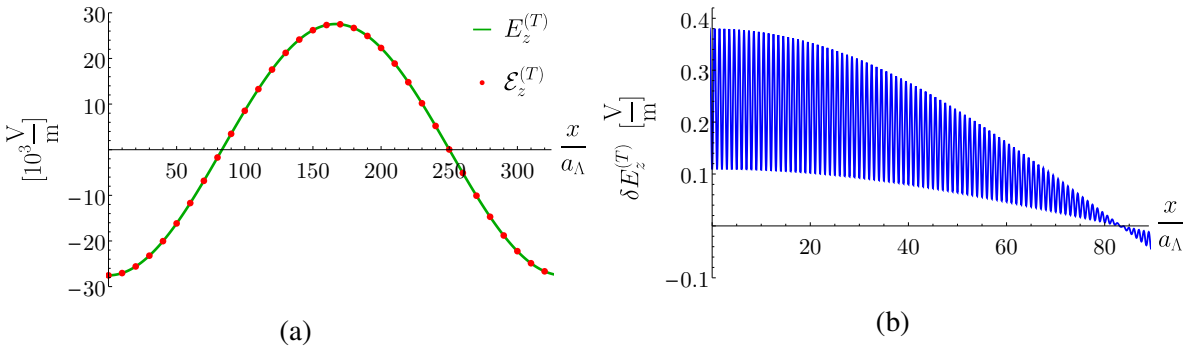

Figure 4.3.1: (a) Spatial variation of the z-components of the transverse local (green) and macroscopic (red) electric fields $E_z^{(\mathrm{T})}(\mathbf{r},\omega)$ and $\mathscr{E}_z^{(\mathrm{T})}(\mathbf{r},\omega)$ given by (3.2.42) and (4.1.9), respectively, for the same parameters as in figure 3.4.4. (b) Spatial variation of the residue $\delta E_z^{(\mathrm{T})}(\mathbf{r},\omega) = E_z^{(\mathrm{T})}(\mathbf{r},\omega) - \mathscr{E}_z^{(\mathrm{T})}(\mathbf{r},\omega)$, representing the $\mathbf{G} \in \Lambda^{-1}\setminus\{\mathbf{0}\}$ contributions of the lattice sum (compare with (4.3.2)).

both fields essentially coincide except for the residue $\delta E_z^{(\mathrm{T})}(\mathbf{r},\omega)$, which turns out to be smaller by a factor of 10^{-5} compared to the size of the original amplitudes $E_z^{(\mathrm{T})}(\mathbf{r},\omega)$ and $\mathscr{E}_z^{(\mathrm{T})}(\mathbf{r},\omega)$, respectively. This matter of fact reasons the success with which the macroscopic Maxwell fields have been applied to a multitude of problems concerning electromagnetic wave propagation in highly diverse media. Nonetheless, attention should be paid with respect to an uncritical usage of the macroscopic field equations instead of the local ones for the description of radiation processes. For instance, when one is establishing a transport theory of light intensity inside a (possibly disordered) material, the product $\delta E_a^{(\mathrm{T})}(\mathbf{r},\omega)\,\delta E_b^{(\mathrm{T})}(\mathbf{r}',\omega)$ may comprise a spatially slowly varying interference contribution, that can never be obtained by the product $\mathscr{E}_a^{(\mathrm{T})}(\mathbf{r},\omega)\,\mathscr{E}_b^{(\mathrm{T})}(\mathbf{r}',\omega)$ of two macroscopic fields. While the transverse local electric field is in well agreement with its associated transverse macroscopic electric field, there is a significant discrepancy with respect to the longitudinal fields. Just as the externally applied electric field $E_{\mathrm{ext},z}(\mathbf{r},\omega) = E_{\mathrm{ext},z}^{(\mathrm{T})}(\mathbf{r},\omega)$ is purely transverse in the setup under consideration, so is the macroscopic electric field in this case too, i.e. $\mathscr{E}_z(\mathbf{r},\omega) = \mathscr{E}_z^{(\mathrm{T})}(\mathbf{r},\omega)$. In contrast, the local electric field also exhibits a non-vanishing longitudinal contribution $E_z^{(\mathrm{L})}(\mathbf{r},\omega)$, whose magnitude essentially depends on the density ν_{P} of polarizable atoms inside the crystal (see figures 3.4.4 and 3.4.5). For instance, if one is interested to set up a theory for secure optical information transfer, it should be based on the local field description instead of the macroscopic one because the former allows to estimate the amount of information about the external signal, which is stored in the medium (e.g. in the glass fiber or in the receiver) in terms of the non-radiative longitudinal field.

Comparing the local magnetic induction field $B_a(\mathbf{r},\omega)$ given by (3.2.46) with the macroscopic magnetic induction field $\mathscr{B}_a(\mathbf{r},\omega)$ given by (4.1.19), enables to express $B_a(\mathbf{r},\omega)$ in terms of $\mathscr{B}_a(\mathbf{r},\omega)$ according to

$$B_a(\mathbf{r},\omega) = \mathscr{B}_a(\mathbf{r},\omega) + \delta B_a(\mathbf{r},\omega)\,, \tag{4.3.3}$$

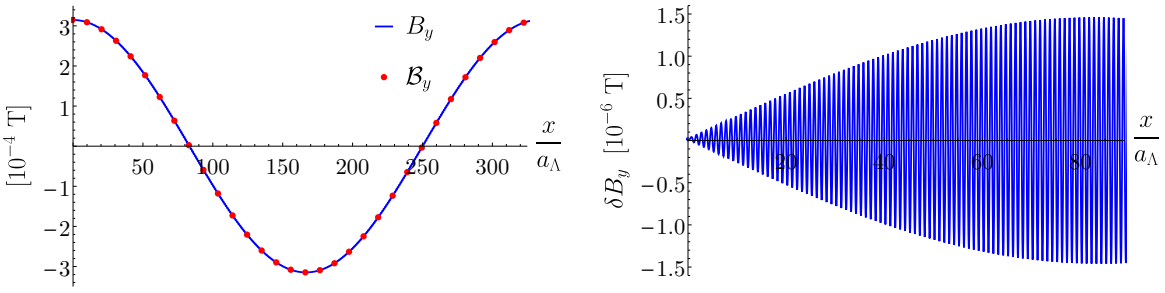

(a) (b)

Figure 4.3.2: (a) Spatial variation of the y-components of the local (blue) and macroscopic (red) magnetic induction fields $B_y(\mathbf{r},\omega)$ and $\mathscr{B}_y(\mathbf{r},\omega)$ given by (3.2.46) and (4.1.19), respectively, for the same parameters as in figure 3.4.2 (b). (b) Spatial variation of the residue $\delta B_y(\mathbf{r},\omega) = B_y(\mathbf{r},\omega) - \mathscr{B}_y(\mathbf{r},\omega)$, representing the $\mathbf{G} \in \Lambda^{-1}\setminus\{\mathbf{0}\}$ contribution of the lattice sum according to (4.3.4).

where

$$\delta B_a(\mathbf{r},\omega) = \frac{1}{\omega}\frac{1}{|C_\Lambda|}\sum_{b,c,d,e=1}^{3}\sum_{\mathbf{G}\in\Lambda^{-1}\setminus\{\mathbf{0}\}} \varepsilon_{abc}\,(q_b+G_b)\,e^{i(\mathbf{q}+\mathbf{G})\cdot\mathbf{r}}\tilde{\mathscr{G}}_{cd}(\mathbf{q}+\mathbf{G},\omega)\,\tilde{K}_{de}(\mathbf{G},\mathbf{q},\omega)\,\tilde{E}^{(\mathrm{ext})}_{\mathbf{q}\omega,e} \tag{4.3.4}$$

denotes again the contribution[5] of the sum over reciprocal lattice vectors $\mathbf{G} \in \Lambda^{-1}\setminus\{\mathbf{0}\}$. In figure 4.3.2 the spatial variation of the local magnetic induction field $B_y(\mathbf{r},\omega)$ calculated from (3.2.46) is compared to the spatial variation of its associated macroscopic magnetic induction field $\mathscr{B}_y(\mathbf{r},\omega)$ given by (4.1.19). Similar to the transverse electric field case, the local and macroscopic magnetic induction fields essentially coincide except for the residue $\delta B_y(\mathbf{r},\omega)$, which is smaller by a factor of $\frac{1}{200}$ when compared to the size of the original amplitudes $B_y(\mathbf{r},\omega)$ and $\mathscr{B}_y(\mathbf{r},\omega)$, respectively. Note, that in the electric field case the residue was even considerably smaller.

Obviously, the macroscopic radiation fields $\mathscr{E}^{(\mathrm{T})}_a(\mathbf{r},\omega)$ and $\mathscr{B}_a(\mathbf{r},\omega)$ represent very good approximate descriptions for the local radiation fields $E^{(\mathrm{T})}_a(\mathbf{r},\omega)$ and $B_a(\mathbf{r},\omega)$. Therefore, the next section deals with the optical properties of crystalline dielectrics that come along with the macroscopic description of electromagnetic wave propagation in this kind of materials.

4.4 Discussion of the dielectric tensor

In this section, the dielectric tensor $\varepsilon_\Lambda(\mathbf{q},\omega)$ given by (4.1.17), which reflects the material as well as the electromagnetic response within the framework of macroscopic electrodynamics, is calculated and discussed for a variety of diverse dielectric crystals, solely with the crystalline structure and the individual electronic and ionic polarizabilities as an input. Besides certain limiting cases that show agreement

[5] It should be noticed, that $\sum_{b,c=1}^{3}\varepsilon_{abc}k_b\tilde{\mathscr{G}}_{cd}(\mathbf{k},\omega) \sim \frac{\omega^2}{c^2}$. Hence, $\delta B_a(\mathbf{r},\omega)$ behaves well in the limit $\omega \to 0$.

with general considerations on stability and causality, various optical properties are discussed on basis of its derivative $\varepsilon^{(\mathrm{T})}(\mathbf{q},\omega)$. For a monograph on crystal optics from a phenomenological point of view, the reader is referred to [1].

4.4.1 Static limit of $\varepsilon_\Lambda(\mathbf{q},\omega)$ for monatomic Bravais lattices

Before discussing diverse effects incorporated into the dielectric tensor $\varepsilon_\Lambda(\mathbf{q},\omega)$ by its arguments $\mathbf{q}$ and ω that represent spatial or chromatic dispersion, it is reasonable to start with its analysis in the static limit and to check certain limiting cases which are related to a monatomic (i.e. $M=1$) crystal structure. Without loss of generality, the atom is assumed to be located at the origin $\eta^{(1)}=\mathbf{0}$ of the Wigner-Seitz cell C_Λ, so that with $\alpha_{ab}(\omega)\equiv\alpha_{ab}^{(1,1)}(\mathbf{q},\omega)$ (4.1.5) assumes the guise

$$\tilde{K}(\mathbf{q},\omega)=\frac{1}{\varepsilon_0}\alpha(\omega)\circ\left(\delta-\frac{1}{\varepsilon_0}\zeta_\Lambda^{(0)}(\mathbf{q},\omega)\circ\alpha(\omega)\right)^{-1}. \tag{4.4.1}$$

Then the dielectric tensor given by (4.1.17) reads

$$\varepsilon_\Lambda(\mathbf{q},\omega)=\delta+\frac{1}{|C_\Lambda|}\left[\varepsilon_0\alpha^{-1}(\omega)-\left(\zeta_\Lambda^{(0)}(\mathbf{q},\omega)-\frac{1}{|C_\Lambda|}\tilde{\mathscr{G}}(\mathbf{q},\omega)\right)\right]^{-1}, \tag{4.4.2}$$

where the lattice sum $\left(\zeta_\Lambda^{(0)}(\mathbf{q},\omega)-\frac{1}{|C_\Lambda|}\tilde{\mathscr{G}}(\mathbf{q},\omega)\right)$ is conveniently evaluated in the sense of Ewald's summation technique[6] [30–33]. It should be mentioned, that for simple cubic lattices the evaluation of $\left(\zeta_\Lambda^{(0)}(\mathbf{q},\omega)-\frac{1}{|C_\Lambda|}\tilde{\mathscr{G}}(\mathbf{q},\omega)\right)$ is also possible by means of Jacobi's third theta function $\vartheta_3(z,\tau)=\sum_{m=-\infty}^{\infty}e^{-m^2\pi\tau}e^{2\pi imz}$, which converges normally on $\left\{(z,\tau)\in\mathbb{C}^2:\mathrm{Re}(\tau)>0\right\}$ [39, 60, 61]. The static limit of the dielectric tensor (4.4.2) for monatomic crystal structures is then obtained by first taking $|\mathbf{q}|\to 0$ and subsequently $\omega\to 0$. Introducing the abbreviations

$$\begin{aligned}\varepsilon_\Lambda&\equiv\lim_{\omega\to 0}\lim_{|\mathbf{q}|\to 0}\varepsilon_\Lambda(\mathbf{q},\omega)\\ \alpha&\equiv\lim_{\omega\to 0}\alpha(\omega)\end{aligned} \tag{4.4.3}$$

and identifying the 3×3 Lorentz factor tensor by

$$\mathscr{L}=|C_\Lambda|\lim_{\omega\to 0}\lim_{|\mathbf{q}|\to 0}\left(\zeta_\Lambda^{(0)}(\mathbf{q},\omega)-\frac{1}{|C_\Lambda|}\tilde{\mathscr{G}}(\mathbf{q},\omega)\right), \tag{4.4.4}$$

[6] For details regarding a fast and precise numerical evaluation of the lattice sum $\zeta_\Lambda^{(0)}(\mathbf{q},\omega)$, see appendix F.2.2. The subtraction of the single term $\frac{1}{|C_\Lambda|}\tilde{\mathscr{G}}(\mathbf{q},\omega)$ from $\zeta_\Lambda^{(0)}(\mathbf{q},\omega)$ is straightforward and does not cause any difficulties.

the dielectric tensor (4.4.2) describing monatomic crystal structures can be written in the static limit as (see also [23])

$$\begin{aligned}\varepsilon_\Lambda &= \delta + \frac{1}{|C_\Lambda|}\left[\varepsilon_0\alpha^{-1} - \frac{1}{|C_\Lambda|}\mathscr{L}\right]^{-1} \\ &= \left(\delta + \frac{\nu_P}{\varepsilon_0}(\delta - \mathscr{L})\circ\alpha\right)\circ\left(\delta - \frac{\nu_P}{\varepsilon_0}\mathscr{L}\circ\alpha\right)^{-1},\end{aligned} \tag{4.4.5}$$

where in the second line the density of polarizable atoms has been identified as $\nu_P = \frac{1}{|C_\Lambda|}$.

The Lorentz factor tensor $\mathscr{L}$ plays a central role within the framework of macroscopic "textbook" electrodynamics, when one is interested in the determination of the local electric field inside crystalline dielectrics. More specifically, in the macroscopic theory $\mathscr{L}$ takes into account the crystal's symmetry and corrects in this way the contribution of its polarization to the local electric field. In contrast to the depolarization factor, which corrects the contribution of the crystal's polarization to the macroscopic electric field with respect to the crystal's geometrical shape, the Lorentz factor tensor $\mathscr{L}$ does *not* depend on the shape of the crystal, but solely on its symmetry [62]. From the definition of $\mathscr{L}$ by (4.4.4), there follows immediately the trace identity[7]

$$\mathrm{Tr}\left[\mathscr{L}\right] = 1, \tag{4.4.6}$$

which is in compliance with [63]. The numerical evaluation of $\mathscr{L}$ can easily be carried out for all 14 3-dimensional monatomic Bravais lattices by following the lines indicated in appendix F.2.2. Restricting the ensuing considerations to the uniaxial tetragonal and hexagonal crystal systems, the Lorentz factor tensor $\mathscr{L}_{ab} = \mathscr{L}_a\delta_{ab}$ becomes diagonal with $\mathscr{L}_\perp \equiv \mathscr{L}_1 = \mathscr{L}_2$ and $\mathscr{L}_{||} \equiv \mathscr{L}_3 = 1 - 2\mathscr{L}_\perp$, where at the last equality sign the trace identity (4.4.6) has been deployed. It should be emphasized, that the numerical value of $\mathscr{L}_a$ solely depends on the ratio $\frac{a_{||}}{a_\perp}$ of lattice constants $a_{||}$ and $a_\perp$, that denote the length of the crystalline axes parallel and perpendicular to the distinguished (optical) z-axis. Figure 4.4.1 shows the variation of $\mathscr{L}_{||}$ in dependence of $\frac{a_{||}}{a_\perp}$ for both, the tetragonal and hexagonal crystal system. It is noteworthy that in the case of the body-centered tetragonal monatomic Bravais lattice, $\mathscr{L}_{||}$ adopts the for isotropic systems characteristic value $\frac{1}{3}$ three times. For this reason, this lattice is quasi-isotropic over a remarkable range of ratios $\frac{a_{||}}{a_\perp}$ of lattice constants $a_{||}$ and $a_\perp$. Additionally it should be mentioned, that the Lorentz factors obtained with (4.4.4) for the tetragonal and hexagonal crystal system coincide with the results of [64, 65].

The dielectric tensor ε_Λ (see (4.4.5)) describing monatomic crystal structures in the static limit exhibits a pole structure for positive definite Lorentz factor tensors $\mathscr{L}$ i.e. if all eigenvalues of $\mathscr{L}$ are greater than zero. To ensure stability of the crystalline material, the density of polarizable atoms/ions ν_P is

[7] For a proof of (4.4.6), see appendix G.1.

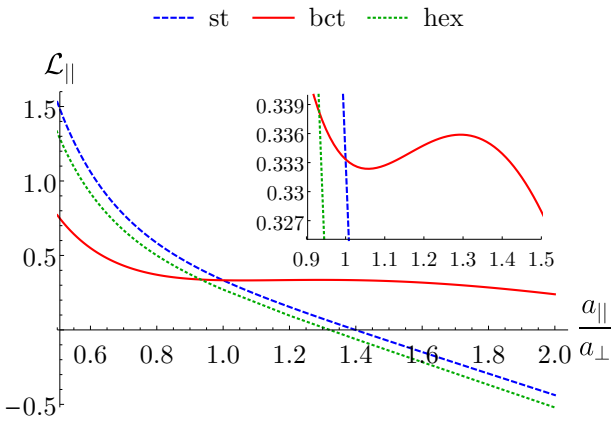

Figure 4.4.1: Plot of the Lorentz factor $\mathscr{L}_{||}$ in dependence of the ratio $\frac{a_{||}}{a_\perp}$ of lattice constants for simple tetragonal (st), body-centered tetragonal (bct) and hexagonal (hex) monatomic Bravais lattices. The inset shows a zoom into the region where $\mathscr{L}_{||}$ assumes a value around $\frac{1}{3}$, which is characteristic for isotropic systems.

bound to values[8]

$$\nu_\mathrm{P} < \nu_\mathrm{P}^{(\mathrm{c})} = \frac{1}{\mathscr{L}_\mathrm{max}^{(+)}} \frac{\varepsilon_0}{\alpha}, \tag{4.4.7}$$

where $\mathscr{L}_\mathrm{max}^{(+)}$ denotes the largest positive eigenvalue of $\mathscr{L}$. As long as the condition (4.4.7) is satisfied, all eigenvalues of ε_Λ are greater than or equal to 1. Therefore the stability criterion (4.4.7) can be understood as an anisotropic generalization of the result

$$\varepsilon_\Lambda = \varepsilon\delta \quad \text{with} \quad \varepsilon \geq 1, \tag{4.4.8}$$

that has been derived by Kirzhnitz [66] for isotropic media quite apart from a particular model description of the material and solely based on general principles such as causality and thermodynamic stability.

Finally, consider a simple cubic crystal structure. As is shown in appendix G.2, in this case there holds $\mathscr{L}_{ab} = \frac{1}{3}\delta_{ab}$, so that the static dielectric tensor given by (4.4.5) assumes the guise of the well-known Clausius-Mossotti formula

$$\varepsilon_\Lambda = \left(\delta + \frac{2}{3}\frac{\nu_\mathrm{P}}{\varepsilon_0}\alpha\right) \circ \left(\delta - \frac{1}{3}\frac{\nu_\mathrm{P}}{\varepsilon_0}\alpha\right)^{-1}, \tag{4.4.9}$$

which also applies well for a variety of (isotropic, non-polar) materials beyond the crystalline aggregate state, including dielectric liquids and gases. It should be noticed, that in the presented derivation of (4.4.9) the common construction of the so-called Lorentz sphere[9] has been avoided.

[8] It is exactly this critical density $\nu_\mathrm{P}^{(\mathrm{c})}$, that indicates the border of instability in figure 3.4.5.

[9] For a derivation of (4.4.9) within the framework of macroscopic "textbook" electrodynamics that requires the construction of the Lorentz sphere, see e.g. [3].

In this section it has been shown, that the general dielectric tensor $\varepsilon_\Lambda(\mathbf{q},\omega)$ given by (4.1.17) incorporates a number of well-known results regarding monatomic crystal structures in the static limit, thus encouraging the consideration of more complicated crystal structures. Hence, the next section deals with diatomic ionic crystal structures and the analytic structure of $\varepsilon_\Lambda(\omega)$, which plays a crucial role in the context of longitudinal and transverse optical lattice vibrations.

4.4.2 The analytic structure of $\varepsilon_\Lambda(\omega)$ in diatomic ionic crystal structures

In comparison to crystal structures with a monatomic basis ($M=1$), qualitative new effects emerge if $M \geq 2$. Particularly in ionic crystals, the positively and negatively charged ions are displaced in opposite directions from their equilibrium positions under the influence of the local electric field, resulting in an induced ionic displacement polarizability[10]. Because the character of this polarization effect is closely related to lattice vibrations, it only contributes to the total polarizability if the frequency ω of the externally applied signal corresponds to typical lattice vibration frequencies $\omega_{\mathrm{Ph}} \sim 10^{12} - 10^{13} s^{-1}$ or even lower frequencies. For frequencies associated with visible light or even higher, ionic displacement polarizability is usually negligible as the ions are not capable to follow the oscillations of the field because of their relatively big moment of inertia. It is well known from theory and also experimentally confirmed, that in the special case of $M=2$, the dielectric tensor of (cubic) ionic crystal structures is closely related to the optical long-wavelength (i.e. $|\mathbf{q}| \to 0$) lattice vibration modes via the Lyddane-Sachs-Teller relation [3, 67]

$$\frac{\varepsilon_\Lambda^{(0)}}{\varepsilon_\Lambda^{(\infty)}} = \frac{\omega_{\mathrm{L}}^2}{\omega_{\mathrm{T}}^2}. \tag{4.4.10}$$

Here, $\varepsilon_\Lambda^{(0)}$ and $\varepsilon_\Lambda^{(\infty)}$ denote the quasi-static and the high frequency limit of the dielectric tensor

$$\varepsilon_\Lambda(\omega) \equiv \lim_{|\mathbf{q}|\to 0} \varepsilon_\Lambda(\mathbf{q},\omega) = \begin{cases} \varepsilon_\Lambda^{(0)} & \text{if } \omega \ll \omega_0^{(j,j')} \\ \varepsilon_\Lambda^{(\infty)} & \text{if } \omega_0^{(j,j')} \ll \omega \ll \omega_0^{(j)} \end{cases}, \tag{4.4.11}$$

where $\omega_0^{(j)}$ with $j \in \{1,2\}$ represents the resonance frequency of an electronic excitation within the j^{th}-ion and thus being associated with the ultraviolet spectral region. However, $\omega_0^{(j,j')}$ with $j, j' \in \{1,2\}$ and $j \neq j'$ constitutes a resonance frequency of the order of ω_{Ph}, which is typical for lattice vibrations. ω_{L} and ω_{T} describe the frequencies of the longitudinal and transverse optical modes, which are associated with lattice vibrations in the limit[11] $|\mathbf{q}| \to 0$, where $\omega_{\mathrm{L}} > \omega_{\mathrm{T}}$. It should be stressed, that the Lyddane-Sachs-Teller relation (4.4.10) solely results from an interpretation of the roots as well as the poles of the dielectric tensor $\varepsilon_\Lambda(\omega)$ and is therefore a consequence of its functional dependence on ω [3]. Due to this fact, it can also be deduced by means of the Kramers-Kronig relation, if ω_{T} is identified as the

[10] For details, see section 3.1.

[11] It should be pointed out, that a strict distinction between longitudinal and transverse optical modes is only possible in isotropic materials. For this reason, the limit $|\mathbf{q}| \to 0$ is taken although cubic crystals are considered. In anisotropic media, the optical modes exhibit both longitudinal and transverse contributions [3].

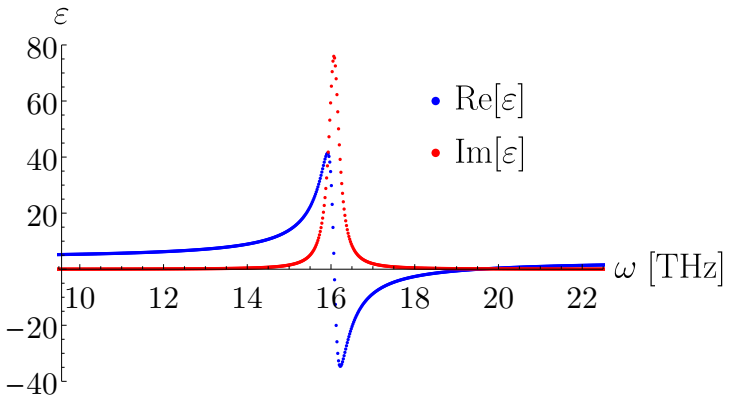

Figure 4.4.2: Plot of the real (blue) and imaginary (red) part of the dielectric tensor $\varepsilon_\Lambda(\omega)$ for the diatomic cubic crystal structure of CsI in the vicinity of the resonance frequency $\omega_0^{(1,2)} = 0.012\text{eV} \hat{=} 18.23\text{THz}$ (see table 4.4.2), which is associated with the ionic displacement polarizability of the Cs and I ions.

frequency where $\text{Im}[\varepsilon_\Lambda(\omega)]$ is peaked and when $\omega_\text{L} > \omega_\text{T}$ denotes the frequency where $\text{Re}[\varepsilon_\Lambda(\omega)]$ is zero [68]. Because of what has been said, (4.4.10) is an indicator that causality has been respected, but it may not be grasped as a rigorous proof for the validity of a theory.

In what follows it is demonstrated, that the dielectric tensor $\varepsilon_\Lambda(\omega) \equiv \lim_{|\mathbf{q}|\to 0} \varepsilon_\Lambda(\mathbf{q},\omega)$ determined by (4.1.17) respects causality in terms of the Lyddane-Sachs-Teller relation (4.4.10). Therefore $\text{Re}[\varepsilon_\Lambda(\omega)]$ and $\text{Im}[\varepsilon_\Lambda(\omega)]$ are calculated for the diatomic cubic crystal structure of CsI (see figure 4.4.2), where the parameters deployed to the respective electronic and ionic displacement polarizability models (3.1.1) and (3.1.2) are given in table 4.4.2[12]. Identifying now the frequencies of the transverse and longitudinal optical modes as $\omega_\text{T} = 16.08\text{THz}$ and $\omega_\text{L} = 19.53\text{THz}$ as well as the quasi-static and the high frequency limit of $\varepsilon_\Lambda(\omega)$ according to $\varepsilon_\Lambda^{(0)} = 4.45$ and $\varepsilon_\Lambda^{(\infty)} \equiv \varepsilon_\Lambda\left(\omega_\text{T}\cdot 10^2\right) = 3.05$, the Lyddane-Sachs-Teller relation (4.4.10) turns out to be satisfied with an accuracy of almost 99%.

Because beside the static limit (see section 4.4.1) the frequency dependence of the dielectric tensor $\varepsilon_\Lambda(\mathbf{q},\omega)$ given by (4.1.17) is compatible with general causality considerations in the long-wavelength limit $|\mathbf{q}| \to 0$ too, it is promising to proceed its discussion in the next section with respect to chromatic and spatial dispersion and their impact on the optical properties of crystalline dielectrics.

4.4.3 Optical properties of crystalline dielectrics governed by $\varepsilon^{(\mathbf{T})}(\mathbf{q},\omega)$

With regard to (4.1.15) it is the dielectric tensor $\varepsilon_\Lambda(\mathbf{q},\omega)$ that relates the Fourier amplitudes of the macroscopic electric field $\tilde{\mathscr{E}}(\mathbf{q},\omega)$ with that of the macroscopic polarization $\tilde{\mathscr{P}}(\mathbf{q},\omega)$ within the framework of macroscopic electrodynamics. Therefore, the microscopic material model of crystalline dielectrics (3.1.5), which has originally been established for the microscopic polarization $\mathbf{P}(\mathbf{r},\omega)$, is

[12] In addition, a small damping parameter $\gamma \equiv \gamma^{(1,2)} = \gamma^{(2,1)} > 0$ has been included into the ionic displacement polarizability (3.1.2) to take into account, that lattice vibrations are in general damped.

incorporated into $\varepsilon_\Lambda(\mathbf{q},\omega)$, as can be seen by inspection of (4.1.17). While the crystalline structure is completely contained within the lattice sums, the specific model of the electromagnetic response of the individual constituents of the crystal is fully described in terms of the electronic and ionic displacement polarizabilities via a Lorentz oscillator model.

Hence it may be surprising at first sight that for a discussion of the optical properties of dielectric crystals, it is *not* the dielectric tensor $\varepsilon_\Lambda(\mathbf{q},\omega)$ but rather its transverse part $\varepsilon^{(\mathrm{T})}(\mathbf{q},\omega)$, which constitutes the relevant physical quantity. This is owed to the fact, that only the transverse part $\tilde{\mathscr{E}}^{(\mathrm{T})}(\mathbf{q},\omega)$ of $\tilde{\mathscr{E}}(\mathbf{q},\omega)$ obeys under certain requirements to a wave(-like) equation (see section 4.2.2 and in particular (4.2.21) and (4.2.22)) and thus describes electromagnetic radiation, while the longitudinal part $\tilde{\mathscr{E}}^{(\mathrm{L})}(\mathbf{q},\omega)$ satisfies under specific conditions a Poisson(-like) equation (see section 4.2.1 and in particular (4.2.16) and (4.2.18)) and consequently represents a non-radiative field. It is exactly this wave(-like) equation (4.2.21) or (4.2.22), where $\varepsilon^{(\mathrm{T})}(\mathbf{q},\omega)$ enters instead of $\varepsilon_\Lambda(\mathbf{q},\omega)$ and therefore the former describes all optical effects possessed by the material under consideration.

Because the transverse dielectric tensor $\varepsilon^{(\mathrm{T})}(\mathbf{q},\omega)$ as given by (4.2.20) can be easily deduced from $\varepsilon_\Lambda(\mathbf{q},\omega)$ via the projection procedure (4.2.8), it naturally contains all the information about the underlying microscopic material model, too. Furthermore, various optical effects are encoded in its arguments ω and $\mathbf{q}$ representing chromatic and spatial dispersion, respectively. A material is commonly said to be chromatic dispersive, when electromagnetic waves of distinct frequencies propagate with different phase velocities inside that material, so that a traversing wave packet which comprises optical signals of different frequencies tends to spread out[13]. However, microscopic considerations based on first principles reveal, that chromatic dispersion of e.g. the index of refraction is directly connected to the retarded response of the polarizable constituents of matter [2]. Moreover, this omnipresent and generally not negligible effect is supplemented by spatial dispersion, whose origin is due to the non-local response of the material's constituents. That is, a charge at point $\mathbf{r}$ recollects the action exerted on it at another position $\mathbf{r}'$ [2, 29]. In other words, a quantity like e.g. the macroscopic polarization $\mathscr{P}(\mathbf{r},\omega)$ is affected by spatial dispersion, if it does not solely depend on the macroscopic electric field $\mathscr{E}(\mathbf{r},\omega)$ at the very same position $\mathbf{r}$ but also on $\mathscr{E}(\mathbf{r}',\omega)$, where $\mathbf{r}'$ is located in the neighbourhood of $\mathbf{r}$ [69]. Compared to chromatic dispersion, spatial dispersion is less popular and often neglected in optics, because its impact is usually considered as miniscule. Nonetheless, it is this $\mathbf{q}$-dependence of the transverse dielectric tensor $\varepsilon^{(\mathrm{T})}(\mathbf{q},\omega)$ that gives rise to a variety of qualitative new optical effects like natural optical activity or spatial dispersion induced birefringence. To gain insight into these effects which are encoded in the $\mathbf{q}$-dependence of $\varepsilon^{(\mathrm{T})}(\mathbf{q},\omega)$, the transverse dielectric tensor is regarded as an analytic function of wave vector $\mathbf{q}$, so that for wave vectors of small modulus it can be expanded into a Taylor series[14] around

[13] It should be noticed that in general each physical quantity that refers to any optical effect, is it the index of refraction, natural optical activity, the Faraday effect or others, depends on frequency ω and therefore shows chromatic dispersion.

[14] Compare with the phenomenological reasoning of spatial dispersion in crystals due to Agranovich and Ginzburg in [1].

$\mathbf{q} = \mathbf{0}$ according to

$$\varepsilon_{ab}^{(\mathrm{T})}(\mathbf{q},\omega) = \varepsilon_{ab}^{(\mathrm{T})}(\omega) + i\sum_{c=1}^{3}\gamma_{abc}(\omega)\,q_c + \sum_{c,d=1}^{3}\alpha_{abcd}(\omega)\,q_c q_d + \ldots. \tag{4.4.12}$$

Notice that the expansion with respect to the wave vector $\mathbf{q}$ in (4.4.12) corresponds in position space to an expansion with respect to $\mathbf{r}$, so that the non-local response is implied by the spatial derivatives.

Starting from the expansion (4.4.12), the quantities $\varepsilon_{ab}^{(\mathrm{T})}(\omega)$, $\gamma_{abc}(\omega)$ and $\alpha_{abcd}(\omega)$ as well as the optical effects associated with them i.e. the index of refraction, natural optical activity and spatial dispersion induced birefringence will be discussed in the next subsections. Additionally it is shown, that the results obtained for these effects from the presented theory coincide well with experimental measurements.

4.4.3.1 Index of refraction

In this section, the principal dielectric constants and their associated principal indices of refraction are discussed for a variety of crystalline dielectrics. Therefore, spatial dispersion is neglected in the remainder of this section, i.e. in the expansion (4.4.12) it is assumed that $\mathbf{q} = \mathbf{0}$, so that there holds $\varepsilon^{(\mathrm{T})}(\mathbf{0},\omega) = \varepsilon^{(\mathrm{T})}(\omega)$. According to section 4.2, the transverse dielectric tensor $\varepsilon^{(\mathrm{T})}(\omega)$ can easily be deduced from the dielectric tensor $\varepsilon_\Lambda(\mathbf{0},\omega) \equiv \varepsilon_\Lambda(\omega)$ given by (4.1.17). For this reason, the dielectric tensor $\varepsilon_\Lambda(\omega)$ is briefly discussed first, followed by a detailed analysis of $\varepsilon^{(\mathrm{T})}(\omega)$ with regard to different crystal structures.

Because only non-absorbing media are considered, $\varepsilon_\Lambda(\omega)$ constitutes a real 3×3 matrix, i.e. there holds $\varepsilon_\Lambda(\omega) = \varepsilon_\Lambda^*(\omega)$. Additionally it can be concluded from considerations requiring the conservation of energy, that $\varepsilon_\Lambda(\omega) = \varepsilon_\Lambda^T(\omega)$ is symmetric [4]. As a consequence, $\varepsilon_\Lambda(\omega)$ can always be transformed to its system of principal axes $\mathbf{a}^{(i)}$ with $i \in \{1,2,3\}$ [70] according to

$$[\varepsilon_\Lambda(\omega)]_{ab} = \varepsilon_a(\omega)\,\delta_{ab} \text{ (system of principal axes).} \tag{4.4.13}$$

In this special coordinate system, $\varepsilon_\Lambda(\omega)$ is diagonal and $\varepsilon_a(\omega)$ with $a \in \{1,2,3\}$ are called the principal dielectric constants[15].

If one is interested in the propagation of electromagnetic waves within a crystalline dielectric in absence of spatial dispersion, the appropriate wave equation determining the transverse electric field $\mathscr{E}^{(\mathrm{T})}(\mathbf{r},\omega)$ is given by (4.2.22). Here $\varepsilon^{(\mathrm{T})}(\omega)$ enters instead of $\varepsilon_\Lambda(\omega)$, because only the degrees of freedom of the material response associated with the radiation field $\mathscr{E}^{(\mathrm{T})}(\mathbf{r},\omega)$ are relevant. All other contributions to the dielectric tensor $\varepsilon_\Lambda(\omega)$ than $\varepsilon^{(\mathrm{T})}(\omega)$ are not related to $\mathscr{E}^{(\mathrm{T})}(\mathbf{r},\omega)$. They have nothing to do

[15] It should be noticed, that besides the principal dielectric constants $\varepsilon_a(\omega)$ also the dielectric principal axes $\mathbf{a}^{(i)}$ may depend on frequency ω. This phenomenon, which is particularly conspicuous in the infrared, is known as *dispersion of the axes* and can only be observed in the monoclinic and triclinic crystal system, where the $\mathbf{a}^{(i)}$ do *not* coincide with the cartesian coordinate axes $\mathbf{e}^{(i)}$ [4].

crystal system	optical classification	refractive indices	principal axes
triclinic	biaxial	$n_1(\omega), n_2(\omega), n_3(\omega)$	$\mathbf{a}^{(1)}(\omega), \mathbf{a}^{(2)}(\omega), \mathbf{a}^{(3)}(\omega)$
monoclinic	biaxial	$n_1(\omega), n_2(\omega), n_3(\omega)$	$\mathbf{a}^{(1)}(\omega), \mathbf{a}^{(2)}(\omega), \mathbf{a}^{(3)}(\omega)$
(ortho-)rhombic	biaxial	$n_1(\omega), n_2(\omega), n_3(\omega)$	$\mathbf{e}^{(1)}, \mathbf{e}^{(2)}, \mathbf{e}^{(3)}$
trigonal	uniaxial	$n_1(\omega) = n_2(\omega), n_3(\omega)$	$\mathbf{e}^{(1)}, \mathbf{e}^{(2)}, \mathbf{e}^{(3)}$
hexagonal	uniaxial	$n_1(\omega) = n_2(\omega), n_3(\omega)$	$\mathbf{e}^{(1)}, \mathbf{e}^{(2)}, \mathbf{e}^{(3)}$
tetragonal	uniaxial	$n_1(\omega) = n_2(\omega), n_3(\omega)$	$\mathbf{e}^{(1)}, \mathbf{e}^{(2)}, \mathbf{e}^{(3)}$
cubic	isotropic	$n_1(\omega) = n_2(\omega) = n_3(\omega)$	$\mathbf{e}^{(1)}, \mathbf{e}^{(2)}, \mathbf{e}^{(3)}$

Table 4.4.1: Optical classification of the seven crystal systems in three dimensions.

with wave propagation and may therefore not be associated with the optical properties of the material. From the general expression (4.2.20) determining $\varepsilon^{(\mathrm{T})}(\mathbf{q},\omega)$ for arbitrary $\mathbf{q}$, $\varepsilon^{(\mathrm{T})}(\omega)$ is obtained when wave propagation along a dielectric principal axis, say $\mathbf{a}^{(i)}$, is considered in the limit $|\mathbf{q}| \to 0$. Within the coordinate system of dielectric principal axes, $\varepsilon^{(\mathrm{T})}(\omega)$ is diagonal, but exhibits solely two non-vanishing eigenvalues instead of three, as was the case for $\varepsilon_\Lambda(\omega)$. This is reasonable, because the purely transverse radiation field $\mathscr{E}^{(\mathrm{T})}(\mathbf{r},\omega)$ is generated from a superposition of two (orthogonal) states of polarization and consequently lacks of a longitudinal part in direction of wave propagation. As is shown in appendix H.1, in the system of principal axes, $\varepsilon^{(\mathrm{T})}(\omega)$ assumes the guise

$$\varepsilon_{ab}^{(\mathrm{T})}(\omega) = \varepsilon_a(\omega)(1-\delta_{ai})\,\delta_{ab} \text{ (system of principal axes)}, \tag{4.4.14}$$

where the index $i \in \{1,2,3\}$ in (4.4.14) labels that dielectric principal axis $\mathbf{a}^{(i)}$, along wave propagation takes place[16].

The principal indices of refraction specifying the phase velocities of the radiation field $\mathscr{E}^{(\mathrm{T})}(\mathbf{r},\omega)$ along the dielectric principal axes are readily deduced from (4.4.14) via the relation

$$n_a(\omega) = \sqrt{\varepsilon_{aa}^{(\mathrm{T})}(\omega)}. \tag{4.4.15}$$

With regard to $n_a(\omega)$, the seven crystal systems existing in three dimensions can be optically classified as summarized in table 4.4.1 (see also [4, 69]).

In what follows, the frequency dependent refractive indices will be calculated on the basis of (4.4.15) for a variety of ionic crystals belonging to the optically isotropic and uniaxial classes. Thanks to exhaustive experimental studies in the field of x-ray and neutron diffraction analysis, the underlying lattice as well as the specific assembly of the ions within the Wigner-Seitz cell C_Λ are well known for all crystal structures considered in this work. In contrast, there are mostly no experimental data avail-

[16] Notice that the term containing the δ_{ai} in (4.4.14) eliminates the non-radiative longitudinal eigenmode which is comprised by $\varepsilon_\Lambda(\omega)$.

crystal	ion/bonding	$\frac{\alpha_0}{4\pi\varepsilon_0}\left[\text{Å}^3\right]$	ω_0 [eV]
CsI	Cs^+	2.884	33.220
	I^-	6.241	8.253
	$Cs^+ - I^-$	1.519	0.012
RbCl	Rb^+	0.285	7.359
	Cl^-	4.500	12.959
	$Rb^+ - Cl^-$	2.214	0.019
BaF_2	Ba^{2+}	1.577	16.353
	F^-	1.165	15.789
CaF_2	Ca^{2+}	0.759	27.484
	F^-	0.866	15.860
SiO_2	Si^{4+}	0.203	17.011
	O^{2-}	1.185	16.123

Table 4.4.2: Estimated fit parameters applied to the (isotropic!) Lorentz oscillator models of electronic and ionic displacement polarizability (3.1.1) and (3.1.2), respectively, for the ionic crystals CsI, RbCl, BaF_2, CaF_2 and SiO_2 ($\alpha-$quartz). In case of SiO_2, the Lorentz oscillator model was fitted to electronic polarizabilities reported in [76].

able regarding the individual chromatic dispersive electronic $\alpha_{ab}^{(\mathrm{el})}\left(\eta^{(j)},\omega\right)$ and ionic displacement polarizability $\alpha_{ab}^{(\mathrm{ion})}\left(\eta^{(j)},\eta^{(j')},\omega\right)$, which are therefore conceived as fit functions of the Lorentz oscillator type (3.1.1) and (3.1.2), respectively[17]. Assuming the respective polarizabilities to be isotropic, i.e. $\alpha_{ab}^{(\mathrm{el})}\left(\eta^{(j)},\omega\right)=\alpha^{(\mathrm{el})}\left(\eta^{(j)},\omega\right)\delta_{ab}$ and $\alpha_{ab}^{(\mathrm{ion})}\left(\eta^{(j)},\eta^{(j')},\omega\right)=\alpha^{(\mathrm{ion})}\left(\eta^{(j)},\eta^{(j')},\omega\right)\delta_{ab}$, the phenomenological Sellmeier fit [71, 72] for the chromatic dispersion of the principal indices of refraction $n_a(\omega)$ is nicely reproduced by means of (4.4.15) with an relative error of less than 1% for the following crystals (see figure 4.4.3): CsI, RbCl, BaF_2, CaF_2, SiO_2 ($\alpha-$quartz). The respective parameters deployed to the Lorentz oscillator models of $\alpha^{(\mathrm{el})}\left(\eta^{(j)},\omega\right)$ and $\alpha^{(\mathrm{ion})}\left(\eta^{(j)},\eta^{(j')},\omega\right)$ are given in table 4.4.2. Since CsI, RbCl, BaF_2 and CaF_2 belong to the cubic crystal system, all principal indices of refraction coincide and the crystals are optically isotropic. Moreover, they represent rather simple crystal structures. The Wigner-Seitz cell C_Λ of the first two crystals comprises $M=2$, that of the last two comprises $M=3$ ions. However, the (laevorotatory)[18] $\alpha-$quartz modification of SiO_2 ($M=9$) belongs to the trigonal crystal system and is therefore optically uniaxial. Its two distinct principal indices of refraction n_o and n_e are called the ordinary and extraordinary index of refraction, respectively. It should be emphasized, that for the calculation of the refractive indices $n_a(\omega)$ within the spectral range extending from the ultraviolet to the near-infrared, solely taking into account the electronic polarizabilities of the

[17] In principle, the calculation of both kinds of polarizability is possible within a microscopic theory, but this is beyond the scope of this work.

[18] The laevorotatory modification of $\alpha-$quartz is allocated to space group $P3_121$. The knowledge of the space group will be important when natural optical activity is discussed in the next section, because there also exists a dextrorotatory modification belonging to space group $P3_221$.

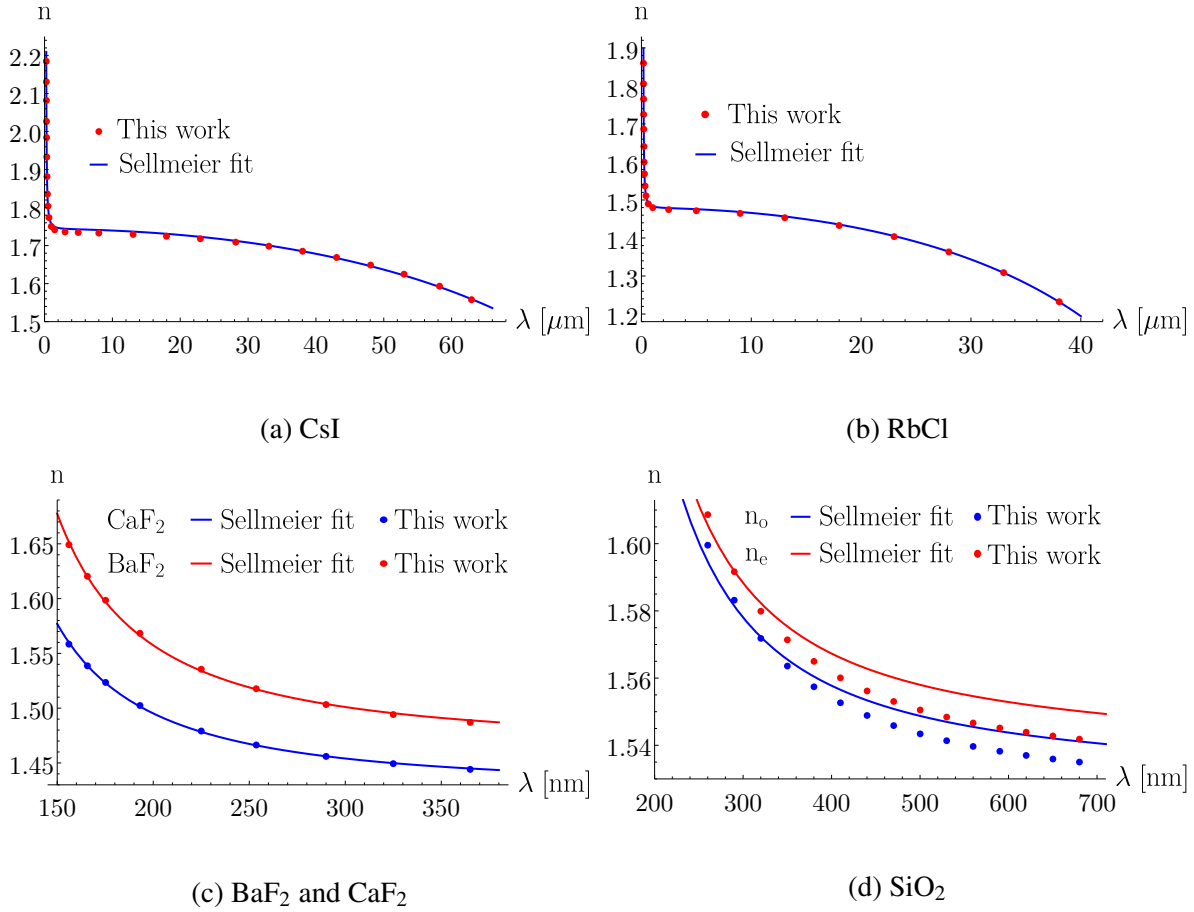

(a) CsI

(b) RbCl

(c) BaF_2 and CaF_2

(d) SiO_2

Figure 4.4.3: Plot of principal indices of refraction $n_a(\omega)$ vs. free space wavelength $\lambda = \frac{2\pi c}{\omega}$ for CsI, RbCl, BaF_2, CaF_2 and SiO_2. Displayed are values (dots) calculated from (4.4.15), solely with the crystalline structure and the electronic polarizabilities of the individual ions (supplemented by the ionic displacement polarizabilities in case of CsI and RbCl) as input. The respective parameters entering the polarizability models are given in table 4.4.2. The solid lines show a fit to experimental data of the refractive indices by means of the phenomenological, multi-parameter Sellmeier formula [73–75]. The relative error in $n_a(\omega)$ between this work and the Sellmeier fit is less than 1% for all considered crystals.

individual ions is sufficient (see e.g. BaF_2, CaF_2 and SiO_2). But, if the calculation of $n_a(\omega)$ is extended from the near- to the mid- or even far-infrared spectral regime (see CsI and RbCl), the frequency dependence of the index of refraction is essentially determined by the ionic displacement polarizabilities[19]. It is noteworthy, that the presented approach for the calculation of $n_a(\omega)$ resting upon (4.4.15) warrants considerably fewer fit parameters compared to the Sellmeier formula. For instance, the reproduction of the experimentally observed chromatic dispersion of CsI, ranging from the ultraviolet to the far-infrared spectral regime, requires 17 fit parameters, when the Sellmeier formula [73] is consulted, but solely 6 parameters, if (4.4.15) is utilized. In case of the uniaxial crystal SiO_2, the ordinary and extraordinary index of refraction are already contained within (4.4.15), because the complete crystal symmetry is inherently taken into account by the lattice sums, which are incorporated into the transverse dielectric tensor. In contrast, the Sellmeier formula is unaware of the crystalline structure, so that it takes one Sellmeier fit for each refractive index.

Finally, the applicability of the presented approach is demonstrated for various sophisticated crystal structures covering the cubic and all uniaxial crystal systems (see table 4.4.3). The number of ions comprised by the Wigner-Seitz cell C_Λ varies between $M = 4$ (for hexagonal BeO) and $M = 66$ (for cubic $Bi_{12}TiO_{20}$ and $Bi_{12}SiO_{20}$) for the considered crystals. Similar to the results shown in figure 4.4.3 (d) for SiO_2, all calculations of $n^{(\mathrm{calc})}$ in table 4.4.3 solely rest on published data of electronic polarizabilities (in the visible spectral regime), which have been obtained by a number of different experimental and theoretical studies. As the maximal relative error between $n^{(\mathrm{calc})}$ and $n^{(\mathrm{exp})}$ of all crystals is about 2%, the presented theory proves to be compatible with these studies.

After the presented theory had proved valuable for the calculation of the principal indices of refraction for $\mathbf{q} = \mathbf{0}$, the impact of a finite wave vector $\mathbf{q} \neq \mathbf{0}$ on the transverse dielectric tensor $\varepsilon_{ab}^{(\mathrm{T})}(\mathbf{q}, \omega)$ is investigated. Starting with the first order $\mathbf{q}-$correction in the expansion (4.4.12) of $\varepsilon_{ab}^{(\mathrm{T})}(\mathbf{q}, \omega)$, the interplay between crystalline structure and finite wave vector gives rise to an optical effect called natural optical activity. The next section is dedicated to its discussion.

4.4.3.2 Natural optical activity

The story of natural optical activity[20] begins with an observation made by the astronomer Arago in 1811 when he found, that beams of polarized sunlight traversing a quartz crystal give rise to two solar images, whose colors change when considered through a rotating analyzer crystal. However, it was Biot in 1812 who gave a physical interpretation of Arago's results. He concluded, that the plane of polarisation of a linearly polarized light wave is rotated, when passing through a quartz crystal. Additionally, this rotation has to depend on the light's wavelength. With these two conclusions, the effect of natural optical activity was formulated for the first time. The first and rather phenomenological theory of this

[19] Notice, that $\alpha^{(\mathrm{el})}\left(\eta^{(j)}, \omega\right)$ essentially assumes its static value in the infrared regime, while $\alpha^{(\mathrm{ion})}\left(\eta^{(j)}, \eta^{(j')}, \omega\right)$ basically vanishes in the visible and the ultraviolet.

[20] A comprehensive review on the early history of natural optical activity is given in [56].

crystal	space group	λ [nm]	$\alpha = \frac{\alpha^{(\mathrm{el})}}{4\pi\varepsilon_0}\left[\mathrm{\AA}^3\right]$	$n^{(\mathrm{exp})}$	$n^{(\mathrm{calc})}$	references
$\beta-SiO_2$*	$P6_222$	517	$\alpha_{Si}=0.185$ $\alpha_O=1.250$	$n_o=1.536$ $n_e=1.544$	$n_o=1.534$ $n_e=1.539$	[76, 77]
TiO_2	$P4_2/mnm$	589	$\alpha_{Ti}=0.1862$ $\alpha_O^{\parallel}=2.6006$ $\alpha_O^{\perp}=2.2863$	$n_o=2.613$ $n_e=2.909$	$n_o=2.600$ $n_e=2.921$	[78–80]
BeO	$P6_3mc$	633	$\alpha_{Be}=0.007$ $\alpha_O=1.290$	$n_o=1.717$ $n_e=1.732$	$n_o=1.713$ $n_e=1.717$	[81–83]
$NaClO_3$*	$P2_13$	633	$\alpha_{Na}=0.290$ $\alpha_{Cl}=0.010$ $\alpha_O=1.600$	$n=1.514$	$n=1.526$	[76, 84, 85]
$SrTiO_3$	$Pm\bar{3}m$	589	$\alpha_{Sr}=1.0666$ $\alpha_{Ti}=0.1859$ $\alpha_O=2.3940$	$n=2.410$	$n=2.409$	[83, 86, 87]
$Bi_{12}TiO_{20}$*	I23	633	$\alpha_{Bi}=0.0625$ $\alpha_{Ti}=0.272$ $\alpha_O=3.725$	$n=2.562$	$n=2.553$	[83, 88]
$Bi_{12}SiO_{20}$*	I23	650	$\alpha_{Bi}=0.150$ $\alpha_{Si}=0.001$ $\alpha_O=3.540$	$n=2.52$	$n=2.50$	[76, 83, 89]
$\alpha-AlPO_4$*	$P3_121$	633	$\alpha_{Al}=0.050$ $\alpha_P=0.050$ $\alpha_O=1.370$	$n_o=1.524$ $n_e=1.533$	$n_o=1.541$ $n_e=1.545$	[76, 83, 90]
$BaTiO_3$	P4mm	589	$\alpha_{Ba}=1.9460$ $\alpha_{Ti}=0.1859$ $\alpha_O=2.3940$	$n_o=2.426$ $n_e=2.380$	$n_o=2.400$ $n_e=2.380$	[87, 91, 92]
$CaCO_3$	$R\bar{3}cH$	589	$\alpha_{Ca}=0.792$ $\alpha_C=0.000$ $\alpha_O^{\parallel}=1.384$ $\alpha_O^{\perp}=1.328$	$n_o=1.658$ $n_e=1.486$	$n_o=1.626$ $n_e=1.513$	[75, 93, 94]
$Tm_2Ge_2O_7$*	$P4_12_12$	633	Due to complex structure of α_X's see references	$n_o=1.900$ $n_e=1.890$	$n_o=1.899$ $n_e=1.900$	[95]

Table 4.4.3: Calculation of the principal indices of refraction $n^{(\mathrm{calc})}$ and comparison with experimental results $n^{(\mathrm{exp})}$ for various optically isotropic as well as uniaxial ionic crystals. The employed data regarding the crystalline structures and the electronic polarizabilities entering the calculations via (4.4.15), as well as the experimental data for $n^{(\mathrm{exp})}$, are taken from the publications cited in the column "references". In case of anisotropic polarizabilities occurring in the uniaxial crystals TiO_2 and $CaCO_3$, $\alpha_O^{\parallel}$ and $\alpha_O^{\perp}$ denote the polarizabilities of the oxygen ion parallel and perpendicular to the optical z-axis. Crystals marked with an asterisk "$*$" show natural optical activity, too (see table 4.4.4).

effect was then proposed by Fresnel in 1822, solely resting on interference theory and without taking into account the structure of specific material substances. He elucidated that a linearly polarized light wave, incident on a suitable material like quartz, is decomposed into two opposing (left and right) circular polarization states when passing this material, both propagating with different velocities and thus experiencing a relative phase shift. The superposition of both circular polarization states after the material has been traversed then results again in a linearly polarized light wave, albeit its plane of polarization being rotated with respect to that of the incident wave due to the phase shift.

Following the phenomenological reasoning of Agranovich and Ginzburg [1] as well as that of Sommerfeld [69], natural optical activity is caused by the *non-local* response of the material's constituents, which shows up in the dependence of the transverse dielectric tensor on wave vector[21] $\mathbf{q} \neq \mathbf{0}$ according to

$$\varepsilon_{ab}^{(\mathrm{T})}(\mathbf{q},\omega) = \varepsilon_{ab}^{(\mathrm{T})}(\omega) + i\sum_{c=1}^{3}\gamma_{abc}(\omega)\,q_c. \tag{4.4.16}$$

Consequently, natural optical activity manifests the most important optical effect resulting from spatial dispersion in the expansion (4.4.12), provided it is not prohibited by any point group symmetry of the respective material substance. While in crystals the rotatory power, i.e. the ability to rotate the plane of polarization, is attributed to helical structures (of specific chirality) formed by the most polarizable atoms/ions [96], in optically active fluids like e.g. tartaric acid or a solution of glucose in water [56], the rotatory power originates from the presence of chiral molecules in these otherwise isotropic substances[22].

Restricting the ensuing discussion of natural optical activity to ionic crystalline dielectrics, rotatory power can only be observed in crystals that lack of a center of inversion [1, 69, 97]. In total, there exist 21 non-centrosymmetric crystallographic point groups. However, if wave vector $\mathbf{q}$ is arbitrarily orientated, rotatory power is hardly evidenced experimentally, because in non-cubic crystals it is masked by the crystal's own birefringence, whose effect by far exceeds that of natural optical activity. Therefore, in the remainder of this section, only wave propagation with $\mathbf{q} = q\mathbf{e}^{(3)}$ along the (optical) z-axis of cubic and uniaxial crystal structures is considered, so that birefringence has no effect. The relevant point groups that are dealt with read: 23 and 432 (cubic), 3 and 32 (trigonal), 4 and 422 (tetragonal) as well as 6 and 622 (hexagonal) [97]. As is shown in appendix H.2, for crystal structures exhibiting these point group symmetries, the transverse dielectric tensor assumes the guise

$$\varepsilon_{ab}^{(\mathrm{T})}(\mathbf{q},\omega) = \varepsilon_a(\omega)\left(1 - e_a^{(3)}\right)\delta_{ab} + i\varepsilon_{ab3}\gamma(q,\omega), \tag{4.4.17}$$

where $e_a^{(3)}$ and ε_{ab3} denote the a^{th} component of the unit vector pointing in z-direction and the Levi-Civita symbol, respectively. The strength of rotatory power is assigned to $\gamma(q,\omega) \propto q$, that possesses

[21] Recall, that the propagable modes inside a material are determined by the photonic band structure $\omega_n(\mathbf{q})$.

[22] Notice, that there exist materials like e.g. rubidium tartrate, where optical activity is related to the individual molecules as well as to their assembly within a crystalline structure, with the interesting result, that laevorotatory crystals are deposited from a dextrorotatory solution [57]. Therefore, such materials stay optically active, even when their state of aggregation changes from the solid state to the liquid one.

the for natural optical activity characteristic properties

$$\gamma(0,\omega) = 0 \tag{4.4.18}$$

$$\gamma(-q,\omega) = -\gamma(q,\omega)\,. \tag{4.4.19}$$

In matrix notation, (4.4.17) reads

$$\varepsilon^{(\mathrm{T})}(\mathbf{q},\omega) = \begin{pmatrix} \varepsilon_1(\omega) & i\gamma(q,\omega) & 0 \\ -i\gamma(q,\omega) & \varepsilon_1(\omega) & 0 \\ 0 & 0 & 0 \end{pmatrix}. \tag{4.4.20}$$

The propagable modes of the transverse macroscopic radiation field $\tilde{\mathscr{E}}^{(\mathrm{T})}(\mathbf{q},\omega)$ within a crystal correspond to the eigenmodes of that crystal. Since $\tilde{\mathscr{E}}^{(\mathrm{T})}(\mathbf{q},\omega)$ is determined by the inhomogeneous wavelike equation (4.2.21), the crystalline eigenmodes are readily obtained from that by eliminating all external sources[23], i.e. by setting $\tilde{\mathbf{j}}^{(\mathrm{T})}_{\mathrm{ext}}(\mathbf{q},\omega) = \mathbf{0}$. As a consequence, the inhomogeneous wavelike equation (4.2.21) reduces to the homogeneous equation

$$\left(|\mathbf{q}|^2\,\delta - \frac{\omega^2}{c^2}\varepsilon^{(\mathrm{T})}(\mathbf{q},\omega)\right)\cdot\tilde{\mathscr{E}}^{(\mathrm{T})}(\mathbf{q},\omega) = \mathbf{0}, \tag{4.4.21}$$

which may be grasped as an effective 2×2 eigenvalue problem, because of (4.4.20) there immediately follows $\tilde{\mathscr{E}}^{(\mathrm{T})}_3(\mathbf{q},\omega) = 0$. Therefore, (4.4.21) is equivalent to

$$\begin{pmatrix} \varepsilon_1(\omega) & i\gamma(q,\omega) \\ -i\gamma(q,\omega) & \varepsilon_1(\omega) \end{pmatrix}\cdot\tilde{\mathbf{e}}_\pm(\mathbf{q},\omega) = n^2_\pm(\mathbf{q},\omega)\,\tilde{\mathbf{e}}_\pm(\mathbf{q},\omega)\,, \tag{4.4.22}$$

where $n^2_\pm(\mathbf{q},\omega) = \frac{c^2}{\omega^2}|\mathbf{q}|^2$ has been abbreviated. The computation of the eigenvalues $n^2_\pm(\mathbf{q},\omega)$ and eigenvectors $\tilde{\mathbf{e}}_\pm(\mathbf{q},\omega)$ associated with (4.4.22) is straightforward and yields

$$n^2_\pm(\mathbf{q},\omega) = \varepsilon_1(\omega) \pm \gamma(q,\omega) \tag{4.4.23}$$

$$\tilde{\mathbf{e}}_\pm(\mathbf{q},\omega) = \frac{1}{\sqrt{2}}\begin{pmatrix} \pm i \\ 1 \end{pmatrix}. \tag{4.4.24}$$

Obviously, this result substantiates Fresnel's interpretation of natural optical activity, because only waves of left $(-)$ and right $(+)$ circular polarization[24] $\tilde{\mathbf{e}}_\pm(\mathbf{q},\omega)$ are capable to propagate along the (optical) z-axis in cubic and uniaxial crystal structures exhibiting rotatory power. Likewise, the speed of light is renormalized for both polarization states with respect to distinct indices of refraction

$$n_\pm(\mathbf{q},\omega) = \sqrt{\varepsilon_1(\omega)\pm\gamma(q,\omega)} \approx n_1(\omega) \pm \frac{\gamma(q,\omega)}{2n_1(\omega)}, \tag{4.4.25}$$

[23] Compare with the determination of the photonic band structure $\omega_n(\mathbf{q})$ in section 3.3.

[24] Compare to the Jones formalism [97] for an interpretation of the shorthand notation $\tilde{\mathbf{e}}_\pm(\mathbf{q},\omega)$ given in (4.4.24).

so that the phases

$$\varphi_{\pm}(\mathbf{q},\omega)=\mathbf{q}_{\pm}\cdot\mathbf{r}=\frac{\omega}{c}n_{\pm}(\mathbf{q},\omega)z\approx\frac{\omega}{c}\left(n_1(\omega)\pm\frac{\gamma(q,\omega)}{2n_1(\omega)}\right)z \tag{4.4.26}$$

of left and right circular polarized waves differ when propagating the same distance z inside the crystal. Apparently, natural optical activity is a consequence of spatial dispersion induced circular birefringence, where spatial dispersion is considered as a small correction to the principal dielectric constants, so that the approximation in (4.4.25) is justified due to $\gamma(q,\omega)\ll\varepsilon_1(\omega)$.

Retaining the two dimensional description of polarization, the superposition of the left and right circularly polarized modes results in

$$\begin{aligned}\mathbf{e}(\mathbf{r},\omega)&=\tilde{\mathbf{e}}_{-}(\mathbf{q},\omega)\,e^{i\varphi_{-}(\mathbf{q},\omega)}+\tilde{\mathbf{e}}_{+}(\mathbf{q},\omega)\,e^{i\varphi_{+}(\mathbf{q},\omega)}\\&=\sqrt{2}e^{\frac{i}{2}(\varphi_{-}(\mathbf{q},\omega)+\varphi_{+}(\mathbf{q},\omega))}\begin{pmatrix}\sin\left[\frac{1}{2}(\varphi_{-}(\mathbf{q},\omega)-\varphi_{+}(\mathbf{q},\omega))\right]\\\cos\left[\frac{1}{2}(\varphi_{-}(\mathbf{q},\omega)-\varphi_{+}(\mathbf{q},\omega))\right]\end{pmatrix},\end{aligned} \tag{4.4.27}$$

after the wave traveled some distance z. It should be emphasized, that $e^{\frac{i}{2}(\varphi_{-}(\mathbf{q},\omega)+\varphi_{+}(\mathbf{q},\omega))}=e^{i\frac{\omega}{c}n_1(\omega)z}$ constitutes a global phase factor which is independent of spatial dispersion and does *not* affect the polarization state. Without loss of generality, assume that the crystal extends in z-direction from $z=0$ to $z=d$. Noticing that $\varphi_{\pm}(\mathbf{q},\omega)=0$ if $z=0$, it is easily seen from (4.4.27), that the wave $\mathbf{e}_{\text{in}}(\mathbf{r},\omega)$ incident on the crystal at $z=0$ is linearly polarized in y-direction, i.e. $\mathbf{e}_{\text{in}}(\mathbf{r},\omega)=\sqrt{2}(0\;1)^T$, while the wave $\mathbf{e}_{\text{out}}(\mathbf{r},\omega)$ passing out the crystal at $z=d$ is also linearly polarized, but its polarization direction is rotated with respect to $\mathbf{e}_{\text{in}}(\mathbf{r},\omega)$ by the angle

$$\beta(\mathbf{q},\omega)=\frac{1}{2}(\varphi_{-}(\mathbf{q},\omega)-\varphi_{+}(\mathbf{q},\omega))=-\frac{\omega}{c}\frac{\gamma(q,\omega)}{2n_1(\omega)}d. \tag{4.4.28}$$

The crystal's rotatory power $\rho(q,\omega)$ is then defined as angle of rotation per propagation length, so that one immediately obtains from (4.4.28) (with $\frac{\omega}{c}=\frac{2\pi}{\lambda}$)

$$\rho(q,\omega)=-\frac{\pi}{\lambda}\frac{\gamma(q,\omega)}{n_1(\omega)}, \tag{4.4.29}$$

which can also be written in the form

$$\rho(q,\omega)=\frac{\pi}{\lambda}(n_{-}(\mathbf{q},\omega)-n_{+}(\mathbf{q},\omega)), \tag{4.4.30}$$

so that it becomes manifest, that circular birefringence is the origin of rotatory power[25]. By convention, a crystal is said to be dextrorotatory, if for an observer looking at the (light) source through the crystal, the plane of polarization of the linearly polarized wave rotates to the right, i.e. clockwise. On the other hand, if the plane of polarization rotates to the left, i.e. counter-clockwise, the crystal is said to be

[25]It should be noted, that the dimensional unit of $\rho(q,\omega)$ is $\frac{\text{rad}}{\text{m}}$.

laevorotatory. In case of a dextrorotatory crystal, the phase velocity of the propagating right circular polarization state is larger than that of the left circular, so that $n_+(\mathbf{q},\omega) < n_-(\mathbf{q},\omega)$. As a consequence, there holds $\rho(q,\omega) > 0$ in dextrorotatory crystals. In laevorotatory crystals, the converse remains valid, so that $\rho(q,\omega) < 0$. The representation of $\rho(q,\omega)$ by means of $\gamma(q,\omega)$ (see (4.4.29)) reveals two characteristics of natural optical activity. First, rotatory power vanishes when spatial dispersion is neglected, i.e. if $\mathbf{q} = \mathbf{0}$, because of (4.4.18). Second, if the propagation direction of the electromagnetic wave is reversed, $\rho(q,\omega)$ changes sign due to (4.4.19). Hence, the helicity of the path traced by the polarization vector remains unaltered, so that natural optical activity constitutes a reciprocal optical effect[26].

Because the story of natural optical activity has begun with SiO_2 ($\alpha-$quartz), we start with the calculation of its frequency dependent rotatory power $\rho(q,\omega)$ on the basis of (4.4.29) or (4.4.30), where the electromagnetic wave is assumed to propagate along the optical z-axis, i.e. $\mathbf{q} = |\mathbf{q}|\,\mathbf{e}^{(3)}$. To be exact, the modulus $|\mathbf{q}|$ of the wave vector $\mathbf{q}$ for a given frequency ω is set by the photonic band structure $\omega_n(\mathbf{q})$, which reveals the existence of a left and a right circularly polarized propagable mode in the optical spectral regime. However, for these rather low frequencies, there holds $||\mathbf{q}_+| - |\mathbf{q}_-|| = \frac{\omega}{c}|n_+(\mathbf{q},\omega) - n_-(\mathbf{q},\omega)| = \frac{\omega}{c}\left|\frac{\gamma(q,\omega)}{n_1(\omega)}\right| \ll \frac{\omega}{c}$, so that for practical calculations the parameterization of $|\mathbf{q}|$ by the principal index of refraction $n_1(\omega)$ alone according to $|\mathbf{q}| = \frac{\omega}{c}n_1(\omega)$ is an excellent approximation[27]. Utilizing an isotropic Lorentz oscillator model for the electronic polarizabilities with parameters given in table 4.4.2, the experimental data regarding the rotatory power of the laevorotatory SiO_2 ($\alpha-$quartz) of space group $P3_121$ are nicely reproduced by means of (4.4.29), see figure 4.4.4. The relative error between experimental data and the presented theory does not exceed 3.2%. It should be pointed out, that better agreement could easily be achieved by allowing the electronic polarizabilities to be anisotropic.

Finally, the rotatory power $\rho(q,\omega)$ is calculated and compared to experimental data for all optically active crystals from table 4.4.3 marked with an asterisk "$*$". The results are summarized in table 4.4.4, where the calculations have been carried out for the wavelengths and polarizabilities which are reported in table 4.4.3, of course. It is apparent that the presented theory always yields the correct direction of rotation. In this context it is interesting to note, that the laevorotatory $\alpha-$quartz (see figure 4.4.4) and the dextrorotatory $\alpha-AlPO_4$ (see table 4.4.4) belong to the same space group $P3_121$. This fact clearly evidences, that rotatory power is not simply a consequence of the chirality provided by the space group, but rather by the helical structures formed by the most polarizable atoms within the Wigner-Seitz cell C_Λ. Altogether, $\rho^{(\mathrm{calc})}$ matches $\rho^{(\mathrm{exp})}$ quite well. The appearing discrepancies may be attributed to the fact that, on the one hand, the assumption of isotropic polarizabilities is an oversimplification, and on the other hand, that even ions of identical sort may possess distinct polarizabilities because of their

[26] A physical process is said to be reciprocal, if the time-reversed process leads to a mental picture of something that is physically conceivable, and when this time-reversed process shows *no* characteristic distinctions with respect to the original one. Popular examples are natural optical activity and Brownian motion in thermal equilibrium [54].

[27] Throughout this section, the paramaterization $|\mathbf{q}| = \frac{\omega}{c}n_1(\omega)$ is used, where $n_1(\omega) = n(\omega)$ in cubic and $n_1(\omega) = n_o(\omega)$ in uniaxial crystal structures.

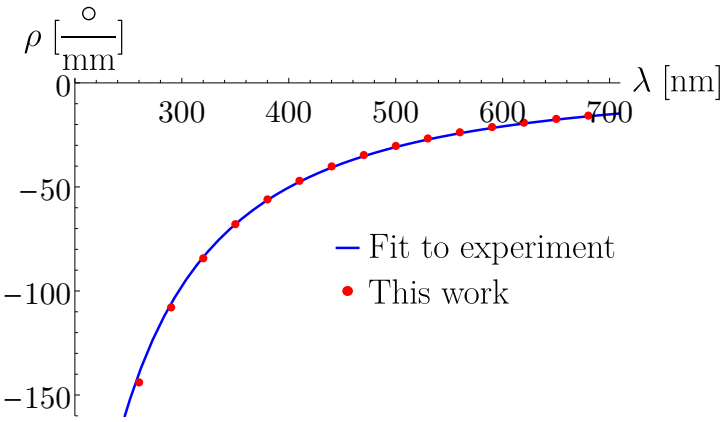

Figure 4.4.4: Plot of rotatory power $\rho\,(q,\omega)$ vs. free space wavelength $\lambda = \frac{2\pi c}{\omega}$ for laevorotatory SiO_2 ($\alpha-$quartz) of space group $P3_121$ with regard to wave propagation along its optical z-axis. Displayed are values (red dots) calculated from (4.4.29), solely with the crystalline structure [98] and the isotropic electronic polarizabilities of the individual ions as input. The respective parameters entering the electronic polarizability model of the Lorentz oscillator type (3.1.1) are given in table 4.4.2. The blue line represents a fit to experimental data of rotatory power taken from [56]. The relative error in $\rho\,(q,\omega)$ between experiment and theory does not exceed 3.2%.

crystal	space group	λ [nm]	$\rho^{(\mathrm{exp})}\ [\frac{°}{\mathrm{mm}}]$	$\rho^{(\mathrm{calc})}\ [\frac{°}{\mathrm{mm}}]$	references
$\beta-SiO_2$	$P6_222$	517	+33.6	+29.84	[56]
$NaClO_3$	$P2_13$	633	+2.44	+3.76	[99]
$Bi_{12}TiO_{20}$	I23	633	-5.9	-6.12	[100]
$Bi_{12}SiO_{20}$	I23	650	-20.5	-19.35	[101]
$\alpha-AlPO_4$	$P3_121$	633	+14.6	+11.23	[97]
$Tm_2Ge_2O_7$	$P4_12_12$	633	-15.0	-14.49	[95]

Table 4.4.4: Calculation of the rotatory power $\rho^{(\mathrm{calc})}$ and comparison with experimental results $\rho^{(\mathrm{exp})}$ for all optically active crystal structures marked with an asterisk "$*$" in table 4.4.3. While the data on crystal structures and electronic polarizabilities, both entering the calculation of $\rho^{(\mathrm{calc})}$ via (4.4.29), are taken from table 4.4.3, the experimental data for $\rho^{(\mathrm{exp})}$ have been inferred from the publications cited in the column "references".

different locations within C_Λ(for instance, see $Tm_2Ge_2O_7$ [95]).

In this section it has been shown, that natural optical activity is a consequence of spatial dispersion induced circular birefringence in non-centrosymmetric crystal structures. Simultaneously, this optical effect represented by $\gamma_{abc}(\omega)$ constituted the lowest order correction to the transverse dielectric tensor $\varepsilon_{ab}^{(\mathrm{T})}(\mathbf{q},\omega)$, when the latter is expanded with respect to wave vector $\mathbf{q}$ (see (4.4.12)). When considering centrosymmetric crystal structures, the lowest order contribution of spatial dispersion to $\varepsilon_{ab}^{(\mathrm{T})}(\mathbf{q},\omega)$ will be due to $\alpha_{abcd}(\omega)$, because $\gamma_{abc}(\omega)=0$. Irrespective of its negligible magnitude in the visible spectral regime, the effect of spatial dispersion induced birefringence represented by $\alpha_{abcd}(\omega)$ gives reason for concern regarding the imaging quality of dielectric lenses made from crystalline dielectrics, a topic of prime importance when designing modern lithographic optical systems in the (deep) ultraviolet [9, 102]. Therefore, the next section addresses the consequences on the optical properties of crystalline structures, when $\alpha_{abcd}(\omega)$ is no longer negligible.

Addendum: Magnetic induction field induced circular birefringence or the Faraday effect Suppose that a dielectric (non-magnetic) crystal is put into an externally controlled *static* magnetic induction field $\mathbf{B}^{(0)}$. Then the former state of equilibrium of each constituent of the crystal, represented by its individual electronic polarizability $\alpha_{ab}^{(\mathrm{el})}\left(\eta^{(j)},\omega\right)$ with $j\in\{1,2,\ldots,M\}$, is changed due to the interaction between the charge carriers comprised by that constituent and $\mathbf{B}^{(0)}$. As a consequence, a new state of equilibrium is established in each constituent, described by a polarizability $\alpha_{ab}^{(\mathrm{el})}\left(\eta^{(j)},\omega;\mathbf{B}^{(0)}\right)$. Assuming that $\alpha_{ab}^{(\mathrm{el})}\left(\eta^{(j)},\omega;\mathbf{B}^{(0)}\right)$ is an analytic function with respect to $\mathbf{B}^{(0)}$, its Taylor expansion around $\mathbf{B}^{(0)}=\mathbf{0}$ readily yields to first order[28]

$$\alpha_{ab}^{(\mathrm{el})}\left(\eta^{(j)},\omega;\mathbf{B}^{(0)}\right)=\alpha_{ab}^{(\mathrm{el})}\left(\eta^{(j)},\omega\right)+i\sum_{c=1}^{3}\beta_{abc}^{(j)}(\omega)\,B_c^{(0)}, \tag{4.4.31}$$

where $\alpha_{ab}^{(\mathrm{el})}\left(\eta^{(j)},\omega\right)$ represents the frequency dependent electronic polarizability of the j^{th}-constituent typically associated with the Lorentz oscillator model[29] (3.1.1). Additionally there holds $\beta_{abc}^{(j)}(\omega)=\left[\beta_{abc}^{(j)}(\omega)\right]^{*}$. It is important to realize, that $\beta_{abc}^{(j)}(\omega)$ constitutes an axial tensor of odd rank. Hence, there is a priori *no* symmetry argument requiring that $\beta_{abc}^{(j)}(\omega)$ vanishes in any of the 32 crystallographic point groups, when Neumann's principle is applied [5].

Because the dielectric tensor is a functional of $\alpha_{ab}^{(\mathrm{el})}\left(\eta^{(j)},\omega;\mathbf{B}^{(0)}\right)$, it is invariably affected by the magnetic induction field if $\mathbf{B}^{(0)}\neq\mathbf{0}$. Of course, the same holds true for the transverse dielectric tensor, so that now there is $\varepsilon^{(\mathrm{T})}\left(\mathbf{q},\omega;\mathbf{B}^{(0)}\right)$ instead of $\varepsilon^{(\mathrm{T})}(\mathbf{q},\omega)$. Its expansion with respect to $\mathbf{q}$ and $\mathbf{B}^{(0)}$ up to

[28] Compare with (3.3.8) and the discussion that is given there.

[29] A simple formula for $\alpha_{ab}^{(\mathrm{el})}\left(\eta^{(j)},\omega;\mathbf{B}^{(0)}\right)$ can be derived within the framework of the classical, driven Lorentz oscillator model, see [26]. However, this oversimplified model shows some shortcomings, when consulted for the description of the Faraday effect in crystals. For a discussion see [103].

second order

$$\begin{aligned}\varepsilon_{ab}^{(\mathrm{T})}\left(\mathbf{q},\omega;\mathbf{B}^{(0)}\right) =& \varepsilon_{ab}^{(\mathrm{T})}(\omega) + i\sum_{c=1}^{3}\gamma_{abc}(\omega)\,q_c + i\sum_{c=1}^{3}\gamma_{abc}^{(\mathrm{F})}(\omega)\,B_c^{(0)} \\ &+ \sum_{c,d=1}^{3} A_{abcd}^{(\mathrm{MISD})}(\omega)\,q_c B_d^{(0)} + \sum_{c,d=1}^{3}\alpha_{abcd}(\omega)\,q_c q_d + \sum_{c,d=1}^{3} A_{abcd}^{(\mathrm{CM})}(\omega)\,B_c^{(0)} B_d^{(0)}\end{aligned} \tag{4.4.32}$$

(compare with [1]) reveals several new optical effects in comparison to (4.4.12). Here, $\gamma_{abc}^{(\mathrm{F})}(\omega)$ describes the Faraday effect, $A_{abcd}^{(\mathrm{MISD})}$ the effect of magnetically induced spatial dispersion and $A_{abcd}^{(\mathrm{CM})}(\omega)$ the Cotton-Mouton effect [104].

Assuming that spatial dispersion is negligible, (4.4.32) reduces to

$$\varepsilon_{ab}^{(\mathrm{T})}\left(\omega;\mathbf{B}^{(0)}\right) \equiv \varepsilon_{ab}^{(\mathrm{T})}\left(\mathbf{0},\omega;\mathbf{B}^{(0)}\right) = \varepsilon_{ab}^{(\mathrm{T})}(\omega) + i\sum_{c=1}^{3}\gamma_{abc}^{(\mathrm{F})}(\omega)\,B_c^{(0)}, \tag{4.4.33}$$

provided that $A_{abcd}^{(\mathrm{CM})}(\omega)$ is insignificantly small. In analogy to natural optical activity, the propagable crystalline eigenmodes are determined from the wavelike equation (4.2.21) for $\tilde{\mathbf{j}}_{\mathrm{ext}}^{(\mathrm{T})}(\mathbf{q},\omega) = \mathbf{0}$, where now the transverse dielectric tensor is given by (4.4.33). In general, these crystalline eigenmodes correspond to elliptically polarized waves, that traverse the magneto-optically active material described by $\varepsilon_{ab}^{(\mathrm{T})}\left(\omega;\mathbf{B}^{(0)}\right)$ with different phase velocities. As a result, a linearly polarized electromagnetic wave incident upon such a material emerges from this as an elliptically polarized wave. The angle enclosed by the linear polarization state of the incident wave and the major axis of the emerging elliptically polarized wave is called Faraday rotation angle ψ, where the ratio of minor to major axis of the ellipse (the Faraday ellipticity) is usually described by an angle χ [105].

If $\mathbf{q}\times\mathbf{B}^{(0)} = \mathbf{0}$ and additionally wave propagation along a highly symmetrical, say (optical) z-axis (i.e. $\mathbf{q} = q\mathbf{e}^{(3)}$) in cubic and uniaxial crystal structures is assumed, $\varepsilon^{(\mathrm{T})}\left(\omega;\mathbf{B}^{(0)}\right)$ is formally equivalent to (4.4.20), solely the replacement $\gamma(q,\omega) \to \gamma\left(B_3^{(0)},\omega\right)$ with $\gamma\left(B_3^{(0)},\omega\right) \propto B_3^{(0)}$ has to be done. Of course, the two crystalline eigenmodes now correspond to a left and a right circularly polarized wave respectively, both traveling with different phase velocities. Once the crystal of thickness d has been traversed, their superposition results in a linearly polarized wave, whose plane of polarization is rotated with respect to the incident one by an angle

$$\psi = V B_3^{(0)} d, \tag{4.4.34}$$

where V denotes the frequency and temperature dependent material-specific Verdet-"constant" [97].

In contrast to natural optical activity, the thus induced circular birefringence is unaware of spatial dispersion. It is solely a consequence of the broken time-reversal symmetry caused by the static magnetic induction field $\mathbf{B}^{(0)}$ [54]. As a consequence, the angle of rotation ψ does *not* change sign, if

the propagation direction of the electromagnetic wave is reversed, i.e. the helicity of the path traced by the polarization vector changes its orientation when $q \to -q$. For that reason the Faraday effect is called a non-reciprocal[30] optical effect, in contrast to natural optical activity which is reciprocal. This non-reciprocity is applicable for a variety of technical practices, because it allows for instance the construction of magneto-optical isolators or the design of magnetic field sensors [106, 107]. Although Faraday's discovery of magnetic induction field induced circular birefringence is traced back to the year 1845 [56], it is still a subject of current interest in fundamental research, in particular in the context of graphene [108].

4.4.3.3 Spatial dispersion induced birefringence

As has already been pointed out by Lorentz [109], the commonly presumed optical isotropy of cubic crystals is broken when they are traversed by an electromagnetic wave because of a symmetry breaking accompanied by the finite wave vector $\mathbf{q}$, resulting in spatial dispersion induced birefringence. Although this omnipresent optical effect is known for a long time, it received only little attention because of its negligible magnitude in the visible spectral regime. However, with the progress made by the lithography industry in producing smaller and smaller semiconductor structures by means of optical systems operating in the deep ultraviolet (DUV) spectral regime, spatial dispersion induced birefringence has been "rediscovered". Since inherent isotropic optics made of glassy materials are inappropriate in the DUV spectral regime due to their high absorption, cubic crystalline materials like CaF_2 or BaF_2 are utilized to realize modern optical lithography systems. Since the wave vector $\mathbf{q}$ is no longer negligible in this spectral regime, the so designed imaging systems suffer from spatial dispersion induced birefringence. In particular, this intrinsic birefringence[31] implicates a significant loss in image quality and contrast [9, 102], both being crucial parameters with regard to the patterning of semiconductor circuits on microscopic length scales. Beside already established technologies like optical lithography, spatial dispersion induced birefringence is also relevant in the context of photonic crystals or metamaterials, which may possess exceptional optical properties. For instance, they can exhibit a negative index of refraction [110, 111] and thus allow the design of optics that provide perfect optical imaging [112], given that $n = -1$ holds exactly and is not altered by the magnitude and direction of the wave vector $\mathbf{q}$. Also, the implementation of optical cloaking devices [113, 114] is possible by tailoring the index of refraction n accurately. Because the effect of spatial dispersion induced birefrigence Δn in such artificial materials can be comparable in magnitude with the usual index of refraction n [115], a profound knowledge is required to develop appropriate compensation techniques for Δn, that could allow

[30] A physical process is said to be non-reciprocal, if the time-reversed process leads to a mental picture of something that is physically conceivable, but shows characteristic distinctions with respect to the original situation. Popular examples are the Faraday and the Fizeau effect [54].

[31] Note, that the 157nm lithography target specification regarding birefringence is $\Delta n = 10^{-7}$, while the experimentally determined induced birefringence due to spatial dispersion in CaF_2 and BaF_2 is of order $\Delta n \sim 10^{-6}$ at $\lambda = \frac{2\pi c}{\omega} = 156.1$nm [9], if $\mathbf{q} || (110)^T$. Even the birefringence caused by residual stresses, which is a consequence of polishing the crystal, may be exceeded by that of spatial dispersion by a multiple [102].

a wide-ranging technical applicability of these materials, similar to these of modern optical lithography systems [116, 117].

A genuine analysis of spatial dispersion induced birefringence mediated by $\alpha_{abcd}(\omega)$ in the expansion (4.4.12) of the transverse dielectric tensor $\varepsilon_{ab}^{(\mathrm{T})}(\mathbf{q},\omega)$ requires the exclusion of spatial dispersion induced effects, whose influences on $\varepsilon_{ab}^{(\mathrm{T})}(\mathbf{q},\omega)$ are of comparable or even larger magnitude than those associated with $\alpha_{abcd}(\omega)$. Therefore, in the remainder of this section, only centrosymmetric crystals are considered. This implies the elimination of natural optical activity because of $\gamma_{abc}(\omega)=0$, so that in the expansion (4.4.12), $\alpha_{abcd}(\omega)$ constitutes the leading order contribution to $\varepsilon_{ab}^{(\mathrm{T})}(\mathbf{q},\omega)$ with respect to spatial dispersion, i.e. there holds[32]

$$\varepsilon_{ab}^{(\mathrm{T})}(\mathbf{q},\omega)=\varepsilon_{ab}^{(\mathrm{T})}(\omega)+\sum_{c,d=1}^{3}\alpha_{abcd}(\omega)\,q_c q_d. \tag{4.4.35}$$

Notice, that in contrast to natural optical activity represented by $\gamma_{abc}(\omega)$, the *non-local* response of the material's constituents implied by $\alpha_{abcd}(\omega)$ is omnipresent, i.e. there exists a priori *no* crystallographic point group symmetry that makes $\alpha_{abcd}(\omega)$ vanishing. The realization of 157nm lithography systems requires optics made of materials, whose birefringence is maximally $\Delta n=10^{-7}$ [9]. This target specification is only achievable by means of cubic crystals, so that the ensuing discussion of spatial dispersion induced birefringence is restricted to the cubic crystal system[33], which is optically isotropic in the limit $\mathbf{q}=\mathbf{0}$. In particular, the cubic crystals CaF_2, BaF_2, CsI and RbCl are considered, each of them exhibiting the crystallographic point group symmetry $m\bar{3}m$. For wave propagation along a plane diagonal of the Wigner-Seitz cell C_Λ, say the diagonal of the x-y plane where $\mathbf{q}=\frac{|\mathbf{q}|}{\sqrt{2}}(110)^T$, spatial dispersion induced birefringence assumes its maximum value [9]. In this special case, the transverse dielectric tensor (4.4.35) can be written formally (in cartesian coordinates) in the condensed form

$$\varepsilon^{(\mathrm{T})}(\mathbf{q},\omega)=\varepsilon(\omega)\begin{pmatrix}\frac{1}{2}&-\frac{1}{2}&0\\-\frac{1}{2}&\frac{1}{2}&0\\0&0&1\end{pmatrix}+|\mathbf{q}|^2\begin{pmatrix}\xi_1(\omega)+\xi_2(\omega)&-\xi_1(\omega)-\xi_2(\omega)&0\\-\xi_1(\omega)-\xi_2(\omega)&\xi_1(\omega)+\xi_2(\omega)&0\\0&0&4\xi_2(\omega)\end{pmatrix}, \tag{4.4.36}$$

as is shown in appendix H.3. In (4.4.36), $\varepsilon(\omega)$ denotes the familiar frequency dependent scalar dielectric function associated with cubic crystals, while the abbreviations $\xi_1(\omega)$ and $\xi_2(\omega)$ can be grasped as two independent parameters that subsume the individual contributions of $\alpha_{abcd}(\omega)$.

In analogy to the previous section 4.4.3.2, the propagable modes of the transverse macroscopic radiation field $\tilde{\mathscr{E}}^{(\mathrm{T})}(\mathbf{q},\omega)$ in crystals in consideration of spatial dispersion induced birefringence are determined from the wavelike equation (4.2.21) by eliminating the external current source. Utilizing the abbrevia-

[32] Of course, there exist higher-order contributions of spatial dispersion to $\varepsilon_{ab}^{(\mathrm{T})}(\mathbf{q},\omega)$ than $\alpha_{abcd}(\omega)$. However, these come first into play for frequencies beyond the spectral regime, that is relevant for applications like 157nm lithography.

[33] Notice, that the birefringence inherently possessed by uniaxial and biaxial crystals is typically of the order $\Delta n\sim 10^{-2}-10^{-1}$ and thus constitutes a show-stopper in the design of optical imaging systems for lithographic applications.

tion $n^2(\mathbf{q},\omega) = \frac{c^2}{\omega^2}|\mathbf{q}|^2$, the resulting eigenvalue problem can be cast into

$$\boldsymbol{\varepsilon}^{(\mathrm{T})}(\mathbf{q},\omega)\cdot\tilde{\mathscr{E}}^{(\mathrm{T})}(\mathbf{q},\omega) = n^2(\mathbf{q},\omega)\,\tilde{\mathscr{E}}^{(\mathrm{T})}(\mathbf{q},\omega). \tag{4.4.37}$$

As a consequence of (4.4.37), there exist two propagable linearly polarized modes

$$\tilde{\mathscr{E}}^{(\mathrm{T})}_{(001)}(\mathbf{q},\omega) = \begin{pmatrix} 0 \\ 0 \\ 1 \end{pmatrix} \text{ with } n^2_{(001)}(\mathbf{q},\omega) = \varepsilon(\omega) + 4\xi_2(\omega)|\mathbf{q}|^2 \tag{4.4.38}$$

$$\tilde{\mathscr{E}}^{(\mathrm{T})}_{(1\bar{1}0)}(\mathbf{q},\omega) = \frac{1}{\sqrt{2}}\begin{pmatrix} 1 \\ -1 \\ 0 \end{pmatrix} \text{ with } n^2_{(1\bar{1}0)}(\mathbf{q},\omega) = \varepsilon(\omega) + 2\left(\xi_1(\omega)+\xi_2(\omega)\right)|\mathbf{q}|^2, \tag{4.4.39}$$

which correspond to the two mutually orthogonal polarization degrees of freedom of the electromagnetic radiation field[34]. Obviously, this result confirms Lorentz's note on breaking the symmetry of optical isotropy, which is commonly attributed to cubic crystals, as a consequence of the finiteness of the wave vector $\mathbf{q}$. While for $|\mathbf{q}| = 0$ the indices of refraction associated with the propagable modes $\tilde{\mathscr{E}}^{(\mathrm{T})}_{(001)}(\mathbf{q},\omega)$ and $\tilde{\mathscr{E}}^{(\mathrm{T})}_{(1\bar{1}0)}(\mathbf{q},\omega)$ coincide according to $n_{(001)}(\mathbf{0},\omega) = n_{(1\bar{1}0)}(\mathbf{0},\omega) = \sqrt{\varepsilon(\omega)} \equiv n(\omega)$ and thus preserve the optical isotropy of cubic crystals, they slightly differ (in agreement with [118]) by the amount

$$\Delta n(\mathbf{q},\omega) = n_{(1\bar{1}0)}(\mathbf{q},\omega) - n_{(001)}(\mathbf{q},\omega) \tag{4.4.40}$$

$$\approx \frac{\xi_1(\omega)-\xi_2(\omega)}{n(\omega)}|\mathbf{q}|^2, \tag{4.4.41}$$

when the realistic case of a wave vector with finite modulus $|\mathbf{q}| > 0$ is considered[35]. Generally speaking, birefringence $\Delta n(\mathbf{q},\omega)$ is induced in the cubic crystal when it is traversed by an electromagnetic wave in direction of a plane diagonal[36] of its Wigner-Seitz cell C_Λ. However, it should be realized, that there could exist a certain frequency $\omega = \omega_{\mathrm{iso}}$, which would allow for $\xi_1(\omega_{\mathrm{iso}}) = \xi_2(\omega_{\mathrm{iso}})$, so that due to (4.4.41) the spatial dispersion induced birefringence $\Delta n(\mathbf{q},\omega_{\mathrm{iso}})$ exactly vanishes.

In what follows, the frequency dependence of spatial dispersion induced birefringence $\Delta n(\mathbf{q},\omega)$ is computed, which is experienced by an electromagnetic wave with wave vector $\mathbf{q} = \frac{|\mathbf{q}|}{\sqrt{2}}(110)^T$, when

[34] Of course, the eigenvalue problem (4.4.37) possesses a third solution, namely $\tilde{\mathscr{E}}^{(\mathrm{T})}_{(110)}(\mathbf{q},\omega) = \frac{1}{\sqrt{2}}(110)^T$ with $n^2_{(110)}(\mathbf{q},\omega) = 0$. However, due to the vanishing eigenvalue, the mode $\tilde{\mathscr{E}}^{(\mathrm{T})}_{(110)}(\mathbf{q},\omega)$ which is orientated parallel to the wave vector $\mathbf{q}$, is *not* capable to propagate within the crystal.

[35] In the derivation of (4.4.41) it has been assumed, that $\varepsilon(\omega)$ constitutes the dominant contribution to $n_{(1\bar{1}0)}(\mathbf{q},\omega)$ and $n_{(001)}(\mathbf{q},\omega)$ respectively, while the $\mathbf{q}$-dependent terms only represent small corrections. For a microscopic justification on basis of a band-model, see [119].

[36] Notice, that for directions of higher symmetry, i.e. $\mathbf{q}||(100)$ and $\mathbf{q}||(111)$ as well as all symmetrically equivalent directions, the principal index of refraction of the cubic crystal is slightly modified due to spatial dispersion, while its optical isotropy is conserved.

traversing the cubic crystals CsI, RbCl, CaF_2 and BaF_2 that belong to the crystallographic point group $m\bar{3}m$. Thereto, the transverse dielectric tensor $\varepsilon^{(T)}(\mathbf{q},\omega)$ is initially deduced from the dielectric tensor $\varepsilon_\Lambda(\mathbf{q},\omega)$ given by (4.1.17), where solely the crystalline structure as well as the isotropic Lorentz oscillator models (3.1.1) and (3.1.2) for the electronic or ionic displacement polarizabilities, with parameters given in table 4.4.2, enter its calculation. Since the formal structure of the so obtained $\varepsilon^{(T)}(\mathbf{q},\omega)$ is equivalent to that in (4.4.36), the subsequent computation of $\Delta n(\mathbf{q},\omega)$ via (4.4.40) follows the lines indicated above. Again it should be stressed, that the modulus $|\mathbf{q}|$ of the wave vector $\mathbf{q}$, which is associated with a propagable mode of frequency ω, is set by the photonic band structure $\omega_n(\mathbf{q})$, which now reveals the existence of two mutually orthogonal linearly polarized radiation modes $\tilde{\mathscr{E}}^{(T)}_{(001)}(\mathbf{q},\omega)$ and $\tilde{\mathscr{E}}^{(T)}_{(1\bar{1}0)}(\mathbf{q},\omega)$. However, because the two distinct wave vectors associated with these modes solely differ by the amount $\left|\left|\mathbf{q}_{(1\bar{1}0)}\right| - \left|\mathbf{q}_{(001)}\right|\right| = \frac{\omega}{c}|\Delta n(\mathbf{q},\omega)| \ll \frac{\omega}{c}$, for practical calculations the parameterization of $|\mathbf{q}|$ by means of the principal index of refraction $n(\omega)$ according to $|\mathbf{q}| = \frac{\omega}{c}n(\omega)$ is an excellent approximation[37], that will be used for the calculation of $\Delta n(\mathbf{q},\omega)$ in the remainder of this section. Figure 4.4.5 shows a comparison of calculated values of the frequency dependence of spatial dispersion induced birefringence on the basis of (4.4.40) with experimental data for CsI and RbCl [118] as well as CaF_2 and BaF_2 [9]. In each case, the experimental results are nicely reproduced by the presented theory. With regard to 157nm lithography, the consequences of spatial dispersion induced birefringence in CaF_2 and BaF_2 (see figure 4.4.5 (c) and (d)) seem fatal, as it exceeds the target specification for birefringence $\Delta n = 10^{-7}$ by a multiple. Nonetheless, there is no need to surrender, because the opposite sign of this optical effect in these two materials suggests the combination of optical components made of both materials. Furthermore, an appropriate mixed solid solution $Ca_{1-x}Ba_xF_2$ could eliminate this disruptive effect at the desired wavelength [9, 117].

[37] Compare with the discussion of natural optical activity in section 4.4.3.2.

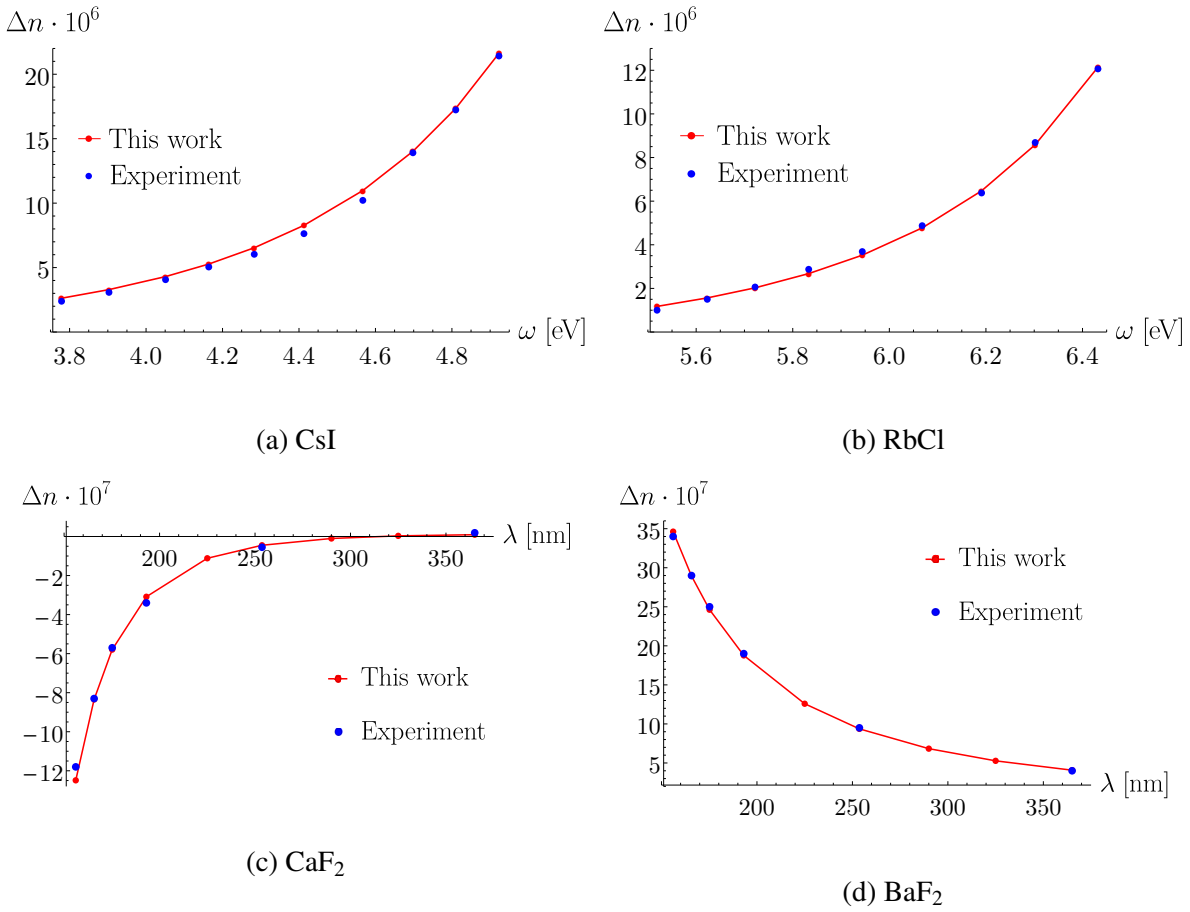

(a) CsI

(b) RbCl

(c) CaF_2

(d) BaF_2

Figure 4.4.5: Comparison of experimental data (blue), taken from [9, 118], on the frequency dependence of spatial dispersion induced birefringence $\Delta n(\mathbf{q},\omega)$ in (a) CsI (b) RbCl (c) CaF_2 and (d) BaF_2 with calculated values (red) resulting from the $\mathbf{q}$-dependence of the transverse dielectric tensor $\varepsilon^{(\mathrm{T})}(\mathbf{q},\omega)$. In all cases there is $\mathbf{q}||(110)^T$. For CsI and RbCl, the experimental values of $\Delta n(\mathbf{q},\omega)$ have been read of a plot. The estimated error in reading is about $\pm 0.2 \cdot 10^{-6}$.

Chapter 5

Summary

In this work, a self-contained theory of the local electromagnetic field in crystalline dielectrics and its relation to macroscopic electrodynamics is established, where the presented integral equation approach substantially differs from conventional expositions on this subject (see e.g. [4, 28, 120]). Initially, deploying the Helmholtz decomposition theorem to the microscopic Maxwell (differential) equations, the independent degrees of freedom of the electromagnetic theory corresponding to its irrotational (longitudinal) and solenoidal (transverse) contributions are identified (compare with [18]). This allows to restate the differential equations determining the local electromagnetic field in terms of equivalent inhomogeneous integral equations. The material model of the dielectric crystal under investigation, including electronic as well as ionic displacement polarizability effects, is completely described by the lattice periodic dielectric susceptibility kernel $\chi_{ab}(\mathbf{r},\mathbf{r}',\omega)$ (see (3.1.6)), which relates the microscopic polarization $\mathbf{P}(\mathbf{r},\omega)$ with the local electric field $\mathbf{E}(\mathbf{r},\omega)$ via a convolution integral.

In view of Bloch's theory [3] it seems natural to expand $\mathbf{E}(\mathbf{r},\omega)$ with respect to a complete and orthonormal set of eigenfunctions of the translation operator $\hat{T}_{\mathbf{R}}$, whose action on a function $f(\mathbf{r})$ is to shift its argument by a lattice vector $\mathbf{R}\in\Lambda$ according to $\hat{T}_{\mathbf{R}}f(\mathbf{r})=f(\mathbf{r}+\mathbf{R})$. However, the popular basis system of plane waves $\left\{e^{i(\mathbf{q}+\mathbf{G})\cdot\mathbf{r}}\right\}_{\mathbf{q}\in C_{\Lambda^{-1}},\mathbf{G}\in\Lambda^{-1}}$, constructed from eigenfunctions of the momentum operator, turns out to be unsuited for this purpose, as it requires for each wave vector $\mathbf{q}\in C_{\Lambda^{-1}}$ the handling of huge, completely filled matrices, that are labeled by reciprocal lattice vectors $\mathbf{G},\mathbf{G}'\in\Lambda^{-1}$. Instead, the basis system of non-standard Bloch functions $\{w(\mathbf{r};\mathbf{s},\mathbf{k})\}_{\mathbf{s}\in C_{\Lambda},\mathbf{k}\in C_{\Lambda^{-1}}}$ (see (3.2.9)) is deployed, which can be constructed from eigenfunctions of the position operator. This allows to deal with small sparse matrices, so that various (numerical) difficulties and inaccuracies that are related to the truncation or inversion of huge matrices can be avoided. In addition, it allows to solve the inhomogeneous integral equations determining the local electromagnetic field within crystalline dielectrics exactly (see (3.2.39) and (3.2.46)).

The propagable modes inside the crystalline dielectric including their dispersion relation $\omega_n(\mathbf{q})$, that is also called photonic band structure, are then obtained by considering the associated homogeneous integral equations (3.3.1), where $\omega_n(\mathbf{q})$ turns out to be the solvability condition of the corresponding

$3M \times 3M$ eigenvalue problem (3.3.2), with M denoting the number of atoms or ions comprised by the Wigner-Seitz cell C_Λ. In particular, $\omega_n(\mathbf{q})$ is calculated for the monatomic sc-, fcc- and bcc-lattices as well as for the diatomic diamond lattice, where radiation damping initially has been neglected. In all cases, the presented computations agree well with previously published results on the photonic band structures which have been obtained by different methods. Taking radiation damping given by (3.3.4) into account, it is shown that the concept of a photonic band structure $\omega_n(\mathbf{q})$ including many band branches looses its meaning for real crystalline materials with microscopic lattice constants, if ω exceeds a critical frequency ω_c. Finally, the removal of band degeneracies in the photonic band structure is demonstrated by applying a static magnetic induction field to the crystal.

From the solution of the inhomogeneous integral equations determining the local electric field $\mathbf{E}(\mathbf{r},\omega)$ in presence of a slowly varying time harmonic external signal $\mathbf{E}_{\text{ext}}(\mathbf{r},\omega)$ it is found, that solely modes of frequency ω and wave vector $\mathbf{q}$ located in the immediate proximity to the photonic band structure $\omega_n(\mathbf{q})$ are capable to propagate inside the crystal with sufficient intensity (see figure 3.4.3). As is shown in figure 3.4.2, these modes display rapid spatial variations, whose length scale is set by the lattice constant, on the back of a slowly varying envelope. The latter's length scale is set by the spatially slowly varying external signal $\mathbf{E}_{\text{ext}}(\mathbf{r},\omega)$. Within a dielectric crystal, $\mathbf{E}(\mathbf{r},\omega)$ consists in general of a radiative (transverse) and a non-radiative (longitudinal) part $\mathbf{E}^{(\text{T})}(\mathbf{r},\omega)$ or $\mathbf{E}^{(\text{L})}(\mathbf{r},\omega)$, even though $\mathbf{E}_{\text{ext}}(\mathbf{r},\omega)$ is purely transverse (see figure 3.4.4). Whether $\mathbf{E}^{(\text{T})}(\mathbf{r},\omega)$ or $\mathbf{E}^{(\text{L})}(\mathbf{r},\omega)$ constitutes the dominant contribution to $\mathbf{E}(\mathbf{r},\omega)$ strongly depends on the density of polarizable atoms ν_{P} within the crystal. While in high-density materials there holds $\mathbf{E}(\mathbf{r},\omega) \approx \mathbf{E}^{(\text{L})}(\mathbf{r},\omega)$, in very low-density media one finds $\mathbf{E}(\mathbf{r},\omega) \approx \mathbf{E}^{(\text{T})}(\mathbf{r},\omega)$ (compare with figure 3.4.5 (a)).

Now, the local electromagnetic field represented by $\mathbf{E}(\mathbf{r},\omega)$ and $\mathbf{B}(\mathbf{r},\omega)$ is related to the macroscopic electromagnetic field denoted by $\mathscr{E}(\mathbf{r},\omega)$ and $\mathscr{B}(\mathbf{r},\omega)$ by conceiving the latter as the spatially low-pass filtered local electromagnetic field. In other words, the macroscopic field corresponds to the spatially slowly varying part of the local field. In this context it is shown in figures 4.3.1 and 4.3.2, that the macroscopic electromagnetic field essentially coincides with the radiative (transverse) parts of the local electromagnetic field in case that the external signal $\mathbf{E}_{\text{ext}}(\mathbf{r},\omega)$ was purely transverse. Similarly, the macroscopic polarization $\mathscr{P}(\mathbf{r},\omega)$ is conceived as the spatially low-pass filtered microscopic polarization $\mathbf{P}(\mathbf{r},\omega)$. Relating the respective Fourier amplitudes $\tilde{\mathscr{P}}(\mathbf{q},\omega)$ and $\tilde{\mathscr{E}}(\mathbf{q},\omega)$ in the familiar way owed to macroscopic electrodynamics according to $\tilde{\mathscr{P}}(\mathbf{q},\omega) = \varepsilon_0(\boldsymbol{\varepsilon}_\Lambda(\mathbf{q},\omega) - \boldsymbol{\delta}) \cdot \tilde{\mathscr{E}}(\mathbf{q},\omega)$, an exact expression determining the dielectric 3×3 tensor $\boldsymbol{\varepsilon}_\Lambda(\mathbf{q},\omega)$ (see (4.1.17)) emerges, whose arguments ω and $\mathbf{q}$ reflect the retarded and non-local response of the individual atoms/ions to an electromagnetic signal, respectively. The only input for the calculation of $\boldsymbol{\varepsilon}_\Lambda(\mathbf{q},\omega)$ are the crystalline structure under consideration as well as the individual electronic and ionic displacement polarizabilities.

Starting from equation (4.1.14), a set of coupled (differential) equations determining the longitudinal and transverse parts of the macroscopic electric field are deduced without having any prior knowledge of the local electric field (see (4.2.10) and (4.2.11)). In case the external signal $\mathbf{E}_{\text{ext}}(\mathbf{r},\omega)$ is purely longitudinal, a Poisson type equation determining a scalar potential $\phi(\mathbf{r},\omega)$ emerges, so that the non-radiative

(longitudinal) macroscopic electric field can be derived from $\mathscr{E}^{(\mathrm{L})}(\mathbf{r},\omega) = -\nabla_{\mathbf{r}}\phi(\mathbf{r},\omega)$. In this context, electric field screening is described by the longitudinal dielectric tensor $\varepsilon^{(\mathrm{L})}(\mathbf{q},\omega)$ given by (4.2.14). Provided $\mathbf{E}_{\mathrm{ext}}(\mathbf{r},\omega)$ is purely transverse, a wave-like equation determining the radiative (transverse) macroscopic electric field $\mathscr{E}^{(\mathrm{T})}(\mathbf{r},\omega)$ arises, where the re-normalization of the speed of light within a crystalline dielectric is governed by the transverse dielectric tensor $\varepsilon^{(\mathrm{T})}(\mathbf{q},\omega)$ (see (4.2.20)). Notice that both, the longitudinal as well as the transverse dielectric tensor $\varepsilon^{(\mathrm{L})}(\mathbf{q},\omega)$ or $\varepsilon^{(\mathrm{T})}(\mathbf{q},\omega)$, can easily be deduced from the dielectric tensor $\varepsilon_{\Lambda}(\mathbf{q},\omega)$.

In the static limit, an exact expression for the dielectric tensor $\varepsilon_{\Lambda} \equiv \lim_{\omega\to 0}\lim_{|\mathbf{q}|\to 0}\varepsilon_{\Lambda}(\mathbf{q},\omega)$ is derived that applies for all 14 (monatomic) three-dimensional Bravais lattices, where the respective crystal symmetry is incorporated via the Lorentz factor tensor $\mathscr{L}$ (see (4.4.5)). Additionally, the expression for ε_{Λ} conforms with general stability criteria deduced from causality and thermodynamic considerations [66] and in particular it reduces to the well-known Clausius-Mossotti formula in case of cubic symmetry. Moreover, it is demonstrated using the example of CsI, that the analytic structure of the dielectric tensor $\varepsilon_{\Lambda}(\omega) \equiv \lim_{|\mathbf{q}|\to 0}\varepsilon_{\Lambda}(\mathbf{q},\omega)$ in absence of spatial dispersion complies with the Lyddane-Sachs-Teller relation, which is valid for cubic diatomic ionic crystals.

A Taylor expansion of the transverse dielectric tensor $\varepsilon^{(\mathrm{T})}(\mathbf{q},\omega)$ around $\mathbf{q}=\mathbf{0}$ according to $\varepsilon^{(\mathrm{T})}_{ab}(\mathbf{q},\omega) = \varepsilon^{(\mathrm{T})}_{ab}(\omega) + i\sum_{c=1}^{3}\gamma_{abc}(\omega)\,q_c + \sum_{c,d=1}^{3}\alpha_{abcd}(\omega)\,q_c q_d + \ldots$ provides insight into various optical effects related to light propagation in dielectric crystals, in full agreement with [1]. This includes the principal indices of refraction $n_a(\omega) = \sqrt{\varepsilon^{(\mathrm{T})}_{aa}(\omega)}$, natural optical activity specified by $\gamma_{abc}(\omega)$ and spatial dispersion induced birefringence represented by $\alpha_{abcd}(\omega)$ as well as the chromatic dispersion of these quantities. Considering various sophisticated dielectric crystal structures with up to 66 atoms per Wigner-Seitz cell and with polarizabilities known for a specific wavelength from the literature, it is shown in tables 4.4.3 and 4.4.4 that the calculated principal indices of refraction and also the rotatory power of natural optical activity agree well with experimental results. By modeling the frequency dependence of the electronic and ionic displacement polarizabilities by means of Lorentz oscillators, whose frequency dependence is in accordance with fundamental quantum mechanical considerations on atom-individual polarizabilities [23], the chromatic dispersion of all afore mentioned optical effects can be described with high accuracy over wide frequency intervals. Using the example of CsI and RbCl it is demonstrated in figure 4.4.3 (a) and (b), that the calculated chromatic dispersion of the index of refraction agrees well with experimental measurements over a frequency range extending from the ultraviolet to the far-infrared. Similarly, the utility of the presented theory is exemplified by comparing the calculated chromatic dispersion of rotatory power with experimental findings for laevorotatory $\alpha-$quartz (see figure 4.4.4). Finally, the applicability of the theory is proven in figure 4.4.5 by modeling the frequency dependence of spatial dispersion induced birefringence with high accuracy in i.a. CaF_2 and BaF_2, a quantity that is of prime importance in the design of optical imaging systems for lithographic systems operating in the ultraviolet spectral region.

Last but not least it should be emphasized, that the presented theory of the macroscopic electromagnetic field does *not* make use of the displacement field $\mathscr{D}(\mathbf{r},\omega)$ and the magnetic field $\mathscr{H}(\mathbf{r},\omega)$.

Chapter 6

Outlook

With high confidence, the presented integral equation approach for calculating the local electromagnetic field in dielectric crystals of perfect symmetry can be deployed without major difficulties to crystalline materials that lack of perfect lattice periodicity. For instance, assuming the electronic polarizability of the j^{th}-atom/ion to be not solely dependent on its position $\eta^{(j)} \in C_\Lambda$ within the Wigner-Seitz cell, but also on the unit cell itself, i.e. $\alpha_{ab}^{(\text{el})}\left(\eta^{(j)},\omega\right) \to \alpha_{ab}^{(\text{el})}\left(\mathbf{R}+\eta^{(j)},\omega\right)$ with $\mathbf{R} \in \Lambda$, the model of the dielectric susceptibility kernel $\chi_{ab}(\mathbf{r},\mathbf{r}',\omega)$ (see (3.1.6)) can be extended to crystalline materials possessing either a single impurity center or even a substitutional site disorder. Potential areas of application include the investigation of the local electromagnetic field in the vicinity of single nitrogen vacancy centers in diamond, used as single photon sources or electric field sensors [121, 122], as well as light propagation and localization in disordered media, the latter being based on the phenomenological macroscopic Maxwell equations up to now [123–126]. Additionally, a theory of the dielectric tensor for disordered materials within the framework of the coherent potential approximation (CPA) [27, 127] is enabled.

Similarly, $\alpha_{ab}^{(\text{el})}\left(\mathbf{R}+\eta^{(j)},\omega\right)$ allows to consider from a microscopic point of view the electrodynamics of the so-called half-space problem (see e.g. [128, 129]), where the part of $\mathbb{R}^3$ with $z \leq 0$ is filled by a polarizable crystalline dielectric, while the part with $z > 0$ is assumed to be free of any material (vacuum). Considering an electromagnetic plane wave of wavelength $\lambda = \frac{2\pi c}{\omega} \gg a_\Lambda$ incident from the region with $z > 0$ on the interface at $z = 0$, the law of reflection as well as Snell's law of refraction should be deducible without taking into account any boundary conditions, a fact owed to the integral equation approach. Simultaneously, when decreasing the wavelength, the emergence of Bragg's law of diffraction is expected once $\lambda = \frac{2\pi c}{\omega}$ is comparable to the lattice constant a_Λ, so that the presented local field formalism could provide a unified framework of electrodynamics ranging from long-wavelength (or visible) optics down to x-ray optics. Of course, this would also include a description of the Goos-Hänchen and Imbert-Fedorov effect [130], both associated with the total reflection of light beams possessing a finite waist.

The extension of the local field integral equation approach to crystalline thin film or even atomic mono-

layer materials like e.g. graphene as well as to fluids is considered as possible, too. In the latter case, the strict periodic arrangement of the individual atoms has to be renounced. Instead, the material structure has to be described statistically by means of particle densities and particle distribution functions [131].

Lattice vibrations associated with the motion of the atomic/ionic cores around their equilibrium positions could explicitly be considered in the material model by taking into account the finite temperature of the crystalline system. This would allow to include the (strong) coupling of lattice vibrations to the local electromagnetic radiation field, thus providing access to a theory of polaritons [132] based on a microscopic point of view.

Appendix A

Helmholtz decomposition and projection operators

Starting from Poisson's equation, the essence of the Helmholtz decomposition theorem is established by representing a (regular) vector field as a sum of its curl-free (longitudinal) and divergence-free (transverse) components. Once the formal solution of Poisson's equation has been constructed by means of Green's function, these components are explicitly calculated. As a result, explicit representations of the longitudinal and transverse projection operators in real (and reciprocal) space are obtained, that will be used extensively in the course of this work.

A.1 Helmholtz decomposition

As a starting point for the decomposition of a vector field $\mathbf{V}(\mathbf{r})$ into a sum consisting of its irrotational (longitudinal) and solenoidal (transverse) contributions, follow [24, 133] by considering Poisson's equation

$$-\nabla_{\mathbf{r}}^2 A_a(\mathbf{r}) = V_a(\mathbf{r}) \quad ; \quad a \in \{1,2,3\} \tag{A.1.1}$$

for the a^{th} component of $\mathbf{V}(\mathbf{r})$ in cartesian coordinates. Its particular solution is given by

$$A_a(\mathbf{r}) = \lim_{\eta \to 0^+} \int_{\mathbb{R}^3 \setminus \mathscr{S}(\mathbf{r},\eta)} d^3r'\, g(\mathbf{r}-\mathbf{r}')\, V_a(\mathbf{r}') \tag{A.1.2}$$

$$= \int_{\mathbb{R}^3} d^3r'\, g(\mathbf{r}-\mathbf{r}')\, V_a(\mathbf{r}')\,, \tag{A.1.3}$$

where

$$g(\mathbf{r}-\mathbf{r}') = \frac{1}{4\pi}\frac{1}{|\mathbf{r}-\mathbf{r}'|} \tag{A.1.4}$$

denotes the Green function of Poisson's equation (A.1.1) that satisfies

$$-\nabla_{\mathbf{r}}^2 g\left(\mathbf{r}-\mathbf{r}'\right)=\delta\left(\mathbf{r}-\mathbf{r}'\right), \tag{A.1.5}$$

while

$$\mathscr{S}\left(\mathbf{r},\eta\right)=\left\{\mathbf{r}'\in\mathbb{R}^3:\left|\mathbf{r}-\mathbf{r}'\right|<\eta\right\} \tag{A.1.6}$$

represents the set of all points $\mathbf{r}'\in\mathbb{R}^3$ lying inside a sphere[1] of radius η around the point $\mathbf{r}$. With the identity

$$\nabla_{\mathbf{r}}\times\nabla_{\mathbf{r}}\times\mathbf{A}\left(\mathbf{r}\right)=\nabla_{\mathbf{r}}\nabla_{\mathbf{r}}\cdot\mathbf{A}\left(\mathbf{r}\right)-\nabla_{\mathbf{r}}^2\mathbf{A}\left(\mathbf{r}\right), \tag{A.1.7}$$

(A.1.1) can be rewritten as

$$\mathbf{V}\left(\mathbf{r}\right)=-\nabla_{\mathbf{r}}\nabla_{\mathbf{r}}\cdot\mathbf{A}\left(\mathbf{r}\right)+\nabla_{\mathbf{r}}\times\nabla_{\mathbf{r}}\times\mathbf{A}\left(\mathbf{r}\right)\equiv\mathbf{V}^{(\mathrm{L})}\left(\mathbf{r}\right)+\mathbf{V}^{(\mathrm{T})}\left(\mathbf{r}\right), \tag{A.1.8}$$

where

$$\mathbf{V}^{(\mathrm{L})}\left(\mathbf{r}\right)=-\nabla_{\mathbf{r}}\nabla_{\mathbf{r}}\cdot\mathbf{A}\left(\mathbf{r}\right)=-\lim_{\eta\to0^+}\nabla_{\mathbf{r}}\nabla_{\mathbf{r}}\cdot\int_{\mathbb{R}^3\setminus\mathscr{S}(\mathbf{r},\eta)}d^3r'\,g\left(\mathbf{r}-\mathbf{r}'\right)\mathbf{V}\left(\mathbf{r}'\right) \tag{A.1.9}$$

$$\mathbf{V}^{(\mathrm{T})}\left(\mathbf{r}\right)=\nabla_{\mathbf{r}}\times\nabla_{\mathbf{r}}\times\mathbf{A}\left(\mathbf{r}\right)=\lim_{\eta\to0^+}\nabla_{\mathbf{r}}\times\nabla_{\mathbf{r}}\times\int_{\mathbb{R}^3\setminus\mathscr{S}(\mathbf{r},\eta)}d^3r'\,g\left(\mathbf{r}-\mathbf{r}'\right)\mathbf{V}\left(\mathbf{r}'\right) \tag{A.1.10}$$

denote the longitudinal and transverse components of the vector field $\mathbf{V}\left(\mathbf{r}\right)$, respectively. Evidently, there holds by construction

$$\nabla_{\mathbf{r}}\times\mathbf{V}^{(\mathrm{L})}\left(\mathbf{r}\right)=\mathbf{0} \tag{A.1.11}$$

$$\nabla_{\mathbf{r}}\cdot\mathbf{V}^{(\mathrm{T})}\left(\mathbf{r}\right)=0. \tag{A.1.12}$$

In essence, equations (A.1.8)-(A.1.12) constitute the Helmholtz decomposition theorem. Regarding its range of validity, uniqueness as well as potential generalization schemes the reader is referred to [15, 17]. For a comprehensive overview of application fields of the Helmholtz (-Hodge) decomposition including their temporal evolution, see [16]. Obviously, equations (A.1.9) and (A.1.10) give an explicit rule for the construction of the longitudinal and transverse components of a given vector field $\mathbf{V}\left(\mathbf{r}\right)$. Following this rule then allows the identification of the longitudinal and transverse projection operator, as is shown in the next section.

[1] The exclusion of an infinitesimal (spherical) volume $\mathscr{S}\left(\mathbf{r},\eta\right)$ in (A.1.2) is not required at this point for solving the Poisson equation (A.1.1), because the integral is well-behaved as long as $V_a\left(\mathbf{r}\right)$ is assumed to be regular everywhere. However, this volume already indicates the necessity for a regularization which is essential in the derivation of the longitudinal and transverse projection operators in the next section. The reason for this is that this derivation involves the interchange of second-order derivatives with the integral, a procedure which would lead otherwise to a bad singularity at the point $\mathbf{r}=\mathbf{r}'$, see e.g. [134].

A.2 Projection operators

Projecting out the longitudinal and transverse contributions $\mathbf{V}^{(\mathrm{L})}(\mathbf{r})$ and $\mathbf{V}^{(\mathrm{T})}(\mathbf{r})$ of a given vector field $\mathbf{V}(\mathbf{r})$ can be achieved with the help of the so-called longitudinal and transverse projection operators, also known as longitudinal or transverse delta function. They can be constructed explicitly by means of (A.1.9) and (A.1.10), whereby it should be pointed out, that when one of the two projection operators is known, the other one can easily be deduced from (A.1.8) according to Helmholtz's decomposition. Therefore it suffices to consider, for example, the longitudinal contribution of a given vector field $\mathbf{V}(\mathbf{r})$, as is done in the following. Initially, one obtains for the a^{th} component of $\mathbf{V}^{(\mathrm{L})}(\mathbf{r})$ given by (A.1.9) with $a \in \{1,2,3\}$ in cartesian coordinates

$$\begin{aligned} V_a^{(\mathrm{L})}(\mathbf{r}) &= -\frac{\partial}{\partial r_a}\sum_{b=1}^{3}\frac{\partial}{\partial r_b}A_b(\mathbf{r}) \\ &= -\lim_{\eta\to 0^+}\sum_{b=1}^{3}\frac{\partial}{\partial r_a}\frac{\partial}{\partial r_b}\int_{\mathbb{R}^3\setminus\mathscr{S}(\mathbf{r},\eta)} d^3r'\, g\left(\mathbf{r}-\mathbf{r}'\right)V_b\left(\mathbf{r}'\right). \end{aligned} \tag{A.2.1}$$

It looks like that the calculation of the derivatives in (A.2.1) is impeded by the fact, that the range of integration depends on the position vector $\mathbf{r}$. Nevertheless, because $\mathscr{S}(\mathbf{r},\eta)$ represents a sphere, the $\mathbf{r}$-dependence of the integration range can be easily lifted with the help of the Heaviside step function defined as

$$\Theta_{\mathrm{H}}(x) = \begin{cases} 0 & x<0 \\ 1 & x\geq 0 \end{cases}, \tag{A.2.2}$$

allowing to rewrite (A.2.1) according to [24] as

$$V_a^{(\mathrm{L})}(\mathbf{r}) = -\lim_{\eta\to 0^+}\sum_{b=1}^{3}\frac{\partial}{\partial r_a}\frac{\partial}{\partial r_b}\int_{\mathbb{R}^3} d^3r'\,\Theta_{\mathrm{H}}\left(\left|\mathbf{r}-\mathbf{r}'\right|-\eta\right)g\left(\mathbf{r}-\mathbf{r}'\right)V_b\left(\mathbf{r}'\right). \tag{A.2.3}$$

Interchanging the first derivative and the integral yields

$$\begin{aligned} V_a^{(\mathrm{L})}(\mathbf{r}) = -\frac{1}{4\pi}\lim_{\eta\to 0^+}\sum_{b=1}^{3}\frac{\partial}{\partial r_a}\int_{\mathbb{R}^3} d^3r' \Bigg[&\delta\left(\left|\mathbf{r}-\mathbf{r}'\right|-\eta\right)\frac{r_b-r_b'}{\left|\mathbf{r}-\mathbf{r}'\right|^2}V_b\left(\mathbf{r}'\right) \\ &-\Theta_{\mathrm{H}}\left(\left|\mathbf{r}-\mathbf{r}'\right|-\eta\right)\frac{r_b-r_b'}{\left|\mathbf{r}-\mathbf{r}'\right|^3}V_b\left(\mathbf{r}'\right)\Bigg], \end{aligned} \tag{A.2.4}$$

where (A.1.4) and

$$\frac{\partial}{\partial r_a}g\left(\mathbf{r}-\mathbf{r}'\right) = -\frac{1}{4\pi}\frac{r_a-r_a'}{\left|\mathbf{r}-\mathbf{r}'\right|^3} \tag{A.2.5}$$

have been used. The delta function in the first integrand in (A.2.4) restricts $\mathbf{r}'$ to the surface $\partial\mathscr{S}(\mathbf{r},\eta)$ of the sphere $\mathscr{S}(\mathbf{r},\eta)$, so that the integration can be carried out directly in spherical coordinates with

the help of the substitutions

$$\begin{aligned} \mathbf{s} &= \mathbf{r}' - \mathbf{r} \equiv \eta \mathbf{n} \\ \mathbf{n} &= \frac{\mathbf{r}' - \mathbf{r}}{|\mathbf{r}' - \mathbf{r}|}. \end{aligned} \tag{A.2.6}$$

As a result, the respective integral is proportional to η and therefore vanishes in the limit $\eta \to 0^+$. As a consequence, (A.2.4) reduces to

$$V_a^{(\mathrm{L})}(\mathbf{r}) = \frac{1}{4\pi} \lim_{\eta \to 0^+} \sum_{b=1}^{3} \frac{\partial}{\partial r_a} \int_{\mathbb{R}^3} d^3 r' \, \Theta_{\mathrm{H}}\left(|\mathbf{r} - \mathbf{r}'| - \eta\right) \frac{r_b - r_b'}{|\mathbf{r} - \mathbf{r}'|^3} V_b(\mathbf{r}'). \tag{A.2.7}$$

Interchanging the remaining derivative with the integral then gives

$$\begin{aligned} V_a^{(\mathrm{L})}(\mathbf{r}) =& \frac{1}{4\pi} \lim_{\eta \to 0^+} \sum_{b=1}^{3} \int_{\mathbb{R}^3} d^3 r' \left[\delta\left(|\mathbf{r} - \mathbf{r}'| - \eta\right) \frac{(r_a - r_a')(r_b - r_b')}{|\mathbf{r} - \mathbf{r}'|^4} V_b(\mathbf{r}') \right. \\ & \left. + \Theta_{\mathrm{H}}\left(|\mathbf{r} - \mathbf{r}'| - \eta\right) \frac{\delta_{ab} |\mathbf{r} - \mathbf{r}'|^2 - 3(r_a - r_a')(r_b - r_b')}{|\mathbf{r} - \mathbf{r}'|^5} V_b(\mathbf{r}') \right] \\ \equiv & V_a^{(\mathrm{L},1)}(\mathbf{r}) + V_a^{(\mathrm{L},2)}(\mathbf{r}), \end{aligned} \tag{A.2.8}$$

where the abbreviations

$$V_a^{(\mathrm{L},1)}(\mathbf{r}) = \frac{1}{4\pi} \lim_{\eta \to 0^+} \sum_{b=1}^{3} \int_{\mathbb{R}^3} d^3 r' \, \delta\left(|\mathbf{r} - \mathbf{r}'| - \eta\right) \frac{(r_a - r_a')(r_b - r_b')}{|\mathbf{r} - \mathbf{r}'|^4} V_b(\mathbf{r}') \tag{A.2.9}$$

$$V_a^{(\mathrm{L},2)}(\mathbf{r}) = \frac{1}{4\pi} \lim_{\eta \to 0^+} \sum_{b=1}^{3} \int_{\mathbb{R}^3} d^3 r' \, \Theta_{\mathrm{H}}\left(|\mathbf{r} - \mathbf{r}'| - \eta\right) \frac{\delta_{ab} |\mathbf{r} - \mathbf{r}'|^2 - 3(r_a - r_a')(r_b - r_b')}{|\mathbf{r} - \mathbf{r}'|^5} V_b(\mathbf{r}') \tag{A.2.10}$$

have been introduced. The delta function in (A.2.9) restricts $\mathbf{r}'$ to the surface $\partial \mathscr{S}(\mathbf{r}, \eta)$, so that the situation is similar as in the case of equation (A.2.4). Therefore, the integral may be evaluated in

spherical coordinates with the help of (A.2.6) according to[2]

$$\begin{aligned} V_a^{(\mathrm{L},1)}(\mathbf{r}) &= \frac{1}{4\pi}\lim_{\eta\to 0^+}\sum_{b=1}^{3}\int_{\mathbb{R}^3} d^3s\,\delta(|\mathbf{s}|-\eta)\,\frac{1}{|\mathbf{s}|^2}n_a n_b V_b(\mathbf{r}+\eta\mathbf{n}) \\ &= \frac{1}{4\pi}\lim_{\eta\to 0^+}\sum_{b=1}^{3}\int_0^\infty ds\int d\Omega\,\delta(s-\eta)\,n_a n_b V_b(\mathbf{r}+\eta\mathbf{n}) \\ &= \frac{1}{4\pi}\sum_{b=1}^{3}\int d\Omega\,n_a n_b V_b(\mathbf{r}) \\ &= \frac{1}{3}V_a(\mathbf{r}). \end{aligned} \tag{A.2.11}$$

Inserting (A.2.10) and (A.2.11) in (A.2.8) then finally yields

$$\begin{aligned} V_a^{(\mathrm{L})}(\mathbf{r}) &= \sum_{b=1}^{3}\int_{\mathbb{R}^3} d^3r'\left[\frac{1}{3}\delta_{ab}\delta(\mathbf{r}-\mathbf{r}') + \Theta_{\mathrm{H}}\left(|\mathbf{r}-\mathbf{r}'|-0^+\right)\frac{\delta_{ab}|\mathbf{r}-\mathbf{r}'|^2 - 3(r_a-r_a')(r_b-r_b')}{4\pi|\mathbf{r}-\mathbf{r}'|^5}\right]V_b(\mathbf{r}') \\ &\equiv \sum_{b=1}^{3}\int_{\mathbb{R}^3} d^3r'\,\Pi_{ab}^{(\mathrm{L})}(\mathbf{r}-\mathbf{r}')\,V_b(\mathbf{r}'), \end{aligned} \tag{A.2.12}$$

where in the second line the matrix element of the longitudinal projection operator $\Pi_{ab}^{(\mathrm{L})}(\mathbf{r}-\mathbf{r}')$ has been defined as

$$\Pi_{ab}^{(\mathrm{L})}(\mathbf{r}-\mathbf{r}') = \frac{1}{3}\delta_{ab}\delta(\mathbf{r}-\mathbf{r}') + \Theta_{\mathrm{H}}\left(|\mathbf{r}-\mathbf{r}'|-0^+\right)\frac{\delta_{ab}|\mathbf{r}-\mathbf{r}'|^2 - 3(r_a-r_a')(r_b-r_b')}{4\pi|\mathbf{r}-\mathbf{r}'|^5}. \tag{A.2.13}$$

The transverse component $\mathbf{V}^{(\mathrm{T})}(\mathbf{r})$ of the vector field $\mathbf{V}(\mathbf{r})$ can now easily be deduced from (A.1.8), since

$$\begin{aligned} V_a^{(\mathrm{T})}(\mathbf{r}) &= V_a(\mathbf{r}) - V_a^{(\mathrm{L})}(\mathbf{r}) \\ &= \sum_{b=1}^{3}\int_{\mathbb{R}^3} d^3r'\left[\delta_{ab}\delta(\mathbf{r}-\mathbf{r}') - \Pi_{ab}^{(\mathrm{L})}(\mathbf{r}-\mathbf{r}')\right]V_b(\mathbf{r}') \\ &\equiv \sum_{b=1}^{3}\int_{\mathbb{R}^3} d^3r'\,\Pi_{ab}^{(\mathrm{T})}(\mathbf{r}-\mathbf{r}')\,V_b(\mathbf{r}'), \end{aligned} \tag{A.2.14}$$

[2]When interchanging the *second* derivative with the integral (see (A.2.8) and (A.2.11)), the exclusion of the infinitesimal (spherical) volume $\mathscr{S}(\mathbf{r},\eta)$ from the range of integration, i.e. the integral's regularization, has now a *non*-vanishing effect on the longitudinal field $V_a^{(\mathrm{L})}(\mathbf{r})$, as it avoids the occurrence of the bad singularity $\frac{\partial}{\partial r_a}\frac{\partial}{\partial r_b}g(\mathbf{r}-\mathbf{r}')V_b(\mathbf{r}')$ in the integrand (compare with [134]). The same applies when calculating the transverse field $V_a^{(\mathrm{T})}(\mathbf{r})$. In contrast, for integrands of the type $\nabla_{\mathbf{r}}^2 g(\mathbf{r}-\mathbf{r}')V_b(\mathbf{r}')$ the regularization of the integral can be waived, because of the identity $-\nabla_{\mathbf{r}}^2 g(\mathbf{r}-\mathbf{r}') = \delta(\mathbf{r}-\mathbf{r}')$ the integral behaves well at $\mathbf{r}=\mathbf{r}'$.

where in the last line the matrix element of the transverse projection operator $\Pi_{ab}^{(\mathrm{T})}(\mathbf{r}-\mathbf{r}')$ has been defined as

$$\begin{aligned}\Pi_{ab}^{(\mathrm{T})}(\mathbf{r}-\mathbf{r}') &= \delta_{ab}\delta(\mathbf{r}-\mathbf{r}') - \Pi_{ab}^{(\mathrm{L})}(\mathbf{r}-\mathbf{r}') \\ &= \frac{2}{3}\delta_{ab}\delta(\mathbf{r}-\mathbf{r}') - \Theta_{\mathrm{H}}\left(|\mathbf{r}-\mathbf{r}'|-0^{+}\right)\frac{\delta_{ab}|\mathbf{r}-\mathbf{r}'|^{2}-3(r_a-r_a')(r_b-r_b')}{4\pi|\mathbf{r}-\mathbf{r}'|^{5}}. \end{aligned} \tag{A.2.15}$$

It should be pointed out, that the values of the integrals (A.2.9) and (A.2.10) appearing in the derivation of $V_a^{(\mathrm{L})}(\mathbf{r})$ or $\Pi_{ab}^{(\mathrm{L})}(\mathbf{r}-\mathbf{r}')$ (and so too for $V_a^{(\mathrm{T})}(\mathbf{r})$ or $\Pi_{ab}^{(\mathrm{T})}(\mathbf{r}-\mathbf{r}')$) depend individually on the geometry of the excluded volume (here: the sphere $\mathscr{S}(\mathbf{r},\eta)$). However, the sum of both integrals gives the unique field $V_a^{(\mathrm{L})}(\mathbf{r})$ (and so too $V_a^{(\mathrm{T})}(\mathbf{r})$) whose value is *independent* of the geometry of the excluded volume [134].

Equations (A.2.12) and (A.2.14) give an explicit rule for the construction of the longitudinal and transverse components $\mathbf{V}^{(\mathrm{L})}(\mathbf{r})$ and $\mathbf{V}^{(\mathrm{T})}(\mathbf{r})$ of a given vector field $\mathbf{V}(\mathbf{r})$ in real space in terms of convolution integrals. However, in reciprocal space these correspond to simple multiplications according to

$$\tilde{V}_a^{(A)}(\mathbf{k}) = \sum_{b=1}^{3}\tilde{\Pi}_{ab}^{(A)}(\mathbf{k})\,\tilde{V}_b(\mathbf{k}) \quad ; \quad A\in\{\mathrm{L},\mathrm{T}\}, \tag{A.2.16}$$

where the longitudinal and transverse projection operator $\tilde{\Pi}_{ab}^{(\mathrm{L})}(\mathbf{k})$ and $\tilde{\Pi}_{ab}^{(\mathrm{T})}(\mathbf{k})$ in reciprocal space are given by

$$\tilde{\Pi}_{ab}^{(\mathrm{L})}(\mathbf{k}) = \frac{k_a k_b}{|\mathbf{k}|^2} \tag{A.2.17}$$

$$\tilde{\Pi}_{ab}^{(\mathrm{T})}(\mathbf{k}) = \delta_{ab} - \frac{k_a k_b}{|\mathbf{k}|^2}. \tag{A.2.18}$$

For a refined proof that $\tilde{\Pi}_{ab}^{(\mathrm{L})}(\mathbf{k})$ and $\tilde{\Pi}_{ab}^{(\mathrm{T})}(\mathbf{k})$ given by (A.2.17) or (A.2.18) obey to the Fourier integral representation

$$\Pi_{ab}^{(A)}(\mathbf{r}) = \frac{1}{(2\pi)^3}\int_{\mathbb{R}^3} d^3k\, e^{i\mathbf{k}\cdot\mathbf{r}}\tilde{\Pi}_{ab}^{(A)}(\mathbf{k}) \quad ; \quad A\in\{\mathrm{L},\mathrm{T}\} \tag{A.2.19}$$

and thus constitute the correct Fourier transforms of $\Pi_{ab}^{(\mathrm{L})}(\mathbf{r})$ and $\Pi_{ab}^{(\mathrm{T})}(\mathbf{r})$ given by (A.2.13) and (A.2.15) respectively, see [18]. The characteristic properties of projection operators are summarized below in abstract operator notation, where "$\circ$" denotes the common matrix product in reciprocal space or a

convolution integral in real space, while $\mathbb{I}$ and $\mathbb{O}$ represent the corresponding unity and zero operator.

$$\mathbf{\Pi}^{(\mathrm{L})} + \mathbf{\Pi}^{(\mathrm{T})} = \mathbb{I} \tag{A.2.20}$$

$$\mathbf{\Pi}^{(\mathrm{L})} \circ \mathbf{\Pi}^{(\mathrm{L})} = \mathbf{\Pi}^{(\mathrm{L})} \tag{A.2.21}$$

$$\mathbf{\Pi}^{(\mathrm{T})} \circ \mathbf{\Pi}^{(\mathrm{T})} = \mathbf{\Pi}^{(\mathrm{T})} \tag{A.2.22}$$

$$\mathbf{\Pi}^{(\mathrm{L})} \circ \mathbf{\Pi}^{(\mathrm{T})} = \mathbf{\Pi}^{(\mathrm{T})} \circ \mathbf{\Pi}^{(\mathrm{L})} = \mathbb{O}. \tag{A.2.23}$$

In particular, a verification of (A.2.20) - (A.2.23) is trivial in reciprocal space.

Appendix B

Derivation of the local electromagnetic field integral equations

Starting from Helmholtz's equation for $E_a^{(\mathrm{T})}(\mathbf{r},\omega)$, the integral equation (2.2.6) is derived by making use of Green's second identity [24]. In particular, special attention is paid to the *non-local* character of the transverse current density $j_a^{(\mathrm{T})}(\mathbf{r},\omega)$, that poses the source term for $E_a^{(\mathrm{T})}(\mathbf{r},\omega)$. As a byproduct, the Ewald-Oseen extinction theorem emerges.

To find an integral equation for the cartesian components of the transverse electric field $E_a^{(\mathrm{T})}(\mathbf{r},\omega)$ with $a \in \{1,2,3\}$, which describes the same physics as Helmholtz's equation (compare with (2.1.38))

$$\left(-\nabla_{\mathbf{r}}^2 - \frac{\omega^2}{c^2}\right) E_a^{(\mathrm{T})}(\mathbf{r},\omega) = i\omega\mu_0 j_a^{(\mathrm{T})}(\mathbf{r},\omega), \tag{B.0.1}$$

the method of Green functions is applied. The particular Green function $g(\mathbf{r}-\mathbf{r}',\omega)$, which is associated with (B.0.1) satisfies

$$\left(-\nabla_{\mathbf{r}}^2 - \frac{\omega^2}{c^2}\right) g(\mathbf{r}-\mathbf{r}',\omega) = \delta(\mathbf{r}-\mathbf{r}') \tag{B.0.2}$$

and is given for our purposes by[1]

$$g(\mathbf{r}-\mathbf{r}',\omega) = \frac{1}{4\pi}\frac{e^{i\frac{\omega}{c}|\mathbf{r}-\mathbf{r}'|}}{|\mathbf{r}-\mathbf{r}'|}. \tag{B.0.3}$$

Obviously, there holds

$$g(\mathbf{r}-\mathbf{r}',\omega) = g(\mathbf{r}'-\mathbf{r},\omega) \tag{B.0.4}$$

$$\nabla_{\mathbf{r}} g(\mathbf{r}-\mathbf{r}',\omega) = -\nabla_{\mathbf{r}'} g(\mathbf{r}-\mathbf{r}',\omega). \tag{B.0.5}$$

[1] It should be pointed out, that the retarded Green function given by (B.0.3) behaves like an outgoing spherical wave and corresponds to homogeneous boundary conditions, where the boundary is at infinity [133].

In what follows, the combination of (B.0.1) and (B.0.2) as well as subsequent application of Green's second identity

$$\int_V d^3r \left(\phi(\mathbf{r})\nabla_{\mathbf{r}}^2\psi(\mathbf{r}) - \psi(\mathbf{r})\nabla_{\mathbf{r}}^2\phi(\mathbf{r})\right) = \int_{\partial V} d^2r\, \mathbf{n}\cdot\left(\phi(\mathbf{r})\nabla_{\mathbf{r}}\psi(\mathbf{r}) - \psi(\mathbf{r})\nabla_{\mathbf{r}}\phi(\mathbf{r})\right) \tag{B.0.6}$$

will allow to work out the desired integral equation. For this, multiply (B.0.1) by $g(\mathbf{r}-\mathbf{r}',\omega)$ and (B.0.2) by $E_a^{(\mathrm{T})}(\mathbf{r},\omega)$ in each case from the left-hand side and subtract, exchanging $\mathbf{r}$ and $\mathbf{r}'$ at the same time. This results in

$$\begin{aligned} &E_a^{(\mathrm{T})}(\mathbf{r}',\omega)\nabla_{\mathbf{r}'}^2 g(\mathbf{r}'-\mathbf{r},\omega) - g(\mathbf{r}'-\mathbf{r},\omega)\nabla_{\mathbf{r}'}^2 E_a^{(\mathrm{T})}(\mathbf{r}',\omega) \\ =&i\omega\mu_0 g(\mathbf{r}'-\mathbf{r},\omega) j_a^{(\mathrm{T})}(\mathbf{r}',\omega) - E_a^{(\mathrm{T})}(\mathbf{r}',\omega)\delta(\mathbf{r}'-\mathbf{r}), \end{aligned} \tag{B.0.7}$$

which constitutes the basis for further purposes. Let Ω denote the domain of non-vanishing current density, i.e. $\mathbf{j}(\mathbf{r},\omega)\neq\mathbf{0}$ when $\mathbf{r}\in\Omega$ and $\mathbf{j}(\mathbf{r},\omega)=\mathbf{0}$ when $\mathbf{r}\notin\Omega$. Then, by integration of (B.0.7) with respect to $\mathbf{r}'$ over Ω and subsequent application of Green's identity (B.0.6), one readily obtains

$$\begin{aligned} &i\omega\mu_0\int_\Omega d^3r'\, g(\mathbf{r}'-\mathbf{r},\omega) j_a^{(\mathrm{T})}(\mathbf{r}',\omega) \\ &-\int_{\partial\Omega} d^2r'\,\mathbf{n}'\cdot\left(E_a^{(\mathrm{T})}(\mathbf{r}',\omega)\nabla_{\mathbf{r}'} g(\mathbf{r}'-\mathbf{r},\omega) - g(\mathbf{r}'-\mathbf{r},\omega)\nabla_{\mathbf{r}'}E_a^{(\mathrm{T})}(\mathbf{r}',\omega)\right) \\ =&\begin{cases} E_a^{(\mathrm{T})}(\mathbf{r},\omega) & \mathbf{r}\in\Omega \\ 0 & \mathbf{r}\notin\Omega \end{cases}, \end{aligned} \tag{B.0.8}$$

where $\mathbf{n}'$ denotes the normal unit vector of the closed surface $\partial\Omega$ pointing away from the interior of the domain Ω. Now, let $\mathbf{n}''$ the normal unit vector of the closed surface $\partial\left(\mathbb{R}^3\backslash\Omega\right)$ pointing away from the interior of the domain $\mathbb{R}^3\backslash\Omega$. Then, integration of (B.0.7) with respect to $\mathbf{r}'$ over $\mathbb{R}^3\backslash\Omega$ and utilization of Green's identity (B.0.6) directly gives

$$\begin{aligned} &\int_{\partial(\mathbb{R}^3\backslash\Omega)} d^2r'\,\mathbf{n}''\cdot\left(E_a^{(\mathrm{T})}(\mathbf{r}',\omega)\nabla_{\mathbf{r}'} g(\mathbf{r}'-\mathbf{r},\omega) - g(\mathbf{r}'-\mathbf{r},\omega)\nabla_{\mathbf{r}'}E_a^{(\mathrm{T})}(\mathbf{r}',\omega)\right) \\ =&i\omega\mu_0\int_{\mathbb{R}^3\backslash\Omega} d^3r'\, g(\mathbf{r}'-\mathbf{r},\omega) j_a^{(\mathrm{T})}(\mathbf{r}',\omega) - \int_{\mathbb{R}^3\backslash\Omega} d^3r'\, E_a^{(\mathrm{T})}(\mathbf{r}',\omega)\delta(\mathbf{r}'-\mathbf{r}). \end{aligned} \tag{B.0.9}$$

At this point it has to be stressed that, while $\mathbf{j}(\mathbf{r},\omega)=\mathbf{0}$ holds for $\mathbf{r}\notin\Omega$ and $\mathbf{j}(\mathbf{r},\omega)\neq\mathbf{0}$ if $\mathbf{r}\in\Omega$, there is in general *no* such restriction for its transverse component $\mathbf{j}^{(\mathrm{T})}(\mathbf{r},\omega)$ because of the non-local projection procedure (2.1.19) in real space. Thus, the volume integral in (B.0.9) containing $j_a^{(\mathrm{T})}(\mathbf{r}',\omega)$ does *not* vanish. As the set of points $\mathbf{r}'\in\mathbb{R}^3$ lying on the surface $\partial\Omega$ and $\partial\left(\mathbb{R}^3\backslash\Omega\right)$, respectively, is

identical in both cases and since $\mathbf{n}'' = -\mathbf{n}'$ holds by construction, there follows at once[2] from (B.0.9)

$$\begin{aligned} & i\omega\mu_0 \int_{\mathbb{R}^3\setminus\Omega} d^3r'\, g\left(\mathbf{r}'-\mathbf{r},\omega\right) j_a^{(\mathrm{T})}\left(\mathbf{r}',\omega\right) \\ & + \int_{\partial\Omega} d^2r'\, \mathbf{n}' \cdot \left(E_a^{(\mathrm{T})}\left(\mathbf{r}',\omega\right) \nabla_{\mathbf{r}'} g\left(\mathbf{r}'-\mathbf{r},\omega\right) - g\left(\mathbf{r}'-\mathbf{r},\omega\right) \nabla_{\mathbf{r}'} E_a^{(\mathrm{T})}\left(\mathbf{r}',\omega\right) \right) \\ = & \begin{cases} 0 & \mathbf{r}\in\Omega \\ E_a^{(\mathrm{T})}\left(\mathbf{r},\omega\right) & \mathbf{r}\notin\Omega \end{cases} . \end{aligned} \tag{B.0.10}$$

Finally, combining (B.0.8) with (B.0.10) and taking account of (B.0.4) yields

$$E_a^{(\mathrm{T})}\left(\mathbf{r},\omega\right) = i\omega\mu_0 \int_{\mathbb{R}^3} d^3r'\, g\left(\mathbf{r}-\mathbf{r}',\omega\right) j_a^{(\mathrm{T})}\left(\mathbf{r}',\omega\right), \tag{B.0.11}$$

which constitutes an integral equation[3] determining $E_a^{(\mathrm{T})}\left(\mathbf{r},\omega\right)$ for $\mathbf{r}\in\mathbb{R}^3$. To specify the integral equation (B.0.11) to the geometry proposed in section 2.2 (see figure 2.2.1), the current density $\mathbf{j}\left(\mathbf{r},\omega\right)$ is split into

$$\mathbf{j}\left(\mathbf{r},\omega\right) = \begin{cases} \mathbf{j}_{\mathrm{ext}}\left(\mathbf{r},\omega\right) & \mathbf{r}\in\Omega_{\mathrm{S}} \\ \mathbf{j}_{\mathrm{ind}}\left(\mathbf{r},\omega\right) & \mathbf{r}\in\Omega_{\mathrm{P}} \\ \mathbf{0} & \mathbf{r}\notin\Omega \end{cases}, \tag{B.0.12}$$

where Ω_{S} and Ω_{P} denote two disjoint domains (particularly the source and the probe volume with $\Omega_{\mathrm{S}}\cap\Omega_{\mathrm{P}}=\emptyset$) that contain distinct non-vanishing current densities $\mathbf{j}_{\mathrm{ext}}\left(\mathbf{r},\omega\right)$ and $\mathbf{j}_{\mathrm{ind}}\left(\mathbf{r},\omega\right)$, respectively, while $\Omega=\Omega_{\mathrm{S}}\cup\Omega_{\mathrm{P}}$ represents the total domain of non-vanishing current density. Because $\mathbf{j}_{\mathrm{ext}}\left(\mathbf{r},\omega\right)$ is externally controlled and a priori known, the same holds true for its transverse component $\mathbf{j}_{\mathrm{ext}}^{(\mathrm{T})}\left(\mathbf{r},\omega\right)$, whereas $\mathbf{j}_{\mathrm{ind}}^{(\mathrm{T})}\left(\mathbf{r},\omega\right)$ depends on the specific model of the material that is incorporated into $\mathbf{j}_{\mathrm{ind}}\left(\mathbf{r},\omega\right)$. Due to (B.0.12), the transverse current density $\mathbf{j}^{(\mathrm{T})}\left(\mathbf{r},\omega\right)$ entering (B.0.11) thus comprises two contributions, namely $\mathbf{j}_{\mathrm{ext}}^{(\mathrm{T})}\left(\mathbf{r},\omega\right)$ and $\mathbf{j}_{\mathrm{ind}}^{(\mathrm{T})}\left(\mathbf{r},\omega\right)$, that in general do *not* vanish if $\mathbf{r}\notin\Omega$, so that $\mathbf{j}^{(\mathrm{T})}\left(\mathbf{r},\omega\right)$ may be written as

$$\mathbf{j}^{(\mathrm{T})}\left(\mathbf{r},\omega\right) = \mathbf{j}_{\mathrm{ext}}^{(\mathrm{T})}\left(\mathbf{r},\omega\right) + \mathbf{j}_{\mathrm{ind}}^{(\mathrm{T})}\left(\mathbf{r},\omega\right). \tag{B.0.13}$$

Inserting (B.0.13) in (B.0.11) and identifying the externally controlled transverse electric field as

$$E_{\mathrm{ext},a}^{(\mathrm{T})}\left(\mathbf{r},\omega\right) = i\omega\mu_0 \int_{\mathbb{R}^3} d^3r'\, g\left(\mathbf{r}-\mathbf{r}',\omega\right) j_{\mathrm{ext},a}^{(\mathrm{T})}\left(\mathbf{r}',\omega\right), \tag{B.0.14}$$

[2] The first line in (B.0.10) reveals, that the field generated by the transverse current density flowing inside the domain $\mathbb{R}^3\setminus\Omega$ and the field created by the probe's surface $\partial\Omega$ extinguish each other within Ω. This reflects the essence of the (Ewald-Oseen) extinction theorem [4, 30, 38, 135], whose historical origin lies in dispersion theory.

[3] Incidentally, (B.0.11) constitutes a particulate solution of Helmholtz's equation (B.0.1), which is well-known from textbooks. But it should be emphasized, that the outlined approach includes a derivation of the extinction theorem (B.0.10) and additionally gives deeper insight into the non-local character of $\mathbf{j}^{(\mathrm{T})}\left(\mathbf{r},\omega\right)$.

finally allows to write the transverse electric field according to

$$E_a^{(\mathrm{T})}(\mathbf{r},\omega) = E_{\mathrm{ext},a}^{(\mathrm{T})}(\mathbf{r},\omega) + i\omega\mu_0 \int_{\mathbb{R}^3} d^3r'\, g\left(\mathbf{r}-\mathbf{r}',\omega\right) j_{\mathrm{ind},a}^{(\mathrm{T})}\left(\mathbf{r}',\omega\right). \tag{B.0.15}$$

It should be pointed out, that $E_{\mathrm{ext},a}^{(\mathrm{T})}(\mathbf{r},\omega)$ plays the role of a parameter, which can be controlled precisely in arbitrary fashion, independent of the probe under investigation[4]. Under this requirement, there is no need for a specific material model underlying $\mathbf{j}_{\mathrm{ext}}(\mathbf{r},\omega)$, and the impact on the externally controlled current density $\mathbf{j}_{\mathrm{ext}}(\mathbf{r},\omega)$ by the induced current density $\mathbf{j}_{\mathrm{ind}}(\mathbf{r},\omega)$ is completely prohibited.

[4]Of course, the same holds true for the externally controlled longitudinal electric field $E_{\mathrm{ext},a}^{(\mathrm{L})}(\mathbf{r},\omega)$, defined by (2.2.5).

Appendix C

Translation invariance and Fourier transform of $\mathscr{G}_{ab}(\mathbf{r},\mathbf{r}',\omega)$ and its link to dyadic Green's function

In this appendix, first the translation invariance of the electromagnetic kernel $\mathscr{G}_{ab}(\mathbf{r},\mathbf{r}',\omega)$ with respect to a simultaneous shift of its spatial arguments by a constant vector is shown. Subsequently, its Fourier transform $\tilde{\mathscr{G}}_{ab}(\mathbf{k},\omega)$ is calculated (following [24]), which plays a significant role for the representation and evaluation of the arising lattice sums (see e.g. (3.2.24)). Finally, the relation between the electromagnetic kernel and the dyadic Green function associated with the vector wave equation for the electric field is revealed.

C.1 Translation invariance

To realize, that the electromagnetic kernel

$$\mathscr{G}_{ab}(\mathbf{r},\mathbf{r}',\omega) = \frac{\omega^2}{c^2}\int_{\mathbb{R}^3} d^3x\, g(\mathbf{r}-\mathbf{x},\omega)\,\Pi_{ab}^{(\mathrm{T})}(\mathbf{x}-\mathbf{r}') - \Pi_{ab}^{(\mathrm{L})}(\mathbf{r}-\mathbf{r}') \tag{C.1.1}$$

is translation invariant with respect to a simultaneous shift of its spatial arguments by a constant vector $\mathbf{a}$, consider

$$\begin{aligned}\mathscr{G}_{ab}(\mathbf{r}+\mathbf{a},\mathbf{r}'+\mathbf{a},\omega) &= \frac{\omega^2}{c^2}\int_{\mathbb{R}^3} d^3x\, g(\mathbf{r}+\mathbf{a}-\mathbf{x},\omega)\,\Pi_{ab}^{(\mathrm{T})}(\mathbf{x}-\mathbf{r}'-\mathbf{a}) - \Pi_{ab}^{(\mathrm{L})}(\mathbf{r}-\mathbf{r}') \\ &= \frac{\omega^2}{c^2}\int_{\mathbb{R}^3} d^3y\, g(\mathbf{r}-\mathbf{y},\omega)\,\Pi_{ab}^{(\mathrm{T})}(\mathbf{y}-\mathbf{r}') - \Pi_{ab}^{(\mathrm{L})}(\mathbf{r}-\mathbf{r}') \\ &= \mathscr{G}_{ab}(\mathbf{r},\mathbf{r}',\omega),\end{aligned} \tag{C.1.2}$$

so that one readily concludes

$$\mathscr{G}_{ab}\left(\mathbf{r},\mathbf{r}',\omega\right)=\mathscr{G}_{ab}\left(\mathbf{r}-\mathbf{r}',\omega\right). \tag{C.1.3}$$

C.2 Fourier transform

Utilizing the Fourier integral representation of the longitudinal and transverse projection operators in real space (compare with appendix A.2)

$$\Pi_{ab}^{(A)}(\mathbf{r})=\frac{1}{(2\pi)^3}\int_{\mathbb{R}^3}d^3k\,e^{i\mathbf{k}\cdot\mathbf{r}}\tilde{\Pi}_{ab}^{(A)}(\mathbf{k})\quad;\quad A\in\{\mathrm{L},\mathrm{T}\}, \tag{C.2.1}$$

where

$$\tilde{\Pi}_{ab}^{(\mathrm{L})}(\mathbf{k})=\frac{k_a k_b}{|\mathbf{k}|^2} \tag{C.2.2}$$

$$\tilde{\Pi}_{ab}^{(\mathrm{T})}(\mathbf{k})=\delta_{ab}-\frac{k_a k_b}{|\mathbf{k}|^2} \tag{C.2.3}$$

denote their corresponding Fourier transforms, the electromagnetic kernel $\mathscr{G}_{ab}(\mathbf{r}-\mathbf{r}',\omega)$ given by (C.1.1) can be written as

$$\begin{aligned}\mathscr{G}_{ab}\left(\mathbf{r}-\mathbf{r}',\omega\right)&=\frac{\omega^2}{c^2}\int_{\mathbb{R}^3}d^3x\,g(\mathbf{r}-\mathbf{x},\omega)\,\Pi_{ab}^{(\mathrm{T})}\left(\mathbf{x}-\mathbf{r}'\right)-\Pi_{ab}^{(\mathrm{L})}\left(\mathbf{r}-\mathbf{r}'\right)\\&=\frac{1}{(2\pi)^3}\int_{\mathbb{R}^3}d^3k\,e^{i\mathbf{k}\cdot(\mathbf{r}-\mathbf{r}')}\left[\frac{\omega^2}{c^2}\int_{\mathbb{R}^3}d^3x\,g(\mathbf{r}-\mathbf{x},\omega)\,e^{-i\mathbf{k}\cdot(\mathbf{r}-\mathbf{x})}\tilde{\Pi}_{ab}^{(\mathrm{T})}(\mathbf{k})-\tilde{\Pi}_{ab}^{(\mathrm{L})}(\mathbf{k})\right].\end{aligned} \tag{C.2.4}$$

Obviously, the integral with respect to the spatial coordinates in (C.2.4) represents the Fourier transform of the Helmholtz propagator

$$g\left(\mathbf{r}-\mathbf{r}',\omega\right)=\frac{1}{4\pi}\frac{e^{i\frac{\omega}{c}|\mathbf{r}-\mathbf{r}'|}}{|\mathbf{r}-\mathbf{r}'|}, \tag{C.2.5}$$

that is evaluated to

$$\int_{\mathbb{R}^3}d^3x\,g(\mathbf{r}-\mathbf{x},\omega)\,e^{-i\mathbf{k}\cdot(\mathbf{r}-\mathbf{x})}=\frac{1}{|\mathbf{k}|^2-\frac{\omega^2}{c^2}}. \tag{C.2.6}$$

Finally, insertion of (C.2.6) into (C.2.4) leads to

$$\begin{aligned}\mathscr{G}_{ab}\left(\mathbf{r}-\mathbf{r}',\omega\right)&=\frac{1}{(2\pi)^3}\int_{\mathbb{R}^3}d^3k\,e^{i\mathbf{k}\cdot(\mathbf{r}-\mathbf{r}')}\left[\frac{\omega^2}{c^2}\frac{1}{|\mathbf{k}|^2-\frac{\omega^2}{c^2}}\tilde{\Pi}_{ab}^{(\mathrm{T})}(\mathbf{k})-\tilde{\Pi}_{ab}^{(\mathrm{L})}(\mathbf{k})\right]\\&=\frac{1}{(2\pi)^3}\int_{\mathbb{R}^3}d^3k\,e^{i\mathbf{k}\cdot(\mathbf{r}-\mathbf{r}')}\tilde{\mathscr{G}}_{ab}(\mathbf{k},\omega),\end{aligned} \tag{C.2.7}$$

where in the second line the Fourier transformed electromagnetic kernel

$$\tilde{\mathscr{G}}_{ab}(\mathbf{k},\omega) = \frac{\omega^2}{c^2}\frac{1}{|\mathbf{k}|^2-\frac{\omega^2}{c^2}}\tilde{\Pi}^{(\mathrm{T})}_{ab}(\mathbf{k}) - \tilde{\Pi}^{(\mathrm{L})}_{ab}(\mathbf{k}) \tag{C.2.8}$$

$$= \frac{\frac{\omega^2}{c^2}\delta_{ab} - k_a k_b}{|\mathbf{k}|^2-\frac{\omega^2}{c^2}} \tag{C.2.9}$$

has been identified.

C.3 Relation between electromagnetic kernel and dyadic Green's function

The vector wave equation for the electric field, which can easily be deduced from microscopic Maxwell equations (2.1.12) and (2.1.13), reads

$$\nabla_{\mathbf{r}} \times \nabla_{\mathbf{r}} \times \mathbf{E}(\mathbf{r},\omega) - \frac{\omega^2}{c^2}\mathbf{E}(\mathbf{r},\omega) = i\omega\mu_0 \mathbf{j}(\mathbf{r},\omega). \tag{C.3.1}$$

Its associated dyadic Green function

$$G(\mathbf{r},\mathbf{r}',\omega) = \left(\mathbb{I} + \frac{c^2}{\omega^2}\nabla_{\mathbf{r}}\nabla_{\mathbf{r}}^T\right) g(\mathbf{r}-\mathbf{r}',\omega), \tag{C.3.2}$$

that obeys to the outgoing radiation condition then satisfies[1]

$$\nabla_{\mathbf{r}} \times \nabla_{\mathbf{r}} \times G(\mathbf{r},\mathbf{r}',\omega) - \frac{\omega^2}{c^2}G(\mathbf{r},\mathbf{r}',\omega) = \delta(\mathbf{r}-\mathbf{r}')\,\mathbb{I}, \tag{C.3.3}$$

where $g(\mathbf{r}-\mathbf{r}',\omega)$ represents the scalar Helmholtz propagator given by (C.2.5). Inserting the Fourier integral representation of the Helmholtz propagator

$$g(\mathbf{r}-\mathbf{r}',\omega) = \frac{1}{(2\pi)^3}\int_{\mathbb{R}^3} d^3k\, e^{i\mathbf{k}\cdot(\mathbf{r}-\mathbf{r}')}\frac{1}{|\mathbf{k}|^2-\frac{\omega^2}{c^2}} \tag{C.3.4}$$

into (C.3.2), one readily obtains for the cartesian components of the dyadic Green function

$$G_{ab}(\mathbf{r},\mathbf{r}',\omega) = \frac{c^2}{\omega^2}\frac{1}{(2\pi)^3}\int_{\mathbb{R}^3} d^3k\, e^{i\mathbf{k}\cdot(\mathbf{r}-\mathbf{r}')}\frac{\frac{\omega^2}{c^2}\delta_{ab}-k_a k_b}{|\mathbf{k}|^2-\frac{\omega^2}{c^2}}$$

$$= \frac{c^2}{\omega^2}\mathscr{G}_{ab}(\mathbf{r}-\mathbf{r}',\omega), \tag{C.3.5}$$

[1] For a thorough derivation of (C.3.2), see [134].

where in the second line the Fourier integral representation of the electromagnetic kernel (C.2.7) has been identified. Evidently, the electromagnetic kernel $\mathscr{G}_{ab}(\mathbf{r}-\mathbf{r}',\omega)$ is equivalent to the dyadic Green function $G_{ab}(\mathbf{r},\mathbf{r}',\omega)$. However, the benefit in employing $\mathscr{G}_{ab}(\mathbf{r}-\mathbf{r}',\omega)$ instead of $G_{ab}(\mathbf{r},\mathbf{r}',\omega)$ certainly rests upon its straightforward decomposition into longitudinal and transverse components, that allows the identification of radiative and non-radiative contributions of the electromagnetic field at a glance as well as to carry out further calculations on the basis of the well-know properties of the projection operators $\Pi_{ab}^{(\mathrm{L})}(\mathbf{r}-\mathbf{r}')$ and $\Pi_{ab}^{(\mathrm{T})}(\mathbf{r}-\mathbf{r}')$.

Appendix D

Non-standard system of Bloch functions

In this appendix it is shown (see also [23, 24]), that the newly discovered set of non-standard Bloch functions $\{w(\mathbf{r};\mathbf{s},\mathbf{k})\}_{\mathbf{s}\in C_\Lambda,\mathbf{k}\in C_{\Lambda^{-1}}}$ with

$$w(\mathbf{r};\mathbf{s},\mathbf{k}) = \frac{e^{i\mathbf{k}\cdot\mathbf{r}}}{\sqrt{N_\mathrm{P}}} \sum_{\mathbf{R}'\in\Lambda} \delta\left(\mathbf{r}-\mathbf{s}-\mathbf{R}'\right) \tag{D.0.1}$$

constitutes a complete and orthonormal set of eigenfunctions of the translation operator $\hat{T}_\mathbf{R}$, whose action on a function $f(\mathbf{r})$ is defined by $\hat{T}_\mathbf{R} f(\mathbf{r}) = f(\mathbf{r}+\mathbf{R})$ with $\mathbf{R}\in\Lambda$. Notice, that N_P denotes the number of Wigner-Seitz cells C_Λ, whose periodic arrangement builds up the crystal of probe volume $|\Omega_\mathrm{P}|$.

Eigenfunction of $\hat{T}_\mathbf{R}$ One readily confirms, that $w(\mathbf{r};\mathbf{s},\mathbf{k})$ is an eigenfunction of $\hat{T}_\mathbf{R}$. There holds

$$\begin{aligned}
\hat{T}_\mathbf{R} w(\mathbf{r};\mathbf{s},\mathbf{k}) &= w(\mathbf{r}+\mathbf{R};\mathbf{s},\mathbf{k}) \\
&= \frac{e^{i\mathbf{k}\cdot(\mathbf{r}+\mathbf{R})}}{\sqrt{N_\mathrm{P}}} \sum_{\mathbf{R}'\in\Lambda} \delta\left(\mathbf{r}+\mathbf{R}-\mathbf{s}-\mathbf{R}'\right) \\
&= e^{i\mathbf{k}\cdot\mathbf{R}} \frac{e^{i\mathbf{k}\cdot\mathbf{r}}}{\sqrt{N_\mathrm{P}}} \sum_{\mathbf{R}''\in\Lambda} \delta\left(\mathbf{r}-\mathbf{s}-\mathbf{R}''\right) \\
&= e^{i\mathbf{k}\cdot\mathbf{R}} w(\mathbf{r};\mathbf{s},\mathbf{k}),
\end{aligned} \tag{D.0.2}$$

where in the second last line the index transformation $\mathbf{R}'' = \mathbf{R}' - \mathbf{R}$ has been deployed. Notice, that the associated eigenvalue $e^{i\mathbf{k}\cdot\mathbf{R}}$ is highly degenerate.

Completeness relation The completeness relation for the set of functions $\{w(\mathbf{r};\mathbf{s},\mathbf{k})\}_{\mathbf{s}\in C_\Lambda,\mathbf{k}\in C_{\Lambda^{-1}}}$ is shown by calculating

$$\begin{aligned}&\sum_{\mathbf{k}\in C_{\Lambda^{-1}}}\int_{C_\Lambda} d^3s\, w(\mathbf{r};\mathbf{s},\mathbf{k})\, w^\dagger\left(\mathbf{r}';\mathbf{s},\mathbf{k}\right)\\ =&\frac{1}{N_\mathrm{P}}\sum_{\mathbf{k}\in C_{\Lambda^{-1}}} e^{i\mathbf{k}\cdot(\mathbf{r}-\mathbf{r}')}\int_{C_\Lambda} d^3s \sum_{\mathbf{R},\mathbf{R}'\in\Lambda}\delta(\mathbf{r}-\mathbf{s}-\mathbf{R})\,\delta\left(\mathbf{r}'-\mathbf{s}-\mathbf{R}'\right).\end{aligned} \tag{D.0.3}$$

As every point $\mathbf{r},\mathbf{r}'\in\Omega_\mathrm{P}$ can be represented by

$$\mathbf{r}=\mathbf{r}_0+\mathbf{R}_0 \tag{D.0.4}$$

$$\mathbf{r}'=\mathbf{r}_0'+\mathbf{R}_0', \tag{D.0.5}$$

with $\mathbf{r}_0,\mathbf{r}_0'\in C_\Lambda$ and $\mathbf{R}_0,\mathbf{R}_0'\in\Lambda_\mathrm{P}$, (D.0.3) can be evaluated further to

$$\begin{aligned}&\sum_{\mathbf{k}\in C_{\Lambda^{-1}}}\int_{C_\Lambda} d^3s\, w(\mathbf{r};\mathbf{s},\mathbf{k})\, w^\dagger\left(\mathbf{r}';\mathbf{s},\mathbf{k}\right)\\ =&\frac{1}{N_\mathrm{P}}\sum_{\mathbf{k}\in C_{\Lambda^{-1}}} e^{i\mathbf{k}\cdot\left(\mathbf{r}_0+\mathbf{R}_0-\mathbf{r}_0'-\mathbf{R}_0'\right)}\int_{C_\Lambda} d^3s \sum_{\mathbf{R},\mathbf{R}'\in\Lambda}\delta_{\mathbf{R}\mathbf{R}_0}\delta_{\mathbf{R}'\mathbf{R}_0'}\,\delta(\mathbf{r}_0-\mathbf{s})\,\delta\left(\mathbf{r}_0'-\mathbf{s}\right)\\ =&\frac{1}{N_\mathrm{P}}\sum_{\mathbf{k}\in C_{\Lambda^{-1}}} e^{i\mathbf{k}\cdot\left(\mathbf{r}_0+\mathbf{R}_0-\mathbf{r}_0'-\mathbf{R}_0'\right)}\,\delta\left(\mathbf{r}_0-\mathbf{r}_0'\right)\\ =&\frac{1}{N_\mathrm{P}}\sum_{\mathbf{k}\in C_{\Lambda^{-1}}} e^{i\mathbf{k}\cdot\left(\mathbf{R}_0-\mathbf{R}_0'\right)}\,\delta\left(\mathbf{r}_0-\mathbf{r}_0'\right)\\ =&\frac{|C_\Lambda|}{(2\pi)^3}\int_{C_{\Lambda^{-1}}} d^3k\, e^{i\mathbf{k}\cdot\left(\mathbf{R}_0-\mathbf{R}_0'\right)}\,\delta\left(\mathbf{r}_0-\mathbf{r}_0'\right),\end{aligned} \tag{D.0.6}$$

where in the last line the limit $N_\mathrm{P}\to\infty$ was carried out, so that the sum over wave vectors $\mathbf{k}\in C_{\Lambda^{-1}}$ may be replaced by an integral according to

$$\sum_{\mathbf{k}\in C_{\Lambda^{-1}}}\longrightarrow\frac{|\Omega_\mathrm{P}|}{(2\pi)^3}\int_{C_{\Lambda^{-1}}} d^3k\,. \tag{D.0.7}$$

Identifying $|C_{\Lambda^{-1}}|=\frac{(2\pi)^3}{|C_\Lambda|}$ as the volume of the first Brillouin zone and deploying the identity[1]

$$\frac{1}{|C_{\Lambda^{-1}}|}\int_{C_{\Lambda^{-1}}} d^3k\, e^{i\mathbf{k}\cdot\mathbf{R}}=\delta_{\mathbf{R}\mathbf{0}} \tag{D.0.8}$$

[1] An overview on identities commonly used in solid state and crystal physics is e.g. given in [136].

to (D.0.6), the completeness relation for $\{w(\mathbf{r};\mathbf{s},\mathbf{k})\}_{\mathbf{s}\in C_\Lambda,\mathbf{k}\in C_{\Lambda^{-1}}}$ is readily proved

$$\begin{aligned}\sum_{\mathbf{k}\in C_{\Lambda^{-1}}}\int_{C_\Lambda} d^3s\, w(\mathbf{r};\mathbf{s},\mathbf{k})\, w^\dagger\left(\mathbf{r}';\mathbf{s},\mathbf{k}\right) &= \delta_{\mathbf{R}_0\mathbf{R}_0'}\,\delta\left(\mathbf{r}_0-\mathbf{r}_0'\right)\\ &= \delta\left(\mathbf{r}-\mathbf{r}'\right).\end{aligned} \tag{D.0.9}$$

Orthonormality relation The orthonormality relation for the set of functions $\{w(\mathbf{r};\mathbf{s},\mathbf{k})\}_{\mathbf{s}\in C_\Lambda,\mathbf{k}\in C_{\Lambda^{-1}}}$ is shown by calculating the integral

$$\begin{aligned}&\int_{\Omega_\mathrm{P}} d^3r\, w^\dagger(\mathbf{r};\mathbf{s},\mathbf{k})\, w\left(\mathbf{r};\mathbf{s}',\mathbf{k}'\right)\\ =&\frac{1}{N_\mathrm{P}}\sum_{\mathbf{R},\mathbf{R}'\in\Lambda}\int_{\Omega_\mathrm{P}} d^3r\, e^{-i(\mathbf{k}-\mathbf{k}')\cdot\mathbf{r}}\,\delta(\mathbf{r}-\mathbf{s}-\mathbf{R})\,\delta\left(\mathbf{r}-\mathbf{s}'-\mathbf{R}'\right)\\ =&\frac{1}{N_\mathrm{P}}\sum_{\mathbf{R}\in\Lambda_\mathrm{P}}\sum_{\mathbf{R}'\in\Lambda} e^{-i(\mathbf{k}-\mathbf{k}')\cdot(\mathbf{s}+\mathbf{R})}\,\delta\left(\mathbf{s}+\mathbf{R}-\mathbf{s}'-\mathbf{R}'\right)\\ =&e^{-i(\mathbf{k}-\mathbf{k}')\cdot\mathbf{s}}\,\delta\left(\mathbf{s}-\mathbf{s}'\right)\frac{1}{N_\mathrm{P}}\sum_{\mathbf{R}\in\Lambda_\mathrm{P}} e^{-i(\mathbf{k}-\mathbf{k}')\cdot\mathbf{R}}.\end{aligned} \tag{D.0.10}$$

Applying now the identity

$$\frac{1}{N_\mathrm{P}}\sum_{\mathbf{R}\in\Lambda_\mathrm{P}} e^{-i\mathbf{k}\cdot\mathbf{R}} = \sum_{\mathbf{G}\in\Lambda^{-1}}\delta_{\mathbf{k}+\mathbf{G},\mathbf{0}}, \tag{D.0.11}$$

the orthonormality relation is readily proved

$$\begin{aligned}\int_{\Omega_\mathrm{P}} d^3r\, w^\dagger(\mathbf{r};\mathbf{s},\mathbf{k})\, w\left(\mathbf{r};\mathbf{s}',\mathbf{k}'\right) &= e^{-i(\mathbf{k}-\mathbf{k}')\cdot\mathbf{s}}\,\delta\left(\mathbf{s}-\mathbf{s}'\right)\sum_{\mathbf{G}\in\Lambda^{-1}}\delta_{\mathbf{k}\mathbf{k}'}\delta_{\mathbf{G}\mathbf{0}}\\ &= \delta\left(\mathbf{s}-\mathbf{s}'\right)\delta_{\mathbf{k}\mathbf{k}'}.\end{aligned} \tag{D.0.12}$$

Appendix E

Auxiliary calculations

Due to their extent, various auxiliary calculations are presented in this appendix, as they would disturb the line of thought in the main text[1].

E.1 Matrix elements of $[\mathscr{G}\circ\chi]_{ab}$ in the basis $\{w(\mathbf{r};\mathbf{s},\mathbf{k})\}_{\mathbf{s}\in C_\Lambda,\mathbf{k}\in C_{\Lambda^{-1}}}$

According to equation (3.2.15), the matrix elements of the kernel $[\mathscr{G}\circ\chi]_{ab}$ represented in the basis $\{w(\mathbf{r};\mathbf{s},\mathbf{k})\}_{\mathbf{s}\in C_\Lambda,\mathbf{k}\in C_{\Lambda^{-1}}}$, with

$$w(\mathbf{r};\mathbf{s},\mathbf{k}) = \frac{e^{i\mathbf{k}\cdot\mathbf{r}}}{\sqrt{N_\mathrm{P}}}\sum_{\mathbf{R}'\in\Lambda}\delta\left(\mathbf{r}-\mathbf{s}-\mathbf{R}'\right), \tag{E.1.1}$$

are defined by

$$\langle\mathbf{s},\mathbf{k}\,|[\mathscr{G}\circ\chi]_{ab}|\,\mathbf{s}',\mathbf{k}'\rangle \equiv \int_{\Omega_\mathrm{P}} d^3r\int_{\mathbb{R}^3} d^3r'\,w^\dagger(\mathbf{r};\mathbf{s},\mathbf{k})\,[\mathscr{G}\circ\chi]_{ab}\left(\mathbf{r},\mathbf{r}',\omega\right)w\left(\mathbf{r}';\mathbf{s}',\mathbf{k}'\right), \tag{E.1.2}$$

where (see (3.1.10))

$$[\mathscr{G}\circ\chi]_{ab}\left(\mathbf{r},\mathbf{r}',\omega\right) = \sum_{c=1}^{3}\int_{\mathbb{R}^3} d^3r''\,\mathscr{G}_{ac}\left(\mathbf{r}-\mathbf{r}'',\omega\right)\chi_{cb}\left(\mathbf{r}'',\mathbf{r}',\omega\right) \tag{E.1.3}$$

holds. Deploying the model for the dielectric susceptibility kernel (3.1.6) in (E.1.3), $[\mathscr{G}\circ\chi]_{ab}(\mathbf{r},\mathbf{r}',\omega)$ is readily evaluated to

$$[\mathscr{G}\circ\chi]_{ab}\left(\mathbf{r},\mathbf{r}',\omega\right) = \frac{1}{\varepsilon_0}\sum_{c=1}^{3}\sum_{\mathbf{R}\in\Lambda_\mathrm{P}}\sum_{j,j'=1}^{M}\mathscr{G}_{ac}\left(\mathbf{r}-\mathbf{R}-\eta^{(j)},\omega\right)\alpha_{cb}\left(\eta^{(j)},\eta^{(j')},\omega\right)\delta\left(\mathbf{r}'-\mathbf{R}-\eta^{(j')}\right). \tag{E.1.4}$$

[1] Essentially, the calculations follow [23, 24].

Initially, there follows by inserting (E.1.1) into (E.1.2)

$$\begin{aligned}
&\langle \mathbf{s},\mathbf{k}\,|[\mathscr{G}\circ\chi]_{ab}|\,\mathbf{s}',\mathbf{k}'\rangle \\
=&\frac{1}{N_\mathrm{P}}\int_{\Omega_\mathrm{P}} d^3r \sum_{\mathbf{R}\in\Lambda} e^{-i\mathbf{k}\cdot\mathbf{r}}\delta\left(\mathbf{r}-\mathbf{s}-\mathbf{R}\right)\int_{\mathbb{R}^3} d^3r' \sum_{\mathbf{R}'\in\Lambda} e^{i\mathbf{k}'\cdot\mathbf{r}'}\delta\left(\mathbf{r}'-\mathbf{s}'-\mathbf{R}'\right)[\mathscr{G}\circ\chi]_{ab}\left(\mathbf{r},\mathbf{r}',\omega\right) \\
=&\frac{1}{N_\mathrm{P}}\sum_{\mathbf{R}'\in\Lambda} e^{i\mathbf{k}'\cdot(\mathbf{s}'+\mathbf{R}')}\int_{\Omega_\mathrm{P}} d^3r \sum_{\mathbf{R}\in\Lambda} e^{-i\mathbf{k}\cdot\mathbf{r}}\delta\left(\mathbf{r}-\mathbf{s}-\mathbf{R}\right)[\mathscr{G}\circ\chi]_{ab}\left(\mathbf{r},\mathbf{s}'+\mathbf{R}',\omega\right) \\
=&\frac{1}{N_\mathrm{P}}\sum_{\mathbf{R}\in\Lambda_\mathrm{P}}\sum_{\mathbf{R}'\in\Lambda} e^{-i\mathbf{k}\cdot(\mathbf{s}+\mathbf{R})}[\mathscr{G}\circ\chi]_{ab}\left(\mathbf{s}+\mathbf{R},\mathbf{s}'+\mathbf{R}',\omega\right)e^{i\mathbf{k}'\cdot(\mathbf{s}'+\mathbf{R}')},
\end{aligned} \tag{E.1.5}$$

so that subsequent insertion of (E.1.4) leads to

$$\begin{aligned}
&\langle \mathbf{s},\mathbf{k}\,|[\mathscr{G}\circ\chi]_{ab}|\,\mathbf{s}',\mathbf{k}'\rangle \\
=&\frac{1}{\varepsilon_0}\frac{1}{N_\mathrm{P}}\sum_{c=1}^{3}\sum_{j,j'=1}^{M}\sum_{\mathbf{R},\mathbf{R}''\in\Lambda_\mathrm{P}}\sum_{\mathbf{R}'\in\Lambda} \\
&\cdot e^{-i\mathbf{k}\cdot(\mathbf{s}+\mathbf{R})}\mathscr{G}_{ac}\left(\mathbf{s}+\mathbf{R}-\mathbf{R}''-\eta^{(j)},\omega\right)\alpha_{cb}\left(\eta^{(j)},\eta^{(j')},\omega\right)\delta\left(\mathbf{s}'+\mathbf{R}'-\mathbf{R}''-\eta^{(j')}\right)e^{i\mathbf{k}'\cdot(\mathbf{s}'+\mathbf{R}')} \\
=&\frac{1}{\varepsilon_0}\frac{1}{N_\mathrm{P}}\sum_{c=1}^{3}\sum_{j,j'=1}^{M}\sum_{\mathbf{R},\mathbf{R}'\in\Lambda_\mathrm{P}} \\
&\cdot e^{-i\mathbf{k}\cdot(\mathbf{s}+\mathbf{R})}\mathscr{G}_{ac}\left(\mathbf{s}+\mathbf{R}-\mathbf{R}'-\eta^{(j)},\omega\right)\alpha_{cb}\left(\eta^{(j)},\eta^{(j')},\omega\right)e^{i\mathbf{k}'\cdot(\mathbf{s}'+\mathbf{R}')}\delta\left(\mathbf{s}'-\eta^{(j')}\right),
\end{aligned} \tag{E.1.6}$$

where in the last line

$$\delta\left(\mathbf{s}'+\mathbf{R}'-\mathbf{R}''-\eta^{(j')}\right)=\delta_{\mathbf{R}'\mathbf{R}''}\delta\left(\mathbf{s}'-\eta^{(j')}\right) \tag{E.1.7}$$

has been used. Assuming from now on the crystal to be infinitely extended, i.e. $\Lambda_\mathrm{P}=\Lambda$, an index transformation $\mathbf{R}''=\mathbf{R}'-\mathbf{R}$ can be applied to (E.1.6), so that finally[2]

$$\begin{aligned}
&\langle \mathbf{s},\mathbf{k}\,|[\mathscr{G}\circ\chi]_{ab}|\,\mathbf{s}',\mathbf{k}'\rangle \\
=&\frac{e^{-i\mathbf{k}\cdot\mathbf{s}}}{\varepsilon_0}\frac{1}{N_\mathrm{P}}\sum_{c=1}^{3}\sum_{j,j'=1}^{M}\sum_{\mathbf{R},\mathbf{R}'\in\Lambda} e^{-i(\mathbf{k}-\mathbf{k}')\cdot\mathbf{R}}\mathscr{G}_{ac}\left(\mathbf{s}-\mathbf{R}'-\eta^{(j)},\omega\right)\alpha_{cb}\left(\eta^{(j)},\eta^{(j')},\omega\right)e^{i\mathbf{k}'\cdot(\mathbf{s}'+\mathbf{R}')}\delta\left(\mathbf{s}'-\eta^{(j')}\right) \\
=&\frac{e^{-i\mathbf{k}\cdot\mathbf{s}}}{\varepsilon_0}\frac{(2\pi)^3}{|C_\Lambda|}\frac{1}{N_\mathrm{P}}\sum_{c=1}^{3}\sum_{j,j'=1}^{M}\sum_{\mathbf{R}'\in\Lambda} \\
&\cdot\mathscr{G}_{ac}\left(\mathbf{s}-\mathbf{R}'-\eta^{(j)},\omega\right)\alpha_{cb}\left(\eta^{(j)},\eta^{(j')},\omega\right)e^{i\mathbf{k}'\cdot(\mathbf{s}'+\mathbf{R}')}\delta\left(\mathbf{s}'-\eta^{(j')}\right)\delta\left(\mathbf{k}-\mathbf{k}'\right)
\end{aligned} \tag{E.1.8}$$

emerges, where at the last equality sign the well-known identity (see e.g. [136])

$$\sum_{\mathbf{R}\in\Lambda} e^{-i\mathbf{k}\cdot\mathbf{R}}=\frac{(2\pi)^3}{|C_\Lambda|}\sum_{\mathbf{G}\in\Lambda^{-1}}\delta\left(\mathbf{G}+\mathbf{k}\right) \tag{E.1.9}$$

[2]Notice, that after the index transformation the new summation index has been renamed according to $\mathbf{R}''\to\mathbf{R}'$ to keep the notation short.

in conjunction with

$$\delta\left(\mathbf{G}+\mathbf{k}-\mathbf{k}'\right)=\delta_{\mathbf{G}\mathbf{0}}\delta\left(\mathbf{k}-\mathbf{k}'\right) \tag{E.1.10}$$

has been utilized.

E.2 Derivation of equation (3.2.27) and reasoning for a definition by cases of $[\zeta_\Lambda(\mathbf{s},\mathbf{k},\omega)]_{ab}$

According to (3.2.19), the expansion coefficients $\mathfrak{e}_a(\mathbf{s},\mathbf{k},\omega)$ with $\mathbf{s}\in C_\Lambda$ are determined by

$$\mathfrak{e}_a(\mathbf{s},\mathbf{k},\omega)=\mathfrak{e}_{\mathrm{ext},a}(\mathbf{s},\mathbf{k},\omega)+\frac{1}{\varepsilon_0}\sum_{b,c=1}^{3}\sum_{j,j'=1}^{M}\left[\zeta_\Lambda\left(\mathbf{s}-\eta^{(j)},\mathbf{k},\omega\right)\right]_{ab}\alpha_{bc}^{(j,j')}(\mathbf{k},\omega)\,\mathfrak{e}_c^{(j')}(\mathbf{k},\omega), \tag{E.2.1}$$

where use has been made of the lattice sum's definition (see (3.2.21) for $\mathbf{s}\neq\mathbf{0}$)

$$[\zeta_\Lambda(\mathbf{s},\mathbf{k},\omega)]_{ab}=\sum_{\mathbf{R}\in\Lambda}e^{-i\mathbf{k}\cdot(\mathbf{s}+\mathbf{R})}\mathscr{G}_{ab}(\mathbf{s}+\mathbf{R},\omega). \tag{E.2.2}$$

The determination of $\mathfrak{e}_a(\mathbf{s},\mathbf{k},\omega)$ requires the knowledge of $\mathfrak{e}_c^{(j')}(\mathbf{k},\omega)$ for $j'\in\{1,2,\ldots,M\}$, which can in principle be achieved by taking the limit $\mathbf{s}\to\eta^{(j'')}$ successively in (E.2.1) for any $j''\in\{1,2,\ldots,M\}$. Nonetheless, attention has to be paid in this limiting process because of a singularity which is hold by the lattice sum $\zeta_\Lambda\left(\mathbf{s}-\eta^{(j)},\mathbf{k},\omega\right)$ defined by (E.2.2). It originates from the lattice sum's $\mathbf{R}=\mathbf{0}$ contribution if $\mathbf{s}\to\eta^{(j'')}=\eta^{(j)}$. Therefore, omitting this singular contribution occurring at $\mathbf{R}=\mathbf{0}$ in the limit $\mathbf{s}\to\eta^{(j'')}$ if $j''=j$, (E.2.1) initially assumes the guise[3]

$$\begin{aligned}\mathfrak{e}_a^{(j'')}(\mathbf{k},\omega)=&\mathfrak{e}_{\mathrm{ext},a}^{(j'')}(\mathbf{k},\omega)+\frac{1}{\varepsilon_0}\sum_{b,c=1}^{3}\sum_{j,j'=1}^{M}\lim_{\mathbf{s}\to\eta^{(j'')}}\left[\zeta_\Lambda\left(\mathbf{s}-\eta^{(j)},\mathbf{k},\omega\right)\right]_{ab}\alpha_{bc}^{(j,j')}(\mathbf{k},\omega)\,\mathfrak{e}_c^{(j')}(\mathbf{k},\omega)\\&-\frac{1}{\varepsilon_0}\sum_{b,c=1}^{3}\sum_{j'=1}^{M}\lim_{\mathbf{s}\to\eta^{(j'')}}\mathscr{G}_{ab}\left(\mathbf{s}-\eta^{(j'')},\omega\right)\alpha_{bc}^{(j'',j')}(\mathbf{k},\omega)\,\mathfrak{e}_c^{(j')}(\mathbf{k},\omega).\end{aligned} \tag{E.2.3}$$

[3] Physically speaking, omitting this singular contribution is equivalent to the statement that a point dipole does not interact with the field that is produced by itself.

Decomposing now the sum with respect to j into two contributions according to $j = j''$ and $j \neq j''$, there directly follows

$$\begin{aligned}
\mathfrak{e}_a^{(j'')}(\mathbf{k},\omega) =& \mathfrak{e}_{\mathrm{ext},a}^{(j'')}(\mathbf{k},\omega) + \frac{1}{\varepsilon_0}\sum_{b,c=1}^{3}\sum_{j'=1}^{M}\sum_{j\neq j''}\left[\zeta_\Lambda\left(\eta^{(j'')}-\eta^{(j)},\mathbf{k},\omega\right)\right]_{ab}\alpha_{bc}^{(j,j')}(\mathbf{k},\omega)\,\mathfrak{e}_c^{(j')}(\mathbf{k},\omega) \\
&+\frac{1}{\varepsilon_0}\sum_{b,c=1}^{3}\sum_{j'=1}^{M}\lim_{|\mathbf{s}|\to 0}\left(\left[\zeta_\Lambda(\mathbf{s},\mathbf{k},\omega)\right]_{ab}-\mathscr{G}_{ab}(\mathbf{s},\omega)\right)\alpha_{bc}^{(j'',j')}(\mathbf{k},\omega)\,\mathfrak{e}_c^{(j')}(\mathbf{k},\omega) \\
=& \mathfrak{e}_{\mathrm{ext},a}^{(j'')}(\mathbf{k},\omega) + \frac{1}{\varepsilon_0}\sum_{b,c=1}^{3}\sum_{j'=1}^{M}\sum_{j\neq j''}\left[\zeta_\Lambda\left(\eta^{(j'')}-\eta^{(j)},\mathbf{k},\omega\right)\right]_{ab}\alpha_{bc}^{(j,j')}(\mathbf{k},\omega)\,\mathfrak{e}_c^{(j')}(\mathbf{k},\omega) \\
&+\frac{1}{\varepsilon_0}\sum_{b,c=1}^{3}\sum_{j'=1}^{M}\left[\zeta_\Lambda^{(0)}(\mathbf{k},\omega)\right]_{ab}\alpha_{bc}^{(j'',j')}(\mathbf{k},\omega)\,\mathfrak{e}_c^{(j')}(\mathbf{k},\omega),
\end{aligned} \tag{E.2.4}$$

where in the last line the non-singular lattice sum $\zeta_\Lambda^{(0)}(\mathbf{k},\omega)$ (compare with (3.2.26)) has been defined by

$$\begin{aligned}
\left[\zeta_\Lambda^{(0)}(\mathbf{k},\omega)\right]_{ab} &= \lim_{|\mathbf{s}|\to 0}\left(\left[\zeta_\Lambda(\mathbf{s},\mathbf{k},\omega)\right]_{ab}-\mathscr{G}_{ab}(\mathbf{s},\omega)\right) \\
&= \sum_{\mathbf{R}\in\Lambda\setminus\{\mathbf{0}\}} e^{-i\mathbf{k}\cdot\mathbf{R}}\mathscr{G}_{ab}(\mathbf{R},\omega) \\
&\equiv \left[\zeta_\Lambda(\mathbf{0},\mathbf{k},\omega)\right]_{ab}.
\end{aligned} \tag{E.2.5}$$

Combining (E.2.2) and (E.2.5) results in the by cases defined lattice sum (3.2.21), so that equation (E.2.4) determining the expansion coefficients at the atomic positions assumes the guise

$$\mathfrak{e}_a^{(j'')}(\mathbf{k},\omega) = \mathfrak{e}_{\mathrm{ext},a}^{(j'')}(\mathbf{k},\omega) + \frac{1}{\varepsilon_0}\sum_{b,c=1}^{3}\sum_{j,j'=1}^{M}\left[\zeta_\Lambda\left(\eta^{(j'')}-\eta^{(j)},\mathbf{k},\omega\right)\right]_{ab}\alpha_{bc}^{(j,j')}(\mathbf{k},\omega)\,\mathfrak{e}_c^{(j')}(\mathbf{k},\omega), \tag{E.2.6}$$

which is in accordance with (3.2.27).

E.3 Derivation of equation (3.2.32)

Under the assumption of an infinitely extended crystal (compare with (3.2.17)), the expansion of the local electric field (3.2.10) with respect to the system of functions $\{w(\mathbf{r};\mathbf{s},\mathbf{k})\}_{\mathbf{s}\in C_\Lambda,\mathbf{k}\in C_{\Lambda^{-1}}}$ formally reads

$$E_a(\mathbf{r},\omega) = \frac{|\Omega_\mathrm{P}|}{(2\pi)^3}\int_{C_{\Lambda^{-1}}} d^3k \int_{C_\Lambda} d^3s\, w(\mathbf{r};\mathbf{s},\mathbf{k})\,\mathfrak{e}_a(\mathbf{s},\mathbf{k},\omega), \tag{E.3.1}$$

where $w(\mathbf{r};\mathbf{s},\mathbf{k})$ has already been defined in (3.2.9) according to

$$w(\mathbf{r};\mathbf{s},\mathbf{k}) = \frac{e^{i\mathbf{k}\cdot\mathbf{r}}}{\sqrt{N_\mathrm{P}}}\sum_{\mathbf{R}'\in\Lambda}\delta\left(\mathbf{r}-\mathbf{s}-\mathbf{R}'\right). \tag{E.3.2}$$

The expansion coefficients $\mathfrak{e}_a(\mathbf{s},\mathbf{k},\omega)$ are readily obtained by inserting (3.2.31) into (3.2.19), so that

$$\begin{aligned}\mathfrak{e}_a(\mathbf{s},\mathbf{k},\omega) =& \mathfrak{e}_{\mathrm{ext},a}(\mathbf{s},\mathbf{k},\omega) + \frac{1}{\varepsilon_0}\sum_{b,c,d=1}^{3}\sum_{j,j',j''=1}^{M} \\ &\cdot\left[\zeta_\Lambda\left(\mathbf{s}-\eta^{(j)},\mathbf{k},\omega\right)\right]_{ab}\alpha^{(j,j')}_{bc}(\mathbf{k},\omega)\left[\left(\delta-\Gamma(\mathbf{k},\omega)\right)^{-1}\right]^{(j'j'')}_{cd}\mathfrak{e}^{(j'')}_{\mathrm{ext},d}(\mathbf{k},\omega). \qquad \text{(E.3.3)}\end{aligned}$$

Expanding the external field in analogy to $E_a(\mathbf{r},\omega)$ according to

$$E_{\mathrm{ext},a}(\mathbf{r},\omega) = \frac{|\Omega_{\mathrm{P}}|}{(2\pi)^3}\int_{C_{\Lambda^{-1}}} d^3k \int_{C_\Lambda} d^3s\, w(\mathbf{r};\mathbf{s},\mathbf{k})\,\mathfrak{e}_{\mathrm{ext},a}(\mathbf{s},\mathbf{k},\omega), \qquad \text{(E.3.4)}$$

$E_a(\mathbf{r},\omega)$ finally assumes the guise

$$\begin{aligned}&E_a(\mathbf{r},\omega)\\ =&E_{\mathrm{ext},a}(\mathbf{r},\omega) + \frac{1}{\varepsilon_0}\frac{|\Omega_{\mathrm{P}}|}{(2\pi)^3}\sum_{b,c,d=1}^{3}\sum_{j,j',j''=1}^{M}\\ &\cdot\int_{C_{\Lambda^{-1}}} d^3k\int_{C_\Lambda} d^3s\, w(\mathbf{r};\mathbf{s},\mathbf{k})\left[\zeta_\Lambda\left(\mathbf{s}-\eta^{(j)},\mathbf{k},\omega\right)\right]_{ab}\alpha^{(j,j')}_{bc}(\mathbf{k},\omega)\left[\left(\delta-\Gamma(\mathbf{k},\omega)\right)^{-1}\right]^{(j'j'')}_{cd}\mathfrak{e}^{(j'')}_{\mathrm{ext},d}(\mathbf{k},\omega)\\ =&E_{\mathrm{ext},a}(\mathbf{r},\omega) + \frac{1}{\varepsilon_0}\frac{1}{(2\pi)^3}\frac{|\Omega_{\mathrm{P}}|}{\sqrt{N_{\mathrm{P}}}}\sum_{b,c,d=1}^{3}\sum_{j,j',j''=1}^{M}\\ &\cdot\int_{C_{\Lambda^{-1}}} d^3k\, e^{i\mathbf{k}\cdot\mathbf{r}}\left[\zeta_\Lambda\left(\mathbf{r}-\eta^{(j)},\mathbf{k},\omega\right)\right]_{ab}\alpha^{(j,j')}_{bc}(\mathbf{k},\omega)\left[\left(\delta-\Gamma(\mathbf{k},\omega)\right)^{-1}\right]^{(j'j'')}_{cd}\mathfrak{e}^{(j'')}_{\mathrm{ext},d}(\mathbf{k},\omega), \qquad \text{(E.3.5)}\end{aligned}$$

where in the last line the integral with respect to $\mathbf{s}$ has been carried out by taking account of the lattice periodicity of the lattice sum $\zeta_\Lambda\left(\mathbf{r}-\eta^{(j)},\mathbf{k},\omega\right)$.

E.4 Relation between the expansion coefficients $\tilde{E}^{(\mathbf{ext})}_{\mathbf{q}\omega,a}$ and $\mathfrak{e}_{\mathbf{ext},a}(\mathbf{s},\mathbf{k},\omega)$

Expanding the externally applied electric field $E_{\mathrm{ext},a}(\mathbf{r},\omega)$ on the one hand with respect to plane waves and on the other hand in terms of $\{w(\mathbf{r};\mathbf{s},\mathbf{k})\}_{\mathbf{s}\in C_\Lambda,\mathbf{k}\in C_{\Lambda^{-1}}}$, a relation is established between the corresponding expansion coefficients $\tilde{E}^{(\mathrm{ext})}_{\mathbf{q}\omega,a}$ and $\mathfrak{e}_{\mathrm{ext},a}(\mathbf{s},\mathbf{k},\omega)$, respectively. There holds

$$E_{\mathrm{ext},a}(\mathbf{r},\omega) = \sum_{\mathbf{q}}\tilde{E}^{(\mathrm{ext})}_{\mathbf{q}\omega,a}e^{i\mathbf{q}\cdot\mathbf{r}} \qquad \text{(E.4.1)}$$

$$\stackrel{!}{=}\sum_{\mathbf{k}\in C_{\Lambda^{-1}}}\int_{C_\Lambda} d^3s\, w(\mathbf{r};\mathbf{s},\mathbf{k})\,\mathfrak{e}_{\mathrm{ext},a}(\mathbf{s},\mathbf{k},\omega), \qquad \text{(E.4.2)}$$

where up to this point no restrictions have been imposed on $\mathbf{q}$. According to (3.2.12), one obtains for the expansion coefficient $\mathfrak{e}_{\mathrm{ext},a}(\mathbf{s},\mathbf{k},\omega)$

$$\begin{aligned}\mathfrak{e}_{\mathrm{ext},a}(\mathbf{s},\mathbf{k},\omega) &= \int_{\Omega_\mathrm{P}} d^3r\, w^\dagger(\mathbf{r};\mathbf{s},\mathbf{k})\, E_{\mathrm{ext},a}(\mathbf{r},\omega) \\ &= \frac{1}{\sqrt{N_\mathrm{P}}} \sum_{\mathbf{R}'\in\Lambda_\mathrm{P}} e^{-i\mathbf{k}\cdot(\mathbf{s}+\mathbf{R}')} E_{\mathrm{ext},a}\left(\mathbf{s}+\mathbf{R}',\omega\right) \\ &= \frac{e^{-i\mathbf{k}\cdot\mathbf{s}}}{\sqrt{N_\mathrm{P}}} \sum_{\mathbf{q}} \tilde{E}^{(\mathrm{ext})}_{\mathbf{q}\omega,a} e^{i\mathbf{q}\cdot\mathbf{s}} \sum_{\mathbf{R}'\in\Lambda_\mathrm{P}} e^{-i(\mathbf{k}-\mathbf{q})\cdot\mathbf{R}'} \\ &= \frac{e^{-i\mathbf{k}\cdot\mathbf{s}}}{\sqrt{N_\mathrm{P}}} \frac{(2\pi)^3}{|C_\Lambda|} \sum_{\mathbf{q}} \tilde{E}^{(\mathrm{ext})}_{\mathbf{q}\omega,a} e^{i\mathbf{q}\cdot\mathbf{s}} \sum_{\mathbf{G}\in\Lambda^{-1}} \delta(\mathbf{k}-\mathbf{q}+\mathbf{G}), \end{aligned} \tag{E.4.3}$$

where in the last line the crystal was assumed to be infinitely extended (i.e. $\Lambda_\mathrm{P}=\Lambda$), so that the well-known identity (see e.g. [136])

$$\sum_{\mathbf{R}\in\Lambda} e^{-i\mathbf{k}\cdot\mathbf{R}} = \frac{(2\pi)^3}{|C_\Lambda|} \sum_{\mathbf{G}\in\Lambda^{-1}} \delta(\mathbf{k}+\mathbf{G}) \tag{E.4.4}$$

can be applied. It should be emphasized, that the assumption $\Lambda_\mathrm{P}=\Lambda$ is in total accordance with the considerations given in section 3.2. Restricting now $\mathbf{q}$ to the first Brillouin zone, i.e. $\mathbf{q}\in C_{\Lambda^{-1}}$, the rather complicated relation (E.4.3) between $\mathfrak{e}_{\mathrm{ext},a}(\mathbf{s},\mathbf{k},\omega)$ and $\tilde{E}^{(\mathrm{ext})}_{\mathbf{q}\omega,a}$ simplifies, as only the $\mathbf{G}=\mathbf{0}$ term contributes to the sum over reciprocal lattice vectors, so that finally

$$\mathfrak{e}_{\mathrm{ext},a}(\mathbf{s},\mathbf{k},\omega) = \frac{e^{-i\mathbf{k}\cdot\mathbf{s}}}{\sqrt{N_\mathrm{P}}} \frac{(2\pi)^3}{|C_\Lambda|} \sum_{\mathbf{q}\in C_{\Lambda^{-1}}} \tilde{E}^{(\mathrm{ext})}_{\mathbf{q}\omega,a} e^{i\mathbf{q}\cdot\mathbf{s}} \delta(\mathbf{k}-\mathbf{q}). \tag{E.4.5}$$

E.5 Calculation of macroscopic polarization

The low-pass filtered Fourier amplitude $\tilde{\mathscr{P}}_a(\mathbf{q},\omega)$ associated with the microscopic polarization $P_a(\mathbf{r},\omega)$ given by (3.1.5) according to

$$P_a(\mathbf{r},\omega) = \varepsilon_0 \sum_{b=1}^{3} \int_{\mathbb{R}^3} d^3r'\, \chi_{ab}\left(\mathbf{r},\mathbf{r}',\omega\right) E_b\left(\mathbf{r}',\omega\right), \tag{E.5.1}$$

where

$$\chi_{ab}\left(\mathbf{r},\mathbf{r}',\omega\right) = \frac{1}{\varepsilon_0} \sum_{\mathbf{R}\in\Lambda} \sum_{j,j'=1}^{M} \alpha_{ab}\left(\eta^{(j)},\eta^{(j')},\omega\right) \delta\left(\mathbf{r}-\mathbf{R}-\eta^{(j)}\right) \delta\left(\mathbf{r}'-\mathbf{R}-\eta^{(j')}\right) \tag{E.5.2}$$

denotes the dielectric susceptibility kernel (see (3.1.6)) for an infinitely extended crystal (i.e. $\Lambda_P = \Lambda$), is defined by (see (4.1.10))

$$\tilde{\mathscr{P}}_a(\mathbf{q},\omega) = \int_{\mathbb{R}^3} d^3r\, e^{-i\mathbf{q}\cdot\mathbf{r}} P_a(\mathbf{r},\omega) \quad \text{with} \quad \mathbf{q} \in C_{\Lambda^{-1}}. \tag{E.5.3}$$

Initially there follows by inserting (E.5.1) and (E.5.2) into (E.5.3)

$$\tilde{\mathscr{P}}_a(\mathbf{q},\omega) = \sum_{b=1}^{3} \sum_{j,j'=1}^{M} \sum_{\mathbf{R}\in\Lambda} e^{-i\mathbf{q}\cdot\left(\mathbf{R}+\eta^{(j)}\right)} \alpha_{ab}\left(\eta^{(j)},\eta^{(j')},\omega\right) E_b\left(\mathbf{R}+\eta^{(j')},\omega\right). \tag{E.5.4}$$

As the local electric field can be represented according to (3.2.39) by

$$E_a(\mathbf{r},\omega) = \tilde{E}^{(\mathrm{ext})}_{\mathbf{q}\omega,a} e^{i\mathbf{q}\cdot\mathbf{r}} + \frac{1}{|C_\Lambda|} \sum_{b,d=1}^{3} \sum_{\mathbf{G}\in\Lambda^{-1}} e^{i(\mathbf{q}+\mathbf{G})\cdot\mathbf{r}} \tilde{\mathscr{G}}_{ab}(\mathbf{q}+\mathbf{G},\omega)\, \tilde{K}_{bd}(\mathbf{G},\mathbf{q},\omega)\, \tilde{E}^{(\mathrm{ext})}_{\mathbf{q}\omega,d} \tag{E.5.5}$$

one obtains

$$\begin{aligned}
&\tilde{\mathscr{P}}_a(\mathbf{q},\omega) \\
&= \sum_{b,d=1}^{3} \sum_{j,j'=1}^{M} \sum_{\mathbf{R}\in\Lambda} \alpha_{ab}\left(\eta^{(j)},\eta^{(j')},\omega\right) \Bigg(e^{-i(\mathbf{q}-\mathbf{q}')\cdot\mathbf{R}} e^{-i\mathbf{q}\cdot\eta^{(j)}} e^{i\mathbf{q}'\cdot\eta^{(j')}} \delta_{bd} \\
&\quad + \frac{1}{|C_\Lambda|} \sum_{c=1}^{3} \sum_{\mathbf{G}\in\Lambda^{-1}} e^{-i(\mathbf{q}-\mathbf{q}'-\mathbf{G})\cdot\mathbf{R}} e^{-i\mathbf{q}\cdot\eta^{(j)}} e^{i(\mathbf{q}'+\mathbf{G})\cdot\eta^{(j')}} \tilde{\mathscr{G}}_{bc}\left(\mathbf{q}'+\mathbf{G},\omega\right) \tilde{K}_{cd}\left(\mathbf{G},\mathbf{q}',\omega\right) \Bigg) \tilde{E}^{(\mathrm{ext})}_{\mathbf{q}'\omega,d} \\
&= \frac{(2\pi)^3}{|C_\Lambda|} \delta(\mathbf{q}-\mathbf{q}') \sum_{b,d=1}^{3} \sum_{j,j'=1}^{M} \alpha_{ab}\left(\eta^{(j)},\eta^{(j')},\omega\right) \Bigg(\delta_{bd} e^{-i\mathbf{q}\cdot\eta^{(j)}} e^{i\mathbf{q}'\cdot\eta^{(j')}} \\
&\quad + \frac{1}{|C_\Lambda|} \sum_{c=1}^{3} \sum_{\mathbf{G}\in\Lambda^{-1}} e^{-i\mathbf{q}\cdot\eta^{(j)}} e^{i(\mathbf{q}'+\mathbf{G})\cdot\eta^{(j')}} \tilde{\mathscr{G}}_{bc}\left(\mathbf{q}'+\mathbf{G},\omega\right) \tilde{K}_{cd}\left(\mathbf{G},\mathbf{q}',\omega\right) \Bigg) \tilde{E}^{(\mathrm{ext})}_{\mathbf{q}'\omega,d},
\end{aligned} \tag{E.5.6}$$

where in the last line the identity

$$\sum_{\mathbf{R}\in\Lambda} e^{-i\mathbf{k}\cdot\mathbf{R}} = \frac{(2\pi)^3}{|C_\Lambda|} \sum_{\mathbf{G}\in\Lambda^{-1}} \delta(\mathbf{G}+\mathbf{k}) \tag{E.5.7}$$

has been deployed. Additionally, use has been made of the fact that $\mathbf{q},\mathbf{q}' \in C_{\Lambda^{-1}}$. Now introducing the abbreviation (see (3.2.20))

$$\alpha^{(j,j')}_{bc}(\mathbf{k},\omega) \equiv e^{-i\mathbf{k}\cdot\eta^{(j)}} \alpha_{bc}\left(\eta^{(j)},\eta^{(j')},\omega\right) e^{i\mathbf{k}\cdot\eta^{(j')}} \tag{E.5.8}$$

together with the definition (3.2.38), i.e.

$$\tilde{K}_{bd}(\mathbf{G},\mathbf{q},\omega) = \frac{1}{\varepsilon_0} \sum_{c=1}^{3} \sum_{j,j',j''=1}^{M} e^{-i\mathbf{G}\cdot\eta^{(j)}} \alpha^{(j,j')}_{bc}(\mathbf{q},\omega) \left[\left(\delta - \Gamma(\mathbf{q},\omega)\right)^{-1}\right]^{(j'j'')}_{cd}, \tag{E.5.9}$$

there follows

$$\begin{aligned}
&\tilde{\mathscr{P}}_a(\mathbf{q},\omega)\\
=&\frac{(2\pi)^3}{|C_\Lambda|}\delta(\mathbf{q}-\mathbf{q}')\sum_{b,d=1}^{3}\sum_{j,j'=1}^{M}\alpha_{ab}^{(j,j')}(\mathbf{q},\omega)\left(\delta_{bd}+\frac{1}{\varepsilon_0}\frac{1}{|C_\Lambda|}\sum_{c,e=1}^{3}\sum_{j'',j'''=1}^{M}\sum_{\mathbf{G}\in\Lambda^{-1}}\right.\\
&\left.\cdot\tilde{\mathscr{G}}_{bc}(\mathbf{q}+\mathbf{G},\omega)\,e^{i\mathbf{G}\cdot\left(\eta^{(j')}-\eta^{(j'')}\right)}\alpha_{ce}^{(j'',j''')}(\mathbf{q},\omega)\left[(\delta-\Gamma(\mathbf{q},\omega))^{-1}\right]_{ed}^{(j'''j'''')}\right)\tilde{E}_{\mathbf{q}\omega,d}^{(\mathrm{ext})}.
\end{aligned}\tag{E.5.10}$$

The subsequent identification of (see (3.2.24) and (3.2.28))

$$[\zeta_\Lambda(\mathbf{s},\mathbf{k},\omega)]_{ab}=\frac{1}{|C_\Lambda|}\sum_{\mathbf{G}\in\Lambda^{-1}}\tilde{\mathscr{G}}_{ab}(\mathbf{k}+\mathbf{G},\omega)\,e^{i\mathbf{G}\cdot\mathbf{s}}\tag{E.5.11}$$

$$\Gamma_{ac}^{(j'',j')}(\mathbf{k},\omega)=\frac{1}{\varepsilon_0}\sum_{b=1}^{3}\sum_{j=1}^{M}\left[\zeta_\Lambda\left(\eta^{(j'')}-\eta^{(j)},\mathbf{k},\omega\right)\right]_{ab}\alpha_{bc}^{(j,j')}(\mathbf{k},\omega)\tag{E.5.12}$$

then yields

$$\begin{aligned}
&\tilde{\mathscr{P}}_a(\mathbf{q},\omega)\\
=&\frac{(2\pi)^3}{|C_\Lambda|}\delta(\mathbf{q}-\mathbf{q}')\sum_{b,d=1}^{3}\sum_{j,j'=1}^{M}\alpha_{ab}^{(j,j')}(\mathbf{q},\omega)\left(\delta_{bd}\right.\\
&\left.+\sum_{e=1}^{3}\sum_{j''',j''''=1}^{M}\Gamma_{be}^{(j',j''')}(\mathbf{q},\omega)\left[(\delta-\Gamma(\mathbf{q},\omega))^{-1}\right]_{ed}^{(j'''j'''')}\right)\tilde{E}_{\mathbf{q}\omega,d}^{(\mathrm{ext})}\\
=&\frac{(2\pi)^3}{|C_\Lambda|}\delta(\mathbf{q}-\mathbf{q}')\sum_{b,d=1}^{3}\sum_{j,j'=1}^{M}\alpha_{ab}^{(j,j')}(\mathbf{q},\omega)\left(\delta_{bd}+\sum_{j''''=1}^{M}\left[\Gamma(\mathbf{q},\omega)\circ(\delta-\Gamma(\mathbf{q},\omega))^{-1}\right]_{bd}^{(j'j'''')}\right)\tilde{E}_{\mathbf{q}\omega,d}^{(\mathrm{ext})},
\end{aligned}\tag{E.5.13}$$

where the symbol $\circ$ denotes the appropriate (block-) matrix multiplication. Obviously there holds[4]

$$\begin{aligned}
\Gamma(\mathbf{q},\omega)\circ(\delta-\Gamma(\mathbf{q},\omega))^{-1}&=-\left((\delta-\Gamma(\mathbf{q},\omega))-\delta\right)\circ(\delta-\Gamma(\mathbf{q},\omega))^{-1}\\
&=(\delta-\Gamma(\mathbf{q},\omega))^{-1}-\delta,
\end{aligned}\tag{E.5.14}$$

so that with the help of (4.1.5), i.e.

$$\tilde{K}_{bd}(\mathbf{q},\omega)=\frac{1}{\varepsilon_0}\sum_{c=1}^{3}\sum_{j,j',j''=1}^{M}\alpha_{bc}^{(j,j')}(\mathbf{q},\omega)\left[(\delta-\Gamma(\mathbf{q},\omega))^{-1}\right]_{cd}^{(j'j'')},\tag{E.5.15}$$

[4] δ denotes the (block-) identity matrix.

the low-pass filtered Fourier amplitude of the microscopic polarization finally emerges

$$\begin{aligned}
&\tilde{\mathscr{P}}_a(\mathbf{q},\omega)\\
=&\frac{(2\pi)^3}{|C_\Lambda|}\delta(\mathbf{q}-\mathbf{q}')\sum_{b,d=1}^{3}\sum_{j,j',j''''=1}^{M}\alpha_{ab}^{(j,j')}(\mathbf{q},\omega)\left[(\delta-\Gamma(\mathbf{q},\omega))^{-1}\right]_{bd}^{(j'j'''')}\tilde{E}_{\mathbf{q}\omega,d}^{(\mathrm{ext})}\\
=&\varepsilon_0\frac{(2\pi)^3}{|C_\Lambda|}\delta(\mathbf{q}-\mathbf{q}')\sum_{d=1}^{3}\tilde{K}_{ad}(\mathbf{q},\omega)\tilde{E}_{\mathbf{q}\omega,d}^{(\mathrm{ext})}.
\end{aligned}\tag{E.5.16}$$

According to (4.1.11), the macroscopic polarization $\mathscr{P}_a(\mathbf{r},\omega)$ in real space then readily follows

$$\begin{aligned}
\mathscr{P}_a(\mathbf{r},\omega)&=\frac{1}{(2\pi)^3}\int_{C_{\Lambda^{-1}}}d^3q\,e^{i\mathbf{q}\cdot\mathbf{r}}\tilde{\mathscr{P}}_a(\mathbf{q},\omega)\\
&=\frac{\varepsilon_0}{|C_\Lambda|}\sum_{d=1}^{3}\tilde{K}_{ad}(\mathbf{q}',\omega)\tilde{E}_{\mathbf{q}'\omega,d}^{(\mathrm{ext})}e^{i\mathbf{q}'\cdot\mathbf{r}}.
\end{aligned}\tag{E.5.17}$$

Appendix F

The lattice sum $\left[\zeta_\Lambda(\mathbf{s},\mathbf{k},\omega)\right]_{ab}$

Initially, an alternative representation of the lattice sum $\left[\zeta_\Lambda(\mathbf{s},\mathbf{k},\omega)\right]_{ab}$ based on its Fourier series expansion for $\mathbf{s}\neq\mathbf{0}$ is presented, that proves to be useful for the forthcoming derivations in the remainder of this work. Concerning the numerical evaluation of $\left[\zeta_\Lambda(\mathbf{s},\mathbf{k},\omega)\right]_{ab}$, a technique in the sense of the well-known Ewald summation is presented to ensure its fast and precise computation for $\mathbf{s}\neq\mathbf{0}$ as well as $\mathbf{s}=\mathbf{0}$. The thus derived expressions for the lattice sum constitute the basis for all calculations regarding the photonic band structure, the local electromagnetic field or the dielectric tensor. The calculations outlined below have been elaborated previously by Prof. N. Schopohl in [24] and have been published in the supplementary material to [23].

F.1 Fourier series expansion

If $\mathbf{s}\neq\mathbf{0}$, the lattice sum

$$\left[\zeta_\Lambda(\mathbf{s},\mathbf{k},\omega)\right]_{ab}=\sum_{\mathbf{R}\in\Lambda}e^{-i\mathbf{k}\cdot(\mathbf{s}+\mathbf{R})}\mathscr{G}_{ab}(\mathbf{s}+\mathbf{R},\omega) \tag{F.1.1}$$

possesses the periodicity of the lattice Λ, so that for $\mathbf{R}'\in\Lambda$ there holds $\zeta_\Lambda(\mathbf{s}+\mathbf{R}',\mathbf{k},\omega)=\zeta_\Lambda(\mathbf{s},\mathbf{k},\omega)$. Hence, (F.1.1) can be expanded into a Fourier series according to

$$\left[\zeta_\Lambda(\mathbf{s},\mathbf{k},\omega)\right]_{ab}=\sum_{\mathbf{G}\in\Lambda^{-1}}\left[\tilde{\zeta}_\Lambda(\mathbf{G},\mathbf{k},\omega)\right]_{ab}e^{i\mathbf{G}\cdot\mathbf{s}}, \tag{F.1.2}$$

where the expansion coefficients $\left[\tilde{\zeta}_\Lambda(\mathbf{G},\mathbf{k},\omega)\right]_{ab}$ are easily evaluated to

$$\begin{aligned}\left[\tilde{\zeta}_\Lambda(\mathbf{G},\mathbf{k},\omega)\right]_{ab} &= \frac{1}{|C_\Lambda|}\int_{C_\Lambda} d^3s\, e^{-i\mathbf{G}\cdot\mathbf{s}}\left[\zeta_\Lambda(\mathbf{s},\mathbf{k},\omega)\right]_{ab} \\ &= \frac{1}{|C_\Lambda|}\int_{C_\Lambda} d^3s\, e^{-i\mathbf{G}\cdot\mathbf{s}}\sum_{\mathbf{R}\in\Lambda} e^{-i\mathbf{k}\cdot(\mathbf{s}+\mathbf{R})}\mathscr{G}_{ab}(\mathbf{s}+\mathbf{R},\omega) \\ &= \frac{1}{|C_\Lambda|}\int_{\mathbb{R}^3} d^3r\, e^{-i(\mathbf{k}+\mathbf{G})\cdot\mathbf{r}}\mathscr{G}_{ab}(\mathbf{r},\omega) \\ &= \frac{1}{|C_\Lambda|}\tilde{\mathscr{G}}_{ab}(\mathbf{k}+\mathbf{G},\omega)\,. \end{aligned} \tag{F.1.3}$$

In the last line the Fourier transform of the electromagnetic kernel $\mathscr{G}_{ab}(\mathbf{r},\omega)$ has been identified. By utilizing (C.2.8) and (C.2.9) respectively, the Fourier series expansion (F.1.2) can be written as

$$[\zeta_\Lambda(\mathbf{s},\mathbf{k},\omega)]_{ab} = \frac{1}{|C_\Lambda|}\sum_{\mathbf{G}\in\Lambda^{-1}} e^{i\mathbf{G}\cdot\mathbf{s}}\left(\frac{\omega^2}{c^2}\frac{1}{|\mathbf{k}+\mathbf{G}|^2-\frac{\omega^2}{c^2}}\tilde{\Pi}^{(\mathrm{T})}_{ab}(\mathbf{k}+\mathbf{G}) - \tilde{\Pi}^{(\mathrm{L})}_{ab}(\mathbf{k}+\mathbf{G})\right) \tag{F.1.4}$$

$$= \frac{1}{|C_\Lambda|}\sum_{\mathbf{G}\in\Lambda^{-1}} e^{i\mathbf{G}\cdot\mathbf{s}}\frac{\frac{\omega^2}{c^2}\delta_{ab}-(k_a+G_a)(k_b+G_b)}{|\mathbf{k}+\mathbf{G}|^2-\frac{\omega^2}{c^2}}. \tag{F.1.5}$$

The representation (F.1.4) of the lattice sum $[\zeta_\Lambda(\mathbf{s},\mathbf{k},\omega)]_{ab}$ turns out to be valuable when decomposing the local electric field into its longitudinal and transverse components (see (3.2.41) and (3.2.42)), while (F.1.5) constitutes the starting point for its numerical evaluation in the sense of Ewald's summation method [30–33], which is presented in the following.

F.2 "Ewald summation technique" for numerical calculations

The basic idea of the analytical treatment of poorly converging lattice sums like e.g. $\zeta_\Lambda(\mathbf{s},\mathbf{k},\omega)$ given by (F.1.5) is to transform such sums into other sums that converge rapidly. For illustration, the common approach is exemplified first (see in particular [62] and references therein) before it is explicitly applied to $\zeta_\Lambda(\mathbf{s},\mathbf{k},\omega)$.

Assume, that the function $f(\mathbf{R})$ with $\mathbf{R}\in\Lambda$ vanishes slowly if $|\mathbf{R}|\to\infty$ and that it is possibly infinite at $\mathbf{R}=\mathbf{0}$. Then, the sum

$$S = \sum_{\mathbf{R}\in\Lambda} f(\mathbf{R})$$

will converge slowly. To improve convergence, a function $F(\mathbf{R})$ is introduced that vanishes rapidly if $|\mathbf{R}|\to\infty$ and that is finite at $\mathbf{R}=\mathbf{0}$. This allows to rewrite S in the guise

$$S = \sum_{\mathbf{R}\in\Lambda} f(\mathbf{R})F(\mathbf{R}) + \sum_{\mathbf{R}\in\Lambda} f(\mathbf{R})(1-F(\mathbf{R}))\,,$$

where the *first* sum is already fast converging. Now, if $f(\mathbf{R})(1-F(\mathbf{R}))$ is a slowly varying smooth

function in real space, then its Fourier transform is a rapidly decaying function in reciprocal space, so that the *second* slowly convergent sum over real lattice vectors $\mathbf{R} \in \Lambda$ can be transformed to a rapidly converging sum over reciprocal lattice vectors $\mathbf{G} \in \Lambda^{-1}$ by means of Poisson's summation formula [137]. In case that $f(\mathbf{R})$ goes to infinity for $\mathbf{R} = \mathbf{0}$, then $1 - F(\mathbf{R})$ has to vanish simultaneously in such a way, that the smoothness of $f(\mathbf{R})(1 - F(\mathbf{R}))$ is ensured.

Notice, that this procedure to represent a poorly convergent lattice sum as a sum of two lattice sums, where one is rapidly convergent in real and the other in reciprocal space, has been established in solid state and crystal physics by Ewald [30, 31] by utilization of the Jacobi theta function transformation formula [60].

F.2.1 Case 1: $\mathbf{s} \neq \mathbf{0}$

As the starting point for a fast and precise numerical evaluation of $[\zeta_\Lambda(\mathbf{s},\mathbf{k},\omega)]_{ab}$ for $\mathbf{s} \neq \mathbf{0}$, its representation (F.1.5) is consulted, i.e.

$$[\zeta_\Lambda(\mathbf{s},\mathbf{k},\omega)]_{ab} = \frac{1}{|C_\Lambda|} \sum_{\mathbf{G}\in\Lambda^{-1}} e^{i\mathbf{G}\cdot\mathbf{s}} \frac{\frac{\omega^2}{c^2}\delta_{ab} - (k_a + G_a)(k_b + G_b)}{|\mathbf{k}+\mathbf{G}|^2 - \frac{\omega^2}{c^2}}. \tag{F.2.1}$$

Introducing a splitting parameter[1] $\xi > 0$, the original lattice sum (F.2.1) can be rewritten as

$$[\zeta_\Lambda(\mathbf{s},\mathbf{k},\omega)]_{ab} = \left[\zeta_\Lambda^{(\mathrm{G})}(\mathbf{s},\mathbf{k},\omega;\xi)\right]_{ab} + \left[\zeta_\Lambda^{(\mathrm{R})}(\mathbf{s},\mathbf{k},\omega;\xi)\right]_{ab}, \tag{F.2.2}$$

where

$$\left[\zeta_\Lambda^{(\mathrm{G})}(\mathbf{s},\mathbf{k},\omega;\xi)\right]_{ab} = \frac{1}{|C_\Lambda|} \sum_{\mathbf{G}\in\Lambda^{-1}} e^{i\mathbf{G}\cdot\mathbf{s}} \frac{\frac{\omega^2}{c^2}\delta_{ab} - (k_a + G_a)(k_b + G_b)}{|\mathbf{k}+\mathbf{G}|^2 - \frac{\omega^2}{c^2}} e^{-\xi^2\left(|\mathbf{k}+\mathbf{G}|^2 - \frac{\omega^2}{c^2}\right)} \tag{F.2.3}$$

$$\left[\zeta_\Lambda^{(\mathrm{R})}(\mathbf{s},\mathbf{k},\omega;\xi)\right]_{ab} = \frac{1}{|C_\Lambda|} \sum_{\mathbf{G}\in\Lambda^{-1}} e^{i\mathbf{G}\cdot\mathbf{s}} \frac{\frac{\omega^2}{c^2}\delta_{ab} - (k_a + G_a)(k_b + G_b)}{|\mathbf{k}+\mathbf{G}|^2 - \frac{\omega^2}{c^2}} \left[1 - e^{-\xi^2\left(|\mathbf{k}+\mathbf{G}|^2 - \frac{\omega^2}{c^2}\right)}\right] \tag{F.2.4}$$

represent new lattice sums. Obviously, $\zeta_\Lambda^{(\mathrm{G})}(\mathbf{s},\mathbf{k},\omega;\xi)$ is a fast converging sum over reciprocal lattice vectors $\mathbf{G} \in \Lambda^{-1}$, while $\zeta_\Lambda^{(\mathrm{R})}(\mathbf{s},\mathbf{k},\omega;\xi)$ is not. Nonetheless, $\zeta_\Lambda^{(\mathrm{R})}(\mathbf{s},\mathbf{k},\omega;\xi)$ can be transformed into a fast converging sum over real lattice vectors $\mathbf{R} \in \Lambda$, so that finally a fast convergence of the originally slowly converging lattice sum (F.2.1) can be achieved. Deploying the identity

$$\begin{aligned} 1 - e^{-\xi^2\left(|\mathbf{k}+\mathbf{G}|^2 - \frac{\omega^2}{c^2}\right)} &= \int_0^\infty d\tau \, \frac{d}{d\tau} \exp\left[-e^{-\tau}\xi^2\left(|\mathbf{k}+\mathbf{G}|^2 - \frac{\omega^2}{c^2}\right)\right] \\ &= \xi^2\left(|\mathbf{k}+\mathbf{G}|^2 - \frac{\omega^2}{c^2}\right) \int_0^\infty d\tau \exp\left[-\tau - e^{-\tau}\xi^2\left(|\mathbf{k}+\mathbf{G}|^2 - \frac{\omega^2}{c^2}\right)\right] \end{aligned} \tag{F.2.5}$$

[1] A good but certainly not optimal choice of ξ that anyhow ensures a fast convergence of the appearing lattice sums prooves to be $\xi = \frac{1}{2}a_\Lambda$.

to (F.2.4), there directly follows

$$\begin{aligned}
&\left[\zeta_\Lambda^{(\mathrm{R})}(\mathbf{s},\mathbf{k},\omega;\xi)\right]_{ab}\\
=&\xi^2\frac{e^{-i\mathbf{k}\cdot\mathbf{s}}}{|C_\Lambda|}\int_0^\infty d\tau\, e^{-\tau}\sum_{\mathbf{G}\in\Lambda^{-1}} e^{i(\mathbf{k}+\mathbf{G})\cdot\mathbf{s}}\left[\frac{\omega^2}{c^2}\delta_{ab}-(k_a+G_a)(k_b+G_b)\right]\exp\left[-e^{-\tau}\xi^2\left(|\mathbf{k}+\mathbf{G}|^2-\frac{\omega^2}{c^2}\right)\right]\\
=&\xi^2\frac{e^{-i\mathbf{k}\cdot\mathbf{s}}}{|C_\Lambda|}\int_0^\infty d\tau\, e^{-\tau}\left[\frac{\omega^2}{c^2}\delta_{ab}+\frac{\partial^2}{\partial s_a\partial s_b}\right]\sum_{\mathbf{G}\in\Lambda^{-1}} e^{i(\mathbf{k}+\mathbf{G})\cdot\mathbf{s}}\exp\left[-e^{-\tau}\xi^2\left(|\mathbf{k}+\mathbf{G}|^2-\frac{\omega^2}{c^2}\right)\right]\\
\equiv&\xi^2\frac{e^{-i\mathbf{k}\cdot\mathbf{s}}}{|C_\Lambda|}\int_0^\infty d\tau\, e^{-\tau}\left[\frac{\omega^2}{c^2}\delta_{ab}+\frac{\partial^2}{\partial s_a\partial s_b}\right]S^{(\mathrm{R})}(\mathbf{s},\mathbf{k},\omega,\tau;\xi).
\end{aligned}\tag{F.2.6}$$

Because

$$S^{(\mathrm{R})}(\mathbf{s},\mathbf{k},\omega,\tau;\xi)=\sum_{\mathbf{G}\in\Lambda^{-1}} e^{i(\mathbf{k}+\mathbf{G})\cdot\mathbf{s}}\exp\left[-e^{-\tau}\xi^2\left(|\mathbf{k}+\mathbf{G}|^2-\frac{\omega^2}{c^2}\right)\right]\tag{F.2.7}$$

is invariant with respect to any translations by reciprocal lattice vectors $\mathbf{G}'\in\Lambda^{-1}$, it possesses a Fourier series representation according to

$$S^{(\mathrm{R})}(\mathbf{s},\mathbf{k},\omega,\tau;\xi)=\sum_{\mathbf{R}\in\Lambda}\tilde{S}^{(\mathrm{R})}(\mathbf{s},\mathbf{R},\omega,\tau;\xi)\,e^{-i\mathbf{k}\cdot\mathbf{R}},\tag{F.2.8}$$

where the expansion coefficients are given by

$$\begin{aligned}
\tilde{S}^{(\mathrm{R})}(\mathbf{s},\mathbf{R},\omega,\tau;\xi)&=\frac{|C_\Lambda|}{(2\pi)^3}\int_{C_{\Lambda^{-1}}} d^3k\, e^{i\mathbf{k}\cdot\mathbf{R}}S^{(\mathrm{R})}(\mathbf{s},\mathbf{k},\omega,\tau;\xi)\\
&=\frac{|C_\Lambda|}{(2\pi)^3}\int_{C_{\Lambda^{-1}}} d^3k\, e^{i\mathbf{k}\cdot\mathbf{R}}\sum_{\mathbf{G}\in\Lambda^{-1}} e^{i(\mathbf{k}+\mathbf{G})\cdot\mathbf{s}}\exp\left[-e^{-\tau}\xi^2\left(|\mathbf{k}+\mathbf{G}|^2-\frac{\omega^2}{c^2}\right)\right]\\
&=\frac{|C_\Lambda|}{(2\pi)^3}\int_{\mathbb{R}^3} d^3q\, e^{i\mathbf{q}\cdot(\mathbf{s}+\mathbf{R})}\exp\left[-e^{-\tau}\xi^2\left(|\mathbf{q}|^2-\frac{\omega^2}{c^2}\right)\right]\\
&=\frac{|C_\Lambda|}{(2\pi)^3}\left(\frac{\pi}{e^{-\tau}\xi^2}\right)^{\frac{3}{2}}\exp\left[-\frac{-\left(2e^{-\tau}\xi^2\frac{\omega}{c}\right)^2+|\mathbf{s}+\mathbf{R}|^2}{4e^{-\tau}\xi^2}\right].
\end{aligned}\tag{F.2.9}$$

Consequently, (F.2.6) emerges as a fast converging sum over real lattice vectors $\mathbf{R}\in\Lambda$ according to

$$\begin{aligned}
&\left[\zeta_\Lambda^{(\mathrm{R})}(\mathbf{s},\mathbf{k},\omega;\xi)\right]_{ab}\\
=&\frac{e^{-i\mathbf{k}\cdot\mathbf{s}}}{8\xi\pi^{\frac{3}{2}}}\int_0^\infty d\tau\,\exp\left[\frac{\tau}{2}+e^{-\tau}\xi^2\frac{\omega^2}{c^2}\right]\sum_{\mathbf{R}\in\Lambda} e^{-i\mathbf{k}\cdot\mathbf{R}}\left[\frac{\omega^2}{c^2}\delta_{ab}+\frac{\partial^2}{\partial s_a\partial s_b}\right]\exp\left[\frac{-|\mathbf{s}+\mathbf{R}|^2}{4e^{-\tau}\xi^2}\right]\\
=&\frac{1}{4\xi^3\pi^{\frac{3}{2}}}\int_1^\infty du\,\exp\left[\frac{1}{u^2}\xi^2\frac{\omega^2}{c^2}\right]\\
&\cdot\sum_{\mathbf{R}\in\Lambda} e^{-i\mathbf{k}\cdot(\mathbf{s}+\mathbf{R})}\left[\left(\xi^2\frac{\omega^2}{c^2}-\frac{u^2}{2}\right)\delta_{ab}+\frac{u^4}{4\xi^2}(s_a+R_a)(s_b+R_b)\right]\exp\left[-u^2\frac{|\mathbf{s}+\mathbf{R}|^2}{4\xi^2}\right],
\end{aligned}\tag{F.2.10}$$

where for obtaining the last line $u = e^{\frac{\tau}{2}}$ has been substituted. Inserting (F.2.3) and (F.2.10) in (F.2.2) then finally yields a representation of the lattice sum $\left[\zeta_\Lambda(\mathbf{s},\mathbf{k},\omega)\right]_{ab}$ for $\mathbf{s} \neq \mathbf{0}$, that ensures its fast and precise numerical computation.

F.2.2 Case 2: $\mathbf{s} = \mathbf{0}$

Taking into account the results from the previous section, an expression that ensures a fast and precise numerical evaluation of the lattice sum $\zeta_\Lambda^{(0)}(\mathbf{k},\omega) \equiv \zeta_\Lambda(\mathbf{0},\mathbf{k},\omega)$ can be obtained, when its representation (see (3.2.26))

$$\begin{aligned}
&\left[\zeta_\Lambda^{(0)}(\mathbf{k},\omega)\right]_{ab} \\
&= \lim_{|\mathbf{s}|\to 0}\left(\left[\zeta_\Lambda(\mathbf{s},\mathbf{k},\omega)\right]_{ab} - \mathscr{G}_{ab}(\mathbf{s},\omega)\right) \\
&\equiv \lim_{|\mathbf{s}|\to 0}\left\{\left[\zeta_\Lambda^{(\mathrm{G})}(\mathbf{s},\mathbf{k},\omega;\xi)\right]_{ab} - \mathscr{G}_{ab}^{(\mathrm{G})}(\mathbf{s},\omega;\xi)\right\} + \lim_{|\mathbf{s}|\to 0}\left\{\left[\zeta_\Lambda^{(\mathrm{R})}(\mathbf{s},\mathbf{k},\omega;\xi)\right]_{ab} - \mathscr{G}_{ab}^{(\mathrm{R})}(\mathbf{s},\omega;\xi)\right\}
\end{aligned} \tag{F.2.11}$$

is consulted. Since $\lim_{|\mathbf{s}|\to 0}\left[\zeta_\Lambda^{(\mathrm{G,R})}(\mathbf{s},\mathbf{k},\omega;\xi)\right]_{ab}$ is already known from the previous section, only $\lim_{|\mathbf{s}|\to 0}\mathscr{G}_{ab}^{(\mathrm{G,R})}(\mathbf{s},\omega;\xi)$ has to be analyzed. By utilizing the Fourier integral representation (C.2.7), the electromagnetic kernel

$$\mathscr{G}_{ab}(\mathbf{s},\omega) = \frac{1}{(2\pi)^3}\int_{\mathbb{R}^3} d^3k\, e^{i\mathbf{k}\cdot\mathbf{s}}\frac{\frac{\omega^2}{c^2}\delta_{ab} - k_a k_b}{|\mathbf{k}|^2 - \frac{\omega^2}{c^2}} \tag{F.2.12}$$

has been decomposed in (F.2.11) according to

$$\mathscr{G}_{ab}(\mathbf{s},\omega) = \mathscr{G}_{ab}^{(\mathrm{G})}(\mathbf{s},\omega;\xi) + \mathscr{G}_{ab}^{(\mathrm{R})}(\mathbf{s},\omega;\xi), \tag{F.2.13}$$

where the new kernels

$$\mathscr{G}_{ab}^{(\mathrm{G})}(\mathbf{s},\omega;\xi) = \frac{1}{(2\pi)^3}\int_{\mathbb{R}^3} d^3k\, e^{i\mathbf{k}\cdot\mathbf{s}}\frac{\frac{\omega^2}{c^2}\delta_{ab} - k_a k_b}{|\mathbf{k}|^2 - \left(\frac{\omega}{c} + i0^+\right)^2}e^{-\xi^2\left(|\mathbf{k}|^2 - \frac{\omega^2}{c^2}\right)} \tag{F.2.14}$$

$$\mathscr{G}_{ab}^{(\mathrm{R})}(\mathbf{s},\omega;\xi) = \frac{1}{(2\pi)^3}\int_{\mathbb{R}^3} d^3k\, e^{i\mathbf{k}\cdot\mathbf{s}}\frac{\frac{\omega^2}{c^2}\delta_{ab} - k_a k_b}{|\mathbf{k}|^2 - \frac{\omega^2}{c^2}}\left[1 - e^{-\xi^2\left(|\mathbf{k}|^2 - \frac{\omega^2}{c^2}\right)}\right] \tag{F.2.15}$$

individually depend on a splitting parameter $\xi > 0$. It should be pointed out, that for $\mathscr{G}_{ab}^{(\mathrm{G})}(\mathbf{s},\omega;\xi)$ the pole occurring in the denominator of the integrand has been shifted from the real axis to the upper complex half plane. This is required to carry out the integral and to ensure causality. In contrast, $|\mathbf{k}| = \frac{\omega}{c}$ does *not* cause trouble for the kernel $\mathscr{G}_{ab}^{(\mathrm{R})}(\mathbf{s},\omega;\xi)$ in compliance with de l'Hospital's rule. Because the integrand of $\mathscr{G}_{ab}^{(\mathrm{G})}(\mathbf{s},\omega;\xi)$ is for $a \neq b$ an odd function of k_a and k_b in the limit $|\mathbf{s}| \to 0$, the off-diagonal

components of $\mathscr{G}^{(\mathrm{G})}_{ab}(\mathbf{s},\omega;\xi)$ where $a\neq b$ vanish exactly in this limit, so that

$$\begin{aligned}\lim_{|\mathbf{s}|\to 0}\mathscr{G}^{(\mathrm{G})}_{ab}(\mathbf{s},\omega;\xi) &= \delta_{ab}\frac{1}{(2\pi)^3}\int_{\mathbb{R}^3}d^3k\,\frac{\frac{\omega^2}{c^2}-k_a^2}{|\mathbf{k}|^2-\left(\frac{\omega}{c}+i0^+\right)^2}e^{-\xi^2\left(|\mathbf{k}|^2-\frac{\omega^2}{c^2}\right)}\\ &= \delta_{ab}\frac{1}{(2\pi)^3}\int_{\mathbb{R}^3}d^3k\,\frac{\frac{\omega^2}{c^2}-\frac{1}{3}|\mathbf{k}|^2}{|\mathbf{k}|^2-\left(\frac{\omega}{c}+i0^+\right)^2}e^{-\xi^2\left(|\mathbf{k}|^2-\frac{\omega^2}{c^2}\right)}\\ &= -\frac{1}{3}\delta_{ab}\frac{1}{(2\pi)^3}\int_{\mathbb{R}^3}d^3k\left[e^{-\xi^2\left(|\mathbf{k}|^2-\frac{\omega^2}{c^2}\right)}-2\frac{\omega^2}{c^2}\frac{e^{-\xi^2\left(|\mathbf{k}|^2-\frac{\omega^2}{c^2}\right)}}{|\mathbf{k}|^2-\left(\frac{\omega}{c}+i0^+\right)^2}\right],\end{aligned}\tag{F.2.16}$$

where in the second line use has been made of the fact, that each component k_a^2 with $a\in\{1,2,3\}$ contributes equally to the integral because of symmetry. The first term in (F.2.16) is a Gaussian integral and readily evaluated to

$$\int_{\mathbb{R}^3}d^3k\,e^{-\xi^2\left(|\mathbf{k}|^2-\frac{\omega^2}{c^2}\right)}=\frac{\pi^{\frac{3}{2}}}{\xi^3}e^{\xi^2\frac{\omega^2}{c^2}}.\tag{F.2.17}$$

For the evaluation of the second integral, see the supplementary material to [23]. It reads

$$\int_{\mathbb{R}^3}d^3k\,\frac{e^{-\xi^2\left(|\mathbf{k}|^2-\frac{\omega^2}{c^2}\right)}}{|\mathbf{k}|^2-\left(\frac{\omega}{c}+i0^+\right)^2}=\frac{2\pi^{\frac{3}{2}}}{\xi}e^{\xi^2\frac{\omega^2}{c^2}}-2\pi^2\frac{\omega}{c}\mathrm{erfi}\left(\frac{\omega}{c}\xi\right)+2i\pi^2\frac{\omega}{c},\tag{F.2.18}$$

where $\mathrm{erfi}(z)=\frac{\mathrm{erf}(iz)}{i}$ denotes the imaginary error function. With (F.2.17) and (F.2.18) one obtains for (F.2.16)

$$\lim_{|\mathbf{s}|\to 0}\mathscr{G}^{(\mathrm{G})}_{ab}(\mathbf{s},\omega;\xi)=\delta_{ab}\left[\frac{1}{6\pi^{\frac{3}{2}}\xi^3}e^{\xi^2\frac{\omega^2}{c^2}}\left(\frac{\omega^2}{c^2}\xi^2-\frac{1}{4}\right)-\frac{1}{6\pi}\frac{\omega^3}{c^3}\mathrm{erfi}\left(\frac{\omega}{c}\xi\right)+\frac{i}{6\pi}\frac{\omega^3}{c^3}\right],\tag{F.2.19}$$

so that the combination of (F.2.3) and (F.2.19) results in

$$\begin{aligned}&\lim_{|\mathbf{s}|\to 0}\left\{\left[\zeta^{(\mathrm{G})}_\Lambda(\mathbf{s},\mathbf{k},\omega;\xi)\right]_{ab}-\mathscr{G}^{(\mathrm{G})}_{ab}(\mathbf{s},\omega;\xi)\right\}\\ =&\frac{1}{|C_\Lambda|}\sum_{\mathbf{G}\in\Lambda^{-1}}\frac{\frac{\omega^2}{c^2}\delta_{ab}-(k_a+G_a)(k_b+G_b)}{|\mathbf{k}+\mathbf{G}|^2-\frac{\omega^2}{c^2}}e^{-\xi^2\left(|\mathbf{k}+\mathbf{G}|^2-\frac{\omega^2}{c^2}\right)}\\ &-\delta_{ab}\left[\frac{1}{6\pi^{\frac{3}{2}}\xi^3}e^{\xi^2\frac{\omega^2}{c^2}}\left(\frac{\omega^2}{c^2}\xi^2-\frac{1}{4}\right)-\frac{1}{6\pi}\frac{\omega^3}{c^3}\mathrm{erfi}\left(\frac{\omega}{c}\xi\right)+\frac{i}{6\pi}\frac{\omega^3}{c^3}\right].\end{aligned}\tag{F.2.20}$$

Deploying the identity (F.2.5) to $\mathscr{G}_{ab}^{(\mathrm{R})}(\mathbf{s},\omega;\xi)$, which is given by (F.2.15), directly yields

$$\begin{aligned}
&\lim_{|\mathbf{s}|\to 0}\mathscr{G}_{ab}^{(\mathrm{R})}(\mathbf{s},\omega;\xi)\\
&=\lim_{|\mathbf{s}|\to 0}\frac{\xi^2}{(2\pi)^3}\int_{\mathbb{R}^3}d^3k\,e^{i\mathbf{k}\cdot\mathbf{s}}\left(\frac{\omega^2}{c^2}\delta_{ab}-k_ak_b\right)\int_0^\infty d\tau\,\exp\left[-\tau-e^{-\tau}\xi^2\left(|\mathbf{k}|^2-\frac{\omega^2}{c^2}\right)\right]\\
&=\lim_{|\mathbf{s}|\to 0}\frac{\xi^2}{(2\pi)^3}\int_0^\infty d\tau\,e^{-\tau}\left(\frac{\omega^2}{c^2}\delta_{ab}+\frac{\partial^2}{\partial s_a\partial s_b}\right)\int_{\mathbb{R}^3}d^3k\,e^{i\mathbf{k}\cdot\mathbf{s}}\exp\left[-e^{-\tau}\xi^2\left(|\mathbf{k}|^2-\frac{\omega^2}{c^2}\right)\right]\\
&=\lim_{|\mathbf{s}|\to 0}\frac{1}{8\xi\pi^{\frac{3}{2}}}\int_0^\infty d\tau\,\exp\left[\frac{\tau}{2}+e^{-\tau}\xi^2\frac{\omega^2}{c^2}\right]\left(\frac{\omega^2}{c^2}\delta_{ab}+\frac{\partial^2}{\partial s_a\partial s_b}\right)\exp\left[-\frac{|\mathbf{s}|^2}{4e^{-\tau}\xi^2}\right]\\
&=\frac{1}{8\xi^3\pi^{\frac{3}{2}}}\int_0^\infty d\tau\,\exp\left[\frac{\tau}{2}+e^{-\tau}\xi^2\frac{\omega^2}{c^2}\right]\left(\xi^2\frac{\omega^2}{c^2}-\frac{1}{2e^{-\tau}}\right)\delta_{ab}\\
&=\frac{1}{4\xi^3\pi^{\frac{3}{2}}}\int_1^\infty du\,\exp\left[\frac{1}{u^2}\xi^2\frac{\omega^2}{c^2}\right]\left(\xi^2\frac{\omega^2}{c^2}-\frac{u^2}{2}\right)\delta_{ab},
\end{aligned}\tag{F.2.21}$$

where for obtaining the last line $u=e^{\frac{\tau}{2}}$ has been substituted. Combining the results (F.2.10) and (F.2.21), one confirms that $\mathscr{G}_{ab}^{(\mathrm{R})}(\mathbf{s},\omega;\xi)$ exactly cancels the $\mathbf{R}=\mathbf{0}$ contribution of $\left[\zeta_\Lambda^{(\mathrm{R})}(\mathbf{s},\mathbf{k},\omega;\xi)\right]_{ab}$ in the limit $|\mathbf{s}|\to 0$ with the outcome, that

$$\begin{aligned}
&\lim_{|\mathbf{s}|\to 0}\left\{\left[\zeta_\Lambda^{(\mathrm{R})}(\mathbf{s},\mathbf{k},\omega;\xi)\right]_{ab}-\mathscr{G}_{ab}^{(\mathrm{R})}(\mathbf{s},\omega;\xi)\right\}\\
&=\frac{1}{4\xi^3\pi^{\frac{3}{2}}}\int_1^\infty du\,\exp\left[\frac{1}{u^2}\xi^2\frac{\omega^2}{c^2}\right]\sum_{\mathbf{R}\in\Lambda\setminus\{\mathbf{0}\}}e^{-i\mathbf{k}\cdot\mathbf{R}}\left[\left(\xi^2\frac{\omega^2}{c^2}-\frac{u^2}{2}\right)\delta_{ab}+\frac{u^4}{4\xi^2}R_aR_b\right]\exp\left[-u^2\frac{|\mathbf{R}|^2}{4\xi^2}\right].
\end{aligned}\tag{F.2.22}$$

Inserting (F.2.20) and (F.2.22) in (F.2.11) finally yields a representation of the lattice sum $\zeta_\Lambda^{(0)}(\mathbf{k},\omega)\equiv\zeta_\Lambda(\mathbf{0},\mathbf{k},\omega)$, that ensures its fast and precise numerical computation. Note, that

$$\Im\left\{\left[\zeta_\Lambda^{(0)}(\mathbf{k},\omega)\right]_{ab}\right\}=\Im\left\{\lim_{|\mathbf{s}|\to 0}\left\{\left[\zeta_\Lambda^{(\mathrm{G})}(\mathbf{s},\mathbf{k},\omega;\xi)\right]_{ab}-\mathscr{G}_{ab}^{(\mathrm{G})}(\mathbf{s},\omega;\xi)\right\}\right\}=-\frac{1}{6\pi}\frac{\omega^3}{c^3}\delta_{ab}.\tag{F.2.23}$$

Appendix G

Lorentz factor $\mathscr{L}_{ab}$

Initially, the trace identity satisfied by the Lorentz factor tensor $\mathscr{L}$ is proven for all (monatomic) Bravais lattices. Based on this, $\mathscr{L}$ is explicitly calculated for a simple cubic lattice by means of a potential-theoretical approach, originally given by Prof. N. Schopohl [24]. An alternative evaluation of the associated lattice sums relying on the third Jacobi theta function can be found in [39].

G.1 Proof of trace identity

With regard to (4.4.4), the cartesian components of the Lorentz factor tensor are defined by

$$\mathscr{L}_{ab} = |C_\Lambda| \lim_{\omega\to 0} \lim_{|\mathbf{k}|\to 0} \left(\left[\zeta_\Lambda^{(0)}(\mathbf{k},\omega) \right]_{ab} - \frac{1}{|C_\Lambda|} \tilde{\mathscr{G}}_{ab}(\mathbf{k},\omega) \right), \tag{G.1.1}$$

where $\left[\zeta_\Lambda^{(0)}(\mathbf{k},\omega) \right]_{ab}$ is given by (3.2.21) according to

$$\left[\zeta_\Lambda^{(0)}(\mathbf{k},\omega) \right]_{ab} = \sum_{\mathbf{R}\in\Lambda\setminus\{\mathbf{0}\}} e^{-i\mathbf{k}\cdot\mathbf{R}} \mathscr{G}_{ab}(\mathbf{R},\omega), \tag{G.1.2}$$

while the Fourier transform of the electromagnetic kernel $\tilde{\mathscr{G}}_{ab}(\mathbf{k},\omega)$ will be represented by its Fourier integral representation

$$\tilde{\mathscr{G}}_{ab}(\mathbf{k},\omega) = \int_{\mathbb{R}^3} d^3r\, e^{-i\mathbf{k}\cdot\mathbf{r}} \mathscr{G}_{ab}(\mathbf{r},\omega). \tag{G.1.3}$$

Recall, that the electromagnetic kernel (see (2.2.15)) reads in real space

$$\mathscr{G}_{ab}(\mathbf{r}-\mathbf{r}',\omega) = \frac{\omega^2}{c^2} \int_{\mathbb{R}^3} d^3x\, g(\mathbf{r}-\mathbf{x},\omega)\, \Pi_{ab}^{(\mathrm{T})}(\mathbf{x}-\mathbf{r}') - \Pi_{ab}^{(\mathrm{L})}(\mathbf{r}-\mathbf{r}'). \tag{G.1.4}$$

Inserting (G.1.2) - (G.1.4) into (G.1.1) immediately leads to

$$\begin{aligned}\mathscr{L}_{ab} &= -|C_\Lambda| \sum_{\mathbf{R}\in\Lambda\setminus\{\mathbf{0}\}} \Pi_{ab}^{(\mathrm{L})}(\mathbf{R}) + \int_{\mathbb{R}^3} d^3r\, \Pi_{ab}^{(\mathrm{L})}(\mathbf{r}) \\ &= \lim_{|\mathbf{s}|\to 0} \frac{\partial^2}{\partial s_a \partial s_b} \left(|C_\Lambda| \sum_{\mathbf{R}\in\Lambda\setminus\{\mathbf{0}\}} \frac{1}{4\pi} \frac{1}{|\mathbf{s}-\mathbf{R}|} - \int_{\mathbb{R}^3} d^3r \frac{1}{4\pi} \frac{1}{|\mathbf{s}-\mathbf{r}|} \right). \end{aligned} \tag{G.1.5}$$

The second line in (G.1.5) applies, since the longitudinal projection operator appearing in the first term within the first line only contributes with its usual non-singular dipole contribution $\lim_{|\mathbf{s}|\to 0} \frac{\partial^2}{\partial s_a \partial s_b} \frac{1}{4\pi} \frac{1}{|\mathbf{s}-\mathbf{R}|}$ because of $\mathbf{R} \in \Lambda\setminus\{\mathbf{0}\}$ (compare with (A.2.13)), while the second term in the first line has been recast by identifying (A.2.1) with (A.2.12). In a final step, summing up the diagonal contributions of $\mathscr{L}$ given by (G.1.5) and deploying the well-known delta function identity

$$-\nabla_{\mathbf{r}}^2 \frac{1}{4\pi} \frac{1}{|\mathbf{r}-\mathbf{r}'|} = \delta(\mathbf{r}-\mathbf{r}'), \tag{G.1.6}$$

one readily proves the trace identity

$$\mathrm{Tr}[\mathscr{L}] = 1, \tag{G.1.7}$$

which is satisfied by the Lorentz factor tensor.

G.2 Calculation of $\mathscr{L}_{ab}$ for a simple cubic lattice

The initial point for the calculation of the Lorentz factors $\mathscr{L}_{ab}$ in terms of a potential-theoretical approach is established by equation (G.1.5), which can be rewritten by means of the function

$$\begin{aligned}\phi(\mathbf{s}) &= |C_\Lambda| \sum_{\mathbf{R}\in\Lambda\setminus\{\mathbf{0}\}} \frac{1}{4\pi} \frac{1}{|\mathbf{s}-\mathbf{R}|} - \int_{\mathbb{R}^3} d^3r \frac{1}{4\pi} \frac{1}{|\mathbf{s}-\mathbf{r}|} \\ &= \int_{\mathbb{R}^3} d^3r \frac{1}{4\pi} \frac{1}{|\mathbf{s}-\mathbf{r}|} \left(|C_\Lambda| \sum_{\mathbf{R}\in\Lambda\setminus\{\mathbf{0}\}} \delta(\mathbf{r}-\mathbf{R}) - 1 \right) \end{aligned} \tag{G.2.1}$$

according to

$$\mathscr{L}_{ab} = \lim_{|\mathbf{s}|\to 0} \frac{\partial^2}{\partial s_a \partial s_b} \phi(\mathbf{s}). \tag{G.2.2}$$

As can be easily verified, $\phi(\mathbf{s})$ constitutes a particular solution of the Poisson equation

$$-\nabla_{\mathbf{s}}^2 \phi(\mathbf{s}) = |C_\Lambda| \sum_{\mathbf{R}\in\Lambda\setminus\{\mathbf{0}\}} \delta(\mathbf{s}-\mathbf{R}) - 1. \tag{G.2.3}$$

Instead of finding the solution to (G.2.3) in a single step, one is also allowed to solve the two equations

$$-\nabla_{\mathbf{s}}^2\phi^{(1)}(\mathbf{s}) = |C_\Lambda| \sum_{\mathbf{R}\in\Lambda\setminus\{\mathbf{0}\}} \delta(\mathbf{s}-\mathbf{R}) \tag{G.2.4}$$

$$-\nabla_{\mathbf{s}}^2\phi^{(2)}(\mathbf{s}) = -1 \tag{G.2.5}$$

and to construct afterwards the solution $\phi(\mathbf{s})$ of (G.2.3) by superimposing $\phi^{(1)}(\mathbf{s})$ and $\phi^{(2)}(\mathbf{s})$ according to

$$\phi(\mathbf{s}) = \phi^{(1)}(\mathbf{s}) + \phi^{(2)}(\mathbf{s}), \tag{G.2.6}$$

which is ensured due to the linearity of the Poisson equation. To determine the Lorentz factors (G.2.2) for a simple cubic lattice, equations (G.2.4) and (G.2.5) have to be discussed in consideration of the requirements imposed by the symmetry of a simple cubic lattice. First of all, $\phi^{(1)}(\mathbf{s})$ and $\phi^{(2)}(\mathbf{s})$ have to be symmetric under the discrete symmetry operation

$$\phi^{(1,2)}(\mathbf{s}) \equiv \phi^{(1,2)}(s_1,s_2,s_3) \stackrel{!}{=} \phi^{(1,2)}(\pm s_1,\pm s_2,\pm s_3), \tag{G.2.7}$$

that directly implies

$$\lim_{|\mathbf{s}|\to 0} \frac{\partial^2}{\partial s_a \partial s_b}\phi^{(1,2)}(\mathbf{s}) = 0 \;\text{ if } a \neq b \tag{G.2.8}$$

as well as

$$\lim_{|\mathbf{s}|\to 0} \frac{\partial^2}{\partial s_1^2}\phi^{(1,2)}(\mathbf{s}) = \lim_{|\mathbf{s}|\to 0} \frac{\partial^2}{\partial s_2^2}\phi^{(1,2)}(\mathbf{s}) = \lim_{|\mathbf{s}|\to 0} \frac{\partial^2}{\partial s_3^2}\phi^{(1,2)}(\mathbf{s}). \tag{G.2.9}$$

Taking into account, that in the calculation of the Lorentz factors (G.2.2) $|\mathbf{s}| \to 0$ and that in the Poisson equation determining $\phi^{(1)}(\mathbf{s})$ the Wigner-Seitz cell $\mathbf{R} = \mathbf{0}$ is excluded, (G.2.4) reduces to the Laplace equation

$$-\nabla_{\mathbf{s}}^2\phi^{(1)}(\mathbf{s}) = 0. \tag{G.2.10}$$

Deploying (G.2.9) to (G.2.10) one readily infers

$$\lim_{|\mathbf{s}|\to 0} \frac{\partial^2}{\partial s_a^2}\phi^{(1)}(\mathbf{s}) = 0 \;\text{ for } a \in \{1,2,3\}, \tag{G.2.11}$$

with the result that

$$\lim_{|\mathbf{s}|\to 0} \frac{\partial^2}{\partial s_a \partial s_b}\phi^{(1)}(\mathbf{s}) = 0 \;\forall a,b \in \{1,2,3\}. \tag{G.2.12}$$

A particular solution to the Poisson equation (G.2.5) determining $\phi^{(2)}(\mathbf{s})$, that is in total agreement with the conditions (G.2.8) and (G.2.9) set by the symmetry of a simple cubic lattice reads (with $\phi_0 = \text{const}$)

$$\phi^{(2)}(\mathbf{s}) = \frac{|\mathbf{s}|^2}{6} + \phi_0, \tag{G.2.13}$$

so that

$$\lim_{|\mathbf{s}|\to 0} \frac{\partial^2}{\partial s_a \partial s_b} \phi^{(2)}(\mathbf{s}) = \frac{1}{3}\delta_{ab} \; \forall a,b \in \{1,2,3\}. \tag{G.2.14}$$

is readily inferred. Combining the results (G.2.12) and (G.2.14), the Lorentz factors (G.2.2) for a simple cubic lattice are deduced to

$$\mathscr{L}_{ab} = \frac{1}{3}\delta_{ab}. \tag{G.2.15}$$

As a corollary one obtains

$$\lim_{\omega\to 0} \lim_{|\mathbf{k}|\to 0} \tilde{\mathscr{G}}_{ab}(\mathbf{k},\omega) = -\frac{1}{3}\delta_{ab}. \tag{G.2.16}$$

Appendix H

Survey on the optical properties of crystals comprised by $\varepsilon^{(\mathrm{T})}(\mathbf{q},\omega)$

In this appendix, several representations of the transverse dielectric tensor $\varepsilon^{(\mathrm{T})}(\mathbf{q},\omega)$ are deduced from the dielectric tensor $\varepsilon_{\Lambda}(\mathbf{q},\omega)$ for distinct "experimental" configurations, where the focus is on the optical properties of crystalline materials like the index of refraction, optical activity as well as spatial dispersion induced birefringence. Finally, these representations form the basis, on which these effects are discussed in section 4.4.3.

H.1 Representation of $\varepsilon^{(\mathrm{T})}(\omega)$ with respect to the dielectric principal axes

The general expression determining $\varepsilon^{(\mathrm{T})}(\mathbf{q},\omega)$ for arbitrary $\mathbf{q}$ reads (see (4.2.20) and (4.2.8))

$$\varepsilon^{(\mathrm{T})}(\mathbf{q},\omega)=\varepsilon^{(\mathrm{T,T})}(\mathbf{q},\omega)-\varepsilon^{(\mathrm{T,L})}(\mathbf{q},\omega)\circ\left[\frac{1}{\varepsilon^{(\mathrm{L,L})}(\mathbf{q},\omega)}\right]\circ\varepsilon^{(\mathrm{L,T})}(\mathbf{q},\omega)\,, \tag{H.1.1}$$

where

$$\varepsilon_{ab}^{(A,B)}(\mathbf{q},\omega)=\sum_{c,d=1}^{3}\tilde{\Pi}_{ac}^{(A)}(\mathbf{q})\left[\varepsilon_{\Lambda}(\mathbf{q},\omega)\right]_{cd}\tilde{\Pi}_{db}^{(B)}(\mathbf{q})\quad\text{with}\quad A,B\in\{\mathrm{L,T}\}\,. \tag{H.1.2}$$

Assuming that spatial dispersion is negligible, i.e. $\mathbf{q}=\mathbf{0}$, there directly follows from (H.1.1) by utilizing the abbreviations $\varepsilon^{(\mathrm{T})}(\mathbf{0},\omega)\equiv\varepsilon^{(\mathrm{T})}(\omega)$ and $\varepsilon^{(A,B)}(\mathbf{0},\omega)\equiv\varepsilon^{(A,B)}(\omega)$ with $A,B\in\{\mathrm{L,T}\}$

$$\varepsilon^{(\mathrm{T})}(\omega)=\varepsilon^{(\mathrm{T,T})}(\omega)-\varepsilon^{(\mathrm{T,L})}(\omega)\circ\left[\frac{1}{\varepsilon^{(\mathrm{L,L})}(\omega)}\right]\circ\varepsilon^{(\mathrm{L,T})}(\omega)\,. \tag{H.1.3}$$

The transverse dielectric tensor $\varepsilon^{(\mathrm{T})}(\omega)$ is thus completely determined by the $\varepsilon^{(A,B)}(\omega)$, which are calculated on the basis of (H.1.2) by taking the limit

$$\varepsilon_{ab}^{(A,B)}(\omega) \equiv \varepsilon_{ab}^{(A,B)}(\mathbf{0},\omega) = \lim_{|\mathbf{q}|\to 0} \sum_{c,d=1}^{3} \tilde{\Pi}_{ac}^{(A)}(\mathbf{q}) \left[\varepsilon_{\Lambda}(\omega)\right]_{cd} \tilde{\Pi}_{db}^{(B)}(\mathbf{q}), \tag{H.1.4}$$

where $\varepsilon_{\Lambda}(\omega) \equiv \varepsilon_{\Lambda}(\mathbf{0},\omega)$ constitutes the dielectric tensor (4.1.17) for $\mathbf{q}=\mathbf{0}$. To perform the projection process in (H.1.4), the wave vector $\mathbf{q}$ is aligned along one of the dielectric principal axes, say $\mathbf{a}^{(i)}$ with $i \in \{1,2,3\}$, that is associated with the symmetric[1] dielectric tensor $\varepsilon_{\Lambda}(\omega)$. Here, the principal axis vector $\mathbf{a}^{(i)}$ is *not* affected by spatial dispersion (i.e. $\mathbf{a}^{(i)}$ is independent of $\mathbf{q}$) and additionally represents a (normalized) eigenvector of $\varepsilon_{\Lambda}(\omega)$ to the real eigenvalue $\varepsilon_i(\omega)$, so that

$$\varepsilon_{\Lambda}(\omega) \cdot \mathbf{a}^{(i)} = \varepsilon_i(\omega)\, \mathbf{a}^{(i)} \tag{H.1.5}$$

with $\left|\mathbf{a}^{(i)}\right| = 1$ and $\varepsilon_i(\omega) \in \mathbb{R}$ holds. Additionally, $\left\{\mathbf{a}^{(j)}\right\}_{j\in\{1,2,3\}}$ establishes a complete and orthonormal basis of $\mathbb{R}^3$. Choosing $\mathbf{q} = q\mathbf{a}^{(i)}$ with $i \in \{1,2,3\}$ and $q \in \mathbb{R}$, (H.1.4) can be readily evaluated.

By utilizing the projection operators in reciprocal space as given in section A.2, one initially obtains e.g. for $A = \mathrm{L}$ and $B = \mathrm{T}$

$$\begin{aligned}
\varepsilon_{ab}^{(\mathrm{L,T})}(\omega) &= \lim_{|\mathbf{q}|\to 0} \sum_{c,d=1}^{3} \tilde{\Pi}_{ac}^{(\mathrm{L})}(\mathbf{q}) \left[\varepsilon_{\Lambda}(\omega)\right]_{cd} \tilde{\Pi}_{db}^{(\mathrm{T})}(\mathbf{q}) \\
&= \sum_{c,d=1}^{3} a_a^{(i)} a_c^{(i)} \left[\varepsilon_{\Lambda}(\omega)\right]_{cd} \left(\delta_{db} - a_d^{(i)} a_b^{(i)}\right).
\end{aligned} \tag{H.1.6}$$

Taking into account the completeness of $\left\{\mathbf{a}^{(j)}\right\}_{j\in\{1,2,3\}}$, there immediately follows from what has been said above

$$\begin{aligned}
\varepsilon_{ab}^{(\mathrm{L,T})}(\omega) &= \sum_{c,d=1}^{3} \sum_{j=1}^{3} a_a^{(i)} a_c^{(i)} \left[\varepsilon_{\Lambda}(\omega)\right]_{cd} a_d^{(j)} a_b^{(j)} - \sum_{c,d=1}^{3} a_a^{(i)} a_c^{(i)} \left[\varepsilon_{\Lambda}(\omega)\right]_{cd} a_d^{(i)} a_b^{(i)} \\
&= \sum_{c=1}^{3} \sum_{j=1}^{3} \varepsilon_j(\omega)\, a_a^{(i)} a_c^{(i)} a_c^{(j)} a_b^{(j)} - \varepsilon_i(\omega) \sum_{c=1}^{3} a_a^{(i)} a_c^{(i)} a_c^{(i)} a_b^{(i)} \\
&= 0.
\end{aligned} \tag{H.1.7}$$

Similarly one shows that $\varepsilon_{ab}^{(\mathrm{T,L})}(\omega) = 0$, so that the second term in (H.1.3) identically vanishes. As a consequence, it is not necessary to calculate $\frac{1}{\varepsilon^{(\mathrm{L,L})}(\omega)}$, as $\varepsilon^{(\mathrm{T})}(\omega)$ reduces to $\varepsilon^{(\mathrm{T,T})}(\omega)$ because of the reasoning given in section 4.2.2. What remains is the calculation of $\varepsilon_{ab}^{(\mathrm{T,T})}(\omega)$. Proceeding in the same

[1] For a proof that $\left[\varepsilon_{\Lambda}(\omega)\right]_{ab} = \left[\varepsilon_{\Lambda}(\omega)\right]_{bc}$, see e.g. [4].

way as before, one obtains

$$\begin{aligned}\varepsilon_{ab}^{(\mathrm{T,T})}(\omega) &= \lim_{|\mathbf{q}|\to 0}\sum_{c,d=1}^{3}\tilde{\Pi}_{ac}^{(\mathrm{T})}(\mathbf{q})\,[\varepsilon_{\Lambda}(\omega)]_{cd}\,\tilde{\Pi}_{db}^{(\mathrm{T})}(\mathbf{q})\\ &= \sum_{c,d=1}^{3}\left(\delta_{ac}-a_a^{(i)}a_c^{(i)}\right)[\varepsilon_{\Lambda}(\omega)]_{cd}\left(\delta_{db}-a_d^{(i)}a_b^{(i)}\right)\\ &= [\varepsilon_{\Lambda}(\omega)]_{ab}-\varepsilon_i(\omega)\,a_a^{(i)}a_b^{(i)}. \end{aligned} \tag{H.1.8}$$

Finally, the transverse dielectric tensor $\varepsilon^{(\mathrm{T})}(\omega)$ is received from (H.1.3) by combining the previously obtained results. Its representation with respect to the cartesian coordinate system $\left\{\mathbf{e}^{(j)}\right\}_{j\in\{1,2,3\}}$ reads

$$\varepsilon_{ab}^{(\mathrm{T})}(\omega) = [\varepsilon_{\Lambda}(\omega)]_{ab}-\varepsilon_i(\omega)\,a_a^{(i)}a_b^{(i)}\ \text{(cartesian coordinates)} \tag{H.1.9}$$

and reveals, that $\varepsilon^{(\mathrm{T})}(\omega)$ is a symmetric matrix just like $\varepsilon_{\Lambda}(\omega)$. But in contrast to the dielectric tensor $\varepsilon_{\Lambda}(\omega)$, the transverse dielectric tensor only exhibits two non-vanishing eigenvalues instead of three, because the second term in (H.1.9) eliminates the non-radiative "longitudinal" eigenmode which is comprised by $\varepsilon_{\Lambda}(\omega)$. What just has been said can immediately be realized by representing $\varepsilon^{(\mathrm{T})}(\omega)$ in the basis of dielectric principal axes $\left\{\mathbf{a}^{(j)}\right\}_{j\in\{1,2,3\}}$, which simultaneously constitute eigenvectors of $\varepsilon_{\Lambda}(\omega)$ and $\varepsilon^{(\mathrm{T})}(\omega)$, as can easily be seen from (H.1.9). Constructing an orthogonal 3×3 matrix S from the orthonormal basis $\left\{\mathbf{a}^{(j)}\right\}_{j\in\{1,2,3\}}$, one readily obtains the transverse dielectric tensor $\varepsilon^{(\mathrm{T})}(\omega)$ within the coordinate system of principal axes according to

$$\varepsilon_{ab}^{(\mathrm{T})}(\omega) = \varepsilon_a(\omega)\,(1-\delta_{ai})\,\delta_{ab}\ \text{(system of principal axes)}. \tag{H.1.10}$$

Remember that the index $i\in\{1,2,3\}$ in (H.1.10) labels that dielectric principal axis $\mathbf{a}^{(i)}$, along wave propagation takes place.

H.2 Rotatory power and the structure of $\varepsilon^{(\mathrm{T})}(\mathbf{q},\omega)$ in cubic and uniaxial crystal systems

Similar to the previous section H.1, the transverse dielectric tensor $\varepsilon^{(\mathrm{T})}(\mathbf{q},\omega)$ defined by (H.1.1) can readily be deduced from the dielectric tensor $\varepsilon_{\Lambda}(\mathbf{q},\omega)$ (see (4.1.17)) by means of the projections (H.1.2). In order to study the rotatory power of various crystals in terms of $\varepsilon^{(\mathrm{T})}(\mathbf{q},\omega)$, start with the expansion of $\varepsilon_{\Lambda}(\mathbf{q},\omega)$ to first order with respect to the wave vector $\mathbf{q}$ around $\mathbf{q}=\mathbf{0}$ according to[2]

$$[\varepsilon_{\Lambda}(\mathbf{q},\omega)]_{ab} = [\varepsilon_{\Lambda}(\omega)]_{ab}+i\sum_{c=1}^{3}\gamma_{abc}^{(\Lambda)}(\omega)\,q_c. \tag{H.2.1}$$

[2]Compare with the expansion (4.4.12) of the transverse dielectric tensor.

point groups	constraints on $G^{(\Lambda)}(\omega)$	
	$\gamma_j(\omega)$	$\chi(\omega)$
23, 432	$\gamma_1(\omega)=\gamma_3(\omega)$	$\chi(\omega)=0$
32, 422, 622	/	$\chi(\omega)=0$
3, 4, 6	/	/

Table H.2.1: Constraints imposed on the gyrotropy tensor $G^{(\Lambda)}(\omega)$ given by (H.2.3) due to the point group symmetry of cubic and uniaxial crystal structures exhibiting rotatory power [5, 97].

$\varepsilon_\Lambda(\omega)$ denotes again the dielectric tensor in absence of spatial dispersion (i.e. for $\mathbf{q}=\mathbf{0}$), which has already been discussed in section 4.4.3.1 and appendix H.1. However, the polar tensor $\gamma^{(\Lambda)}_{abc}(\omega)$ of rank 3 might give rise to rotatory power in particular *non-centrosymmetric* crystal structures and is therefore called gyration tensor. Its components are real, so that $\gamma^{(\Lambda)}_{abc}(\omega)=\left[\gamma^{(\Lambda)}_{abc}(\omega)\right]^*$ holds, as has been shown in [1, 69]. Furthermore, it can be represented in terms of the Levi-Civita tensor ε_{abc} and an axial tensor $G^{(\Lambda)}_{ab}(\omega)$ of rank 2, called gyrotropy tensor, according to [1, 97]

$$\gamma^{(\Lambda)}_{abc}(\omega)=\sum_{d=1}^{3}\varepsilon_{abd}G^{(\Lambda)}_{dc}(\omega)\,. \tag{H.2.2}$$

Of course, there holds by construction $G^{(\Lambda)}_{ab}(\omega)=\left[G^{(\Lambda)}_{ab}(\omega)\right]^*$.

Since the discussion of natural optical activity in section 4.4.3.2 is restricted to crystal structures, where the effect of rotatory power is not masked by the crystal's own birefringence, only wave propagation with $\mathbf{q}=q\mathbf{e}^{(3)}$ along the (optical) z-axis in cubic and uniaxial crystal systems is considered. In total, there exist 8 crystallographic point groups in these crystal systems, that feature rotatory power. For these groups, the gyrotropy tensor can be written in a condensed form by

$$G^{(\Lambda)}(\omega)=\begin{pmatrix}\gamma_1(\omega) & \chi(\omega) & 0\\ -\chi(\omega) & \gamma_1(\omega) & 0\\ 0 & 0 & \gamma_3(\omega)\end{pmatrix}, \tag{H.2.3}$$

where table H.2.1 allows the identification of the specific structure of $G^{(\Lambda)}(\omega)$ for each individual group [5, 97]. Noticing that in the cubic as well as in the uniaxial crystal systems the dielectric principal axes associated with $\varepsilon_\Lambda(\omega)$ coincide with the axes of the cartesian coordinate system (see table 4.4.1), $\varepsilon_\Lambda(\omega)$ is diagonal and reads

$$\left[\varepsilon_\Lambda(\omega)\right]_{ab}=\varepsilon_a(\omega)\,\delta_{ab}\ \text{ with }\ \begin{cases}\varepsilon_1(\omega)=\varepsilon_2(\omega)=\varepsilon_3(\omega) & \text{(cubic)}\\ \varepsilon_1(\omega)=\varepsilon_2(\omega)\neq\varepsilon_3(\omega) & \text{(uniaxial)}\end{cases}. \tag{H.2.4}$$

Additionally, taking into account that the wave vector $\mathbf{q}=q\mathbf{e}^{(3)}$ is aligned along the (optical) z-axis, the

dielectric tensor $\varepsilon_\Lambda(\mathbf{q},\omega)$ given by (H.2.1) assumes the guise

$$[\varepsilon_\Lambda(\mathbf{q},\omega)]_{ab} = \varepsilon_a(\omega)\,\delta_{ab} + i\varepsilon_{ab3}\gamma_3(\omega)\,q. \tag{H.2.5}$$

The representation (H.2.5) of the dielectric tensor $\varepsilon_\Lambda(\mathbf{q},\omega)$ constitutes the starting point for the derivation of the transverse dielectric tensor $\varepsilon^{(\mathrm{T})}(\mathbf{q},\omega)$ featuring rotatory power. By virtue of (H.1.2) it is easily verified, that in the present case $\varepsilon_{ab}^{(\mathrm{T,L})}(\mathbf{q},\omega) = \varepsilon_{ab}^{(\mathrm{L,T})}(\mathbf{q},\omega) = 0$, so that the transverse dielectric tensor reduces to

$$\begin{aligned}\varepsilon_{ab}^{(\mathrm{T})}(\mathbf{q},\omega) &= \varepsilon_{ab}^{(\mathrm{T,T})}(\mathbf{q},\omega)\\ &= \sum_{c,d=1}^{3} \tilde{\Pi}_{ac}^{(\mathrm{T})}(\mathbf{q})\,[\varepsilon_\Lambda(\mathbf{q},\omega)]_{cd}\,\tilde{\Pi}_{db}^{(\mathrm{T})}(\mathbf{q})\\ &= \varepsilon_a(\omega)\left(1-e_a^{(3)}\right)\delta_{ab} + i\varepsilon_{ab3}\gamma_3(\omega)\,q.\end{aligned} \tag{H.2.6}$$

Introducing the abbreviation $\gamma(q,\omega) = \gamma_3(\omega)\,q$, the matrix representation of (H.2.6) is immediately deduced according to

$$\varepsilon^{(\mathrm{T})}(\mathbf{q},\omega) = \begin{pmatrix} \varepsilon_1(\omega) & i\gamma(q,\omega) & 0\\ -i\gamma(q,\omega) & \varepsilon_1(\omega) & 0\\ 0 & 0 & 0\end{pmatrix} \text{ (cartesian coordinates).} \tag{H.2.7}$$

H.3 Spatial dispersion induced birefringence in point group m$\bar{3}$m when $\mathbf{q}||\,(110)^T$

In analogy to the previous sections H.1 and H.2, the transverse dielectric tensor $\varepsilon^{(\mathrm{T})}(\mathbf{q},\omega)$ (see (H.1.1)) describing spatial dispersion induced birefringence, will be deduced from the dielectric tensor $\varepsilon_\Lambda(\mathbf{q},\omega)$ by means of the projections (H.1.2). When only *centrosymmetric* crystals are considered, natural optical activity is inherently absent, i.e. $\gamma_{abc}^{(\Lambda)}(\omega) = 0$ (see section H.2), so that the expansion of the dielectric tensor around $\mathbf{q} = \mathbf{0}$ yields in the lowest non-vanishing order[3]

$$[\varepsilon_\Lambda(\mathbf{q},\omega)]_{ab} = [\varepsilon_\Lambda(\omega)]_{ab} + \sum_{c,d=1}^{3} \alpha_{abcd}^{(\Lambda)}(\omega)\,q_c q_d. \tag{H.3.1}$$

While $[\varepsilon_\Lambda(\omega)]_{ab}$ denotes again the components of the dielectric tensor in absence of spatial dispersion (i.e. for $\mathbf{q} = \mathbf{0}$), $\alpha_{abcd}^{(\Lambda)}(\omega)$ represents the components of a polar tensor of rank 4, that incorporates the effect of spatial dispersion induced birefringence. Additionally, for the latter there holds $\alpha_{abcd}^{(\Lambda)}(\omega) = \left[\alpha_{abcd}^{(\Lambda)}(\omega)\right]^*$ as well as $\alpha_{abcd}^{(\Lambda)}(\omega) = \alpha_{bacd}^{(\Lambda)}(\omega) = \alpha_{abdc}^{(\Lambda)}(\omega)$ [1]. In particular it should be

[3] Compare with the expansion (4.4.12) of the transverse dielectric tensor.

stressed, that there is a priori *no* symmetry argument requiring that $\alpha^{(\Lambda)}_{abcd}(\omega)$ vanishes in any of the 32 crystallographic point groups [1, 5], so that spatial dispersion induced birefringence is an omnipresent effect.

Restricting the ensuing discussion to the centrosymmetric cubic point group $\mathrm{m\bar{3}m}$, additional constraints are imposed on the tensor components $[\varepsilon_\Lambda(\omega)]_{ab}$ and $\alpha^{(\Lambda)}_{abcd}(\omega)$ according to Neumann's principle [5]. While the former coincides with the components of a scalar matrix according to $[\varepsilon_\Lambda(\omega)]_{ab} = \varepsilon(\omega)\,\delta_{ab}$, the latter solely exhibits 3 independent non-vanishing components, namely [1]

$$\begin{aligned}
a_1(\omega) &\equiv \alpha^{(\Lambda)}_{1111}(\omega) = \alpha^{(\Lambda)}_{2222}(\omega) = \alpha^{(\Lambda)}_{3333}(\omega)\\
a_2(\omega) &\equiv \alpha^{(\Lambda)}_{1133}(\omega) = \alpha^{(\Lambda)}_{2211}(\omega) = \alpha^{(\Lambda)}_{3322}(\omega) = \alpha^{(\Lambda)}_{3311}(\omega) = \alpha^{(\Lambda)}_{1122}(\omega) = \alpha^{(\Lambda)}_{2233}(\omega)\\
a_3(\omega) &\equiv \alpha^{(\Lambda)}_{1212}(\omega) = \alpha^{(\Lambda)}_{2323}(\omega) = \alpha^{(\Lambda)}_{3131}(\omega) = \alpha^{(\Lambda)}_{2112}(\omega) = \alpha^{(\Lambda)}_{3223}(\omega) = \alpha^{(\Lambda)}_{1331}(\omega)\\
&= \alpha^{(\Lambda)}_{1221}(\omega) = \alpha^{(\Lambda)}_{2332}(\omega) = \alpha^{(\Lambda)}_{3113}(\omega) = \alpha^{(\Lambda)}_{2121}(\omega) = \alpha^{(\Lambda)}_{3232}(\omega) = \alpha^{(\Lambda)}_{1313}(\omega).
\end{aligned} \tag{H.3.2}$$

As spatial dispersion induced birefringence assumes its maximum value when a wave propagates along one of the plane diagonals of the Wigner-Seitz cell C_Λ [9], these directions are of special interest with regard to the target specification of birefringence $\Delta n = 10^{-7}$ required by 157nm lithography systems. Without loss of generality, the wave vector is thus chosen as $\mathbf{q} = \frac{|\mathbf{q}|}{\sqrt{2}}(110)^T$, so that the dielectric tensor (H.3.1) assumes the guise

$$\varepsilon_\Lambda(\mathbf{q},\omega) = \varepsilon(\omega)\,\delta + \frac{|\mathbf{q}|^2}{2}\begin{pmatrix} a_1(\omega)+a_2(\omega) & 2a_3(\omega) & 0\\ 2a_3(\omega) & a_1(\omega)+a_2(\omega) & 0\\ 0 & 0 & 2a_2(\omega)\end{pmatrix}. \tag{H.3.3}$$

The transverse dielectric tensor $\varepsilon^{(\mathrm{T})}(\mathbf{q},\omega)$ describing spatial dispersion induced birefringence can now readily be deduced from (H.3.3). Initially, by virtue of (H.1.2) it is verified that $\varepsilon^{(\mathrm{T,L})}_{ab}(\mathbf{q},\omega) = \varepsilon^{(\mathrm{L,T})}_{ab}(\mathbf{q},\omega) = 0$. Hence, $\varepsilon^{(\mathrm{T})}(\mathbf{q},\omega)$ given by (H.1.1) reduces to

$$\begin{aligned}
\varepsilon^{(\mathrm{T})}(\mathbf{q},\omega) =& \varepsilon^{(\mathrm{T,T})}(\mathbf{q},\omega)\\
=& \tilde{\Pi}^{(\mathrm{T})}(\mathbf{q}) \circ \varepsilon_\Lambda(\mathbf{q},\omega) \circ \tilde{\Pi}^{(\mathrm{T})}(\mathbf{q})\\
=& \varepsilon(\omega)\begin{pmatrix} \frac{1}{2} & -\frac{1}{2} & 0\\ -\frac{1}{2} & \frac{1}{2} & 0\\ 0 & 0 & 1\end{pmatrix}\\
&+ \frac{|\mathbf{q}|^2}{4}\begin{pmatrix} a_1(\omega)+a_2(\omega)-2a_3(\omega) & -a_1(\omega)-a_2(\omega)+2a_3(\omega) & 0\\ -a_1(\omega)-a_2(\omega)+2a_3(\omega) & a_1(\omega)+a_2(\omega)-2a_3(\omega) & 0\\ 0 & 0 & 4a_2(\omega)\end{pmatrix}.
\end{aligned} \tag{H.3.4}$$

Introducing the notation

$$\xi_1(\omega) \equiv \frac{1}{4}\left(a_1(\omega) - 2a_3(\omega)\right) \text{ and } \xi_2(\omega) \equiv \frac{1}{4}a_2(\omega), \tag{H.3.5}$$

(H.3.4) can be written in a condensed form according to

$$\varepsilon^{(\mathrm{T})}(\mathbf{q},\omega) = \varepsilon(\omega)\begin{pmatrix} \frac{1}{2} & -\frac{1}{2} & 0 \\ -\frac{1}{2} & \frac{1}{2} & 0 \\ 0 & 0 & 1 \end{pmatrix} + |\mathbf{q}|^2 \begin{pmatrix} \xi_1(\omega)+\xi_2(\omega) & -\xi_1(\omega)-\xi_2(\omega) & 0 \\ -\xi_1(\omega)-\xi_2(\omega) & \xi_1(\omega)+\xi_2(\omega) & 0 \\ 0 & 0 & 4\xi_2(\omega) \end{pmatrix}$$

(cartesian coordinates). (H.3.6)

Appendix I

Magnetizable crystalline materials

This appendix deals with the local magnetic induction field in magnetizable crystalline materials and is to be conceived as a supplement to the theory of the local electromagnetic field in dielectric crystals, which is presented in the main part of this thesis. Assuming that electric mono-, di- and quadrupole interactions are negligible, the magnetic dipole interaction represents the leading order with regard to the strength of electromagnetic interactions [25]. Since for high frequency driving fields, like e.g. visible laser light, the widely used concept of the magnetic permeability tensor looses its meaning [138] and because there is additionally no physical justification for a distinction of induced polarization and magnetization currents [2] in this high frequency regime, the discussion of the local magnetic induction field in magnetizable crystals requires the frequencies of the driving fields to be restricted well below the optical regime. Since the approach is similar to that of the local electromagnetic field within dielectric crystals presented in chapters 3 and 4, the elaboration in this appendix is shortened.

I.1 Magnetization model and the integral equations of the local magnetic induction field

For the geometry shown in figure 2.2.1, the integral equation determining the local magnetic induction field is given by (2.2.10). Noticing, that the longitudinal part of the induced current density has vanishing curl, usage of the identity $\nabla_{\mathbf{r}} \times (f(\mathbf{r})\mathbf{V}(\mathbf{r})) = (\nabla_{\mathbf{r}} f(\mathbf{r})) \times \mathbf{V}(\mathbf{r}) + f(\mathbf{r})\nabla_{\mathbf{r}} \times \mathbf{V}(\mathbf{r})$ and subsequent application of Gauß's integral theorem allows to rewrite (2.2.10) according to

$$\mathbf{B}(\mathbf{r},\omega) = \mathbf{B}_{\text{ext}}(\mathbf{r},\omega) - \mu_0 \int_{\mathbb{R}^3} d^3r' \left(\nabla_{\mathbf{r}'} g\left(\mathbf{r}-\mathbf{r}',\omega\right)\right) \times \mathbf{j}_{\text{ind}}\left(\mathbf{r}',\omega\right), \tag{I.1.1}$$

because $\mathbf{j}_{\text{ind}}(\mathbf{r},\omega)$ is restricted to $\mathbf{r} \in \Omega_{\text{P}}$ and hence vanishes when $|\mathbf{r}| \to \infty$. In the following it is assumed, that the probe under investigation is of crystalline order, occupies the volume Ω_{P} and does not posses any permanent electric or magnetic moments. Furthermore it is implied, that the constituents

of the probe, i.e. the atoms or ions, only respond to the local magnetic induction field $\mathbf{B}(\mathbf{r},\omega)$ and *not* to the local electric field $\mathbf{E}(\mathbf{r},\omega)$. More precisely, when an externally applied (not to strong) magnetic induction field $\mathbf{B}_{\text{ext}}(\mathbf{r},\omega)$ of rather low frequency is applied to the crystal, its initial state of equilibrium is disturbed due to the change of the local magnetic induction field $\mathbf{B}(\mathbf{r},\omega)$, and a small additional (Lorentz-) force is exerted onto each charge carrier within the crystal. The barycenter of the positively charged nucleus of the j^{th}- atom/ion inside C_Λ with $j \in \{1,2,\ldots,M\}$ is supposed to be at rest at a *fixed* position $\eta^{(j)}$, irrespective of the presence of $\mathbf{B}_{\text{ext}}(\mathbf{r},\omega)$. In contrast, the barycenter of the electrons bound to this nucleus forms a point-like current loop inside the respective atom/ion due to this additional force, so that finally each individual constituent of the crystal acquires an *induced* magnetic dipole moment, which is proportional to the *local* magnetic induction field $\mathbf{B}(\mathbf{r},\omega)$ as retarded response to the externally applied field $\mathbf{B}_{\text{ext}}(\mathbf{r},\omega)$. The proportionality factor between the induced magnetic dipole moment and the local magnetic induction field for the j^{th}-atom/ion inside C_Λ is given by the cartesian components of the *magnetic* polarizability tensor $\beta_{ab}\left(\eta^{(j)},\omega\right) \equiv \beta_{ab}^{(j)}(\omega)$ with $a,b \in \{1,2,3\}$.

The depicted model of magnetizable crystals can be incorporated into the induced current density according to

$$\mathbf{j}_{\text{ind}}(\mathbf{r},\omega) = \nabla_{\mathbf{r}} \times \mathbf{M}(\mathbf{r},\omega), \tag{I.1.2}$$

where $\mathbf{M}(\mathbf{r},\omega)$ denotes the microscopic magnetizability, that contains all the information about the material and its interaction processes with the local magnetic induction field. The relation between $\mathbf{M}(\mathbf{r},\omega)$ and $\mathbf{B}(\mathbf{r},\omega)$ is conveyed in close analogy to (3.1.5) by the magnetic susceptibility kernel $\chi_{ab}^{(\text{mag})}(\mathbf{r},\mathbf{r}',\omega)$ via

$$M_a(\mathbf{r},\omega) = \frac{1}{\mu_0}\sum_{b=1}^{3}\int_{\mathbb{R}^3} d^3r'\,\chi_{ab}^{(\text{mag})}\left(\mathbf{r},\mathbf{r}',\omega\right)B_b\left(\mathbf{r}',\omega\right). \tag{I.1.3}$$

Referring to (3.1.6), a simple *phenomenological* model for the magnetic susceptibility kernel, that takes into account the afore described magnetization process, is given by[1]

$$\chi_{ab}^{(\text{mag})}\left(\mathbf{r},\mathbf{r}',\omega\right) = \mu_0 \sum_{\mathbf{R}\in\Lambda_{\text{P}}}\sum_{j=1}^{M}\beta_{ab}^{(j)}(\omega)\,\delta\left(\mathbf{r}-\mathbf{R}-\eta^{(j)}\right)\delta\left(\mathbf{r}-\mathbf{r}'\right). \tag{I.1.4}$$

It should be emphasized, that in the limit of an infinitely extended crystal, i.e. if $\Lambda_{\text{P}} = \Lambda$, the magnetic susceptibility kernel (I.1.4) is invariant under a translation by an arbitrary lattice vector $\mathbf{R}' \in \Lambda$ according to

$$\chi_{ab}^{(\text{mag})}\left(\mathbf{r}+\mathbf{R}',\mathbf{r}'+\mathbf{R}',\omega\right) = \chi_{ab}^{(\text{mag})}\left(\mathbf{r},\mathbf{r}',\omega\right). \tag{I.1.5}$$

Inserting (I.1.2) into (I.1.1) initially yields for the cartesian components of the local magnetic induction

[1] Notice, that in the model (I.1.4) for $\chi_{ab}^{(\text{mag})}(\mathbf{r},\mathbf{r}',\omega)$, there is *no* magnetic equivalent to the ionic displacement polarizability. Thereto, compare with the expression of $\chi_{ab}(\mathbf{r},\mathbf{r}',\omega)$, as given in (3.1.6).

field

$$\begin{aligned} B_a(\mathbf{r},\omega) &= B_{\mathrm{ext},a}(\mathbf{r},\omega) - \mu_0 \int_{\mathbb{R}^3} d^3r' \left[\left(\nabla_{\mathbf{r}'} g\left(\mathbf{r}-\mathbf{r}',\omega\right)\right) \times \left(\nabla_{\mathbf{r}'} \times \mathbf{M}\left(\mathbf{r}',\omega\right)\right) \right]_a \\ &= B_{\mathrm{ext},a}(\mathbf{r},\omega) - \mu_0 \sum_{b,d,e=1}^{3} \left(\delta_{ad}\delta_{be} - \delta_{ae}\delta_{bd}\right) \int_{\mathbb{R}^3} d^3r' \left(\frac{\partial}{\partial r'_b} g\left(\mathbf{r}-\mathbf{r}',\omega\right) \right) \frac{\partial}{\partial r'_d} M_e\left(\mathbf{r}',\omega\right), \end{aligned} \tag{I.1.6}$$

where in the second line the identity

$$\sum_{c=1}^{3} \varepsilon_{abc}\varepsilon_{cde} = \delta_{ad}\delta_{be} - \delta_{ae}\delta_{bd} \tag{I.1.7}$$

has been deployed. Noticing that the microscopic magnetization $\mathbf{M}(\mathbf{r},\omega)$ given by (I.1.3) is only non-vanishing within the finite probe volume Ω_{P}, partial integration of (I.1.6) with respect to dr'_d readily results in

$$B_a(\mathbf{r},\omega) = B_{\mathrm{ext},a}(\mathbf{r},\omega) - \mu_0 \sum_{b,d,e=1}^{3} \left(\delta_{ad}\delta_{be} - \delta_{ae}\delta_{bd}\right) \int_{\mathbb{R}^3} d^3r' \, G_{db}\left(\mathbf{r}-\mathbf{r}',\omega\right) M_e\left(\mathbf{r}',\omega\right), \tag{I.1.8}$$

where the cartesian components of the *regularized*[2] second-order partial derivatives of the Helmholtz propagator have been identified as (see e.g. [139])

$$\begin{aligned} & G_{db}\left(\mathbf{r}-\mathbf{r}',\omega\right) \\ \equiv & -\frac{\partial}{\partial r'_d}\frac{\partial}{\partial r'_b} g\left(\mathbf{r}-\mathbf{r}',\omega\right) \qquad\qquad (\text{I.1.9}) \\ = & \frac{1}{3}\delta_{db}\delta\left(\mathbf{r}-\mathbf{r}'\right) - \Theta_{\mathrm{H}}\left(\left|\mathbf{r}-\mathbf{r}'\right| - 0^+\right) \frac{e^{i\frac{\omega}{c}\left|\mathbf{r}-\mathbf{r}'\right|}}{4\pi\left|\mathbf{r}-\mathbf{r}'\right|^5} \\ & \cdot \left[\left|\mathbf{r}-\mathbf{r}'\right|^2 \left(-1 + i\frac{\omega}{c}\left|\mathbf{r}-\mathbf{r}'\right|\right)\delta_{db} + \left(3 - 3i\frac{\omega}{c}\left|\mathbf{r}-\mathbf{r}'\right| - \frac{\omega^2}{c^2}\left|\mathbf{r}-\mathbf{r}'\right|^2\right)\left(r_d - r'_d\right)\left(r_b - r'_b\right) \right]. \end{aligned} \tag{I.1.10}$$

Obviously $G_{ab}(\mathbf{r}-\mathbf{r}',\omega)$ constitutes a symmetric 3×3 matrix, which coincides in the static limit with the longitudinal projection operator $\Pi^{(\mathrm{L})}_{ab}(\mathbf{r}-\mathbf{r}')$ given by (2.1.17), i.e.

$$\lim_{\omega\to 0} G_{ab}\left(\mathbf{r}-\mathbf{r}',\omega\right) = \Pi^{(\mathrm{L})}_{ab}\left(\mathbf{r}-\mathbf{r}'\right). \tag{I.1.11}$$

[2]The regularization in (I.1.10) by means of the delta function is possible and necessary, because the second-order derivative of the Helmholtz propagator appears under an integral and would otherwise lead to a bad singularity of the integrand. Compare with the derivation of the projection operators in appendix A.2.

Introducing as notation the 3×3 matrix kernel[3]

$$\mathscr{G}_{ae}^{(\mathrm{mag})}\left(\mathbf{r}-\mathbf{r}',\omega\right) = G_{ae}\left(\mathbf{r}-\mathbf{r}',\omega\right) - \delta_{ae}\mathrm{Tr}\left[G\left(\mathbf{r}-\mathbf{r}',\omega\right)\right] \tag{I.1.12}$$

and carrying out the summation with respect to b and d in (I.1.8), the local magnetic induction field can be rewritten according to

$$B_a\left(\mathbf{r},\omega\right) = B_{\mathrm{ext},a}\left(\mathbf{r},\omega\right) - \mu_0 \sum_{e=1}^{3} \int_{\mathbb{R}^3} d^3r' \, \mathscr{G}_{ae}^{(\mathrm{mag})}\left(\mathbf{r}-\mathbf{r}',\omega\right) M_e\left(\mathbf{r}',\omega\right). \tag{I.1.13}$$

Deploying now the phenomenological magnetization model (I.1.3), the integral equation determining the local magnetic induction field in magnetizable crystalline materials reads

$$B_a\left(\mathbf{r},\omega\right) = B_{\mathrm{ext},a}\left(\mathbf{r},\omega\right) - \sum_{b=1}^{3} \int_{\mathbb{R}^3} d^3r' \, \left[\mathscr{G}^{(\mathrm{mag})} \circ \chi^{(\mathrm{mag})}\right]_{ab}\left(\mathbf{r},\mathbf{r}',\omega\right) B_b\left(\mathbf{r}',\omega\right), \tag{I.1.14}$$

where the abbreviation

$$\left[\mathscr{G}^{(\mathrm{mag})} \circ \chi^{(\mathrm{mag})}\right]_{ab}\left(\mathbf{r},\mathbf{r}',\omega\right) = \sum_{c=1}^{3} \int_{\mathbb{R}^3} d^3r'' \, \mathscr{G}_{ac}^{(\mathrm{mag})}\left(\mathbf{r}-\mathbf{r}'',\omega\right) \chi_{cb}^{(\mathrm{mag})}\left(\mathbf{r}'',\mathbf{r}',\omega\right) \tag{I.1.15}$$

has been introduced. In the next section, the integral equation (I.1.14) will be solved exactly by expanding the local magnetic induction field in terms of the non-standard system of Bloch functions (3.2.9).

I.2 Solution of the local magnetic induction field integral equation

The following procedure of solving the integral equation (I.1.14) is analogue to that already presented in section 3.2. The local magnetic induction field is expanded with respect to the non-standard system of Bloch functions $w\left(\mathbf{r};\mathbf{s},\mathbf{k}\right)$ according to

$$B_a\left(\mathbf{r},\omega\right) = \sum_{\mathbf{k}\in C_\Lambda^{-1}} \int_{C_\Lambda} d^3s \, w\left(\mathbf{r};\mathbf{s},\mathbf{k}\right) \mathfrak{b}_a\left(\mathbf{s},\mathbf{k},\omega\right), \tag{I.2.1}$$

where the expansion coefficients $\mathfrak{b}_a\left(\mathbf{s},\mathbf{k},\omega\right)$ are defined by

$$\mathfrak{b}_a\left(\mathbf{s},\mathbf{k},\omega\right) = \int_{\Omega_\mathrm{P}} d^3r \, w^\dagger\left(\mathbf{r};\mathbf{s},\mathbf{k}\right) B_a\left(\mathbf{r},\omega\right). \tag{I.2.2}$$

[3] It should be noticed, that the electromagnetic kernel $\mathscr{G}_{ab}\left(\mathbf{r}-\mathbf{r}',\omega\right)$ defined in (2.2.15) is independent of any material model with regard to the induced current density $\mathbf{j}_{\mathrm{ind}}\left(\mathbf{r},\omega\right)$. In contrast, the definition of the kernel $\mathscr{G}_{ab}^{(\mathrm{mag})}\left(\mathbf{r}-\mathbf{r}',\omega\right)$ in (I.1.12) already includes the material model $\mathbf{j}_{\mathrm{ind}}\left(\mathbf{r},\omega\right) = \nabla_\mathbf{r} \times \mathbf{M}\left(\mathbf{r},\omega\right)$.

The expansion coefficients $\mathfrak{b}_{\mathrm{ext},a}(\mathbf{s},\mathbf{k},\omega)$ associated with the externally applied magnetic induction field $B_{\mathrm{ext},a}(\mathbf{r},\omega)$ read

$$\mathfrak{b}_{\mathrm{ext},a}(\mathbf{s},\mathbf{k},\omega)=\int_{\Omega_{\mathrm{P}}}d^3r\,w^{\dagger}(\mathbf{r};\mathbf{s},\mathbf{k})\,B_{\mathrm{ext},a}(\mathbf{r},\omega)\,, \tag{I.2.3}$$

so that insertion of (I.1.14) into (I.2.2) readily yields

$$\mathfrak{b}_a(\mathbf{s},\mathbf{k},\omega)=\mathfrak{b}_{\mathrm{ext},a}(\mathbf{s},\mathbf{k},\omega)-\sum_{b=1}^{3}\int_{\Omega_{\mathrm{P}}}d^3r\int_{\mathbb{R}^3}d^3r'\,w^{\dagger}(\mathbf{r};\mathbf{s},\mathbf{k})\left[\mathscr{G}^{(\mathrm{mag})}\circ\chi^{(\mathrm{mag})}\right]_{ab}(\mathbf{r},\mathbf{r}',\omega)\,B_b(\mathbf{r}',\omega)\,. \tag{I.2.4}$$

Introducing now the abbreviation

$$\langle\mathbf{s},\mathbf{k}\left|\left[\mathscr{G}^{(\mathrm{mag})}\circ\chi^{(\mathrm{mag})}\right]_{ab}\right|\mathbf{s}',\mathbf{k}'\rangle\equiv\int_{\Omega_{\mathrm{P}}}d^3r\int_{\mathbb{R}^3}d^3r'\,w^{\dagger}(\mathbf{r};\mathbf{s},\mathbf{k})\left[\mathscr{G}^{(\mathrm{mag})}\circ\chi^{(\mathrm{mag})}\right]_{ab}(\mathbf{r},\mathbf{r}',\omega)\,w(\mathbf{r}';\mathbf{s}',\mathbf{k}') \tag{I.2.5}$$

and eliminating $B_b(\mathbf{r}',\omega)$ in (I.2.4) by means of (I.2.1), one obtains

$$\mathfrak{b}_a(\mathbf{s},\mathbf{k},\omega)=\mathfrak{b}_{\mathrm{ext},a}(\mathbf{s},\mathbf{k},\omega)-\sum_{b=1}^{3}\sum_{\mathbf{k}'\in C_{\Lambda^{-1}}}\int_{C_\Lambda}d^3s'\,\langle\mathbf{s},\mathbf{k}\left|\left[\mathscr{G}^{(\mathrm{mag})}\circ\chi^{(\mathrm{mag})}\right]_{ab}\right|\mathbf{s}',\mathbf{k}'\rangle\mathfrak{b}_b(\mathbf{s}',\mathbf{k}',\omega)\,. \tag{I.2.6}$$

Assuming from now on the crystal to be infinitely extended, i.e. $\Lambda_{\mathrm{P}}=\Lambda$, $\langle\mathbf{s},\mathbf{k}\left|\left[\mathscr{G}^{(\mathrm{mag})}\circ\chi^{(\mathrm{mag})}\right]_{ab}\right|\mathbf{s}',\mathbf{k}'\rangle$ assumes the guise[4]

$$\begin{aligned}&\langle\mathbf{s},\mathbf{k}\left|\left[\mathscr{G}^{(\mathrm{mag})}\circ\chi^{(\mathrm{mag})}\right]_{ab}\right|\mathbf{s}',\mathbf{k}'\rangle\\&=\frac{\mu_0}{N_{\mathrm{P}}}\frac{(2\pi)^3}{|C_\Lambda|}\sum_{c=1}^{3}\sum_{j=1}^{M}\sum_{\mathbf{R}'\in\Lambda}e^{i\mathbf{k}'\cdot\mathbf{s}'}e^{-i\mathbf{k}\cdot(\mathbf{s}+\mathbf{R}')}\mathscr{G}^{(\mathrm{mag})}_{ac}\left(\mathbf{s}+\mathbf{R}'-\mathbf{s}',\omega\right)\beta^{(j)}_{cb}(\omega)\,\delta\left(\mathbf{s}'-\eta^{(j)}\right)\delta\left(\mathbf{k}-\mathbf{k}'\right).\end{aligned} \tag{I.2.7}$$

Replacing also the sum over wave vectors in (I.2.6) by an integral according to (3.2.17), the equation determining the expansion coefficients $\mathfrak{b}_a(\mathbf{s},\mathbf{k},\omega)$ becomes algebraic

$$\begin{aligned}&\mathfrak{b}_a(\mathbf{s},\mathbf{k},\omega)\\&=\mathfrak{b}_{\mathrm{ext},a}(\mathbf{s},\mathbf{k},\omega)-\mu_0\sum_{b,c=1}^{3}\sum_{j=1}^{M}\sum_{\mathbf{R}\in\Lambda}e^{-i\mathbf{k}\cdot\left(\mathbf{s}+\mathbf{R}-\eta^{(j)}\right)}\mathscr{G}^{(\mathrm{mag})}_{ab}\left(\mathbf{s}+\mathbf{R}-\eta^{(j)},\omega\right)\beta^{(j)}_{bc}(\omega)\,\mathfrak{b}_c\left(\eta^{(j)},\mathbf{k},\omega\right)\\&=\mathfrak{b}_{\mathrm{ext},a}(\mathbf{s},\mathbf{k},\omega)-\mu_0\sum_{b,c=1}^{3}\sum_{j=1}^{M}\left[\zeta^{(\mathrm{mag})}_{\Lambda}\left(\mathbf{s}-\eta^{(j)},\mathbf{k},\omega\right)\right]_{ab}\beta^{(j)}_{bc}(\omega)\,\mathfrak{b}^{(j)}_c(\mathbf{k},\omega)\,,\end{aligned} \tag{I.2.8}$$

where in the last line the abbreviation $\mathfrak{b}_c\left(\eta^{(j)},\mathbf{k},\omega\right)\equiv\mathfrak{b}^{(j)}_c(\mathbf{k},\omega)$ and the cartesian components of the 3×3 matrix of lattice sums

$$\left[\zeta^{(\mathrm{mag})}_{\Lambda}(\mathbf{s},\mathbf{k},\omega)\right]_{ab}=\begin{cases}\sum_{\mathbf{R}\in\Lambda}e^{-i\mathbf{k}\cdot(\mathbf{s}+\mathbf{R})}\mathscr{G}^{(\mathrm{mag})}_{ab}(\mathbf{s}+\mathbf{R},\omega) & \text{if } \mathbf{s}\neq\mathbf{0}\\ \sum_{\mathbf{R}\in\Lambda\setminus\{\mathbf{0}\}}e^{-i\mathbf{k}\cdot\mathbf{R}}\mathscr{G}^{(\mathrm{mag})}_{ab}(\mathbf{R},\omega) & \text{if } \mathbf{s}=\mathbf{0}\end{cases} \tag{I.2.9}$$

[4]For calculational details, see appendix I.4.1.

have been introduced. Similar to the definition of $\zeta_\Lambda(\mathbf{s},\mathbf{k},\omega)$ in (3.2.21), the definition of $\zeta_\Lambda^{(\mathrm{mag})}(\mathbf{s},\mathbf{k},\omega)$ by cases ensures that an atom/ion is *not* magnetized by its self-generated magnetic induction field if $\mathbf{s}=\mathbf{0}$. Obviously, $\zeta_\Lambda^{(\mathrm{mag})}(\mathbf{s},\mathbf{k},\omega)$ is invariant with respect to a translation by any lattice vector $\mathbf{R}'\in\Lambda$ if $\mathbf{s}\neq\mathbf{0}$, so that

$$\zeta_\Lambda^{(\mathrm{mag})}\left(\mathbf{s}+\mathbf{R}',\mathbf{k},\omega\right)=\zeta_\Lambda^{(\mathrm{mag})}(\mathbf{s},\mathbf{k},\omega)\,. \tag{I.2.10}$$

In this case, $\zeta_\Lambda^{(\mathrm{mag})}(\mathbf{s},\mathbf{k},\omega)$ possesses the Fourier series representation[5]

$$\left[\zeta_\Lambda^{(\mathrm{mag})}(\mathbf{s},\mathbf{k},\omega)\right]_{ab}=\frac{1}{|C_\Lambda|}\sum_{\mathbf{G}\in\Lambda^{-1}}e^{i\mathbf{G}\cdot\mathbf{s}}\tilde{\mathscr{G}}_{ab}^{(\mathrm{mag})}(\mathbf{k}+\mathbf{G},\omega) \tag{I.2.11}$$

with

$$\tilde{\mathscr{G}}_{ab}^{(\mathrm{mag})}(\mathbf{k},\omega)=\frac{k_ak_b-\delta_{ab}|\mathbf{k}|^2}{|\mathbf{k}|^2-\frac{\omega^2}{c^2}}=-\frac{|\mathbf{k}|^2}{|\mathbf{k}|^2-\frac{\omega^2}{c^2}}\tilde{\Pi}_{ab}^{(\mathrm{T})}(\mathbf{k})\,. \tag{I.2.12}$$

Special attention has to be paid to the definition by cases of $\zeta_\Lambda^{(\mathrm{mag})}(\mathbf{s},\mathbf{k},\omega)$ in (I.2.9), because of

$$\zeta_\Lambda^{(0)(\mathrm{mag})}(\mathbf{k},\omega)\equiv\zeta_\Lambda^{(\mathrm{mag})}(\mathbf{0},\mathbf{k},\omega)\neq\lim_{|\mathbf{s}|\to0}\zeta_\Lambda^{(\mathrm{mag})}(\mathbf{s},\mathbf{k},\omega)\,. \tag{I.2.13}$$

Instead there holds

$$\zeta_\Lambda^{(0)(\mathrm{mag})}(\mathbf{k},\omega)=\lim_{|\mathbf{s}|\to0}\left(\zeta_\Lambda^{(\mathrm{mag})}(\mathbf{s},\mathbf{k},\omega)-\mathscr{G}_{ab}^{(\mathrm{mag})}(\mathbf{s},\omega)\right). \tag{I.2.14}$$

According to (I.2.8), the expansion coefficients $\mathfrak{b}_a(\mathbf{s},\mathbf{k},\omega)$ for any point $\mathbf{s}\in C_\Lambda$ are completely determined by the expansion coefficients $\mathfrak{b}_c^{(j)}(\mathbf{k},\omega)$ at the atomic positions $\eta^{(j)}\in C_\Lambda$. The latter can be obtained by taking successively the limit $\mathbf{s}\to\eta^{(j')}$ for each $j'\in\{1,2,\ldots,M\}$ in (I.2.8). There follows[6]

$$\mathfrak{b}_a^{(j')}(\mathbf{k},\omega)=\mathfrak{b}_{\mathrm{ext},a}^{(j')}(\mathbf{k},\omega)-\mu_0\sum_{b,c=1}^{3}\sum_{j=1}^{M}\left[\zeta_\Lambda^{(\mathrm{mag})}\left(\eta^{(j')}-\eta^{(j)},\mathbf{k},\omega\right)\right]_{ab}\beta_{bc}^{(j)}(\omega)\,\mathfrak{b}_c^{(j)}(\mathbf{k},\omega)\,, \tag{I.2.15}$$

where $\mathfrak{b}_{\mathrm{ext},a}^{(j)}(\mathbf{k},\omega)\equiv\mathfrak{b}_{\mathrm{ext},a}\left(\eta^{(j)},\mathbf{k},\omega\right)$ has been abbreviated. Introducing the notation

$$\delta_{ac}^{(j',j)}=\delta_{j'j}\delta_{ac} \tag{I.2.16}$$

$$\Gamma_{ac}^{(\mathrm{mag})(j',j)}(\mathbf{k},\omega)=\mu_0\sum_{b=1}^{3}\left[\zeta_\Lambda^{(\mathrm{mag})}\left(\eta^{(j')}-\eta^{(j)},\mathbf{k},\omega\right)\right]_{ab}\beta_{bc}^{(j)}(\omega)\,, \tag{I.2.17}$$

(I.2.15) can be cast into

$$\sum_{c=1}^{3}\sum_{j=1}^{M}\left[\delta_{ac}^{(j',j)}+\Gamma_{ac}^{(\mathrm{mag})(j',j)}(\mathbf{k},\omega)\right]\mathfrak{b}_c^{(j)}(\mathbf{k},\omega)=\mathfrak{b}_{\mathrm{ext},a}^{(j')}(\mathbf{k},\omega)\,, \tag{I.2.18}$$

[5] For a derivation of (I.2.11), see appendix I.4.2.

[6] For technical details, see the electric analogue in section 3.2 and appendix E.2, respectively.

so that the explicit solution for $\mathfrak{b}_c^{(j)}(\mathbf{k},\omega)$ is given by

$$\mathfrak{b}_c^{(j)}(\mathbf{k},\omega)=\sum_{d=1}^{3}\sum_{j'=1}^{M}\left[\left(\delta+\Gamma^{(\mathrm{mag})}(\mathbf{k},\omega)\right)^{-1}\right]_{cd}^{(jj')}\mathfrak{b}_{\mathrm{ext},d}^{(j')}(\mathbf{k},\omega). \tag{I.2.19}$$

Deploying (I.2.19) to (I.2.8) finally determines the expansion coefficients $\mathfrak{b}_a(\mathbf{s},\mathbf{k},\omega)$ for any $\mathbf{s}\in C_\Lambda$. The local magnetic induction field within an infinitely extended magnetizable crystalline material then reads[7]

$$\begin{aligned}B_a(\mathbf{r},\omega)=&B_{\mathrm{ext},a}(\mathbf{r},\omega)-\frac{\mu_0}{\sqrt{N_\mathrm{P}}}\frac{|\Omega_\mathrm{P}|}{(2\pi)^3}\sum_{b,c,d=1}^{3}\sum_{j,j'=1}^{M}\int_{C_{\Lambda^{-1}}}d^3k\\&\cdot e^{i\mathbf{k}\cdot\mathbf{r}}\left[\zeta_\Lambda^{(\mathrm{mag})}\left(\mathbf{r}-\eta^{(j)},\mathbf{k},\omega\right)\right]_{ab}\beta_{bc}^{(j)}(\omega)\left[\left(\delta+\Gamma^{(\mathrm{mag})}(\mathbf{k},\omega)\right)^{-1}\right]_{cd}^{(jj')}\mathfrak{b}_{\mathrm{ext},d}^{(j')}(\mathbf{k},\omega).\end{aligned} \tag{I.2.20}$$

Because $B_{\mathrm{ext},a}(\mathbf{r},\omega)$ represents a solution to an *inhomogeneous* Helmholtz equation (see (2.2.11)) with an externally controlled source term located at finite distance to the probe volume (see figure 2.2.1), its expansion with respect to the basis system of plane waves for fixed frequency ω

$$B_{\mathrm{ext},a}(\mathbf{r},\omega)=\sum_{\mathbf{q}'}\tilde{B}_{\mathbf{q}'\omega,a}^{(\mathrm{ext})}e^{i\mathbf{q}'\cdot\mathbf{r}} \tag{I.2.21}$$

comprises a bunch of wave vectors $\mathbf{q}'$. Thus, there is no justification to hang on to the common dispersion relation in vacuum $|\mathbf{q}'|=\frac{\omega}{c}$. Instead, $\mathbf{q}'$ and ω can be treated as *independent* variables. Assuming from now on the externally applied magnetic induction field $B_{\mathrm{ext},a}(\mathbf{r},\omega)$ to consist of a single beam of wave vector $\mathbf{q}\in C_{\Lambda^{-1}}$, (I.2.21) reduces to

$$B_{\mathrm{ext},a}(\mathbf{r},\omega)=\tilde{B}_{\mathbf{q}\omega,a}^{(\mathrm{ext})}e^{i\mathbf{q}\cdot\mathbf{r}}, \tag{I.2.22}$$

where the corresponding Fourier transform in reciprocal space is given by

$$\tilde{B}_{\mathrm{ext},a}(\mathbf{k},\omega)=\int_{\mathbb{R}^3}d^3r\,e^{-i\mathbf{k}\cdot\mathbf{r}}B_{\mathrm{ext},a}(\mathbf{r},\omega)=(2\pi)^3\,\delta(\mathbf{k}-\mathbf{q})\,\tilde{B}_{\mathbf{q}\omega,a}^{(\mathrm{ext})}. \tag{I.2.23}$$

Accordingly, a simple relation between the expansion coefficients $\mathfrak{b}_{\mathrm{ext},a}(\mathbf{s},\mathbf{k},\omega)$ and $\tilde{B}_{\mathbf{q}\omega,a}^{(\mathrm{ext})}$ can be established[8]

$$\mathfrak{b}_{\mathrm{ext},a}(\mathbf{s},\mathbf{k},\omega)=\frac{e^{-i\mathbf{k}\cdot\mathbf{s}}}{\sqrt{N_\mathrm{P}}}\frac{(2\pi)^3}{|C_\Lambda|}\tilde{B}_{\mathbf{q}\omega,a}^{(\mathrm{ext})}e^{i\mathbf{q}\cdot\mathbf{s}}\delta(\mathbf{k}-\mathbf{q}). \tag{I.2.24}$$

[7] For calculational details, see appendix I.4.3.

[8] The derivation of (I.2.24) is completely analogue to that of (3.2.34). Therefore see appendix E.4.

Combining (I.2.20) with (I.2.24), the local magnetic induction field reads

$$B_a(\mathbf{r},\omega) = B_{\mathrm{ext},a}(\mathbf{r},\omega) - \mu_0 \sum_{b,c,d=1}^{3} \sum_{j,j'=1}^{M} \cdot \left[\zeta_\Lambda^{(\mathrm{mag})}\left(\mathbf{r}-\eta^{(j)},\mathbf{q},\omega\right)\right]_{ab} \beta_{bc}^{(j)}(\omega) \left[\left(\delta + \Gamma^{(\mathrm{mag})}(\mathbf{q},\omega)\right)^{-1}\right]_{cd}^{(jj')} \tilde{B}_{\mathbf{q}\omega,d}^{(\mathrm{ext})} e^{i\mathbf{q}\cdot\mathbf{r}}. \quad \text{(I.2.25)}$$

Finally, utilizing the Fourier series representation (I.2.11) of the lattice sum $\zeta_\Lambda^{(\mathrm{mag})}\left(\mathbf{r}-\eta^{(j)},\mathbf{q},\omega\right)$ in (I.2.25) and introducing the kernel

$$\tilde{K}_{bd}^{(\mathrm{mag})}(\mathbf{G},\mathbf{q},\omega) = \mu_0 \sum_{c=1}^{3} \sum_{j,j'=1}^{M} e^{-i\mathbf{G}\cdot\eta^{(j)}} \beta_{bc}^{(j)}(\omega) \left[\left(\delta + \Gamma^{(\mathrm{mag})}(\mathbf{q},\omega)\right)^{-1}\right]_{cd}^{(jj')}, \quad \text{(I.2.26)}$$

the local magnetic induction field $B_a(\mathbf{r},\omega)$ can be written as

$$B_a(\mathbf{r},\omega) = B_{\mathrm{ext},a}(\mathbf{r},\omega) - \frac{1}{|C_\Lambda|} \sum_{b,d=1}^{3} \sum_{\mathbf{G}\in\Lambda^{-1}} e^{i(\mathbf{q}+\mathbf{G})\cdot\mathbf{r}} \tilde{\mathscr{G}}_{ab}^{(\mathrm{mag})}(\mathbf{q}+\mathbf{G},\omega) \tilde{K}_{bd}^{(\mathrm{mag})}(\mathbf{G},\mathbf{q},\omega) \tilde{B}_{\mathbf{q}\omega,d}^{(\mathrm{ext})}, \quad \text{(I.2.27)}$$

provided that $\mathbf{r}$ does not coincide with an atomic position $\eta^{(j)}$. Notice that (I.2.12) ensures, that a transverse externally applied magnetic induction field always induces a purely transverse (i.e. a divergence-free) local magnetic induction field, as can easily be checked by applying the longitudinal projection operator in real space to (I.2.27). This is in contrast to the electric field case (see sections 3.2 and 3.4).

Starting from the local field equations established in this section, the macroscopic magnetic induction field as well as the macroscopic magnetization will be calculated in the next section in order to derive an equation determining the magnetic permeability tensor.

I.3 Macroscopic magnetic induction field in magnetizable crystals and the magnetic permeability tensor

Similar to the local electromagnetic field in dielectric crystals (see chapter 3), the local magnetic induction field $B_a(\mathbf{r},\omega)$ in magnetizable crystalline materials given by (I.2.27) comprises rapid spatial variations because of terms varying like $e^{i\mathbf{G}\cdot\mathbf{r}}$ with $\mathbf{G}\in\Lambda^{-1}\setminus\{\mathbf{0}\}$ on the back of the slowly varying envelope behaving like $e^{i\mathbf{q}\cdot\mathbf{r}}$ with $\mathbf{q}\in C_{\Lambda^{-1}}$, the latter describing the spatial variation of the macroscopic magnetic induction field $\mathscr{B}_a(\mathbf{r},\omega)$. Following the lines indicated in section 4.1, the macroscopic magnetic induction field $\mathscr{B}_a(\mathbf{r},\omega)$ is obtained by low-pass filtering the local field $B_a(\mathbf{r},\omega)$. The Fourier amplitude of $\mathscr{B}_a(\mathbf{r},\omega)$ is thus given by

$$\tilde{\mathscr{B}}_a(\mathbf{q}',\omega) = \int_{\mathbb{R}^3} d^3r\, e^{-i\mathbf{q}'\cdot\mathbf{r}} B_a(\mathbf{r},\omega) \quad \text{with} \quad \mathbf{q}'\in C_{\Lambda^{-1}}, \quad \text{(I.3.1)}$$

so that in real space

$$\mathscr{B}_a(\mathbf{r},\omega) = \frac{1}{(2\pi)^3}\int_{C_{\Lambda^{-1}}} d^3q'\, e^{i\mathbf{q}'\cdot\mathbf{r}}\tilde{\mathscr{B}}_a(\mathbf{q}',\omega) \tag{I.3.2}$$

holds. Introducing the abbreviation

$$\tilde{K}^{(\mathrm{mag})}_{bd}(\mathbf{q},\omega) \equiv \tilde{K}^{(\mathrm{mag})}_{bd}(\mathbf{0},\mathbf{q},\omega) = \mu_0 \sum_{c=1}^{3}\sum_{j,j'=1}^{M} \beta^{(j)}_{bc}(\omega)\left[\left(\delta + \Gamma^{(\mathrm{mag})}(\mathbf{q},\omega)\right)^{-1}\right]^{(jj')}_{cd} \tag{I.3.3}$$

and combining (I.2.27) with (I.3.1), then yields for the Fourier amplitude of the macroscopic magnetic induction field

$$\begin{aligned}
&\tilde{\mathscr{B}}_a(\mathbf{q}',\omega)\\
&= \int_{\mathbb{R}^3} d^3r\, e^{-i\mathbf{q}'\cdot\mathbf{r}}\left(B_{\mathrm{ext},a}(\mathbf{r},\omega) - \frac{1}{|C_\Lambda|}\sum_{b,d=1}^{3}\sum_{\mathbf{G}\in\Lambda^{-1}} e^{i(\mathbf{q}+\mathbf{G})\cdot\mathbf{r}}\tilde{\mathscr{G}}^{(\mathrm{mag})}_{ab}(\mathbf{q}+\mathbf{G},\omega)\,\tilde{K}^{(\mathrm{mag})}_{bd}(\mathbf{G},\mathbf{q},\omega)\,\tilde{B}^{(\mathrm{ext})}_{\mathbf{q}\omega,d}\right)\\
&= (2\pi)^3\,\delta(\mathbf{q}'-\mathbf{q})\left[\tilde{B}^{(\mathrm{ext})}_{\mathbf{q}\omega,a} - \frac{1}{|C_\Lambda|}\sum_{b,d=1}^{3}\tilde{\mathscr{G}}^{(\mathrm{mag})}_{ab}(\mathbf{q},\omega)\,\tilde{K}^{(\mathrm{mag})}_{bd}(\mathbf{q},\omega)\,\tilde{B}^{(\mathrm{ext})}_{\mathbf{q}\omega,d}\right].
\end{aligned} \tag{I.3.4}$$

In real space (I.3.4) then corresponds to

$$\mathscr{B}_a(\mathbf{r},\omega) = \tilde{B}^{(\mathrm{ext})}_{\mathbf{q}\omega,a}e^{i\mathbf{q}\cdot\mathbf{r}} - \frac{1}{|C_\Lambda|}\sum_{b,d=1}^{3}\tilde{\mathscr{G}}^{(\mathrm{mag})}_{ab}(\mathbf{q},\omega)\,\tilde{K}^{(\mathrm{mag})}_{bd}(\mathbf{q},\omega)\,\tilde{B}^{(\mathrm{ext})}_{\mathbf{q}\omega,d}e^{i\mathbf{q}\cdot\mathbf{r}}. \tag{I.3.5}$$

Applying this low-pass filtering process to the microscopic magnetization $M_a(\mathbf{r},\omega)$ given by (I.1.3), the macroscopic magnetization $\mathscr{M}_a(\mathbf{r},\omega)$ is obtained. First, the low-pass filtered Fourier amplitude of $M_a(\mathbf{r},\omega)$ is calculated[9] according to

$$\begin{aligned}
\tilde{\mathscr{M}}_a(\mathbf{q}',\omega) &= \int_{\mathbb{R}^3} d^3r\, e^{-i\mathbf{q}'\cdot\mathbf{r}} M_a(\mathbf{r},\omega) \quad \text{with} \quad \mathbf{q}' \in C_{\Lambda^{-1}}\\
&= \frac{1}{\mu_0}\frac{(2\pi)^3}{|C_\Lambda|}\delta(\mathbf{q}'-\mathbf{q})\sum_{b=1}^{3}\tilde{K}^{(\mathrm{mag})}_{ab}(\mathbf{q},\omega)\,\tilde{B}^{(\mathrm{ext})}_{\mathbf{q}\omega,b},
\end{aligned} \tag{I.3.6}$$

so that in real space

$$\begin{aligned}
\mathscr{M}_a(\mathbf{r},\omega) &= \frac{1}{(2\pi)^3}\int_{C_{\Lambda^{-1}}} d^3q'\, e^{i\mathbf{q}'\cdot\mathbf{r}}\tilde{\mathscr{M}}_a(\mathbf{q}',\omega)\\
&= \frac{1}{\mu_0}\frac{1}{|C_\Lambda|}\sum_{b=1}^{3}\tilde{K}^{(\mathrm{mag})}_{ab}(\mathbf{q},\omega)\,\tilde{B}^{(\mathrm{ext})}_{\mathbf{q}\omega,b}e^{i\mathbf{q}\cdot\mathbf{r}}
\end{aligned} \tag{I.3.7}$$

[9] For a derivation of (I.3.6), see appendix I.4.4.

results. With the help of (I.3.7), the macroscopic magnetic induction field given by (I.3.5) can be cast into

$$\mathscr{B}_a(\mathbf{r},\omega) = \tilde{B}^{(\mathrm{ext})}_{\mathbf{q}\omega,a} e^{i\mathbf{q}\cdot\mathbf{r}} - \mu_0 \sum_{b=1}^{3} \tilde{\mathscr{G}}^{(\mathrm{mag})}_{ab}(\mathbf{q},\omega)\, \mathscr{M}_b(\mathbf{r},\omega), \tag{I.3.8}$$

which reflects Lorentz's local field correction for magnetizable crystalline materials[10]. Now, the 3×3 magnetic permeability tensor $\mu_\Lambda(\mathbf{q},\omega)$ can be introduced with the help of the material equations

$$\tilde{\mathscr{B}}(\mathbf{q},\omega) = \mu_0 \mu_\Lambda(\mathbf{q},\omega)\cdot\tilde{\mathscr{H}}(\mathbf{q},\omega) \tag{I.3.9}$$

$$\tilde{\mathscr{B}}(\mathbf{q},\omega) = \mu_0\left(\tilde{\mathscr{H}}(\mathbf{q},\omega) + \tilde{\mathscr{M}}(\mathbf{q},\omega)\right), \tag{I.3.10}$$

that are well-known from macroscopic electrodynamics. Eliminating the Fourier amplitude of the macroscopic magnetic field $\tilde{\mathscr{H}}(\mathbf{q},\omega)$ readily yields an equation determining $\mu_\Lambda(\mathbf{q},\omega)$ in terms of the known quantities $\tilde{\mathscr{B}}(\mathbf{q},\omega)$ and $\tilde{\mathscr{M}}(\mathbf{q},\omega)$ according to

$$\left(\delta - \mu_\Lambda^{-1}(\mathbf{q},\omega)\right)\cdot\tilde{\mathscr{B}}(\mathbf{q},\omega) = \mu_0\tilde{\mathscr{M}}(\mathbf{q},\omega). \tag{I.3.11}$$

With (I.3.4) and (I.3.6) there follows

$$\left(\delta - \mu_\Lambda^{-1}(\mathbf{q},\omega)\right)\circ\left[\delta - \frac{1}{|C_\Lambda|}\tilde{\mathscr{G}}^{(\mathrm{mag})}(\mathbf{q},\omega)\circ\tilde{K}^{(\mathrm{mag})}(\mathbf{q},\omega)\right]\cdot\tilde{\mathbf{B}}^{(\mathrm{ext})}_{\mathbf{q}\omega} = \frac{1}{|C_\Lambda|}\tilde{K}^{(\mathrm{mag})}(\mathbf{q},\omega)\cdot\tilde{\mathbf{B}}^{(\mathrm{ext})}_{\mathbf{q}\omega}, \tag{I.3.12}$$

so that the magnetic permeability tensor can be finally identified with

$$\begin{aligned}\mu_\Lambda(\mathbf{q},\omega) &= \left[\delta - \frac{1}{|C_\Lambda|}\tilde{K}^{(\mathrm{mag})}(\mathbf{q},\omega)\circ\left(\delta - \frac{1}{|C_\Lambda|}\tilde{\mathscr{G}}^{(\mathrm{mag})}(\mathbf{q},\omega)\circ\tilde{K}^{(\mathrm{mag})}(\mathbf{q},\omega)\right)^{-1}\right]^{-1} \\ &= \left[\delta - \frac{1}{|C_\Lambda|}\left(\left[\tilde{K}^{(\mathrm{mag})}(\mathbf{q},\omega)\right]^{-1} - \frac{1}{|C_\Lambda|}\tilde{\mathscr{G}}^{(\mathrm{mag})}(\mathbf{q},\omega)\right)^{-1}\right]^{-1}.\end{aligned} \tag{I.3.13}$$

Notice, that the physical meaning of the concept of the magnetic permeability tensor is strongly limited in contrast to the concept of the dielectric tensor. Two reasons for this are the following. As has been pointed out by Landau [138], the concept of a magnetic permeability does only make sense at rather low frequencies, i.e. it is only applicable for frequencies well below the regime of visible light. Additionally it has been emphasized by several authors [1, 2, 29], that the mathematical structure of the macroscopic Maxwell equations allows to include magnetic effects described by $\mu_\Lambda(\mathbf{q},\omega)$ into the $\mathbf{q}$-dependence of the dielectric kernel, so that the latter constitutes the quantity of fundamental interest.

[10] Compare with (4.1.14) for crystalline dielectrics.

I.3.1 Static limit for monatomic Bravais lattices

To conclude the discussion on magnetizable crystalline materials, the static limit of the magnetic permeability tensor $\mu_\Lambda(\mathbf{q},\omega)$ as well as that of the macroscopic magnetic induction field $\mathscr{B}(\mathbf{r},\omega)$ are derived for monatomic (i.e. $M=1$) crystal structures. Without loss of generality, the atom is assumed to be located at the origin $\eta^{(1)}=\mathbf{0}$ of the Wigner-Seitz cell C_Λ, so that with $\beta_{bc}^{(1)}(\omega)\equiv\beta_{bc}(\omega)$ (I.3.3) assumes the guise

$$\tilde{K}^{(\mathrm{mag})}(\mathbf{q},\omega)=\mu_0\beta(\omega)\circ\left(\delta+\mu_0\zeta_\Lambda^{(0)(\mathrm{mag})}(\mathbf{q},\omega)\circ\beta(\omega)\right)^{-1}. \tag{I.3.14}$$

The magnetic permeability tensor given by (I.3.13) then reads for monatomic crystal structures

$$\mu_\Lambda(\mathbf{q},\omega)=\left[\delta-\frac{1}{|C_\Lambda|}\left[\frac{1}{\mu_0}\beta^{-1}(\omega)+\left(\zeta_\Lambda^{(0)(\mathrm{mag})}(\mathbf{q},\omega)-\frac{1}{|C_\Lambda|}\tilde{\mathscr{G}}^{(\mathrm{mag})}(\mathbf{q},\omega)\right)\right]^{-1}\right]^{-1}. \tag{I.3.15}$$

Its static limit is obtained by first taking $|\mathbf{q}|\to 0$ and subsequently $\omega\to 0$, so that with the introduction of the 3×3 matrices

$$\mu_\Lambda\equiv\lim_{\omega\to 0}\lim_{|\mathbf{q}|\to 0}\mu_\Lambda(\mathbf{q},\omega) \tag{I.3.16}$$

$$\beta\equiv\lim_{\omega\to 0}\beta(\omega) \tag{I.3.17}$$

$$\mathscr{L}^{(\mathrm{mag})}=|C_\Lambda|\lim_{\omega\to 0}\lim_{|\mathbf{q}|\to 0}\left(\zeta_\Lambda^{(0)(\mathrm{mag})}(\mathbf{q},\omega)-\frac{1}{|C_\Lambda|}\tilde{\mathscr{G}}^{(\mathrm{mag})}(\mathbf{q},\omega)\right) \tag{I.3.18}$$

there finally follows[11]

$$\begin{aligned}\mu_\Lambda&=\left[\delta-\frac{1}{|C_\Lambda|}\left[\frac{1}{\mu_0}\beta^{-1}+\frac{1}{|C_\Lambda|}\mathscr{L}^{(\mathrm{mag})}\right]^{-1}\right]^{-1}\\&=\left(\delta+\mu_0\nu_\mathrm{P}\mathscr{L}^{(\mathrm{mag})}\circ\beta\right)\circ\left(\delta-\mu_0\nu_\mathrm{P}\left(\delta-\mathscr{L}^{(\mathrm{mag})}\right)\circ\beta\right)^{-1},\end{aligned} \tag{I.3.19}$$

where in the second line the density of (magnetizable) atoms/ions has been identified as $\nu_\mathrm{P}=\frac{1}{|C_\Lambda|}$. The 3×3 tensor $\mathscr{L}^{(\mathrm{mag})}$ can be understood as the magnetic analogue to the Lorentz factor tensor $\mathscr{L}$ defined in (4.4.4). It is independent of the geometrical shape of the crystal but incorporates its symmetry due to the lattice sum $\left(\zeta_\Lambda^{(0)(\mathrm{mag})}(\mathbf{q},\omega)-\frac{1}{|C_\Lambda|}\tilde{\mathscr{G}}^{(\mathrm{mag})}(\mathbf{q},\omega)\right)$ and should thus not be confused with the demagnetization factor, which constitutes a pure geometrical quantity.

Finally, consider the special case of a simple cubic crystal structure. As has been shown in appendix

[11] Compare the structure of μ_Λ in (I.3.19) with that of ε_Λ in (4.4.5).

I.4.5, there holds $\mathscr{L}_{ab}^{(\mathrm{mag})} = \frac{2}{3}\delta_{ab}$, so that the static magnetic permeability tensor (I.3.19) reads

$$\mu_\Lambda = \left(\delta + \frac{2}{3}\mu_0 \nu_\mathrm{P} \beta\right) \circ \left(\delta - \frac{1}{3}\mu_0 \nu_\mathrm{P} \beta\right)^{-1}, \tag{I.3.20}$$

which is in total accordance with [140]. It should be noticed, that (I.3.20) is a Clausius-Mossotti type formula similar to (4.4.9), however the latter has been derived for the static dielectric tensor. Additionally, with the abbreviations

$$\begin{aligned} \lim_{\omega\to 0} \mathscr{B}(\mathbf{r},\omega) &\equiv \mathscr{B}(\mathbf{r}) \\ \lim_{\omega\to 0}\lim_{|\mathbf{q}|\to 0} \tilde{\mathbf{B}}_{\mathbf{q}\omega}^{(\mathrm{ext})} &\equiv \tilde{\mathbf{B}}^{(\mathrm{ext})} \\ \lim_{\omega\to 0} \mathscr{M}(\mathbf{r},\omega) &\equiv \mathscr{M}(\mathbf{r}) \end{aligned} \tag{I.3.21}$$

and (I.4.32), the macroscopic magnetic induction field given by (I.3.8) now assumes the guise

$$\mathscr{B}(\mathbf{r}) = \tilde{\mathbf{B}}^{(\mathrm{ext})} + \frac{2}{3}\mu_0 \mathscr{M}(\mathbf{r}) \tag{I.3.22}$$

and thus agrees with the result obtained in [58]. It is interesting to note, that the expression of the static magnetic permeability (I.3.20) for monatomic simple cubic crystal structures can be obtained from that of the static dielectric tensor (4.4.9) by making the simple replacements $\varepsilon_\Lambda \to \mu_\Lambda$, $\frac{1}{\varepsilon_0} \to \mu_0$ and $\alpha \to \beta$, although the local field corrections in both cases (compare footnote to (4.1.14) with (I.3.22)) differ by a factor of minus two.

I.4 Auxiliary calculations

This section serves as an appendix of the current chapter and provides auxiliary calculations, that are related to the model of magnetizable crystals.

I.4.1 Calculation of the matrix elements $\langle \mathbf{s},\mathbf{k} \left| \left[\mathscr{G}^{(\mathbf{mag})} \circ \chi^{(\mathbf{mag})}\right]_{ab} \right| \mathbf{s}',\mathbf{k}' \rangle$

The matrix elements $\langle \mathbf{s},\mathbf{k} \left| \left[\mathscr{G}^{(\mathrm{mag})} \circ \chi^{(\mathrm{mag})}\right]_{ab} \right| \mathbf{s}',\mathbf{k}' \rangle$ are defined by (I.2.5) according to

$$\langle \mathbf{s},\mathbf{k} \left| \left[\mathscr{G}^{(\mathrm{mag})} \circ \chi^{(\mathrm{mag})}\right]_{ab} \right| \mathbf{s}',\mathbf{k}' \rangle \equiv \int_{\Omega_\mathrm{P}} d^3r \int_{\mathbb{R}^3} d^3r'\, w^\dagger(\mathbf{r};\mathbf{s},\mathbf{k}) \left[\mathscr{G}^{(\mathrm{mag})} \circ \chi^{(\mathrm{mag})}\right]_{ab} (\mathbf{r},\mathbf{r}',\omega)\, w(\mathbf{r}';\mathbf{s}',\mathbf{k}'), \tag{I.4.1}$$

where

$$\left[\mathscr{G}^{(\mathrm{mag})} \circ \chi^{(\mathrm{mag})}\right]_{ab} (\mathbf{r},\mathbf{r}',\omega) = \sum_{c=1}^{3} \int_{\mathbb{R}^3} d^3r''\, \mathscr{G}_{ac}^{(\mathrm{mag})}(\mathbf{r}-\mathbf{r}'',\omega)\, \chi_{cb}^{(\mathrm{mag})}(\mathbf{r}'',\mathbf{r}',\omega) \tag{I.4.2}$$

(see (I.1.15)). By inserting the magnetic susceptibility kernel given by (I.1.4) into (I.4.2), one readily obtains

$$\left[\mathscr{G}^{(\mathrm{mag})}\circ\chi^{(\mathrm{mag})}\right]_{ab}(\mathbf{r},\mathbf{r}',\omega)=\mu_0\sum_{c=1}^{3}\sum_{j=1}^{M}\sum_{\mathbf{R}\in\Lambda_{\mathrm{P}}}\mathscr{G}^{(\mathrm{mag})}_{ac}(\mathbf{r}-\mathbf{r}',\omega)\,\beta^{(j)}_{cb}(\omega)\,\delta\left(\mathbf{r}'-\mathbf{R}-\eta^{(j)}\right). \quad \text{(I.4.3)}$$

Making use of the non-standard system of Bloch functions $\{w(\mathbf{r};\mathbf{s},\mathbf{k})\}_{\mathbf{s}\in C_\Lambda,\mathbf{k}\in C_{\Lambda^{-1}}}$ introduced in (3.2.9), the matrix elements $\langle\mathbf{s},\mathbf{k}\,|\left[\mathscr{G}^{(\mathrm{mag})}\circ\chi^{(\mathrm{mag})}\right]_{ab}|\,\mathbf{s}',\mathbf{k}'\rangle$ assume the guise

$$\begin{aligned}
&\langle\mathbf{s},\mathbf{k}\left|\left[\mathscr{G}^{(\mathrm{mag})}\circ\chi^{(\mathrm{mag})}\right]_{ab}\right|\mathbf{s}',\mathbf{k}'\rangle\\
=&\frac{1}{N_{\mathrm{P}}}\sum_{\mathbf{R}',\mathbf{R}''\in\Lambda}\int_{\Omega_{\mathrm{P}}}d^3r\,\delta\left(\mathbf{r}-\mathbf{s}-\mathbf{R}'\right)e^{-i\mathbf{k}\cdot\mathbf{r}}\int_{\mathbb{R}^3}d^3r'\,\delta\left(\mathbf{r}'-\mathbf{s}'-\mathbf{R}''\right)e^{i\mathbf{k}'\cdot\mathbf{r}'}\left[\mathscr{G}^{(\mathrm{mag})}\circ\chi^{(\mathrm{mag})}\right]_{ab}(\mathbf{r},\mathbf{r}',\omega)\\
=&\frac{1}{N_{\mathrm{P}}}\sum_{\mathbf{R}'\in\Lambda_{\mathrm{P}}}\sum_{\mathbf{R}''\in\Lambda}e^{-i\mathbf{k}\cdot(\mathbf{s}+\mathbf{R}')}\left[\mathscr{G}^{(\mathrm{mag})}\circ\chi^{(\mathrm{mag})}\right]_{ab}(\mathbf{s}+\mathbf{R}',\mathbf{s}'+\mathbf{R}'',\omega)\,e^{i\mathbf{k}'\cdot(\mathbf{s}'+\mathbf{R}'')}. \quad \text{(I.4.4)}
\end{aligned}$$

Subsequent deployment of (I.4.3) then yields

$$\begin{aligned}
&\langle\mathbf{s},\mathbf{k}\left|\left[\mathscr{G}^{(\mathrm{mag})}\circ\chi^{(\mathrm{mag})}\right]_{ab}\right|\mathbf{s}',\mathbf{k}'\rangle\\
=&\frac{\mu_0}{N_{\mathrm{P}}}\sum_{c=1}^{3}\sum_{j=1}^{M}\sum_{\mathbf{R},\mathbf{R}'\in\Lambda_{\mathrm{P}}}\delta\left(\mathbf{s}'-\eta^{(j)}\right)e^{-i\mathbf{k}\cdot(\mathbf{s}+\mathbf{R}')}\mathscr{G}^{(\mathrm{mag})}_{ac}(\mathbf{s}+\mathbf{R}'-\mathbf{s}'-\mathbf{R},\omega)\,\beta^{(j)}_{cb}(\omega)\,e^{i\mathbf{k}'\cdot(\mathbf{s}'+\mathbf{R})}. \quad \text{(I.4.5)}
\end{aligned}$$

Assuming from now on the crystal to be of infinite extent, i.e. $\Lambda_{\mathrm{P}}=\Lambda$, the index transformation $\mathbf{R}''=\mathbf{R}'-\mathbf{R}$ with subsequent application of the identity (E.1.9) finally results in

$$\begin{aligned}
&\langle\mathbf{s},\mathbf{k}\left|\left[\mathscr{G}^{(\mathrm{mag})}\circ\chi^{(\mathrm{mag})}\right]_{ab}\right|\mathbf{s}',\mathbf{k}'\rangle\\
=&\frac{\mu_0}{N_{\mathrm{P}}}\frac{(2\pi)^3}{|C_\Lambda|}\sum_{c=1}^{3}\sum_{j=1}^{M}\sum_{\mathbf{R}'\in\Lambda}e^{i\mathbf{k}'\cdot\mathbf{s}'}e^{-i\mathbf{k}\cdot(\mathbf{s}+\mathbf{R}')}\mathscr{G}^{(\mathrm{mag})}_{ac}(\mathbf{s}+\mathbf{R}'-\mathbf{s}',\omega)\,\beta^{(j)}_{cb}(\omega)\,\delta\left(\mathbf{s}'-\eta^{(j)}\right)\delta(\mathbf{k}-\mathbf{k}'). \quad \text{(I.4.6)}
\end{aligned}$$

I.4.2 Fourier series representation of $\zeta^{(\mathbf{mag})}_{\Lambda}(\mathbf{s},\mathbf{k},\omega)$

Applying the Fourier integral representation of the Helmholtz propagator

$$g(\mathbf{r}-\mathbf{r}',\omega)=\frac{1}{(2\pi)^3}\int_{\mathbb{R}^3}d^3k\,e^{i\mathbf{k}\cdot(\mathbf{r}-\mathbf{r}')}\frac{1}{|\mathbf{k}|^2-\frac{\omega^2}{c^2}} \quad \text{(I.4.7)}$$

to (I.1.9), one initially verifies that

$$\begin{aligned} G_{ab}\left(\mathbf{r}-\mathbf{r}',\omega\right) &= -\frac{\partial}{\partial r'_a}\frac{\partial}{\partial r'_b}g\left(\mathbf{r}-\mathbf{r}',\omega\right) \\ &= \frac{1}{(2\pi)^3}\int_{\mathbb{R}^3} d^3k\, e^{i\mathbf{k}\cdot(\mathbf{r}-\mathbf{r}')}\frac{k_a k_b}{|\mathbf{k}|^2-\frac{\omega^2}{c^2}} \\ &\equiv \frac{1}{(2\pi)^3}\int_{\mathbb{R}^3} d^3k\, e^{i\mathbf{k}\cdot(\mathbf{r}-\mathbf{r}')}\tilde{G}_{ab}\left(\mathbf{k},\omega\right), \end{aligned} \tag{I.4.8}$$

where

$$\tilde{G}_{ab}\left(\mathbf{k},\omega\right) = \frac{k_a k_b}{|\mathbf{k}|^2-\frac{\omega^2}{c^2}} \tag{I.4.9}$$

denotes the Fourier transform of $G_{ab}\left(\mathbf{r}-\mathbf{r}',\omega\right)$. With $(I.4.9)$ follows immediately the Fourier transform of

$$\mathscr{G}^{(\mathrm{mag})}_{ab}\left(\mathbf{r}-\mathbf{r}',\omega\right) = G_{ab}\left(\mathbf{r}-\mathbf{r}',\omega\right) - \delta_{ab}\mathrm{Tr}\left[G\left(\mathbf{r}-\mathbf{r}',\omega\right)\right] \tag{I.4.10}$$

according to

$$\begin{aligned} \tilde{\mathscr{G}}^{(\mathrm{mag})}_{ab}\left(\mathbf{k},\omega\right) &= \tilde{G}_{ab}\left(\mathbf{k},\omega\right) - \delta_{ab}\mathrm{Tr}\left[\tilde{G}\left(\mathbf{k},\omega\right)\right] \\ &= \frac{k_a k_b - \delta_{ab}|\mathbf{k}|^2}{|\mathbf{k}|^2-\frac{\omega^2}{c^2}}. \end{aligned} \tag{I.4.11}$$

Provided that $\mathbf{s}\neq\mathbf{0}$,

$$\left[\zeta^{(\mathrm{mag})}_{\Lambda}\left(\mathbf{s},\mathbf{k},\omega\right)\right]_{ab} = \sum_{\mathbf{R}\in\Lambda} e^{-i\mathbf{k}\cdot(\mathbf{s}+\mathbf{R})}\mathscr{G}^{(\mathrm{mag})}_{ab}\left(\mathbf{s}+\mathbf{R},\omega\right) \tag{I.4.12}$$

exhibits a Fourier series representation according to

$$\left[\zeta^{(\mathrm{mag})}_{\Lambda}\left(\mathbf{s},\mathbf{k},\omega\right)\right]_{ab} = \sum_{\mathbf{G}\in\Lambda^{-1}}\left[\tilde{\zeta}^{(\mathrm{mag})}_{\Lambda}\left(\mathbf{G},\mathbf{k},\omega\right)\right]_{ab} e^{i\mathbf{G}\cdot\mathbf{s}}, \tag{I.4.13}$$

because of its lattice periodicity (I.2.10). The expansion coefficients $\left[\tilde{\zeta}^{(\mathrm{mag})}_{\Lambda}\left(\mathbf{G},\mathbf{k},\omega\right)\right]_{ab}$ are easily evaluated to

$$\begin{aligned} \left[\tilde{\zeta}^{(\mathrm{mag})}_{\Lambda}\left(\mathbf{G},\mathbf{k},\omega\right)\right]_{ab} &= \frac{1}{|C_\Lambda|}\int_{C_\Lambda} d^3s\, e^{-i\mathbf{G}\cdot\mathbf{s}}\left[\zeta^{(\mathrm{mag})}_{\Lambda}\left(\mathbf{s},\mathbf{k},\omega\right)\right]_{ab} \\ &= \frac{1}{|C_\Lambda|}\int_{\mathbb{R}^3} d^3r\, e^{-i(\mathbf{k}+\mathbf{G})\cdot\mathbf{r}}\mathscr{G}^{(\mathrm{mag})}_{ab}\left(\mathbf{r},\omega\right) \\ &= \frac{1}{|C_\Lambda|}\tilde{\mathscr{G}}^{(\mathrm{mag})}_{ab}\left(\mathbf{k}+\mathbf{G},\omega\right), \end{aligned} \tag{I.4.14}$$

so that finally

$$\left[\zeta_{\Lambda}^{(\mathrm{mag})}(\mathbf{s},\mathbf{k},\omega)\right]_{ab} = \frac{1}{|C_{\Lambda}|}\sum_{\mathbf{G}\in\Lambda^{-1}} e^{i\mathbf{G}\cdot\mathbf{s}}\tilde{\mathscr{G}}_{ab}^{(\mathrm{mag})}(\mathbf{k}+\mathbf{G},\omega) \tag{I.4.15}$$

$$= \frac{1}{|C_{\Lambda}|}\sum_{\mathbf{G}\in\Lambda^{-1}} e^{i\mathbf{G}\cdot\mathbf{s}}\frac{(k_a+G_a)(k_b+G_b)-\delta_{ab}|\mathbf{k}+\mathbf{G}|^2}{|\mathbf{k}+\mathbf{G}|^2-\frac{\omega^2}{c^2}} \tag{I.4.16}$$

results.

I.4.3 Derivation of (I.2.20)

For an infinitely extended crystal, the local magnetic induction field can be represented by (compare with (I.2.1))

$$B_a(\mathbf{r},\omega) = \frac{|\Omega_{\mathrm{P}}|}{(2\pi)^3}\int_{C_{\Lambda^{-1}}} d^3k \int_{C_{\Lambda}} d^3s\, w(\mathbf{r};\mathbf{s},\mathbf{k})\,\mathfrak{b}_a(\mathbf{s},\mathbf{k},\omega), \tag{I.4.17}$$

where the expansion coefficients $\mathfrak{b}_a(\mathbf{s},\mathbf{k},\omega)$ are readily obtained by insertion of (I.2.19) into (I.2.8) according to

$$\begin{aligned}\mathfrak{b}_a(\mathbf{s},\mathbf{k},\omega) =& \mathfrak{b}_{\mathrm{ext},a}(\mathbf{s},\mathbf{k},\omega) - \mu_0 \sum_{b,c,d=1}^{3}\sum_{j,j'=1}^{M} \\ &\cdot\left[\zeta_{\Lambda}^{(\mathrm{mag})}\left(\mathbf{s}-\eta^{(j)},\mathbf{k},\omega\right)\right]_{ab}\beta_{bc}^{(j)}(\omega)\left[\left(\delta+\Gamma^{(\mathrm{mag})}(\mathbf{k},\omega)\right)^{-1}\right]_{cd}^{(jj')}\mathfrak{b}_{\mathrm{ext},d}^{(j')}(\mathbf{k},\omega).\end{aligned} \tag{I.4.18}$$

In analogy to (I.4.17), the externally applied field is identified with

$$B_{\mathrm{ext},a}(\mathbf{r},\omega) = \frac{|\Omega_{\mathrm{P}}|}{(2\pi)^3}\int_{C_{\Lambda^{-1}}} d^3k \int_{C_{\Lambda}} d^3s\, w(\mathbf{r};\mathbf{s},\mathbf{k})\,\mathfrak{b}_{\mathrm{ext},a}(\mathbf{s},\mathbf{k},\omega), \tag{I.4.19}$$

so that $B_a(\mathbf{r},\omega)$ finally assumes the guise

$$\begin{aligned}B_a(\mathbf{r},\omega) =& B_{\mathrm{ext},a}(\mathbf{r},\omega) - \mu_0\frac{|\Omega_{\mathrm{P}}|}{(2\pi)^3}\sum_{b,c,d=1}^{3}\sum_{j,j'=1}^{M}\int_{C_{\Lambda^{-1}}} d^3k\int_{C_{\Lambda}} d^3s \\ &\cdot w(\mathbf{r};\mathbf{s},\mathbf{k})\left[\zeta_{\Lambda}^{(\mathrm{mag})}\left(\mathbf{s}-\eta^{(j)},\mathbf{k},\omega\right)\right]_{ab}\beta_{bc}^{(j)}(\omega)\left[\left(\delta+\Gamma^{(\mathrm{mag})}(\mathbf{k},\omega)\right)^{-1}\right]_{cd}^{(jj')}\mathfrak{b}_{\mathrm{ext},d}^{(j')}(\mathbf{k},\omega) \\ =& B_{\mathrm{ext},a}(\mathbf{r},\omega) - \frac{\mu_0}{\sqrt{N_{\mathrm{P}}}}\frac{|\Omega_{\mathrm{P}}|}{(2\pi)^3}\sum_{b,c,d=1}^{3}\sum_{j,j'=1}^{M}\int_{C_{\Lambda^{-1}}} d^3k \\ &\cdot e^{i\mathbf{k}\cdot\mathbf{r}}\left[\zeta_{\Lambda}^{(\mathrm{mag})}\left(\mathbf{r}-\eta^{(j)},\mathbf{k},\omega\right)\right]_{ab}\beta_{bc}^{(j)}(\omega)\left[\left(\delta+\Gamma^{(\mathrm{mag})}(\mathbf{k},\omega)\right)^{-1}\right]_{cd}^{(jj')}\mathfrak{b}_{\mathrm{ext},d}^{(j')}(\mathbf{k},\omega),\end{aligned} \tag{I.4.20}$$

where in addition to the definition of $w(\mathbf{r};\mathbf{s},\mathbf{k})$ (see (3.2.9)) the lattice periodicity (see (I.2.10)) of $\zeta_{\Lambda}^{(\mathrm{mag})}(\mathbf{s},\mathbf{k},\omega)$ in case of $\mathbf{s}\neq\mathbf{0}$ has been deployed, to carry out the integration with respect to the spatial coordinates.

I.4.4 Fourier amplitude of the macroscopic magnetization

The ensuing calculations follow the lines indicated in appendix E.5. The Fourier amplitude of the macroscopic magnetization is defined by (see (I.3.6))

$$\tilde{\mathscr{M}}_a(\mathbf{q}',\omega)=\int_{\mathbb{R}^3} d^3r\, e^{-i\mathbf{q}'\cdot\mathbf{r}} M_a(\mathbf{r},\omega) \quad \text{with} \quad \mathbf{q}'\in C_{\Lambda^{-1}}. \tag{I.4.21}$$

Deploying the model of microscopic magnetization given by (I.1.3) and (I.1.4) with the assumption that $\Lambda_{\mathrm{P}}=\Lambda$, one obtains

$$\tilde{\mathscr{M}}_a(\mathbf{q}',\omega)=\sum_{b=1}^{3}\sum_{j=1}^{M}\sum_{\mathbf{R}\in\Lambda} e^{-i\mathbf{q}'\cdot\left(\mathbf{R}+\eta^{(j)}\right)}\beta_{ab}^{(j)}(\omega)\,B_b\left(\mathbf{R}+\eta^{(j)},\omega\right). \tag{I.4.22}$$

When representing $B_b\left(\mathbf{R}+\eta^{(j)},\omega\right)$ by (I.2.27) and subsequent application of the identity (E.5.7), there immediately follows

$$\begin{aligned}\tilde{\mathscr{M}}_a(\mathbf{q}',\omega)=&\frac{(2\pi)^3}{|C_\Lambda|}\delta(\mathbf{q}'-\mathbf{q})\sum_{b,d=1}^{3}\sum_{j=1}^{M}\\ &\cdot\beta_{ab}^{(j)}(\omega)\left[\delta_{bd}-\frac{1}{|C_\Lambda|}\sum_{c=1}^{3}\sum_{\mathbf{G}\in\Lambda^{-1}} e^{i\mathbf{G}\cdot\eta^{(j)}}\tilde{\mathscr{G}}_{bc}^{(\mathrm{mag})}(\mathbf{q}+\mathbf{G},\omega)\,\tilde{K}_{cd}^{(\mathrm{mag})}(\mathbf{G},\mathbf{q},\omega)\right]\tilde{B}_{\mathbf{q}\omega,d}^{(\mathrm{ext})}.\end{aligned} \tag{I.4.23}$$

Now inserting (I.2.26) yields

$$\begin{aligned}&\tilde{\mathscr{M}}_a(\mathbf{q}',\omega)\\ =&\frac{(2\pi)^3}{|C_\Lambda|}\delta(\mathbf{q}'-\mathbf{q})\sum_{b,d=1}^{3}\sum_{j=1}^{M}\beta_{ab}^{(j)}(\omega)\left[\delta_{bd}-\frac{\mu_0}{|C_\Lambda|}\sum_{c,e=1}^{3}\sum_{j',j''=1}^{M}\sum_{\mathbf{G}\in\Lambda^{-1}}\right.\\ &\left.\cdot e^{i\mathbf{G}\cdot\left(\eta^{(j)}-\eta^{(j')}\right)}\tilde{\mathscr{G}}_{bc}^{(\mathrm{mag})}(\mathbf{q}+\mathbf{G},\omega)\,\beta_{ce}^{(j')}(\omega)\left[\left(\delta+\Gamma^{(\mathrm{mag})}(\mathbf{q},\omega)\right)^{-1}\right]_{ed}^{(j'j'')}\right]\tilde{B}_{\mathbf{q}\omega,d}^{(\mathrm{ext})},\end{aligned} \tag{I.4.24}$$

so that with (I.4.15) and (I.2.17)

$$\begin{aligned}
&\tilde{\mathscr{M}}_a\left(\mathbf{q}',\omega\right)\\
=&\frac{(2\pi)^3}{|C_\Lambda|}\delta\left(\mathbf{q}'-\mathbf{q}\right)\sum_{b,d=1}^{3}\sum_{j=1}^{M}\beta_{ab}^{(j)}(\omega)\left[\delta_{bd}\right.\\
&\left.-\sum_{e=1}^{3}\sum_{j',j''=1}^{M}\Gamma_{be}^{(\mathrm{mag})(j,j')}(\mathbf{q},\omega)\left[\left(\delta+\Gamma^{(\mathrm{mag})}(\mathbf{q},\omega)\right)^{-1}\right]_{ed}^{(j'j'')}\right]\tilde{B}_{\mathbf{q}\omega,d}^{(\mathrm{ext})}\\
=&\frac{(2\pi)^3}{|C_\Lambda|}\delta\left(\mathbf{q}'-\mathbf{q}\right)\sum_{b,d=1}^{3}\sum_{j=1}^{M}\beta_{ab}^{(j)}(\omega)\left[\delta_{bd}-\sum_{j''=1}^{M}\left[\Gamma^{(\mathrm{mag})}(\mathbf{q},\omega)\circ\left(\delta+\Gamma^{(\mathrm{mag})}(\mathbf{q},\omega)\right)^{-1}\right]_{bd}^{(jj'')}\right]\tilde{B}_{\mathbf{q}\omega,d}^{(\mathrm{ext})}.
\end{aligned}\tag{I.4.25}$$

results. Applying an identity similar to (E.5.14) and utilizing (I.3.3), there finally holds

$$\tilde{\mathscr{M}}_a\left(\mathbf{q}',\omega\right)=\frac{1}{\mu_0}\frac{(2\pi)^3}{|C_\Lambda|}\delta\left(\mathbf{q}'-\mathbf{q}\right)\sum_{d=1}^{3}\tilde{K}_{ad}^{(\mathrm{mag})}(\mathbf{q},\omega)\tilde{B}_{\mathbf{q}\omega,d}^{(\mathrm{ext})}.\tag{I.4.26}$$

I.4.5 Evaluation of $\mathscr{L}^{(\mathrm{mag})}$ for simple cubic lattices

The evaluation of $\mathscr{L}^{(\mathrm{mag})}$ follows the lines indicated in appendix G.With the definition (I.2.13) of the lattice sum $\zeta_\Lambda^{(0)(\mathrm{mag})}(\mathbf{q},\omega)$ and the representation of $\tilde{\mathscr{G}}_{ab}^{(\mathrm{mag})}(\mathbf{q},\omega)$ by its Fourier integral

$$\begin{aligned}
\tilde{\mathscr{G}}_{ab}^{(\mathrm{mag})}(\mathbf{q},\omega)&=\int_{\mathbb{R}^3}d^3r\,e^{-i\mathbf{q}\cdot\mathbf{r}}\mathscr{G}_{ab}^{(\mathrm{mag})}(\mathbf{r},\omega)\\
&=\int_{\mathbb{R}^3}d^3r\,e^{-i\mathbf{q}\cdot\mathbf{r}}\left(G_{ab}(\mathbf{r},\omega)-\delta_{ab}\mathrm{Tr}\left[G(\mathbf{r},\omega)\right]\right),
\end{aligned}\tag{I.4.27}$$

the cartesian components of $\mathscr{L}^{(\mathrm{mag})}$ defined in (I.3.18) can initially be written for arbitrary Bravais lattices as (compare with (G.1.5))

$$\begin{aligned}
\mathscr{L}_{ab}^{(\mathrm{mag})}=&|C_\Lambda|\lim_{\omega\to0}\lim_{|\mathbf{q}|\to0}\left(\sum_{\mathbf{R}\in\Lambda\setminus\{\mathbf{0}\}}e^{-i\mathbf{q}\cdot\mathbf{R}}\left(G_{ab}(\mathbf{R},\omega)-\delta_{ab}\mathrm{Tr}\left[G(\mathbf{R},\omega)\right]\right)\right.\\
&\left.-\frac{1}{|C_\Lambda|}\int_{\mathbb{R}^3}d^3r\,e^{-i\mathbf{q}\cdot\mathbf{r}}\left(G_{ab}(\mathbf{r},\omega)-\delta_{ab}\mathrm{Tr}\left[G(\mathbf{r},\omega)\right]\right)\right)\\
=&|C_\Lambda|\sum_{\mathbf{R}\in\Lambda\setminus\{\mathbf{0}\}}\left(\Pi_{ab}^{(\mathrm{L})}(\mathbf{R})-\delta_{ab}\mathrm{Tr}\left[\Pi^{(\mathrm{L})}(\mathbf{R})\right]\right)-\int_{\mathbb{R}^3}d^3r\left(\Pi_{ab}^{(\mathrm{L})}(\mathbf{r})-\delta_{ab}\mathrm{Tr}\left[\Pi^{(\mathrm{L})}(\mathbf{r})\right]\right).
\end{aligned}\tag{I.4.28}$$

In the special case of a simple cubic crystal it has been shown in appendix G, that

$$\sum_{\mathbf{R}\in\Lambda\setminus\{\mathbf{0}\}} \Pi_{ab}^{(\mathrm{L})}(\mathbf{R}) = 0 \;\forall a,b \in \{1,2,3\} \tag{I.4.29}$$

$$\int_{\mathbb{R}^3} d^3r\, \Pi_{ab}^{(\mathrm{L})}(\mathbf{r}) = \frac{1}{3}\delta_{ab} \tag{I.4.30}$$

holds, so that from (I.4.28)

$$\mathscr{L}_{ab}^{(\mathrm{mag})} = \frac{2}{3}\delta_{ab} \tag{I.4.31}$$

can readily be deduced. As a corollary one obtains

$$\lim_{\omega\to 0}\lim_{|\mathbf{q}|\to 0} \mathscr{G}_{ab}^{(\mathrm{mag})}(\mathbf{q},\omega) = -\frac{2}{3}\delta_{ab}. \tag{I.4.32}$$

Bibliography

[1] V. M. Agranovich and V. L. Ginzburg. *Spatial Dispersion in Crystal Optics and the Theory of Excitons*, volume 18 of *Monographs and Texts in Physics and Astronomy*. Interscience Publishers, 1966.

[2] L. V. Keldysh. *The Dielectric Function Of Condensed Systems*, volume 24 of *Modern Problems In Condensed Matter Sciences*. North Holland, 2012. chapter 1.

[3] Neil W. Ashcroft and David N. Mermin. *Festkörperphysik*. Oldenbourg Verlag, 4 edition, 2013.

[4] Max Born and Emil Wolf. *Principles of Optics*. Cambridge University Press, 7 edition, 1999.

[5] R. R. Birss. Macroscopic symmetry in space-time. *Reports on Progress in Physics*, 26:307–360, 1963.

[6] Mathias Schubert. *Infrared Ellipsometry on Semiconductor Layer Structures*, volume 209 of *Springer Tracts in Modern Physics*. Springer Verlag, 1 edition, 2004.

[7] Steven A. Henck. In situ real-time ellipsometry for film thickness measurement and control. *Journal of Vacuum Science & Technology A: Vacuum, Surfaces, and Films*, 10(4):934–938, 1992.

[8] Harold J. Metcalf and Peter van der Straten. *Laser Cooling and Trapping*. Springer Verlag, 1 edition, 1999.

[9] John H. Burnett, Zachary H. Levine, and Eric L. Shirley. Intrinsic birefringence in calcium fluoride and barium fluoride. *Physical Review B*, 65(24):241102, 2001.

[10] Marc Eichhorn. *Laserphysik*. Springer Verlag, 2013.

[11] Suzanne Linsmeier Kilmer and R. Rox Anderson. Clinical use of the q-switched ruby and the q-switched Nd:YAG (1064nm and 532nm) lasers for treatment of tattoos. *The Journal of Dermatologic Surgery and Oncology*, 19(4):330–338, 1993.

[12] Charles R. Taylor and R. Rox Anderson. Treatment of benign pigmented epidermal lesions by q-switched ruby laser. *International Journal of Dermatology*, 32(12):908–912, 1993.

[13] David J. Goldberg and Jeffrey Marcus. The use of the frequency-doubled q-switched Nd:YAG laser in the treatment of small cutaneous vascular lesions. *Dermatologic Surgery*, 22(10):841–844, 1996.

[14] H. Helmholtz. Über Integrale der hydrodynamischen Gleichungen, welche den Wirbelbewegungen entsprechen. *Journal für die reine und angewandte Mathematik*, 55:25–55, 1858.

[15] Otto Blumenthal. Über die Zerlegung unendlicher Vektorfelder. *Mathematische Annalen*, 61(2):235–250, 1905.

[16] Harsh Bhatia, Gregory Norgard, Valerio Pascucci, and Peer-Timo Bremer. The Helmholtz-Hodge decomposition - a survey. *IEEE Transactions on Visualization and Computer Graphics*, 19(8):1386–1404, 2013.

[17] Dietmar Petrascheck and Franz Schwabl. *Elektrodynamik*. Springer Spektrum, 2 edition, 2015.

[18] Claude Cohen-Tannoudji, Jacques Dupont-Roc, and Gilbert Grynberg. *Photons & Atoms*. Wiley-VCH, 1 edition, 1997.

[19] Nouredine Zettili. *Quantum Mechanics - Concepts and Applications*. John Wiley and Sons, Ltd, 2001.

[20] George B. Arfken, Hans J. Weber, and Frank E. Harris. *Mathematical Methods for Physicists*. Academic Press Elsevier, 7 edition, 2013.

[21] Dimitry E. Olshevsky. Integral equations as a method of theoretical physics. *The American Mathematical Monthly*, 37(6):274–281, 1930.

[22] Arvid T. Lonseth. Sources and applications of integral equations. *SIAM Review*, 19(2):241–278, 1977.

[23] Marius Dommermuth and Nils Schopohl. On the theory of light propagation in crystalline dielectrics. *Journal of Physics Communications*, 2(7):075012, 2018.

[24] Nils Schopohl. Private communication.

[25] R. E. Raab and O. L. De Lange. *Multipole Theory in Electromagnetism: Classical, Quantum, and Symmetry Aspects, with Applications*, volume 128 of *International Series of Monographs on Physics*. Oxford University Press, 2005.

[26] N. B. Baranova and B. Ya. Zel'dovich. Theory of a new linear magnetorefractive effect in liquids. *Molecular Physics*, 38(4):1085–1098, 1979.

[27] G. Rickayzen. *Green's Functions and Condensed Matter*. Dover Publications, Inc, 2013. Republication.

[28] Max von Laue. *Röntgenstrahlinterferenzen*. Akademische Verlagsgesellschaft Frankfurt am Main, 3 edition, 1960.

[29] O. V. Dolgov and E. G. Maksimov. *The Dielectric Function Of Condensed Systems*, volume 24 of *Modern Problems In Condensed Matter Sciences*. North Holland, 2012. chapter 4.

[30] P. P. Ewald. Zur Begründung der Kristalloptik. *Annalen der Physik*, 354(1):1–38, 1916.

[31] P. P. Ewald. Optique cristalline (lumière et rayons x) interaction des atomes par rayonnement. *Annales de l' I. H. P.*, 8(2):79–110, 1938.

[32] Max Born and Kun Huang. *Dynamical theory of crystal lattices*. The international series of monographs on physics. Oxford University Press, 1954.

[33] J. M. Ziman. *Principles of the Theory of Solids*. Cambridge University Press, 2 edition, 1972.

[34] Gerald D. Mahan. *Many-Particle Physics*. Physics of Solids and Liquids. Plenum Press, 2 edition, 1990.

[35] Eli Yablonovitch. Inhibited spontaneous emission in solid-state physics and electronics. *Physical Review Letters*, 58(20):2059–2062, 1987.

[36] Sajeev John. Strong localization of photons in certain disordered dielectric superlattices. *Physical Review Letters*, 58(23):2486–2489, 1987.

[37] E. Yablonovitch and T. J. Gmitter. Photonic band structure: The face-centered-cubic case. *Physical Review Letters*, 63(18):1950–1953, 1989.

[38] L. Rosenfeld. *Theory of Electrons*, volume 1 of *Selected Topics in Modern Physics*. North-Holland Publishing Company, 1951.

[39] B. T. Draine and Jeremy Goodman. Beyond Clausius-Mossotti: Wave propagation on a polarizable point lattice and the discrete dipole approximation. *The Astrophysical Journal*, 405:685–697, 1993.

[40] Dirk Werner. *Funktionalanalysis*. Springer, 7 edition, 2011.

[41] J. A. Klugkist, M. Mostovoy, and J. Knoester. Mode softening, ferroelectric transition, and tunable photonic band structures in a point-dipole crystal. *Physical Review Letters*, 96(163903), 2006.

[42] Masatoshi Tokushima, Hideo Kosaka, Akihisa Tomita, and Hirohito Yamada. Lightwave propagation through a 120° sharply bent single-line-defect photonic crystal waveguide. *Applied Physics Letters*, 76(8):952–954, 2000.

[43] Thomas F. Krauss. Planar photonic crystal waveguide devices for integrated optics. *Physica Status Solidi (a)*, 197(3):688–702, 2003.

[44] Sharee J. McNab, Nikolaj Moll, and Yurii A. Vlasov. Ultra-low loss photonic integrated circuit with membrane-type photonic crystal waveguides. *Optics Express*, 11(22):2927–2939, 2003.

[45] Philip Russell. Photonic crystal fibers. *Science*, 299(5605):358–362, 2003.

[46] Katsusuke Tajima, Jian Zhou, Kazuhide Nakajima, and Kiminori Sato. Ultralow loss and long length photonic crystal fiber. *Journal of Lightwave Technology*, 22(1):7–10, 2004.

[47] Mario N. Armenise, Carlo E. Campanella, Caterina Ciminelli, Francesco Dell'Olio, and Vittorio M. N. Passaro. Phononic and photonic band gap structures: modelling and applications. *Physics Procedia*, 3:357–364, 2010. International Congress on Ultrasonics, Universidad de Santiago de Chile, January 2009.

[48] Mauro Antezza and Yvan Castin. Fano-Hopfield model and photonic band gaps for an arbitrary atomic lattice. *Physical Review A*, 80(013816), 2009.

[49] K. M. Leung and Y. F. Liu. Full vector wave calculation of photonic band structures in face-centered-cubic dielectric media. *Physical Review Letters*, 65(21):2646–2649, 1990.

[50] Ze Zhang and Sashi Satpathy. Electromagnetic wave propagation in periodic structures: Bloch wave solution of Maxwell's equations. *Physical Review Letters*, 65(21):2650–2653, 1990.

[51] H. Sami Sözüer and Joseph W. Haus. Photonic bands: simple-cubic lattice. *Journal of the Optical Society of America B*, 10(2):296–302, 1993.

[52] Alvaro Blanco, Emmanuel Chomski, Serguei Grabtchak, Marta Ibisate, Sajeev John, Stephen W. Leonard, Cefe Lopez, Francisco Meseguer, Hernan Miguez, Jessica P. Mondia, Geoffrey A. Ozin, Ovidiu Toader, and Henry M. van Driel. Large-scale synthesis of a silicon photonic crystal with a complete three-dimensional bandgap near 1.5 micrometres. *Nature*, 405:437–440, 2000.

[53] Andreas Frölich, Joachim Fischer, Thomas Zebrowski, Kurt Busch, and Martin Wegener. Titania woodpiles with complete three-dimensional photonic bandgaps in the visible. *Advanced Materials*, 25(26):3588–3592, 2013.

[54] E. J. Post. The logic of time reversal. *Foundations of Physics*, 9:129–161, 1979.

[55] L. D. Barron. Optical activity and time reversal. *Molecular Physics*, 43(6):1395–1406, 1981.

[56] T. Martin Lowry. *Optical Rotatory Power*. Dover Publications Inc New York, 1964.

[57] Eugene Hecht. *Optik*. Oldenbourg Verlag, 5 edition, 2009.

[58] C. J. Durrant, M. P. Hertzberg, and P. W. Kuchel. Magnetic susceptibility: Further insights into macroscopic and microscopic fields and the sphere of Lorentz. *Concepts in Magnetic Resonance Part A*, 18A(1):72–95, 2003.

[59] Stephen L. Adler. Quantum theory of the dielectric constant in real solids. *Physical Review*, 126(2):413–420, 1962.

[60] J. H. Conway and N. J. A. Sloane. *Sphere Packings, Lattices and Groups*, volume 290 of *Grundlehren der mathematischen Wissenschaften*. Springer Verlag, 1 edition, 1988.

[61] R. Remmert and G. Schumacher. *Funktionentheorie 1*. Springer Verlag, 5 edition, 2013.

[62] F. W. De Wette and G. E. Schacher. Internal field in general dipole lattices. *Physical Review*, 137(1A):78–91, 1965.

[63] J. H. P. Colpa. Dipole fields and electric-field gradients in their dependence on the macroscopic and microscopic crystal parameters for orthorhombic and hexagonal lattices. 1. *Physica*, 56:185–204, 1971.

[64] J. H. P. Colpa. Dipole fields and electric-field gradients in their dependence on the macroscopic and microscopic crystal parameters for orthorhombic and hexagonal lattices 2. *Physica*, 56:205–236, 1971.

[65] Davide Vanzo, Benjamin J. Topham, and Zoltán G. Soos. Dipole-field sums, Lorentz factors, and dielectric properties of organic molecular films modeled as crystalline arrays of polarizable points. *Advanced Functional Materials*, 25:2004–2012, 2015.

[66] D. A. Kirzhnitz. *The Dielectric Function Of Condensed Systems*, volume 24 of *Modern Problems In Condensed Matter Sciences*. North Holland, 2012. chapter 2.

[67] R. H. Lyddane, R. G. Sachs, and E. Teller. On the polar vibrations of alkali halides. *Physical Review*, 59:673–676, 1941.

[68] Jr. A. S. Barker. Long-wavelength soft modes, central peaks, and the Lyddane-Sachs-Teller relation. *Physical Review B*, 12(10):4071–4084, 1975.

[69] Arnold Sommerfeld. *Optik*, volume 4 of *Vorlesungen über Theoretische Physik*. Verlag Harri Deutsch, 2011.

[70] Gerd Fischer. *Lineare Algebra*. Grundkurs Mathematik. Springer Spektrum, 18 edition, 2014.

[71] Wilhelm Sellmeier. Zur Erklärung der abnormen Farbenfolge im Spectrum einiger Substanzen. *Annalen der Physik*, 219(6):272–282, 1871.

[72] Volkmar Brückner. *Elements of optical networking: Basics and practice of optical data communication*. Vieweg+Teubner Verlag, 2011.

[73] H. H. Li. Refractive index of alkali halides and its wavelength and temperature derivatives. *Journal of Physical and Chemical Reference Data*, 5(2):329–528, 1976.

[74] H. H. Li. Refractive index of alkaline earth halides and its wavelength and temperature derivatives. *Journal of Physical and Chemical Reference Data*, 9(1):161–289, 1980.

[75] Gorachand Ghosh. Dispersion-equation coefficients for the refractive index and birefringence of calcite and quartz crystals. *Optics Communications*, 163:95–102, 1999.

[76] V. Devarajan and A. M. Glazer. Theory and computation of optical rotatory power in inorganic crystals. *Acta Crystallographica Section A*, 42:560–569, 1986.

[77] R. W. G. Wyckoff. *Crystal structures*. Interscience Publishers, 1963.

[78] R. Restori, D. Schwarzenbach, and J. R. Schneider. Charge density in rutile, TiO_2. *Acta Crystallographica Section B*, 43:251–257, 1987.

[79] Rebecca A. Parker. Lorentz corrections in rutile. *Physical Review*, 124(6):1713–1719, 1961.

[80] J. R. DeVore. Refractive indices of rutile and sphalerite. *Journal of the Optical Society of America*, 41(6):416–419, 1951.

[81] G. Vidal-Valat, J. P. Vidal, K. Kurki-Suonio, and R. Kurki-Suonio. Multipole analysis of x-ray diffraction data on BeO. *Acta Crystallographica Section A*, 43:540–550, 1987.

[82] Vesselin Dimitrov and Takayuki Komatsu. Classification of simple oxides: A polarizability approach. *Journal of Solid State Chemistry*, 163(1):100–112, 2002.

[83] Marvin J. Weber. *Handbook of optical materials*. CRC Press, 2003.

[84] S. C. Abrahams and J. L. Bernstein. Remeasurement of optically active $NaClO_3$ and $NaBrO_3$. *Acta Crystallographica Section B*, 33:3601–3604, 1977.

[85] S. Chandrasekhar and M. S. Madhava. Optical rotatory dispersion of crystals of sodium chlorate and sodium bromate. *Acta Crystallographica*, 23:911–913, 1967.

[86] Yu. A. Abramov, V. G. Tsirelson, V. E. Zavodnik, S. A. Ivanov, and I. D. Brown. The chemical bond and atomic displacements in $SrTiO_3$ from x-ray diffraction analysis. *Acta Crystallographica Section B*, 51:942–951, 1995.

[87] H. Chaib, L. M. Eng, and T. Otto. Dielectric polarization and refractive indices of ultrathin barium titanate films on strontium titanate single crystals. *Journal of Physics: Condensed Matter*, 17(1):161–179, 2005.

[88] D. C. N. Swindells and J. L. Gonzalez. Absolute configuration and optical activity of laevorotatory $Bi_{12}TiO_{20}$. *Acta Crystallographica Section B*, 44:12–15, 1988.

[89] S. C. Abrahams, J. L. Bernstein, and C. Svensson. Crystal structure and absolute piezoelectric d_{14} coefficient in laevorotatory $Bi_{12}SiO_{20}$. *The Journal of Chemical Physics*, 71(2):788–792, 1979.

[90] Ngo Thong and D. Schwarzenbach. The use of electric field gradient calculations in charge density refinements. ii. charge density refinement of the low-quartz structure of aluminum phosphate. *Acta Crystallographica Section A*, 35:658–664, 1979.

[91] C. J. Xiao, C. Q. Jin, and X. H. Wang. Crystal structure of dense nanocrystalline $BaTiO_3$ ceramics. *Materials Chemistry and Physics*, 111(2-3):209–212, 2008.

[92] S. H. Wemple, M. Didomenico Jr., and I. Camlibel. Dielectric and optical properties of melt-grown $BaTiO_3$. *Journal of Physics and Chemistry of Solids*, 29(10):1797–1803, 1968.

[93] E. N. Maslen, V. A. Streltsov, and N. R. Streltsova. X-ray study of the electron density in calcite, $CaCO_3$. *Acta Crystallographica Section B*, 49:636–641, 1993.

[94] W. N. Lawless and R. C. Devries. Oxygen polarizability and point-dipole theory in the carbonate minerals. *Journal of Physics and Chemistry of Solids*, 25(10):1119–1124, 1964.

[95] K. Stadnicka, A. M. Glazer, M. Koralewski, and B. M. Wanklyn. Structure and absolute optical chirality of thulium pyrogermanate crystals. *Journal of Physics: Condensed Matter*, 2:4795–4805, 1990.

[96] A. M. Glazer and K. Stadnicka. On the origin of optical activity in crystal structures. *Journal of Applied Crystallography*, 19:108–122, 1986.

[97] Cécile Malgrange, Christian Ricolleau, and Michel Schlenker. *Symmetry and Physical Properties of Crystals*. Springer Science+Business Media, 2014.

[98] Alessandro F. Gualtieri. Accuracy of XRPD QPA using the combined Rietveld-RIR method. *Journal of Applied Crystallography*, 33:267–278, 2000.

[99] S. C. Abrahams, A. M. Glass, and K. Nassau. Crystal chirality and optical rotation sense in isomorphous $NaClO_3$ and $NaBrO_3$. *Solid State Communications*, 24(8):515–516, 1977.

[100] Albert Feldman, William S. Brower Jr., and Deane Horowitz. Optical activity and Faraday rotation in bismuth oxide compounds. *Applied Physics Letters*, 16(5):201–202, 1970.

[101] S. C. Abrahams, C. Svensson, and A. R. Tanguay Jr. Crystal chirality and optical rotation sense in isomorphous $Bi_{12}SiO_{20}$ and $Bi_{12}GeO_{20}$. *Solid State Communications*, 30(5):293–295, 1979.

[102] A. G. Serebryakov, F. Bociort, and J. Braat. Spatial dispersion of crystals as a critical problem for deep uv lithography. *Journal of Optical Technology*, 70(8):566–569, 2003.

[103] Nadine Suzan Cetin. On the theory of the Faraday effect in crystalline dielectrics. Bachelor thesis, Eberhard Karls Universität Tübingen, 2018.

[104] B. B. Krichevtsov, R. V. Pisarev, A. A. Rzhevskii, V. N. Gridnev, and H.-J. Weber. Magnetically induced spatial dispersion in the cubic magnetic semiconductors $Cd_{1-x}Mn_xTe$. *Journal of Experimental and Theoretical Physics*, 87(3):553–562, 1998.

[105] J. C. Suits. Magneto-optical rotation and ellipticity measurements with a spinning analyzer. *The Review of Scientific Instruments*, 42(1):19–22, 1971.

[106] H. Guerrero, R. Pérez del Real, R. Fernández de Caleya, and G. Rosa. Magnetic field biasing in Faraday effect sensors. *Applied Physics Letters*, 74(24):3702–3704, 1999.

[107] L. Sun, S. Jiang, and J. R. Marciante. All-fiber optical magnetic-field sensor based on Faraday rotation in highly terbium-doped fiber. *Optics Express*, 18(6):5407–5412, 2010.

[108] Iris Crassee, Julien Levallois, Andrew L. Walter, Markus Ostler, Aaron Bostwick, Eli Rotenberg, Thomas Seyller, Dirk van der Marel, and Alexey B. Kuzmenko. Giant Faraday rotation in single- and multilayer graphene. *Nature Physics*, 7, 2011.

[109] *Proceedings of the section of sciences*, volume XXIV. Koninklijke Akademie van Wetenschappen, Amsterdam, 1922. H. A. Lorentz: Double refraction by regular crystals, pp. 333-339.

[110] V. G. Veselago. The electrodynamics of substances with simultaneously negative values of ε and μ. *Soviet Physics Uspekhi*, 10(4):509–514, 1968.

[111] R. A. Shelby, D. R. Smith, and S. Schultz. Experimental verification of a negative index of refraction. *Science*, 292(5514):77–79, 2001.

[112] J. B. Pendry. Negative refraction makes a perfect lens. *Physical Review Letters*, 85(18):3966–3969, 2000.

[113] Jason Valentine, Jensen Li, Thomas Zentgraf, Guy Bartal, and Xiang Zhang. An optical cloak made of dielectrics. *Nature Materials*, 8:568–571, 2009.

[114] Tolga Ergin, Nicolas Stenger, Patrice Brenner, John B. Pendry, and Martin Wegener. Three-dimensional invisibility cloak at optical wavelengths. *Science*, 328(5976):337–339, 2010.

[115] Maxim A. Gorlach, Stanislav B. Glybovski, Anna A. Hurshkainen, and Pavel A. Belov. Giant spatial-dispersion-induced birefringence in metamaterials. *Physical Review B*, 93(20), 2016.

[116] Allan and et al. Intrinsic birefringence compensation for below 200 nanometer wavelength optical lithography components with cubic crystalline structures, US Patent (US 6,785,051 B2), August 2004.

[117] Burnett and et al. Minimizing spatial-dispersion-induced birefringence, US Patent (US 7,163,649 B2), January 2007.

[118] C. Zaldo, C. López, and F. Meseguer. Natural birefringence in alkali halide single crystals. *Physical Review B*, 33(6), 1986.

[119] Peter Y. Yu and Manuel Cardona. Spatial dispersion in the dielectric constant of GaAs. *Solid State Communications*, 9:1421–1424, 1971.

[120] André Authier. Optical properties of x-rays - dynamical diffraction. *Acta Crystallographica Section A*, 68:40–56, 2012. Laue centennial.

[121] Christian Kurtsiefer, Sonja Mayer, Patrick Zarda, and Harald Weinfurter. Stable solid-state source of single photons. *Physical Review Letters*, 85(2):290–293, 2000.

[122] F. Dolde, H. Fedder, M. W. Doherty, T. Nöbauer, F. Rempp, G. Balasubramanian, T. Wolf, F. Reinhard, L. C. L. Hollenberg, F. Jelezko, and H. Wrachtrup. Electric-field sensing using single diamond spins. *Nature Physics*, 7:459–463, 2011.

[123] K. Arya, Z. B. Su, and Joseph L. Birman. Anderson localization of electromagnetic waves in a dielectric medium of randomly distributed metal particles. *Physical Review Letters*, 57(21):2725–2728, 1986.

[124] Alexander Figotin and Abel Klein. Localization of classical waves II: Electromagnetic waves. *Communications in Mathematical Physics*, 184:411–441, 1997.

[125] A. Sheikhan, N. Abedpour, R. Sepehrinia, M. D. Niry, M. Reza Rahimi Tabar, and M. Sahimi. Anderson localization and propagation of electromagnetic waves through disordered media. *Waves in Random and Complex Media*, 20(1):191–200, 2010.

[126] Kevin Vynck, Romain Pierrat, and Rémi Carminati. Polarization and spatial coherence of electromagnetic waves in uncorrelated disordered media. *Physical Review A*, 89:013842, 2014.

[127] B. Velický. Theory of electronic transport in disordered binary alloys: Coherent-potential approximation. *Physical Review*, 184(3):614–628, 1969.

[128] P. P. Ewald. Zur Begründung der Kristalloptik. *Annalen der Physik*, 354(2):117–143, 1916.

[129] K. A. Michalski and J. R. Mosig. The Sommerfeld half-space problem revisited: from radio frequencies and Zenneck waves to visible light and Fano modes. *Journal of Electromagnetic Waves and Applications*, 30(1):1–42, 2016.

[130] K. Y. Bliokh and A. Aiello. Goos-Hänchen and Imbert-Fedorov beam shifts: an overview. *Journal of Optics*, 15:014001, 2013.

[131] Jean-Pierre Hansen and Ian R. McDonald. *Theory of Simple Liquids with Applications to Soft Matter*. Academic Press Elsevier, 4 edition, 2013.

[132] D. L. Mills and E. Burstein. Polaritons: the electromagnetic modes of media. *Reports on Progress in Physics*, 37:817–926, 1974.

[133] Philip M. Morse and Herman Feshbach. *Methods of theoretical physics, part 1*. International series in pure and applied physics. McGraw-Hill Book Company, Inc., 1953.

[134] Arthur D. Yaghjian. Electric dyadic Green's functions in the source region. *Proceedings of the IEEE*, 68(2):248–263, 1980.

[135] C. W. Oseen. Über die Wechselwirkung zwischen zwei elektrischen Dipolen und über die Drehung der Polarisationsebene in Kristallen und Flüssigkeiten. *Annalen der Physik*, 353(17):1–56, 1915.

[136] Gerd Czycholl. *Theoretische Festkörperphysik*. Springer, 3 edition, 2008.

[137] Jean-Pierre Serre. *A course in arithmetic*, volume 7 of *Graduate Texts in Mathematics*. Springer Verlag, 1973.

[138] L. D. Landau and E. M. Lifschitz. *Elektrodynamik der Kontinua*, volume 8 of *Lehrbuch der Theoretischen Physik*. Europa-Lehrmittel, 5 edition, 1990.

[139] Werner Weiglhofer. Delta-function identities and electromagnetic field singularities. *American Journal of Physics*, 57(5):455–456, 1989.

[140] O. V. Porvatkina, A. A. Tishchenko, and M. N. Strikhanov. Permittivity and permeability of semi-infinite metamaterial. *Journal of Physics: Conference Series*, 740(1):012011, 2016.